Dissertation zur Erlangung des Doktorgrades

der Fakultät für Chemie und Pharmazie

der Ludwig-Maximilians-Universität München

Molecular *s*-Triazine and *s*-Heptazine Derivatives as Building Blocks in Coordination Networks, Molecular Salts and Supramolecular Materials

Sophia Janina Makowski

aus

Fürstenfeldbruck

2012

Erklärung

Diese Dissertation wurde im Sinne von § 7 der Promotionsordnung vom 28. November 2011 von Herrn Prof. Dr. Wolfgang Schnick betreut.

Eidesstattliche Versicherung

Diese Dissertation wurde eigenständig und ohne unerlaubte Hilfe erarbeitet.

München,

…….

Sophia Janina Makowski

Dissertation eingereicht am	06.03.2012
1. Gutachter:	Prof. Dr. Wolfgang Schnick
2. Gutachter:	Prof. Dr. Bettina V. Lotsch
Mündliche Prüfung am	08.05.2012

To my parents

Acknowledgements

First and foremost, I would like to express my gratitude to my supervisor Prof. Dr. Wolfgang Schnick for the opportunity to work in his group and his guidance of my research. His knowledge and expertise have been of great value for me and I have very much appreciated the given freedom of research and writing.

I would like to thank Prof. Dr. Bettina V. Lotsch for being co-referee of this thesis.

I am thankful to Prof. Dr. H.-C. Böttcher, Prof. Dr. S. Herres-Pawlis, Prof. Dr. D. Johrendt, and Prof. Dr. H. Langhals for being available as examiners in my viva-voce.

My predecessors and peers in C/N research Nicole Braml, Dr. Barbara Jürgens, Prof. Dr. Bettina V. Lotsch, Dr. Andreas Sattler, and Eva Wirnhier I thank for valuable groundwork, ideas and helpful discussions. Dr. Andreas Sattler I am especially thankful for introducing me into this area of research as well as into numerous working techniques. Special thank goes also to Nicole Braml and Eva Wirnhier for their pleasant company in the lab as well as their constant professional and – sometimes even more important – moral support.

All past and present members of lab D2.103, Yamini Avadhut, Nicole Braml, Dr. Cordula Braun, Dajana Durach, Dr. Stefanie Hering, Christian Minke, Dr. Andreas Sattler, and Eva Wirnhier, I would like to thank for providing a pleasant working atmosphere and for the organization of several lab-meetings by Christian Minke and Dr. Andreas Sattler at their homes. Moreover I thank Yamini Avadhut for enthusiastically introducing us into Indian food.

Special thanks go to my bachelor and research students Evelyn Calta, Pia Köstler, Monika Lacher, Claudia Lermer, Michael Hörmannsdorfer, Saeedeh Manzori Ostad, and Arne Schwarze for their enthusiasm, ideas and for contributing to a lively working atmosphere.

I thank all my C/N cooperation partners for performing measurements, fruitful discussions, helpful ideas and enjoyable meetings in Bayreuth and Munich: Prof. Dr. Jürgen Senker and his co-workers Kilian Bärwinkel, Daniel Gunzelmann, Mario Liebl, Maria Mesch, Nadine Popp, and Julia Wack and Prof. Dr. Bettina V. Lotsch and her co-workers Stephan Hug, Katharina Schwinghammer, Brian Tuffy, and Hongji Wang.

I would like to thank Prof. Dr. Stefan Grimme and Helge Krieg for cooperation with DFT calculations and Dr. Alexander Zurawski for cooperation with research on rare-earth carbon nitrogen chemistry.

Prof. Dr. Oliver Oeckler I am grateful for giving me excellent advice on several crystallographic questions and for his engaged supervision of practical courses.

Thomas Miller and Wolfgang Wünschheim I thank for frequent support with all kinds of technical and security questions.

For technical support and carrying out numerous measurements I would like to thank following colleagues and members of the department:

- Sandra Albrecht, Dr. Peter Mayer, and Thomas Miller for testing numerous single-crystals and collecting single-crystal data
- Christian Minke for solid-state NMR and EDX measurements
- Robert Eicher and Gertraud Käser for plenty of elemental analyses
- Helmut Hartl for ICP–AES analyses and persevering efforts to dissolve my samples
- Brigitte Breitenstein for mass spectra
- Irmgard Peter and Marion Sokoll for IR spectra
- Prof. Dr. Konstantin Karaghiosoff and Peter Mayer for solution-state NMR spectra
- all members of the precision mechanics and the glassblower workshops

All my past and present colleagues of solid-state chemistry I have not explicitly mentioned above I thank for providing such a welcoming, friendly and supporting atmosphere over the last years:

Dominik Baumann, Dr. Daniel Bichler, Erik Flügel, Rainer Frankovsky, Gina Friederichs, Cora Hecht, Elsbeth Hermanns, Christine Hieke, Frauke Hintze, Dr. Christoph Höller, Franziska Hummel, Sebastian Junggeburth, Dr. Juliane Kechele, Catrin Löhnert, Olga Lorenz, Saskia Lupart, Philipp Matthes, Dr. Marianne Martin, Prof. Dr. Klaus Müller-Buschbaum, Dr. Sandro Pagano, Ida Pavlichenko, Florian Pucher, Philipp Pust, Annekathrin Ranft, Dr. Rebecca Römer, Tobias Rosenthal, Jens-Christoph Rybak, Dr. Jörn Schmedt auf der Günne, Sebastian Schmiechen, Dr. Matthias Schneider, Sebastian Schneider, Fabian Schönfeld, Thorsten Schröder, Dr. Stefan Sedlmaier, Markus Seibald, Tobias Stürzer, Dr. Marcus Tegel, Daniel Weber, Dr. Johannes Weber, Stephan Werner, Erwin Wiesenmayer, Dr. Martin Zeuner, Christian Ziegler, and Veronika Zinth.

Particularly I want to thank my parents and my sister Christiane, who have helped me immeasurably by their support and care and by putting problems into perspective. And last but not least special thanks to Georg for everything he did for me.

Learning is a treasure that will follow its owner everywhere.

Contents

1. Introduction

Heterocycles probably represent the largest and manifold family of organic compounds and play a significant role in biology and technology, for instance as building blocks of DNA and amino acids, or as natural and artificial dyes and pigments. The formal replacement of one or more carbon atoms in hydrocarbons with heteroatoms, most commonly oxygen, nitrogen, and sulfur, results in a great variety of heterocyclic structures.[1] Especially among the large group of *N*-heterocycles plenty of compounds with considerable importance, especially for nature but also for technical applications, are known (see Scheme 1). Two of the most prominent examples in the field of biology are certainly pyrimidine and purine, which are the building blocks of the nucleobases, and thereby contained in the genes of every living organism. Widely distributed in nature are also the rings imidazole, pyrrolidine and indole, which are contained in the amino acids histidine, proline, and tryptophane, respectively, and the porphin ring system, which is the parent compound of porphyrins and thereby part of key biological dyes, such as the blood pigment heme or the green leaf pigment chlorophyll. Moreover, *N*-heterocycles are widely used for technical applications. Indigo dyes, which comprise the indole unit, and phthalocyanines are broadly utilized as dyes and pigments, and the *s*-triazine compound melamine is used for the preparation of melamine-formaldehyde resins. These colorless, isolating, and hard materials with high chemical

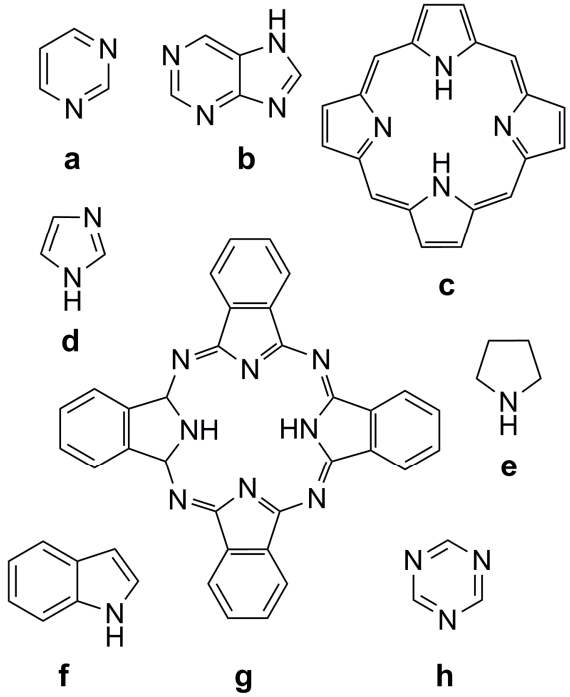

Scheme 1. *N*-heterocycles with significant importance for biology and technology, respectively. Pyrimidine (a), purine (b), porphin (c), imidazole (d), pyrrolidine (e), indole (f), phthalocyanine (g), and *s*-triazine (h).

stability and flame resistance are employed for numerous technical applications, e. g. in moldings and glues.[2]

The nitrogen-rich *s*-triazine C_3N_3 and *s*-heptazine C_6N_7 rings (see Scheme 2) are often regarded as special cases of *N*-heterocycles because they comprise neither C–C nor C–H bonds and therefore formally represent inorganic entities. However, strict differentiation between these inorganic cycles and organic *N*-heterocycles should be applied only cautiously considering their close structural similarity. In fact, *s*-triazine and *s*-heptazine based compounds are usually classified rather inconsistently as inorganic or organic materials depending on the respective point of view. This should be kept in mind when searching for literature or structural data of such compounds, which can be found both in organic and inorganic journals and databases. Nevertheless, a general distinction between hydrocarbons and such nitrogen-rich heterocycles can be meaningful in some cases, for instance if differences in chemical and thermal stability are of interest. High nitrogen contents often increase thermal and oxidative stability of aromatic compounds due to the relatively high bond dissociation energy of carbon nitrogen bonds and the relatively high electronegativity of nitrogen, which causes an enhancement of the oxidation number of carbon and therefore hampers facile oxidation of such compounds.[3] However, although the *s*-triazine and *s*-heptazine core can in general be regarded as examples of nitrogen-rich, symmetric *N*-heterocycles, there are cases where a distinct differentiation between those inorganic rings and organic *N*-heterocycles should be applied: Both the term “carbon nitride” and especially the formula “C_3N_4” refer to a binary compound comprising solely carbon and nitrogen and should therefore not be used to describe various kinds of often undefined materials which contain significant amounts of other elements such as hydrogen.

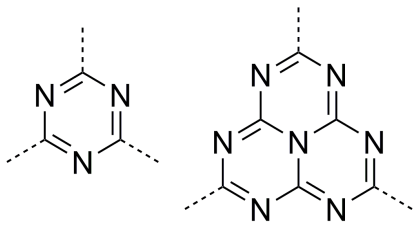

Scheme 2. Molecular structure of the carbon nitrogen rings *s*-triazine (left) and *s*-heptazine (right).

The binary phase C_3N_4 probably represents the carbon nitrogen material which material scientists dream about most. Initial reason for the quest for this compound was the assumption that three-dimensional, cubic C_3N_4 (*c*-C_3N_4) might exhibit material properties comparable to diamond such as high bulk and shear modulus, and high thermal conductivity as is suggested by theoretical calculations.[4] As suitable precursor for the synthesis of *c*-C_3N_4 the two-dimensional, graphite-like modification (*g*-C_3N_4) is considered because DFT calculations have predicted that a conversion of graphitic to cubic C_3N_4 might be possible under high-pressure conditions in analogy to the synthesis of

diamond from graphite.[5] Whereas for *c*-C_3N_4 a number of phases with sp^3-hybridization at the carbon atoms have been theoretically predicted, for *g*-C_3N_4 several structures based on the *s*-triazine and *s*-heptazine unit, respectively, have been proposed.[3,6] However, despite numerous attempts neither the cubic high-pressure modification nor layered C_3N_4 could be prepared without doubt so far,[3,6,7] and not only synthesis of crystalline C_3N_4 proved to be difficult but that of covalently bound C/N/H frameworks in general. Until now only for a couple of such networks preparation and structure elucidation has successfully been performed. *Horvath-Bordon* et al. reported on the first crystalline three-dimensional C/N/H network carbon nitride imide $C_2N_2(NH)$, which was synthesized under high-pressure conditions and crystallizes in a defect wurtzite structure-type analogous to that adopted by sinoite (Si_2N_2O).[8] Moreover, the crystalline two-dimensional networks poly(triazine imide) (PTI) and poly(heptazine imide) (PHI), built up of *s*-triazine and *s*-heptazine cores, respectively, interconnected via imide bridges, (see Scheme 3) were prepared by employing various techniques such as syntheses at moderate high-pressure conditions or reactions in salt melts.[9-11] Also the structure of polymeric melon $[C_6N_7(NH_2)(NH)]_x$, which consists of one-dimensional chains of *s*-heptazine rings interconnected by imide groups, could eventually be elucidated.[12,13] Moreover, by employing the hydrogen-free precursor cyanogen isocyanate C_2N_2O synthesis of an *s*-triazine based resin of composition C_3N_4 was reported recently but the poor crystallinity of product impeded complete structural characterization.[14]

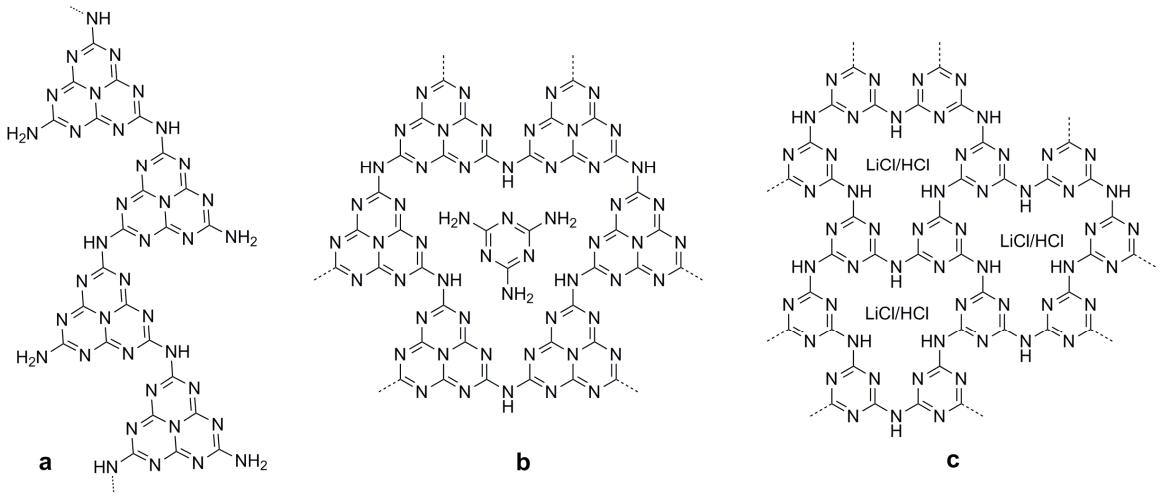

Scheme 3. Crystalline *s*-triazine and *s*-heptazine polymers: one-dimensional melon (a), two-dimensional poly(heptazine imide)·melamine (b) and two-dimensional poly(triazine imide)·LiCl/HCl (c).

For some time, increasing attention has additionally been drawn to C/N-rich polymers with often not exactly defined structures and compositions, which exhibit interesting properties making them valuable compounds for diverse applications.[15] Such materials have for instance been reported to be suitable catalysts for Friedel-Crafts reactions,[16] metal-free CO_2 activation,[17] or photochemical splitting of water.[18] Moreover, carbon nitride type nanoparticles and nano-, micro-, and mesoporous materials with high surface areas have been prepared by polymerization reactions in the presence of hard and soft templates[19] or by dynamic nitrile trimerization in salt melts.[20] However, it has to be noted that for none of these materials a thorough structural characterization has been performed and that elemental analysis – if reported – in general indicated the presence of hydrogen in these compounds. Probably such polymeric materials stated as "*g*-C_3N_4" in the literature actually have to be regarded rather as graphite- or melon-like compounds.[15]

Since the preparation of novel covalently linked *s*-triazine and *s*-heptazine networks with defined structure and composition has proven to be complicated it is indeed worthwhile to take also other kinds of chemical bonds more into account for this purpose. Due to their relatedness to both organic and inorganic compounds the *s*-triazine and *s*-heptazine ring represent borderline cases between different chemical disciplines and are found in various fields of modern chemistry. Especially, the *s*-triazine core is frequently employed as building block of coordinative and supramolecular materials. In contrast, for the *s*-heptazine ring until now only few examples of such compounds are known. Probable reason for this is the limited synthetic access to *s*-heptazine derivatives. The only *s*-heptazine compounds directly accessible by condensation of small molecular C/N/H precursors are melem $C_6N_7(NH_2)_3$[21] and melon $[C_6N_7(NH_2)(NH)]_x$.[12] Any other molecular *s*-heptazine materials are derived either from these starting materials or cyameluric acid $C_6N_7O_3H_3$,[22] which can easily be obtained by hydrolytic treatment of melem and melon. However, all these compounds exhibit poor solubility in common organic solvents making further conversions often difficult. In contrast, *s*-triazine derivatives are not only distinctly better soluble in numerous solvents, but can furthermore be obtained in large variety by facile trimerization of nitriles. However, dependent on their functional groups, also several *s*-triazine compounds exhibit only poor solubility in most solvents. A method which is frequently employed to enable chemistry of such materials in solution anyhow is to utilize salts of these compounds.[23-26] Definite division between molecular salts, coordination compounds, supramolecular materials, and covalently linked frameworks is not always possible but a general differentiation with respect to the nature of interactions which connect single building blocks in the respective materials can be applied. In general, chemical bonds are divided into interatomic and

intermolecular bonds, and for interatomic bonds it is further distinguished between compounds of first order (ionic, metal and covalent interactions) and compounds of higher order (coordinative interactions).[27] However, there is a gradual transition between different bond types, and the actual description of a bonding situation usually depends on the respective point of view. For instance, whereas scientists in the field of coordination chemistry classify coordinative bonds as special cases of interactions, such forces are rather considered as covalent bonds in solid-state chemistry. Therefore, the terms "molecular salts" and "coordination compounds" will be used in the following not in order to strictly classify bonding types but to emphasize the difference between materials in which *s*-triazine and *s*-heptazine cycles are interconnected via metal atoms, and polymers such as melon,[12] PTI[10] or PHI,[9] where these rings are interconnected via imide bridges.

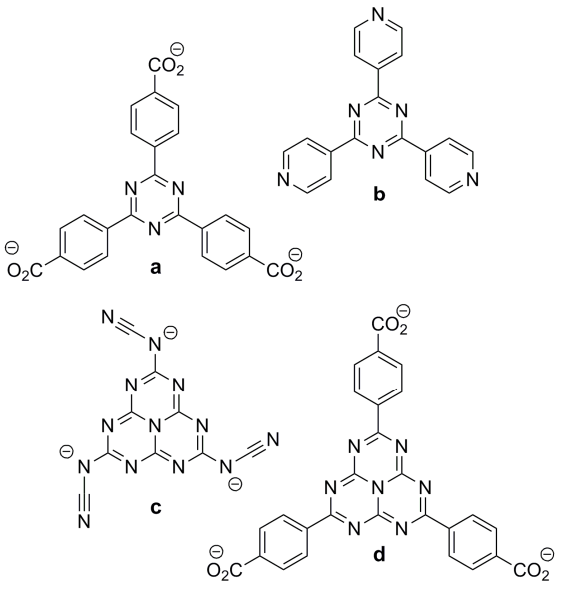

Scheme 4. Examples of ligands comprising the *s*-triazine or *s*-heptazine core: *s*-triazine tribenzoate (a), *s*-triazine-tris(4-pyridyl) (b), melonate (c), and *s*-heptazine tribenzoate (d).

For *s*-heptazine derivatives so far only few coordination frameworks are known, namely networks comprising either melonate anions $(C_6N_7(NCN)_3)^{3-}$ and Cu^{2+} or cyamelurate anions $(H_xC_6N_7O_3)^{(3-x)-}$ and Zn^{2+} or Cu^{2+} [26,28] as well as metal organic frameworks (MOFs) built up of *s*-heptazine tribenzoate and Cu^{2+} or Zn^{2+} (see Scheme 4).[29] In the cyamelurate and melonate based coordination networks a layered arrangement occurs[26,28] as is typically observed for *s*-heptazine compounds. Contrary, binding of three phenyl rings to the *s*-heptazine core in the above mentioned linker *s*-heptazine tribenzoate inhibits formation of a layered structure and enables construction of three-dimensional porous frameworks.[29] Combination of the carbon nitrogen cycle with further aromatic rings in order to obtain multidentate ligands with three-fold symmetry has not only been realized for *s*-heptazine tribenzoate, but also for several *s*-triazine based linkers. Examples for such molecules which are commonly employed as building blocks in MOFs are *s*-triazine tribenzoate[30] and *s*-triazine-tris(4-pyridyl).[31] Moreover, MOFs comprising similar ligands in which chains of two cycles are bound to the *s*-triazine core have been reported.[32] In addition to such linkers, which comprise *s*-triazine cores

combined with several further aromatic cycles, also ligands are known in which *s*-triazine represents the only ring system, for instance cyanuric acid,[33] tricyanomelaminates,[25] *s*-triazine tricarboxylate,[34] or *s*-triazine triyltrisglycine.[35]

Metal organic frameworks are utilized for various applications, for instance catalysis, ion exchange, separation, and gas storage.[36] They are usually prepared by the reaction of suitable ligands and lanthanide or transition metal salts in solution under solvothermal conditions. During this procedure, organic multidentate ligands coordinate the metal ions, and thereby assemble into a three-dimensional porous network. Similarly, in supramolecular structures molecular building units form a specific arrangement by self-assembly which is determined by the interplay of different types of weak noncovalent interactions, e. g. hydrogen bonds, dispersive, and hydrophobic interactions.[37,38] However, differentiation between coordinative and supramolecular structures is not clearly defined, because metal-to-ligand binding is sometimes classified as a separate kind of interaction, and sometimes as one type of noncovalent interactions. Especially pioneering work in the field of supramolecular chemistry, the "chemistry beyond the molecule" (*Lehn*),[39] mainly concerned systems comprising metal ions.[39,40] The concept of supramolecular chemistry plays a key role in biology for molecular recognition and structure formation, for instance in nucleic acids, proteins, and polysaccharides. In 1967, *Pedersen* applied this concept for the first time in synthetic chemistry with the synthesis of crown ethers,[41] which was followed by extensive investigations of host-guest-chemistry by *Lehn* and *Cram*. Eventually, in 1987 the Nobel Prize in Chemistry was awarded jointly to these three scientists "for their development and use of molecules with structure-specific interactions of high selectivity".[42] Among different types of noncovalent interactions in supramolecular assemblies the role of hydrogen bridges is often regarded to be of special importance. Although hydrogen bonds can formally just as well be described as weak covalent or strong dispersive bonds, dependent on their bonding strength, the special attention which is drawn to them can nevertheless be justified considering their enormous biological importance. Hydrogen bonds are not only essential for biological recognition and structure formation, but also responsible for the high melting point of water, which is an inevitable prerequisite for life processes in water. The exceptional role of hydrogen bonds in biology has, among others, in particular been highlighted by *Pauling*, who "believe[d] that […] it will be found that the significance of the hydrogen bond for physiology is greater than that of any other single structural feature".[43]

The role of hydrogen bridges for a specific supramolecular arrangement has also been investigated in detail for a prominent material comprising *s*-triazine units, the 1:1 adduct between cyanuric acid (CA)

and melamine (M).[44,45] In this compound the formation of numerous hydrogen bonds results in self-assembly of CA and M into rosette-like hexamers (see Scheme 5). *Whitesides* et al. have not only extensively studied the formation of a rosette-like structure, but have also developed methods for a directed construction of such motifs.[45] The correctly proposed structure of the CA·M adduct was eventually confirmed by *Rao* et al. who succeeded in obtaining single-crystals of CA·M and of a structurally related adduct of melamine and trithiocyanuric acid $C_3N_3S_3H_3$ under hydrothermal conditions.[46] Next to these adducts melamine also forms co-crystals with several other compounds, for instance with imides,[47] uracil,[48] boric acid,[49] or 4,4'-bipyridyl,[50] and additionally molecular salts comprising melaminium ions and various cyclic anions, such as aromatic carboxylates,[51] aromatic sulfonates,[52] or tricyanomelaminates[24] have been investigated. Contrary, recently reported adduct phases between melamine and melem[53,54] do not represent examples of molecular self-assembly in the classical sense because they are merely obtained as intermediates during thermal condensation of melamine, but not when respective amounts of melamine and melem are reacted.[54]

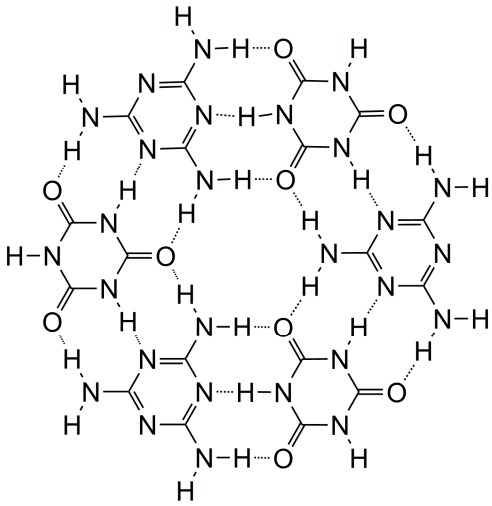

Scheme 5. Hydrogen-bonded rosettes formed between melamine and isocyanuric acid.

Despite countless publications in the field of supramolecular chemistry and plenty of structural data at hand prediction of crystal structures in supramolecular assemblies remains complicated, and the possibilities of chemists for directed construction of desired structures are rather limited – especially when compared to the amazing complexity of biological systems.[38] Therefore, the first step towards targeted synthesis of materials with specific structures, and ideally also desired properties, via crystal engineering, is a detailed investigation of bonding properties of respective building blocks. In an explorative approach, a comprehensive study of motifs for metal coordination, hydrogen bonds, and dispersive interactions contributes to a better understanding of the factors which influence a specific arrangement of building units in the crystal. Additionally, characterization of physical properties of obtained materials, e. g. thermal and chemical stability, allows to estimate under which conditions these compounds can be utilized as starting materials for coordination and supramolecular networks.

In this thesis, several *s*-triazine and *s*-heptazine derivatives, which have been investigated only rarely in this regard so far, are analyzed with respect to their suitability to be employed as building units in molecular salts, coordination compounds, and supramolecular networks. The role of diverse types of interactions on the assembly of molecular entities in the crystal is discussed, and thermal stability as well as selected further physical properties, such as luminescence properties or stability against hydrolysis, of these materials are investigated. Strength of different types of interactions and their relative impact on structural features is studied both by analysis of crystal data and DFT-calculations.

Bibliography

[1] For textbooks, see, for example: a) T. Eicher, S. Hauptmann, *The Chemistry of Heterocycles*; Georg Thieme Verlag: Stuttgart, New York, **1995**; b) J. A. Joule, K. Mills, *Heterocyclic Chemistry*; 4 ed.; Blackwell Publishing: Oxford, **2000**; c) L. D. Quin, J. A. Tyrell, *Fundamentals of heterocyclic chemistry*; John Wiley & Sons: Hoboken, New Jersey, **2010**.

[2] Importance of melamine-formaldehyde resins is illustrated by their annual production which reached $1.5 \cdot 10^6$ t in 2003. Melamine-based resins are the topic of many patents and described in several textbooks, e. g: a) J. Falbe, M. Regitz, (Eds.), *Römpp Chemie Lexikon*; 10 ed.; Georg Thieme Verlag: Stuttgart, New York, **1998**; b) W. Keim, (Ed.), *Kunststoffe - Synthese, Herstellungsverfahren, Apparaturen*; 1 ed.; Wiley-VCH: Weinheim, **2006**; c) K. Weissermel, H.-J. Arpe, *Industrielle Organische Chemie*; 3 ed.; VCH: Weinheim, Basel, **1988**.

[3] E. Kroke, M. Schwarz, *Coord. Chem. Rev.* **2004**, *248*, 493.

[4] a) M. L. Cohen, *Phys. Rev. B* **1985**, *32*, 7988; b) A. Y. Liu, M. L. Cohen, *Science* **1989**, *245*, 841; c) A. Y. Liu, M. L. Cohen, *Phys. Rev. B* **1990**, *41*, 10727.

[5] a) P. Kroll, R. Hoffmann, *J. Am. Chem. Soc.* **1999**, *121*, 4696; b) D. M. Teter, R. J. Hemley, *Science* **1996**, *271*, 53.

[6] G. Goglio, D. Foy, G. Demazeau, *Mater. Sci. Eng. R* **2008**, *58*, 195.

[7] A. Thomas, A. Fischer, F. Goettmann, M. Antonietti, J.-O. Müller, R. Schlögl, J. M. Carlsson, *J. Mater. Chem.* **2008**, *18*, 4893.

[8] E. Horvath-Bordon, R. Riedel, P. F. McMillan, P. Kroll, G. Miehe, P. A. v. Aken, A. Zerr, P. Hoppe, O. Shebanova, I. McLaren, S. Lauterbach, E. Kroke, R. Boehler, *Angew. Chem.* **2007**, *119*, 1498; *Angew. Chem. Int. Ed.* **2007**, *46*, 1476.

[9] M. Döblinger, B. V. Lotsch, J. Wack, J. Thun, J. Senker, W. Schnick, *Chem. Commun.* **2009**, 1541.

[10] E. Wirnhier, M. Döblinger, D. Gunzelmann, J. Senker, B. V. Lotsch, W. Schnick, *Chem. Eur. J.* **2011**, *17*, 3213.

[11] Z. Zhang, K. Leinenweber, M. Bauer, L. A. J. Garvie, P. F. McMillan, G. H. Wolf, *J. Am. Chem. Soc.* **2001**, *123*, 7788.

[12] B. V. Lotsch, M. Döblinger, J. Sehnert, L. Seyfarth, J. Senker, O. Oeckler, W. Schnick, *Chem. Eur. J.* **2007**, *13*, 4969.

[13] L. Seyfarth, J. Seyfarth, B. V. Lotsch, W. Schnick, J. Senker, *Phys. Chem. Chem. Phys.* **2010**, *12*, 2227.

[14] a) C. L. Schmidt, M. Jansen, *J. Mater. Chem.* **2010**, *20*, 4183; b) C. L. Schmidt, M. Jansen, *J. Mater. Chem.* **2010**, *20*, 110.

[15] Y. Wang, X. Wang, M. Antonietti, *Angew. Chem.* **2012**, *124*, 70; *Angew. Chem. Int. Ed.* **2012**, *51*, 68.

[16] a) F. Goettmann, A. Fischer, M. Antonietti, A. Thomas, *Angew. Chem.* **2006**, *118*, 4579; *Angew. Chem. Int. Ed.* **2006**, *45*, 4467; b) A. Vinu, *Adv. Funct. Mater.* **2008**, *18*, 816.

[17] F. Goettmann, A. Thomas, M. Antonietti, *Angew. Chem.* **2007**, *119*, 2773; *Angew. Chem. Int. Ed.* **2007**, *46*, 2717.

[18] a) X. Wang, K. Maeda, A. Thomas, K. Takanabe, G. Xin, J. M. Carlsson, K. Domen, M. Antonietti, *Nat. Mater.* **2009**, *8*, 76; b) J. Zhang, X. Chen, K. Takanabe, K. Maeda, K. Domen, J. D. Epping, X. Fu, M. Antonietti, X. Wang, *Angew. Chem.* **2010**, *122*, 451; *Angew. Chem. Int. Ed.* **2010**, *49*, 441; c) Y. J. Zhang, A. Thomas, M. Antonietti, X. C. Wang, *J. Am. Chem. Soc.* **2009**, *131*, 50; d) G. Liu, P. Niu, C. Sun, S. C. Smith, Z. Chen, G. Q. M. Lu, H.-M. Cheng, *J. Am. Chem. Soc.* **2010**, *132*, 11642.

[19] a) M. Groenewolt, M. Antonietti, *Adv. Mater.* **2005**, *17*, 1789; b) A. Vinu, K. Ariga, T. Mori, T. Nakanishi, S. Hishita, D. Goldberg, Y. Bando, *Adv. Mater.* **2005**, *17*, 1648; c) Y. Wang, X. Wang, M. Antonietti, Y. Zhang, *ChemSusChem* **2010**, *3*, 435.

[20] a) P. Kuhn, M. Antonietti, A. Thomas, *Angew. Chem.* **2008**, *120*, 3499; *Angew. Chem. Int. Ed.* **2008**, *47*, 3450; b) P. Kuhn, A. Forget, D. Su, A. Thomas, M. Antonietti, *J. Am. Chem. Soc.* **2008**, *130*, 13333; c) P. Kuhn, A. Thomas, M. Antonietti, *Macromolecules* **2009**, *42*, 319.

[21] a) B. Jürgens, E. Irran, J. Senker, P. Kroll, H. Müller, W. Schnick, *J. Am. Chem. Soc.* **2003**, *125*, 10288; b) A. Sattler, W. Schnick, *Z. Anorg. Allg. Chem.* **2006**, *632*, 238.

[22] a) A. Sattler, W. Schnick, *Z. Anorg. Allg. Chem.* **2006**, *632*, 1518; b) L. Seyfarth, J. Sehnert, N. E. A. El-Gamel, W. Milius, E. Kroke, J. Breu, J. Senker, *J. Mol. Struct.* **2008**, *889*, 217; c) J. Wagler, N. E. A. El-Gamel, E. Kroke, *Z. Naturforsch.* **2006**, *61b*, 975.

[23] a) A. Sattler, W. Schnick, *Eur. J. Inorg. Chem.* **2009**, 4972; b) A. Sattler, W. Schnick, *Z. Anorg. Allg. Chem.* **2008**, *634*, 457; c) A. Sattler, W. Schnick, *Z. Anorg. Allg. Chem.* **2010**, *636*, 2589; d) A. Sattler, S. Schönberger, W. Schnick, *Z. Anorg. Allg. Chem.* **2010**, *636*, 476; e) A. Sattler, L. Seyfarth, J. Senker, W. Schnick, *Z. Anorg. Allg. Chem.* **2005**, *631*, 2545; f) N. E. A. El-Gamel, L. Seyfarth, J. Wagler, H. Ehrenberg, M. Schwarz, J. Senker, E. Kroke, *Chem. Eur. J.* **2007**, *13*, 1158; g) N. E. A. El-Gamel, J. Wagler, E. Kroke, *J. Mol. Struct.* **2008**, *888*, 204; h) E. Horvath-Bordon, E. Kroke, I. Svoboda, H. Fueß, R. Riedel, S. Neeraj, A. K. Cheetham, *Dalton Trans.*

2004, 3900; i) A. Sattler, W. Schnick, *Z. Anorg. Allg. Chem.* **2006**, *632*, 531; j) A. Sattler, W. Schnick, *Z. Anorg. Allg. Chem.* **2008**, *634*, 1063; k) C. Clauss, J. Wagler, M. Schwarz, A. Schwarzer, E. Kroke, *Z. Anorg. Allg. Chem.* **2010**, *636*, 196; l) E. Horvath-Bordon, E. Kroke, I. Svoboda, H. Fuess, R. Riedel, *New J. Chem.* **2005**, *29*, 693; m) S. J. Makowski, D. Gunzelmann, J. Senker, W. Schnick, *Z. Anorg. Allg. Chem.* **2009**, *635*, 2434; n) S. J. Makowski, W. Schnick, *Z. Anorg. Allg. Chem.* **2009**, *635*, 2197.

[24] B. V. Lotsch, W. Schnick, *Chem. Mater.* **2006**, *18*, 1891.

[25] A. Nag, B. V. Lotsch, J. Schmedt a. d. Günne, O. Oeckler, P. J. Schmidt, W. Schnick, *Chem. Eur. J.* **2007**, *13*, 3512.

[26] A. Sattler, M. R. Budde, W. Schnick, *Z. Anorg. Allg. Chem.* **2009**, *635*, 1933.

[27] a) A. F. Holleman, E. Wiberg, N. Wiberg, *Lehrbuch der Anorganischen Chemie*; 102 ed.; Walter de Gruyter: Berlin, New York, **2007**; b) L. Pauling, *The nature of the chemical bond*; 2 ed.; Cornell University Press: Ithaca, New York, **1948**.

[28] C. Clauss, H. Schmidt, A. Schwarzer, E. Kroke, *Z. Anorg. Allg. Chem.* **2011**, *637*, 2246.

[29] a) Y. Ke, D. J. Collins, D. Sun, H.-C. Zhou, *Inorg. Chem.* **2006**, *45*, 1897; b) S. Ma, D. Sun, M. Ambrogio, J. A. Fillinger, S. Parkin, H.-C. Zhou, *J. Am. Chem. Soc.* **2007**, *129*, 1858.

[30] a) S. Ma, X.-S. Wang, E. S. Manis, C. D. Collier, H.-C. Zhou, *Inorg. Chem.* **2007**, *46*, 3432; b) S. Ma, X.-S. Wang, D. Yuan, H.-C. Zhou, *Angew. Chem.* **2008**, *120*, 4198; *Angew. Chem. Int. Ed.* **2008**, *47*, 4130; c) S. Ma, D. Yuan, X.-S. Wang, H.-C. Zhou, *Inorg. Chem.* **2009**, *48*, 2072; d) S. Ma, H.-C. Zhou, *J. Am. Chem. Soc.* **2006**, *128*, 11734; e) Y. K. Park, S. B. Choi, H. Kim, K. Kim, B.-H. Won, K. Choi, J.-S. Choi, W.-S. Ahn, N. Won, S. Kim, D. H. Jung, S.-H. Choi, G.-H. Kim, S.-S. Cha, Y. H. Jhon, J. K. Yang, J. Kim, *Angew. Chem.* **2007**, *119*, 8378; *Angew. Chem. Int. Ed.* **2007**, *46*, 8230; f) D. Sun, Y. Ke, D. J. Collins, G. A. Lorigan, H.-C. Zhou, *Inorg. Chem.* **2007**, *46*, 2725; g) D. Sun, S. Ma, Y. Ke, D. J. Collins, H.-C. Zhou, *J. Am. Chem. Soc.* **2006**, *128*, 3896; h) D. Sun, S. Ma, Y. Ke, T. M. Petersen, H.-C. Zhou, *Chem. Commun.* **2005**, 2663.

[31] a) J. P. Barrio, J.-N. Rebilly, B. Carter, D. Bradshaw, J. Bacsa, A. Y. Ganin, H. Park, A. Trewin, R. Vaidhyanathan, A. I. Cooper, J. E. Warren, M. J. Rosseinsky, *Chem. Eur. J.* **2008**, *14*, 4521; b) D. N. Dybtsev, H. Chun, K. Kim, *Chem. Commun.* **2004**, 1594; c) M.-X. Li, Z.-X. Miao, M. Shao, S.-W. Liang, S.-R. Zhu, *Inorg. Chem.* **2008**, *47*, 4481; d) W. Li, M.-X. Li, M. Shao, S.-R. Zhu, *Inorg. Chem. Commun.* **2007**, *10*, 753.

[32] a) Dincă, A. Dailly, C. Tsay, J. R. Long, *Inorg. Chem.* **2008**, *47*, 11; b) S.-Y. Wan, Y.-T. Huang, Y.-Z. Li, W.-Y. Sun, *Microporous Mesoporous Mater.* **2004**, *73*, 101.

[33] a) S. Aoki, M. Shiro, T. Koike, E. Kimura, *J. Am. Chem. Soc.* **2000**, *122*, 576; b) L. R. Falvello, M. A. Hitchman, F. Palacio, I. Pascual, A. J. Schultz, H. Stratemeier, M. Tomás, E. P.

Urriolabeitia, D. M. Young, *J. Am. Chem. Soc.* **1999**, *121*, 2808; c) L. R. Falvello, I. Pascual, M. Tomás, *Inorg. Chim. Acta* **1995**, *229*, 135; d) L. R. Falvello, I. Pascual, M. Tomás, E. P. Urriolabeitia, *J. Am. Chem. Soc.* **1997**, *119*, 11894; e) X.-C. Huang, W. Luo, Y.-F. Shen, X.-J. Lin, D. Li, *Chem. Commun.* **2008**, 3995; f) J. Server-Carrió, E. Escrivà, J.-V. Folgado, *Polyhedron* **1998**, *17*, 1495.

[34] J.-R. Galán-Mascarós, J.-M. Clemente-Juan, K. R. Dunbar, *J. Chem. Soc., Dalton Trans.* **2002**, 2710.

[35] S.-N. Wang, H. Xing, Y.-Z. Li, J. Bai, M. Scheer, Y. Pan, X.-Z. You, *Chem. Commun.* **2007**, 2293.

[36] a) A. U. Czaja, N. Trukhan, U. Müller, *Chem. Soc. Rev.* **2009**, *38*, 1284; b) R. J. Kuppler, D. J. Timmons, Q.-R. Fang, J.-R. Li, T. A. Makal, M. D. Young, D. Yuan, D. Zhao, W. Zhuang, H.-C. Zhou, *Coord. Chem. Rev.* **2009**, *253*, 3042.

[37] a) C. B. Aakeröy, N. R. Champness, C. Janiak, *CrystEngComm* **2010**, *12*, 22; b) M. M. Conn, J. Rebek Jr., *Chem. Rev.* **1997**, *97*, 1647; c) M. C. Etter, *J. Phys. Chem.* **1991**, *95*, 4601; d) D. S. Lawrence, T. Jiang, M. Levett, *Chem. Rev.* **1995**, *95*, 2229; e) J.-M. Lehn, *Angew. Chem.* **1990**, *102*, 1347; *Angew. Chem. Int. Ed. Engl.* **1990**, *29*, 1304; f) K. Merz, V. Vasylyeva, *CrystEngComm* **2010**, *12*, 3989; g) D. Philp, J. F. Stoddart, *Angew. Chem.* **1996**, *108*, 1242; *Angew. Chem. Int. Ed. Engl.* **1996**, *35*, 1154; h) L. J. Prins, D. N. Reinhoudt, P. Timmerman, *Angew. Chem.* **2001**, *113*, 2446; *Angew. Chem. Int. Ed.* **2001**, *40*, 2382; i) C. M. Reddy, G. R. Krishna, S. Ghosh, *CrystEngComm* **2010**, *12*, 2296; j) G. M. Whitesides, J. P. Mathias, C. T. Seto, *Science* **1991**, *254*, 1312; k) R. Custelcean, *Chem. Commun.* **2008**, 295.

[38] a) G. R. Desiraju, *Angew. Chem.* **2007**, *119*, 8492; *Angew. Chem. Int. Ed.* **2007**, *46*, 8342; b) M. C. T. Fyfe, J. F. Stoddart, *Acc. Chem. Res.* **1997**, *30*, 393.

[39] J.-M. Lehn, *Angew. Chem.* **1988**, *100*, 91; *Angew. Chem. Int. Ed. Engl.* **1988**, *27*, 89.

[40] a) D. J. Cram, *Angew. Chem.* **1988**, *100*, 1041; *Angew. Chem. Int. Ed. Engl.* **1988**, *27*, 1009; b) C. J. Pedersen, *Angew. Chem.* **1988**, *100*, 1053; *Angew. Chem. Int. Ed. Engl.* **1988**, *27*, 1021.

[41] C. J. Pedersen, *J. Am. Chem. Soc.* **1967**, *89*, 7017.

[42] http://www.nobelprize.org/nobel_prizes/chemistry/laureates/1987/, **accessed 06.02.2012**.

[43] L. Pauling, *The nature of the chemical bond*; 2 ed.; Cornell University Press: Ithaca, New York, **1948**, p. 285.

[44] a) I. S. Choi, X. Li, E. E. Simanek, R. Akaba, G. M. Whitesides, *Chem. Mater.* **1999**, *11*, 684; b) X. Li, D. N. Chin, G. M. Whitesides, *J. Org. Chem.* **1996**, *61*, 1779; c) J. P. Mathias, E. E. Simanek, C. T. Seto, G. M. Whitesides, *Angew. Chem.* **1993**, *105*, 1848; *Angew. Chem. Int. Ed. Engl.* **1993**, *32*, 1766; d) C. T. Seto, J. P. Mathias, G. M. Whitesides, *J. Am. Chem. Soc.* **1993**,

115, 1321; e) C. T. Seto, G. M. Whitesides, *J. Am. Chem. Soc.* **1990**, *112*, 6409; f) C. T. Seto, G. M. Whitesides, *J. Am. Chem. Soc.* **1991**, *113*, 712.

[45] a) G. M. Whitesides, E. E. Simanek, J. P. Mathias, C. T. Seto, D. N. Chin, M. Mammen, D. M. Gordon, *Acc. Chem. Res.* **1995**, *28*, 37; b) J. P. Mathias, C. T. Seto, E. E. Simanek, G. M. Whitesides, *J. Am. Chem. Soc.* **1994**, *116*, 1725; c) C. T. Seto, G. M. Whitesides, *J. Am. Chem. Soc.* **1993**, *115*, 905; d) J. P. Mathias, E. E. Simanek, J. A. Zerkowski, C. T. Seto, G. M. Whitesides, *J. Am. Chem. Soc.* **1994**, *116*, 4316.

[46] A. Ranganathan, V. R. Pedireddi, C. N. R. Rao, *J. Am. Chem. Soc.* **1999**, *121*, 1752.

[47] a) J. Hamblin, S. P. Argent, A. J. Blake, C. Wilson, N. R. Champness, *CrystEngComm* **2008**, *10*, 1782; b) R. F. M. Lange, F. H. Beijer, R. P. Sijbesma, R. W. W. Hooft, H. Kooijman, A. L. Spek, J. Kroon, E. W. Meijer, *Angew. Chem.* **1997**, *109*, 1006; *Angew. Chem. Int. Ed. Engl.* **1997**, *36*, 969; c) G. J. Perpétuo, J. Janczak, *Acta Crystallogr., Sect. C* **2007**, *63*, o301; d) H. Tukada, Y. Mazaki, *Chem. Lett.* **1997**, 441.

[48] R. Thomas, G. U. Kulkarni, *Beilstein J. Org. Chem.* **2007**, *17*, doi:10.1186/1860-5397-3-17.

[49] A. Roy, A. Choudhury, C. N. R. Rao, *J. Mol. Struct.* **2002**, *613*, 61.

[50] K. Sivashankar, A. Ranganathan, V. R. Pedireddi, C. N. R. Rao, *J. Mol. Struct.* **2001**, *559*, 41.

[51] a) G. J. Perpétuo, J. Janczak, *J. Mol. Struct.* **2008**, *891*, 429; b) X.-L. Zhang, X.-M. Chen, *Cryst. Growth Des.* **2005**, *5*, 617.

[52] a) J. Janczak, G. J. Perpétuo, *Acta Crystallogr., Sect. C* **2008**, *64*, o91; b) A. N. Lazar, O. Danylyuk, K. Suwinska, A. W. Coleman, *New J. Chem.* **2006**, *30*, 59.

[53] B. V. Lotsch, W. Schnick, *Chem. Eur. J.* **2007**, *13*, 4956.

[54] A. Sattler, S. Pagano, M. Zeuner, A. Zurawski, D. Gunzelmann, J. Senker, K. Müller-Buschbaum, W. Schnick, *Chem. Eur. J.* **2009**, *15*, 13161.

2. Summary

In this thesis various possibilities to employ *s*-triazine and *s*-heptazine compounds as building blocks in novel materials are presented. Different molecular *s*-triazine and *s*-heptazine derivatives have been utilized as building units in molecular salts, coordination and supramolecular compounds. Special attention has been paid to increased employment of *s*-heptazine derivatives and of molecules which can be classified as intermediates between inorganic carbon nitride type compounds and hydrocarbons. In the obtained materials different types of interactions except for covalent bonds determine specific assemblies of components in the crystal. Detailed analysis of impact and mutual influence of diverse types of noncovalent forces on the arrangement of molecular entities has been performed in order to gain a deeper understanding of these interactions, which will hopefully facilitate more directed syntheses of such materials in the future. Structural characterization has been complemented by analysis of chemical and thermal stability, and thereby the suitability of investigated compounds to be employed as building blocks in novel materials could be evaluated.

2.1 Coordination Compounds and Molecular Salts

Rare-Earth Melonates

(chapter 3, published in *Eur. J. Inorg. Chem.* **2012**, 1832)

Coordination frameworks comprising melonate units $(C_6N_7(NCN)_3)^{3-}$ (see Scheme 6) and trivalent lanthanide ions have been prepared and comprehensively characterized as is described in chapter 3. The obtained materials represent novel examples of *s*-heptazine derivatives with trivalent cations and complement preceding studies of Ln^{3+} tricyanomelaminates and dicyanamides. A series of rare-earth melonates $LnC_6N_7(NCN)_3{\cdot}xH_2O$ (*Ln* = La, Ce, Pr, Nd, Sm, Eu, Tb and *x* = 8-12) has been synthesized by metathesis reactions in aqueous solution. The crystal structure of $LaC_6N_7(NCN)_3{\cdot}8H_2O$ has been solved and refined from single-crystal diffraction data (*C*2, *a* = 1666.2(3), *b* = 669.04(13), *c* = 1751.0(4) pm, β = 108.74(3)°, *V* = 1848.4(6)·10^6 pm^3, *Z* = 4) and structures of isostructural $LnC_6N_7(NCN)_3{\cdot}8H_2O$ (*Ln* = Ce, Pr, Nd, Sm) from powder X-ray diffraction data by Rietveld refinement. In the crystal, melonate units and rare-earth ions form one-dimensional strands which are arranged in corrugated layers (see Figure 1). During syntheses at ambient conditions La and Ce melonate adopt this structure instantaneously, whereas Pr and Nd melonate transform into it only after several days of aging at room temperature. DTA/TG studies and elemental analysis have indicated this transformation to be induced by partial release of crystal water. Alternatively, $LnC_6N_7(NCN)_3{\cdot}8H_2O$ (*Ln* = Pr, Nd, Sm) could

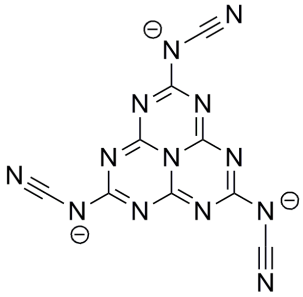

Scheme 6. Molecular structure of melonate.

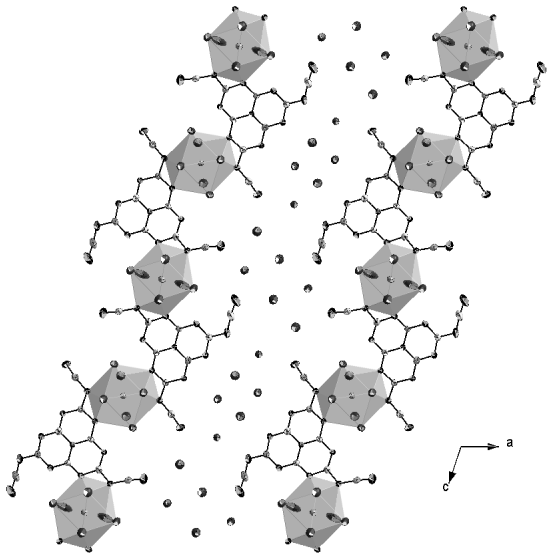

Figure 1. Representation of a single layer in $LaC_6N_7(NCN)_3{\cdot}8H_2O$, illustrating the arrangement of melonate units and La^{3+} in strands along *c* and the localization of crystal water between these strands.

be obtained directly by gradually increasing synthesis temperatures up to hydrothermal conditions. TG/DTA measurements have revealed low thermal stability of rare-earth melonates in comparison to alkali melonates. This might be attributed to the high oxygen affinity of rare-earth metals impeding complete dehydration during heating and consequently potential hydrolysis at elevated temperatures. Whereas Eu melonate does not exhibit luminescence under UV excitation, photoluminescence studies of Tb^{3+} melonate have shown green emission with a maximum at 545 nm due to the $^5D_4 \rightarrow {}^7F_5$ transition.

Alkali and Alkaline Earth Triazine Tricarboxylates

(chapter 4, published in a) *Z. Anorg. Allg. Chem.* **2010**, *636*, 2584; b) *Z. Anorg. Allg. Chem.* **2011**, *637*, 2142; c) *Z. Anorg. Allg. Chem.* **2012**, *638*, 345)

Due to the structural similarity of triazine tricarboxylate (TTC) $(C_3N_3(CO_2)_3)^{3-}$ (see Scheme 7) with benzene tricarboxylate, a compound that is commonly employed as linker in metal organic frameworks, TTC appears to be a suitable linker in coordination networks. In order to gain a better understanding of coordination and thermal properties of triazine tricarboxylates various alkali and alkaline earth salts have been prepared and characterized by means of single-crystal X-ray diffraction, FTIR spectroscopy, and TG/DTA measurements.

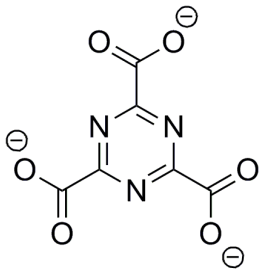

Scheme 7. Molecular structure of triazine tricarboxylate.

Alkali triazine tricarboxylates $Li_3[C_3N_3(CO_2)_3]\cdot 4H_2O$ ($P\bar{1}$, a = 655.10(13), b = 939.84(19), c = 1025.2(2) pm, α = 102.81(3), β = 106.56(3), γ = 91.38(3)°, V = 587.4(2)·10^6 pm^3, Z = 2), $K_3[C_3N_3(CO_2)_3]\cdot 2H_2O$ ($P\bar{1}$, a = 696.63(14), b = 1748.5(3), c = 1756.0(3) pm, α = 119.73(3), β = 91.96(3), γ = 93.84(3)°, V = 1847.6(6)·10^6 pm^3, Z = 6), $Rb_3[C_3N_3(CO_2)_3]\cdot 2H_2O$ ($P2_1/n$, a = 1038.1(2), b = 687.44(14), c = 1807.9(4) pm, β = 92.47(3)°, V = 1289.0(5)·10^6 pm^3, Z = 4), and $Cs_3[C_3N_3(CO_2)_3]\cdot 2H_2O$ (*Cmcm*, a = 2043.3(4), b = 967.51(19), c = 726.54(15) pm, V = 1436.3(5)·10^6 pm^3, Z = 4) have been synthesized by saponification of the respective triethyl ester, and alkaline earth triazine tricarboxylates $Sr_3[C_3N_3(CO_2)_3]_2\cdot 12H_2O$ ($P2_1$/n, a = 1005.4(2), b = 1302.7(3), c = 2107.2(4) pm, β = 97.36(3)°, V = 2737.1(10)·10^6 pm^3, Z = 4) and $Ba_3[C_3N_3(CO_2)_3]_2\cdot 12H_2O$ ($P2_1$/n, a = 1020.9(2), b = 1337.4(3), c = 2139.5(4) pm, β = 95.71(3)°, V = 2906.6(10)·10^6 pm^3, Z = 4) by metathesis

reactions. In the crystal structures, TTC units are arranged in layers with varying degrees of stacking interaction between the layers dependent on the metal ion (see Figure 2). Binding to metal ions via two adjacent carboxylate groups and the intermediate nitrogen atom of the triazine ring has been observed as recurring motif. Alkali triazine tricarboxylates exhibit comparable thermal stability up to 350 °C. Heating above this temperature causes cleavage of the triazine ring for K, Rb and Cs triazine tricarboxylate, but not for Li triazine tricarboxylate. This might be due to more covalent interaction of Li^+ ions.

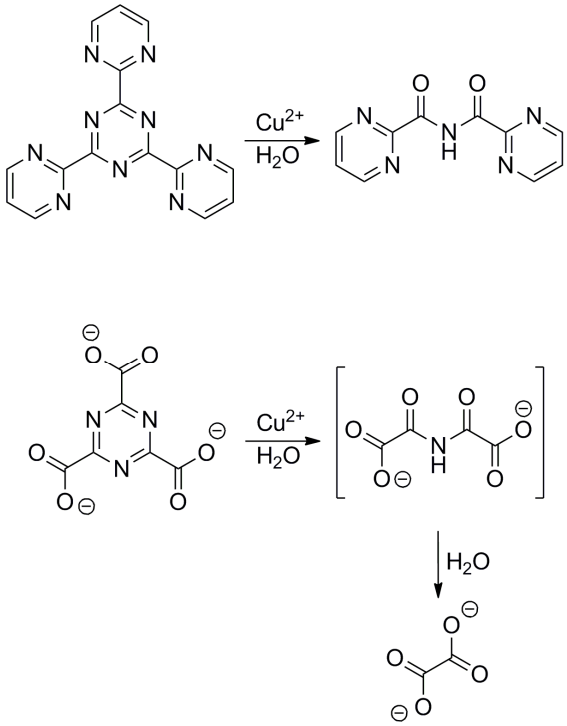

Scheme 8. Hydrolysis of triazine tris(2-pyrimidyl) to bis(2-pyrimidylcarbonyl)amine (top) and of triazine tricarboxylate to oxalate (bottom).

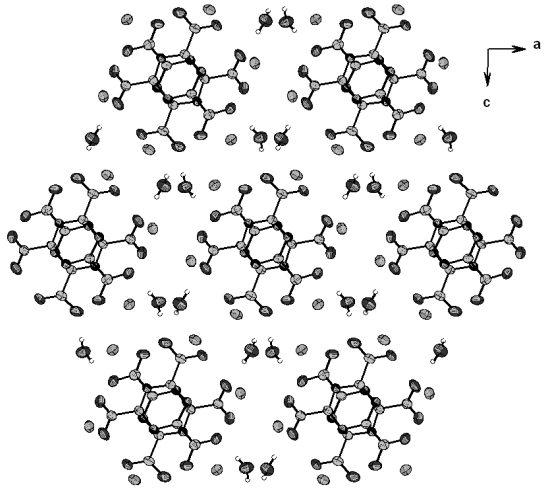

Figure 2. Crystal structure of $Rb_3[C_3N_3(CO_2)_3]\cdot 2H_2O$, representing stacking beween the triazine cores and the hexagonal arrangement of triazine tricarboxylate columns.

Furthermore, stability of TTC in aqueous solutions of Mn^{2+}, Fe^{2+}, Co^{2+}, Ni^{2+}, Cu^{2+} and Zn^{2+} salts has been investigated by means of X-ray diffraction and FTIR spectroscopy. In the presence of most divalent transition metal ions TTC showed tendency towards hydrolysis yielding oxalate. Hydrolysis of TTC can be explained as a result of ring tension which is caused by the coordination of transition metal ions in analogy to the hydrolysis of triazine tris(2-pyrimidyl) (see Scheme 8). TTC is stable in aqueous solutions of Mn^{2+} and Fe^{2+} salts, whereas decreasing ionic radii and consequently decreasing *M*–O and *M*–N distances for Co^{2+}, Ni^{2+}, Cu^{2+} and Zn^{2+} cause intensified ring tension and therefore hydrolysis. Comparison of TTC and triazine tris(2-pyrimidyl) not only allows for an explanation of the

facile hydrolysis of TTC, but also enables the development of strategies for the synthesis of novel TTC coordination networks. Hydrolysis might be avoided by using large metal ions, adding a second, strongly coordinating ligand, or performing syntheses under anhydrous conditions, e. g. in suitable ionic liquids.

Cocrystals of Alkali Triazine Tricarboxylates and Cyanuric Acid

(chapter 5, published in *Z. Anorg. Allg. Chem.* **2011**, *638*, 88)

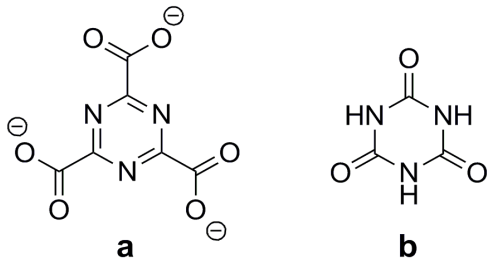

Scheme 9. Molecular structure of triazine tricarboxylate (a) and isocyanuric acid (b).

In order to obtain materials in which the relative influence of different types of interactions on the arrangement of molecular building blocks in the crystal can be studied two different *s*-triazine compounds, namely alkali triazine tricarboxylates and cyanuric acid (see Scheme 9), have been combined to cocrystals. Investigating the reactivity of cyanuric acid $C_3N_3O_3H_3$ towards alkali triazine tricarboxylates $M_3[C_3N_3(CO_2)_3]\cdot xH_2O$ (M = Li, Na, K, Rb, Cs) has revealed that the degree of ion transfer from triazine tricarboxylate to cyanuric acid increases gradually from the Li to Cs salt. This observation can be explained with the HSAB concept and reflects an increasing basicity from Li triazine tricarboxylate to Cs triazine tricarboxylate. The novel cocrystals $M_3[C_3N_3(CO_2)_3][C_3N_3O_3H_3]\cdot H_2O$ (M = K, Rb) have been synthesized this way in aqueous solution at room temperature and analyzed by means of single-crystal X-ray diffraction and thermal analysis. In the crystal structures of $K_3[C_3N_3(CO_2)_3][C_3N_3O_3H_3]\cdot H_2O$ ($P\bar{1}$, a = 709.66(14), b = 964.97(19), c = 1279.1(3) pm, α = 75.83(3), β = 75.38(3), γ = 70.88(3)°, V = 788.1(3)·10^6 pm^3, Z = 2) and $Rb_3[C_3N_3(CO_2)_3][C_3N_3O_3H_3]\cdot H_2O$ ($P2_1/c$, a = 720.01(14), b = 3756.4(8), c = 1256.9(3) pm, β = 101.81(3)°, V = 3327.5(11)·10^6 pm^3, Z = 4) *s*-triazine entities are interconnected by hydrogen bridges to zigzag strands. These strands alternate with corrugated bands of alkali ions forming a layered structure. Next to hydrogen bonds between *s*-triazine units, hydrogen bonds between *s*-triazine entities and crystal water (see Figure 3), and Coulomb interactions between *s*-triazine entities and metal ions also dispersive interactions between *s*-triazine rings occur. However, strength of these dispersive forces has shown to be rather weak in comparison to hydrogen bridges and Coulomb interactions.

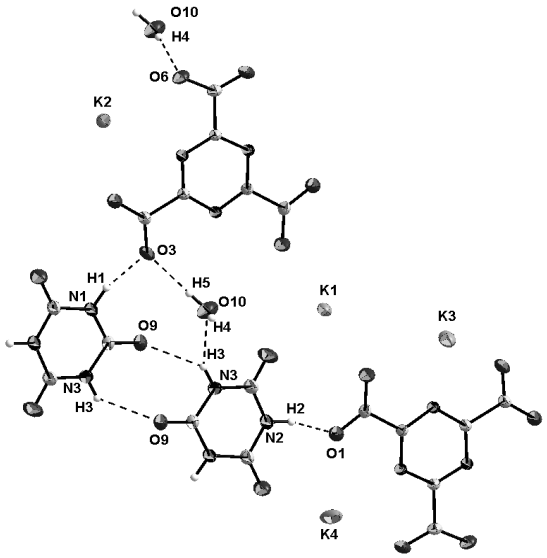

Figure 3. Hydrogen bonding interactions in $K_3[C_3N_3(CO_2)_3][C_3N_3O_3H_3]\cdot H_2O$.

2.2 Supramolecular Assemblies

Melem Hydrate

(chapter 6, published in *Chem. Eur. J.* **2012**, *18*, 3248)

The existence of melem hydrate, which is obtained by treatment of melem $C_6N_7(NH_2)_3$ in boiling water, has been known for some time. As is described in chapter 6, in this work single-crystals of melem hydrate have been obtained by reacting an aqueous suspension of melem under elevated temperature and pressure in an autoclave, and its crystal structure has been elucidated ($R\,\bar{3}c$, a = 2879.0(4), c = 664.01(13) pm, V = 4766.4(13)·10^6 pm^3, Z = 18). Self-assembly of melem units in boiling water leads to the formation of a hydrogen-bonded, hexagonal channel structure (see Figure 4) reminiscent of that of the well known adduct between melamine and cyanuric acid. Due to this

similarity a potential hydrolysis of melem to cyameluric acid has been suspected and could be ruled out by means of solid-state NMR spectroscopy, elemental analysis and mass spectrometry.

In the crystal structure, melem units form hexagonal channels which are filled with crystal water molecules, and perpendicular to the direction of channels melem units are arranged in corrugated layers. Hydrogen bonds interconnect melem units both within and between the layers and are additionally formed between melem and water molecules. Thermal analysis has revealed differing bonding strengths of hydrogen bridges in the structure. Whereas crystal water molecules can be removed from the channels by heating under vacuum, the hexagonal, layered arrangement of melem units is retained even in the dehydrated material. However, withdrawal of water molecules from the structure presumably causes shifting of melem layers perpendicular to the direction of channels, thereby blocking the channels and making them inaccessible for guest molecules.

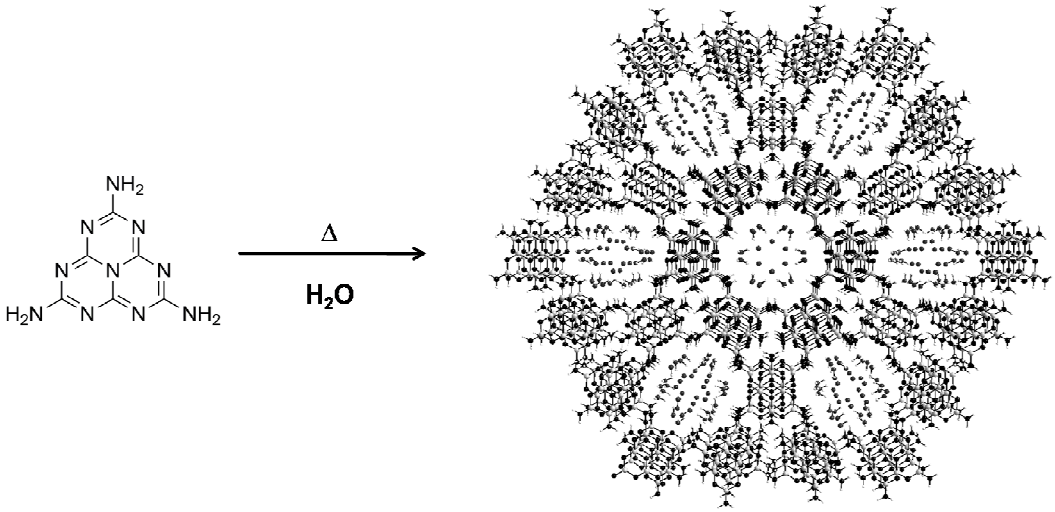

Figure 4. Self-assembly of melem into hydrogen-bonded, hexagonal channels.

Cocrystals of Melamine and *N*-Heterocycles

(chapter 7, published in *J. Mol. Struct.* **2012**, *1013*, 19
chapter 8, unpublished results)

Hydrogen-bonded cocrystals of melamine $C_3N_3(NH_2)_3$ and *N*-heterocycles (see Scheme 10) have been prepared under solvent-free conditions and in aqueous solution. In the obtained 4:3 adduct of melamine and tris(2-pyridyl)-triazine (TPTZ) and the 3:1 adduct of melamine and tetrakis(4-*N*-methylpyridinumyl)porphyrin tetratosylate (TMPyP-Tos) similar structural motifs occur. Both in 4M·3TPTZ (*C*2/*c*, a = 4927.6(10), b = 1212.3(2), c = 2301.6(5) pm, β = 100.85(3)°, V = 13503(5)·10^6 pm^3, Z = 8) and 3M·TMPyP-Tos·9H_2O ($P\bar{1}$, a = 1045.2(2), b = 1462.8(3), c = 1573.6(3) pm, α = 83.26(3), β = 80.34(3), γ = 76.03(3)°, V = 2294.2(8)·10^6 pm^3, Z = 1) *N*-heterocycles are arranged in π-π stacks and melamine molecules are arranged perpendicular to these stacks. This way melamine units are located most suitable as donors and acceptors, respectively, for formation of hydrogen bonds. Next to classical N–H···N, N–H···O, and N–H···S interactions also several nonconventional hydrogen bridges involving C–H donors are present in both adducts. Apart from such nonconventional hydrogen bonds charged porphyrin rings are primarily bound by electrostatic forces. Dispersive interactions between the aromatic rings of *N*-heterocycles have been analyzed with respect to distances and angles between those rings, showing arrangements as typically observed between nitrogen-containing aromatic systems. Thermal analysis of both cocrystals has revealed that noncovalent interactions between components are present even at elevated temperatures.

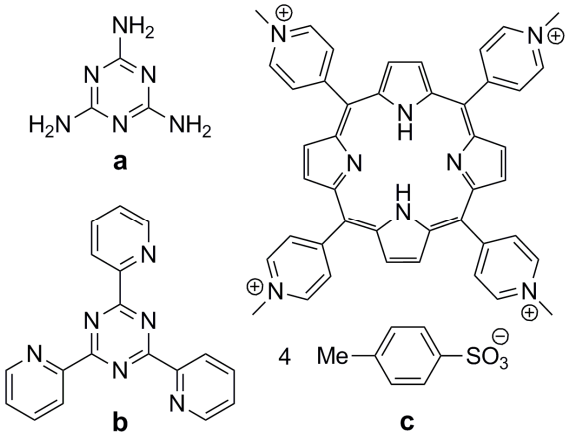

Scheme 10. Molecular structures of a) melamine, b) TPTZ and c) TMPyP-Tos.

Furthermore, the role of dispersive interactions in the adduct phase 4M·3TPTZ in comparison to 2,4,6-tris(2-pyridyl)-1,3,5-triazine (2-TPTZ), 2,4,6-tris(3-pyridyl)-1,3,5-triazine (3-TPTZ), and melamine has been investigated theoretically by density functional theory including dispersion corrections (DFT-D3). Twenty-six smaller complexes from the crystal structures of these compounds were chosen as model systems and noncovalent interactions in these complexes were studied. The applied density functionals were two GGAs (BLYP-D3, PBE-D3), one meta GGA (TPSS-D3) and the

recently proposed double-hybrid density functional PWPB95-D3. A very good agreement for structures obtained from crystal data and structures optimized by using periodic boundary conditions was achieved. For 4M·3TPTZ, 2-TPTZ and 3-TPTZ dispersion interactions in different TPTZ dimers with a varying number of stacked pyridinyl moieties were calculated, and for melamine interactions were calculated both for a π-stacked and a hydrogen bonded dimer. Additionally, for 2-TPTZ and 3-TPTZ the effect of neighboring molecules was studied using PBE-D3 with periodic boundary conditions. For TPTZ units dispersive interactions amount for 40-45 % of the total crystallization energy per molecule, whereas these interactions appeared to be less important between melamine units and between melamine and TPTZ. A contribution to the complexation energy of approximately 4.5 kcal·mol^{-1} for each pair of stacked pyridinyl rings and of approximately 2.4 kcal·mol^{-1} for stacked triazine cores was computed. Consistently, interaction energies of -15.8 kcal·mol^{-1} for 3-TPTZ dimers in which all pyridinyl and triazine rings are stacked, and of -10.5 kcal·mol^{-1} for 2-TPTZ dimers with two stacked pyridinyl units, were calculated. The results indicate that interaction between TPTZ moieties is mainly determined by dispersive forces, whereas these forces are distinctly weaker for interactions between melamine moieties and between melamine and TPTZ. These findings are in good agreement with the results obtained from analysis of single-crystal data.

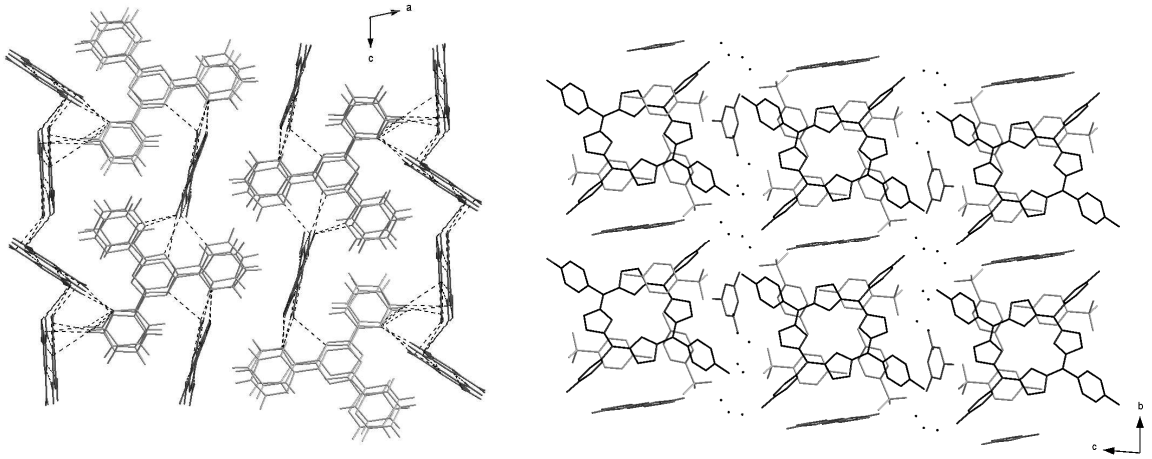

Figure 5. Crystal structures of 4M·3TPTZ (left) and 3M·TMPyP-Tos·9H_2O (right), viewed parallel to the direction of TPTZ and TMPyP stacks, respectively.

3. Rare-Earth Melonates

Melonates $(C_6N_7(NCN)_3)^{3-}$ provide multiple coordination sites and therefore represent suitable ligands for coordination networks. Preceding studies of several alkali and alkaline earth melonates have shown that nitrogen atoms of both *s*-heptazine core and cyanamide side chains contribute to metal coordination. Whereas prior to this work a couple of melonates with mono- and divalent cations have been investigated, no structurally fully characterized melonates with trivalent cations were known so far. In this regard especially lanthanide compounds are of particular interest because Eu^{3+} and Tb^{3+} dicyanamides and tricyanomelaminates have been reported to exhibit photoluminescence under UV excitation. Dicyanamides $(N(CN)_2)^-$, tricyanomelaminates $(C_3N_3(NCN)_3)^{3-}$, and melonates are structurally related, with tricyanomelaminate being the trimerization product of dicyanamide, and melonate representing the *s*-heptazine analog of *s*-triazine based tricyanomelaminate. In this chapter, synthesis, crystal structure, thermal behavior, and luminescence properties of a series of melonates with trivalent rare-earth ions are presented.

Rare-Earth Melonates $LnC_6N_7(NCN)_3 \cdot xH_2O$ (Ln = La, Ce, Pr, Nd, Sm, Eu, Tb; *x* = 8-12): Synthesis, Crystal Structures, Thermal Behavior, and Photoluminescence Properties of Heptazine Salts with Trivalent Cations

Sophia J. Makowski, Arne Schwarze, Peter J. Schmidt, and Wolfgang Schnick

published in: *Eur. J. Inorg. Chem.* **2012**, 1832. DOI: 10.1002/ejic.201101251

Keywords: Lanthanides; Rare earths; Luminescence

Abstract. The rare-earth melonates $LnC_6N_7(NCN)_3 \cdot xH_2O$ (Ln = La, Ce, Pr, Nd, Sm, Eu, Tb; x = 8-12) have been synthesized by metathesis reactions in aqueous solution and characterized by single-crystal and powder XRD, FTIR spectroscopy, thermal analysis, and photoluminescence studies. Powder XRD patterns revealed isotypism of the La–Sm compounds. The structure of $LaC_6N_7(NCN)_3 \cdot 8H_2O$ has been solved and refined from single-crystal diffraction data and those of the remaining salts have been refined from powder XRD data by Rietveld refinement. In the crystal structures, the melonate entities are arranged in corrugated layers, which alternate with layers of crystal water molecules. The lanthanide ions are coordinated by two melonate and six water molecules. $LnC_6N_7(NCN)_3 \cdot xH_2O$ (Ln = Eu, Tb; *x* = 9-12) have also been investigated by photoluminescence studies. Neither hydrated nor dehydrated europium melonate exhibits luminescence under UV excitation, whereas photoluminescence studies of terbium melonate showed green emission with a maximum at 545 nm due to the $^5D_4 \rightarrow {}^7F_5$ transition. Thermal analysis revealed rather low thermal stability of the rare-earth melonates, which is probably due to the tight binding of crystal water that results in hydrolytic decomposition at elevated temperatures.

3.1 Introduction

Molecular and polymeric carbon nitride-type compounds have been extensively studied in recent years, primarily targeting the synthesis of binary C_3N_4 but increasingly with respect to their properties and possible applications.[1] High thermal and oxidation stability as well as semiconducting and catalytic properties make these compounds promising materials to be employed for various technical purposes.[2] Therefore, numerous ternary and quaternary molecular compounds have been synthesized, thoroughly characterized, and employed as starting materials for the preparation of polymeric carbon nitride-type compounds, e.g. substituted *s*-triazines (C_3N_3), such as melamine, cyanuric acid, or cyanuric chloride, and *s*-heptazines (C_6N_7), such as melem, cyameluric acid, or cyameluric chloride (Scheme 1). Furthermore, various salts of anions that contain only carbon and nitrogen in an alternating arrangement have been investigated in this regard. Examples are cyanides $(CN)^-$, cyanamides or carbodiimides $(NCN)^{2-}$, dicyanamides $(N(CN)_2)^-$,[3-5] tricyanomelaminates $(C_3N_3(NCN)_3)^{3-}$,[4,6-9] and melonates $(C_6N_7(NCN)_3)^{3-}$ [10-14] (Scheme 2).

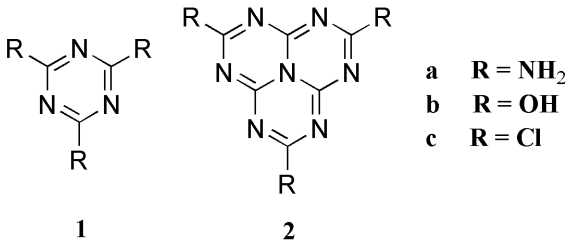

Scheme 1. *s*-Triazine derivatives melamine (**1a**), cyanuric acid (**1b**), and cyanuric chloride (**1c**) and *s*-heptazines melem (**2a**), cyameluric acid (**2b**), and cyameluric chloride (**2c**).

In addition to the structural characterization of a number of these salts, their physical properties and thermal behavior have been investigated. It has been shown that dicyanamides undergo trimerization to the respective tricyanomelaminates under molten conditions[4,7] and nonmetal dicyanamides and tricyanomelaminates transform into *s*-heptazine-based polymeric structures on heating.[8,15] Moreover, photoluminescence studies of dicyanamides and tricyanomelaminates with trivalent rare-earth cations have revealed the red and green luminescence of Eu^{III} and Tb^{III} salts, respectively.[5,9] This luminescence was assigned to $^5D_0 \rightarrow {}^7F_{0\text{-}4}$ transitions with an emission maximum at 615 nm ($^5D_0 \rightarrow {}^7F_2$) for the Eu^{III} compounds and to $^5D_4 \rightarrow {}^7F_{3\text{-}6}$ transitions with an emission maximum at 545 nm ($^5D_4 \rightarrow {}^7F_5$) for the Tb^{III} salts. Furthermore, the potential development of phosphors based on rare-earth dicyanamides and tricyanomelaminates with trivalent cations for applications in light emitting diodes has been discussed.[5,9]

Conversely, no fully structurally characterized *s*-heptazine salts with trivalent cations are known to date. Although several cyamelurates and melonates with trivalent cations have been mentioned in the literature, especially as precursors for the synthesis of functional materials, such as flame retardants or carbon-based nanoparticles,[16] a detailed structural characterization was not reported for any of these compounds. Such materials are usually prepared by metathesis reactions in aqueous solution from the respective alkali salts. Due to the poor solubility of *s*-heptazine salts with multivalent cations, crystalline materials are not easily obtained during this procedure, which is probably reason for the small number of structurally characterized *s*-heptazines with multivalent cations. To date, the crystal structures have been elucidated only for a few examples with divalent cations, namely, calcium, copper, and zinc cyamelurates[17] and calcium and copper melonates.[10,13] In these compounds, sufficient solubility for the growth of single-crystals from solution was achieved by protonation of the *s*-heptazine rings or the addition of ammonia or ethylenediamine.

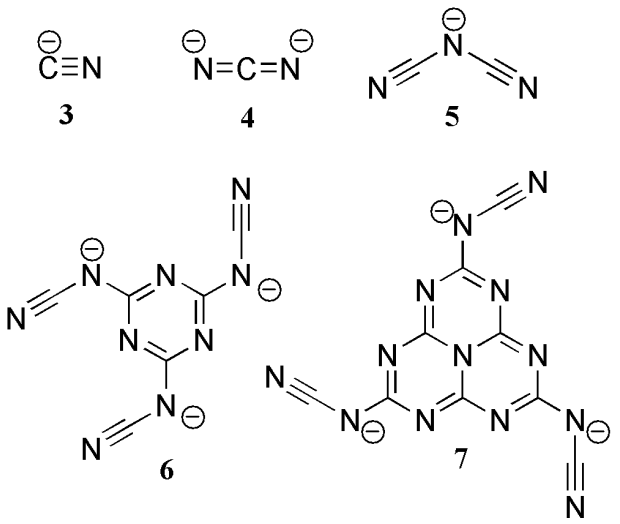

Scheme 2. Molecular structures of anions comprising carbon and nitrogen in an alternating arrangement: cyanide (**3**), cyanamide (**4**), dicyanamide (**5**), tricyanomelaminate (**6**), and melonate (**7**).

With respect to the successful preparation of rare-earth tricyanomelaminates,[9] we chose the structurally related melonates for the attempted synthesis of crystalline *s*-heptazine salts with trivalent rare-earth cations. Melonates have been long known but their detailed characterization has been started only recently. The first report of melonates dates back to 1835, when potassium melonate was obtained as byproduct during the synthesis of potassium thiocyanate.[18] The structure of the melonate anion was correctly proposed in 1937 by Pauling and Sturdivant[19] and was eventually confirmed by Horvath-Bordon et al. by elucidating the crystal structure of potassium melonate pentahydrate.[12] In recent years, a number of alkali and alkaline-earth melonates has been synthesized and structurally characterized.[11,13,14] Moreover, an alternative approach to the original synthesis of melonates from melon and potassium thiocyanate has been established. It has been shown that melonates are also

formed when melon is reacted in cyanate melts and that they eventually decompose in these melts on further heating to yield the related *s*-triazine tricyanomelaminates.[14]

In this contribution, we report the synthesis, structure elucidation, and thermal behavior of the rare-earth melonates $LnC_6N_7(NCN)_3 \cdot 8H_2O$ (Ln = La, Ce, Pr, Nd, Sm), thereby presenting new structurally characterized *s*-heptazine salts with trivalent cations. Additionally, investigations of the photoluminescent properties of $LnC_6N_7(NCN)_3 \cdot xH_2O$ (Ln = Eu, Tb; x = 9-12) complement previous photoluminescence studies of the respective dicyanamides and tricyanomelaminates.

3.2 Results and Discussion

Synthesis and Powder XRD Analysis

Lanthanide melonates $LnC_6N_7(NCN)_3 \cdot xH_2O$ (**7a-g**, Ln = La, Ce, Pr, Nd, Sm, Eu, Tb; x = 8-12) were synthesized by metathesis reactions between ammonium melonate and $LnCl_3 \cdot xH_2O$ in aqueous solution. In analogy to the preparation of lanthanide tricyanomelaminates, the respective ammonium salt had to be used as starting material due to the basic reaction of alkali melonates, which causes the precipitation of lanthanide hydroxides.[9] XRD patterns of the crystalline powders obtained revealed the appearance of three different structures, which are dependent on the nature of the lanthanide. Complexes **7a** and **7b** (Ln = La, Ce) crystallize isostructurally as do **7c**-**7f** (Ln = Pr, Nd, Sm, Eu), whereas another structure and lower crystallinity than that of the other complexes was observed for **7g** (Ln = Tb). However, after several days of aging at room temperature, **7c** and **7d** (Ln = Pr, Nd) transformed into a structure isotypic to that of **7a** and **7b**, and the example of **7d** is shown in Figure 1. Elemental analysis of the as-synthesized and aged samples of **7c** and **7d** indicated that this transformation was due to the partial release of crystal water, which changed the composition of these compounds from $LnC_6N_7(NCN)_3 \cdot 12H_2O$ to $LnC_6N_7(NCN)_3 \cdot 8H_2O$ (Ln = Pr, Nd). The final products $LnC_6N_7(NCN)_3 \cdot 8H_2O$ (Ln = Pr, Nd) were also obtained directly by preparing **7c** and **7d** not at room temperature but by heating the reaction mixtures to approximately 80 °C. Complexes **7e** and **7f** (Ln = Sm, Eu) did not transform into structures isotypic to that of **7a** and **7b** during aging at room temperature but became largely amorphous. However, isotypic $SmC_6N_7(NCN)_3 \cdot 8H_2O$ (**7e**) was obtained by further increasing the synthesis temperature to hydrothermal conditions and reacting an as-synthesized sample of **7e** for 4 h at 120 °C. We therefore assume that $LnC_6N_7(NCN)_3 \cdot 8H_2O$

represents the more stable modification but, due to kinetic reasons, for Ln = Pr, Nd, Sm, $LnC_6N_7(NCN)_3 \cdot 12H_2O$ is formed first during syntheses at room temperature.

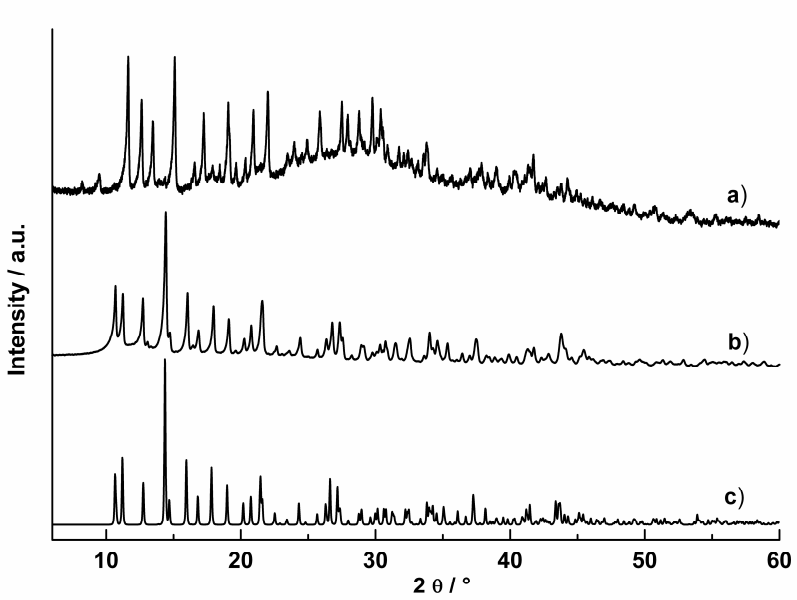

Figure 1. Powder XRD patterns (λ = 154.06 pm, T = 298 K) of a) as-synthesized **7d**, b) **7d**, aged at room temp., and c) **7a** calculated from single-crystal data.

All of the lanthanide melonates investigated were nearly insoluble in water, which impeded single-crystal growth by recrystallization of the immediately precipitating crystalline powders. Single-crystals of **7a** were nevertheless obtained by slow diffusion using agar gel and low-concentration solutions of the starting compounds. The crystal-structure analysis of **7a** (see below) confirmed the composition as octahydrate. Single-crystals of $LnC_6N_7(NCN)_3 \cdot 12H_2O$ (Ln = Pr, Nd, Sm, Eu) were not obtained, and it might be assumed that the general arrangement of melonate entities and lanthanide ions does not significantly differ in the octahydrate and dodecahydrate forms due to their facile transformation to $LnC_6N_7(NCN)_3 \cdot 8H_2O$ (Ln = Pr, Nd, Sm) at room temperature. The characterization of **7g** by FTIR spectroscopy and elemental analysis (see below) indicated a complete exchange of ammonium by Tb^{3+} during the metathesis reaction and an approximate composition of $TbC_6N_7(NCN)_3 \cdot 9H_2O$.

Crystal Structure of 7a

The crystal structure of **7a** was solved from single-crystal XRD data. Complex **7a** crystallizes in the monoclinic space group *C*2 with four formula units in the unit cell. Crystallographic data and details of the structure refinement are summarized in Table 2. The structure is built up of melonate units $[C_6N_7(NCN)_3]^{3-}$, La^{3+} ions, and crystal water molecules (Figure 2). Contrary to the synthesis of lanthanum tricyanomelaminate,[9] ammonium is completely exchanged by lanthanum during the synthesis of **7a** and not present in the structure. As in most alkali and alkaline-earth melonates, the NCN groups are orientated in such a way that the melonate ions show only minor deviations from the point symmetry C_{3h}. The melonate units are nearly planar with bond lengths and angles typically observed for melonate entities. Although the central C–N bonds of the *s*-heptazine core do not contribute to the aromatic system and can therefore be regarded as single bonds (139 pm), the remaining C–N bond lengths of the *s*-heptazine core correspond to conjugated double bonds (131–136 pm). The side chains can be described as carbodiimide groups, –N=C=N–, with a contribution of the resonant cyanamide form, –N–C≡N ($C_{1/3/5}$–$N_{8/9/10}$ 132–135 pm, $N_{8/9/10}$–$C_{7/8/9}$ 130–132 pm, $C_{7/8/9}$–$N_{11/12/13}$ 114–115 pm).

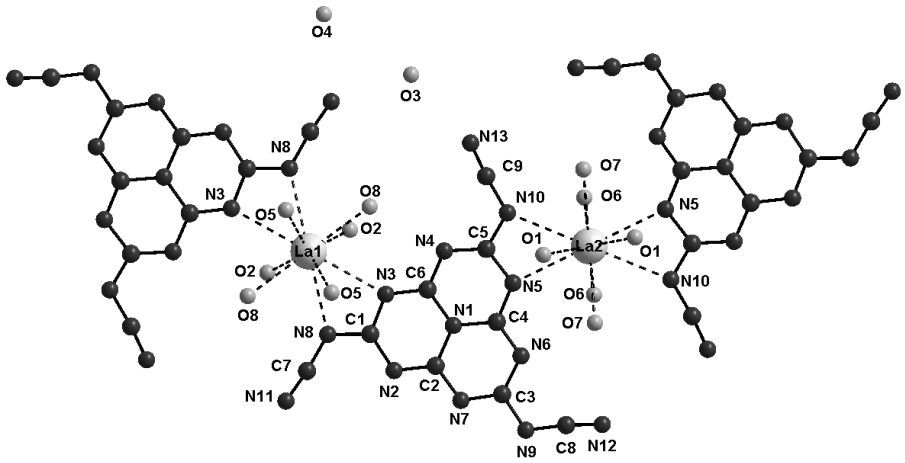

Figure 2. Labeling of atoms and representation of the coordination mode of La^{3+} in the structure of **7a**.

Melonate units and crystal water molecules are arranged in alternating layers perpendicular to the *b* axis, and the La^{3+} ions are located within or slightly above the melonate layers. The melonate entities

are not coplanar but tilted out of the *ac* plane, which results in the formation of a corrugated layer structure (Figure 3). Within one layer, melonate units are arranged in strands along the *c* axis interconnected by La^{3+} ions, and the crystal water molecules are located between these strands (Figure 4). Although the hydrogen-atom positions could not be unambiguously determined from the single-crystal data, N···O (282–308 pm) and O···O (262–267 pm) distances indicate that the water molecules are involved in a hydrogen bonding network that connects the melonate strands.

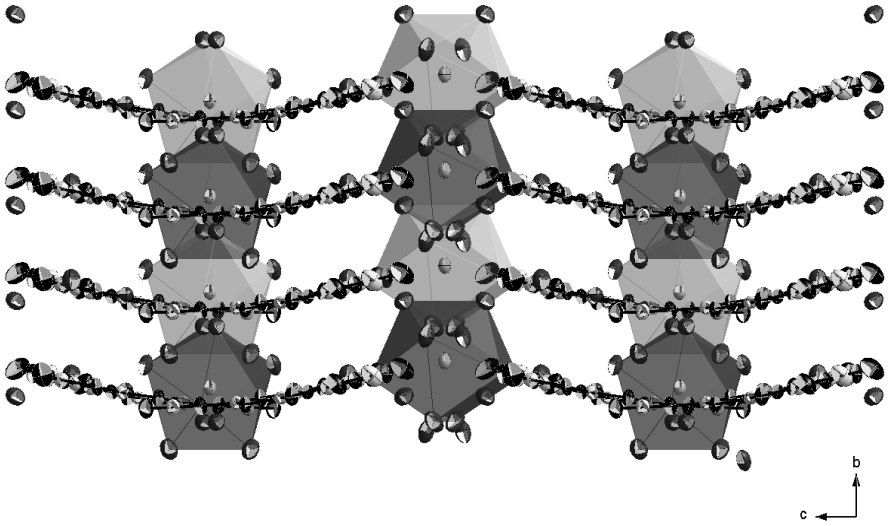

Figure 3. Corrugated layers of melonate units perpendicular to the *b* axis in the crystal structure of **7a**. La^{3+} coordination polyhedrons of adjacent layers are colored light and dark gray, respectively. Thermal ellipsoids are drawn at the 50 % probability level.

Along the *b* axis, the melonate layers are staggered so that adjacent melonate strands do not overlap (Figure 5). The interlayer distance between two melonate layers of 335 pm is similar to values found in alkali and alkaline-earth melonates.[11–14] The La^{3+} ions are coordinated in irregular polyhedrons by two melonate units and six water molecules to achieve coordination numbers of ten. Both the La–O (249–261 pm) and La–N (271–279 pm) distances are in accordance with the sums of the ionic radii[20] and in good agreement with the values for lanthanum tricyanomelaminate.[9] The example of La1 is shown in Figure 6, whereby two melonate units that coordinate one lanthanum ion are not coplanar but tilted with respect to each other. Because of this tilting and the nonuniform distribution of coordinating water molecules above and below the melonate units **7a** crystallizes in the noncentrosymmetric space group *C*2.

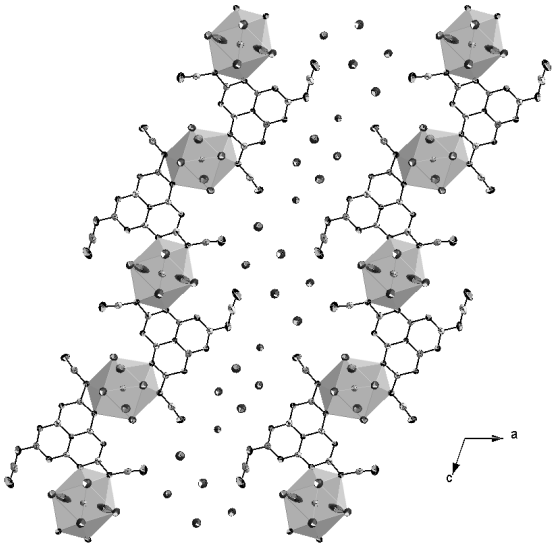

Figure 4. Representation of a single layer in **7a**, which illustrates the arrangement of melonate units and La^{3+} in strands along the *c* axis and the localization of crystal water between these strands. Thermal ellipsoids are drawn at the 50 % probability level.

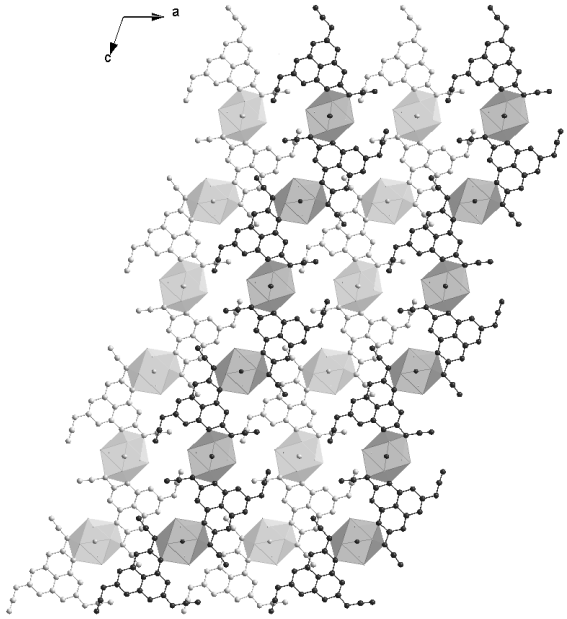

Figure 5. Illustration of the staggered arrangement of melonate layers along the *b* axis in **7a**. The melonate units and La^{3+} coordination polyhedrons of adjacent layers are colored light and dark gray, respectively. Crystal water molecules are omitted for clarity.

The crystal structures of isotypic $LnC_6N_7(NCN)_3 \cdot 8H_2O$ (Ln = Ce, Pr, Nd, Sm; **7b**–**7e**) were refined from powder XRD patterns by the Rietveld method, using the lattice parameters and atomic coordinates of **7a** as the starting values. Bond lengths and angles within the melonate entities were not refined, but the rotation and translation of the melonate units were. Crystallographic data and details of the refinements are given for all compounds in Table 1, and the Rietveld plot of **7b** is shown in Figure 7 as an example. Rietveld plots of **7c**–**e** are given in the Supporting Information (Figures S1–S3). In accordance with our expectations, the lattice parameters and cell volume decreased with the decreasing size of the lanthanide ion from La to Sm, accompanied by a slight increase of the monoclinic angle.

FTIR Spectroscopy

The FTIR spectrum of **7a** shows the characteristic absorption bands of the melonate units (Figure 8, a). Bands at 1200–1700 cm^{-1} are assigned to the stretching vibrations of the *s*-heptazine core, and a sharp band at 807 cm^{-1} to the bending vibrations of the ring. Furthermore, C≡N groups of the side chains give rise to an absorption band at 2184 cm^{-1}, and the ν(OH) signals of the crystal water molecules are observed at 3000–3600 cm^{-1}. The FTIR spectra of **7f** and **7g** (Figure 8, b and c) resemble that of **7a** and are therefore a clear indication of the presence of melonate entities in the samples. Additionally, the absence of ν(NH) bands at around 2800–3000 cm^{-1} shows that the melonate units are not protonated and that a complete exchange of ammonium by Eu^{3+} and Tb^{3+}, respectively, was achieved during the metathesis reaction. This observation is in accordance with the elemental analyses, which give an atomic ratio Ln/C/N of 1:9:13. Hence, for both **7f** and **7g**, the formula $LnC_6N_7(NCN)_3 \cdot xH_2O$ (Ln = Eu, Tb; x = 9–12) can be derived.

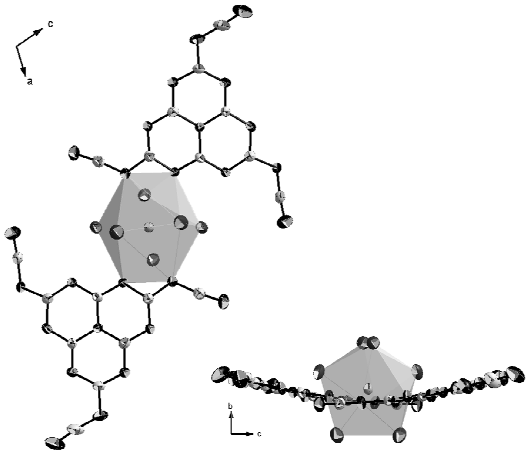

Figure 6. Coordination of La1 by two melonate entities and six crystal water molecules, viewed along the *b* (left) and *a* (right) axes, which illustrates the absence of an inversion center in the crystal structure of **7a**.

Thermal Analysis

The thermal behavior of **7a** was investigated by thermogravimetric (TG) and differential thermal analysis (DTA, Figure 9). At 20–230 °C, the crystal water is partially released. The observed mass loss of 19.6% in this temperature range is smaller than expected for eight water molecules per formula unit (calcd. 25.1%), which indicates that part of the crystal water remains bound in the structure up to elevated temperatures. This observation may be due to the high oxygen affinity of rare-earth elements. Subsequently, at 230–700 °C, a further mass loss of 12.7% occurred slowly and steadily before the sample eventually started to decompose above 700 °C. This high decomposition temperature is typical

Table 1. Crystallographic data and details of the structure refinement for **7b-e**.

$LnC_6N_7(NCN)_3 \cdot 8H_2O$	**7b** (Ln = Ce)	**7c** (Ln = Pr)	**7d** (Ln = Nd)	**7e** (Ln = Sm)
Molar mass /g mol^{-1}	574.43	575.22	578.55	584.67
Crystal system	monoclinic	monoclinic	monoclinic	monoclinic
Space group	*C*2 (no. 5)	*C*2 (no. 5)	*C*2 (no. 5)	*C*2 (no. 5)
Radiation (Cu-$K_{\alpha 1}$), λ /pm	154.06	154.06	154.06	154.06
a /pm	1664.81(5)	1660.12(9)	1657.7(2)	1650.5(2)
b /pm	667.68(2)	665.45(3)	664.89(4)	662.34(4)
c /pm	1749.38(5)	1744.57(7)	1741.99(10)	1736.5(2)
β /°	108.94(1)	109.03(1)	108.99(1)	109.21(1)
V /10^6 pm^3	1839.3(1)	1822.0(2)	1815.5(2)	1792.6(3)
Z	4	4	4	4
Calculated density /g cm^{-3}	2.02	2.04	2.06	2.11
Diffraction range	$2.75° \leq \theta \leq 35°$	$2.75° \leq \theta \leq 35°$	$2.75° \leq \theta \leq 35°$	$2.75° \leq \theta \leq 35°$
Independent parameters	57	52	54	52
Data points	462	459	459	456
GooF	1.588	1.155	1.025	1.221
*R*p, *wR*p	0.0271, 0.0356	0.0175, 0.0232	0.0154, 0.0200	0.0175, 0.0229

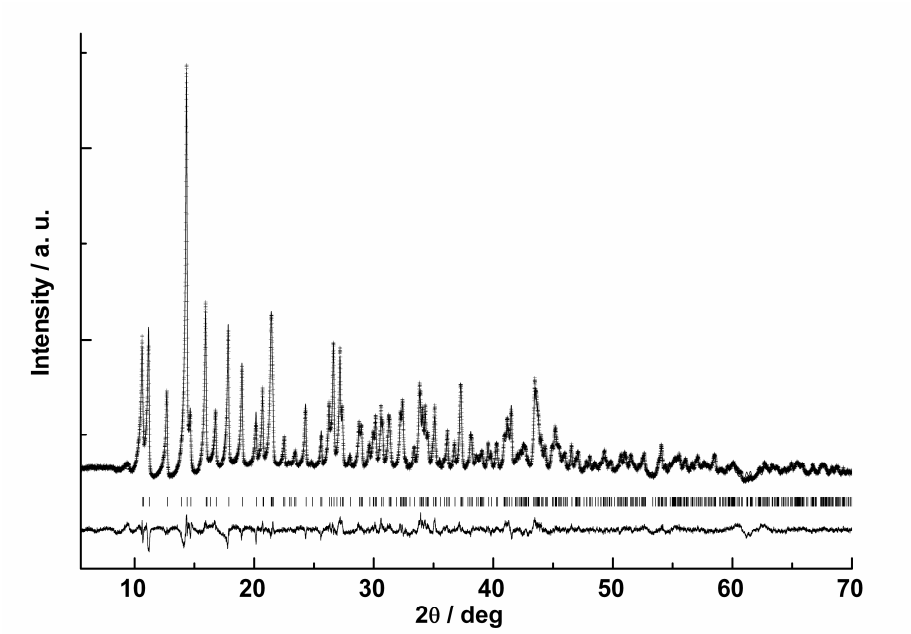

Figure 7. Observed (crosses) and calculated (line) powder XRD patterns and the difference profile of the Rietveld refinement of **7b**. Bragg peaks are indicated by vertical lines. (λ = 154.06 pm, T = 298 K).

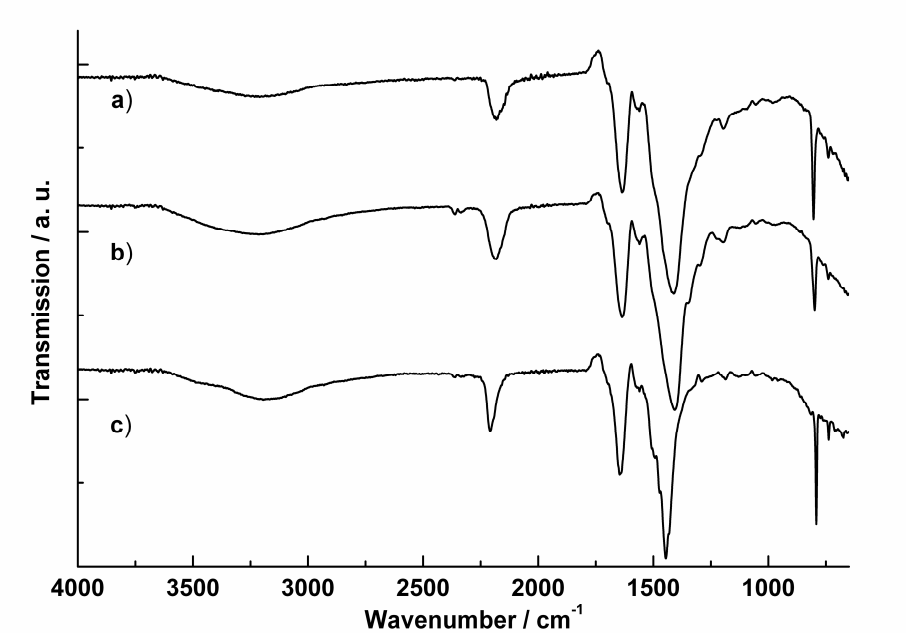

Figure 8. FTIR spectra of a) **7a**, b) **7f**, and c) **7g**.

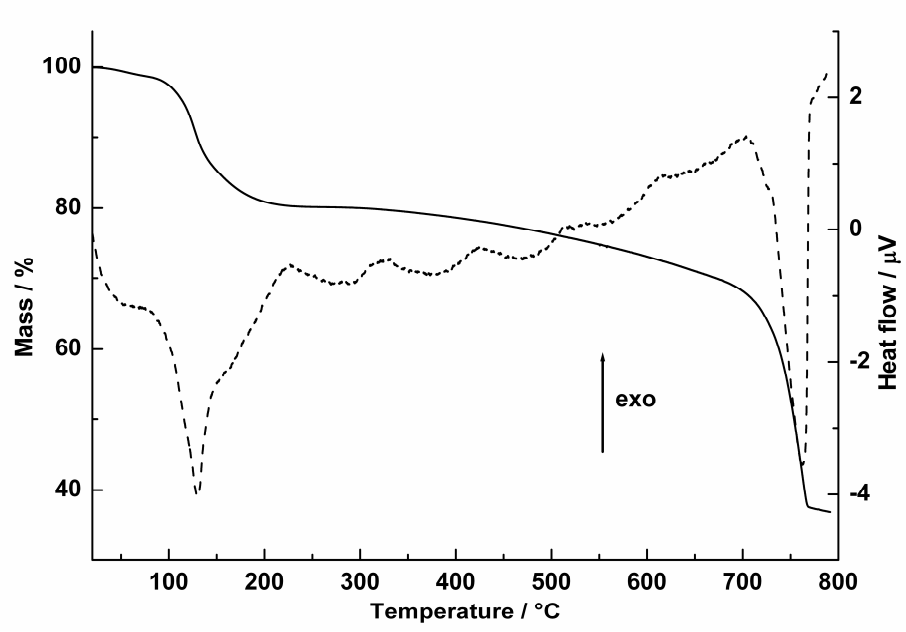

Figure 9. TG (solid) and DTA (dashed) curves of **7a** (17.6 mg), measured with a heating rate of 5 K min^{-1}.

for *s*-heptazine derivatives such as melonates and cyamelurates.[10–12,14,21] However, because the partial mass loss of **7a** began at 230 °C, the thermal stability of this compound has to be regarded as distinctly lower than that of alkali melonates.[11,12,14] We therefore assume that the observed incomplete dehydration of **7a** causes the reaction of the melonate units with the remaining crystal water at elevated temperatures, which leads to another decomposition pathway. Lanthanum oxides or nitrides are presumably obtained as the final products after thermal decomposition. However, their exact composition was not determined. The TG and DTA curves of **7b**–**7e** resemble that of **7a** (Figures S4–S7), which indicates the comparable thermal behavior and stability of all of the rare-earth melonates investigated.

Photoluminescence Studies

Photoluminescence studies were conducted on **7f** and **7g**. Unlike the respective Ln^{III} dicyanamides and tricyanomelaminates, which exhibit luminescence properties both for Eu^{III} and Tb^{III} derivatives, luminescence under UV excitation was only observed for **7g**. Furthermore, quenching was observed for the hydrated form of **7g**. It is well known that the luminescence of compounds with trivalent rare-earth cations is strongly affected by crystal water molecules, which cause nonradiative loss through O–H oscillation.[5,9] Because the luminescence of hydrated **7g** was less pronounced than that of dehydrated **7g**, photoluminescence studies were only carried out for the dehydrated compound (Figure 10). The diffuse reflectance spectrum of dehydrated **7g** shows a broad band at 250–450 nm, which can be attributed to the melonate entities as it also occurs in the spectra of other Ln^{III} melonates and ammonium melonate. In the excitation and emission spectra of **7g**, all peaks can be assigned in accordance with the spectra of Tb^{III} dicyanamide and Tb^{III} tricyanomelaminate.[5,9] The broad band at 250–450 nm in the excitation spectrum originates from the Tb^{III} $4f^8 \rightarrow 4f^7 5d^1$ transition. Sharp peaks that correspond to intra-4f transitions, which are superimposed on this wide band in Tb^{III} dicyanamide and Tb^{III} tricyanomelaminate, cannot be unambiguously assigned in the spectrum of **7g** due to a comparably high background in the excitation spectrum. The emission spectrum, recorded at λ_{exc} = 340 nm, shows several distinctive bands characteristic of Tb^{III} $^5D_4 \rightarrow {}^7F_J$ (J = 3-6) transitions with a maximum green emission at 545 nm (J = 5).

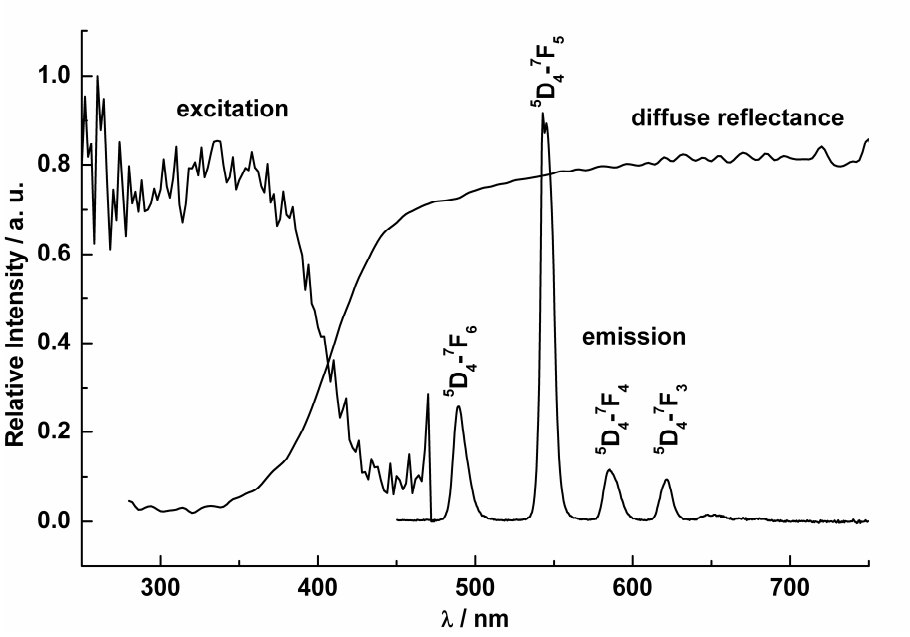

Figure 10. Diffuse reflectance, excitation, and emission spectra of dehydrated **7g** at room temp. (λ_{em} = 545 nm, λ_{exc} = 340 nm).

3.3 Conclusions

We have reported the synthesis, structure elucidation, and thermal behavior of rare-earth melonates $LnC_6N_7(NCN)_3 \cdot 8H_2O$ (Ln = La, Ce, Pr, Nd, Sm), which are new examples of structurally characterized *s*-heptazine salts with trivalent cations. *s*-Heptazines have gained considerable interest in recent years as building units in functional carbon nitride-type materials, but due to the low crystallinity of most *s*-heptazine salts with multivalent cations, their structural characterization is often impeded. However, by employing the long-known concept of gel crystallization in *s*-heptazine chemistry, we have been able to grow single crystals of melonates with trivalent cations suitable for analysis by XRD. In addition to a structural characterization, the thermal properties of lanthanide melonates have been investigated. TG and DTA studies have revealed that their thermal behavior deviates from that of alkali melonates. The high oxygen affinity of rare-earth metals impedes complete dehydration on heating. Consequently, at elevated temperatures, a potential reaction of the lanthanide

melonates with the remaining crystal water decreases the thermal stability in comparison to alkali melonates. Moreover, photoluminescence studies of Eu^{III} and Tb^{III} melonate have complemented previous studies on the luminescent properties of the respective dicyanamides and tricyano-melaminates. These results contribute to the systematic investigation of the structures and properties of molecular Ln/C/N compounds and illustrate possibilities for the synthesis of numerous new *s*-heptazine salts by employing multivalent cations.

3.4 Experimental Section

Syntheses

The rare-earth melonates $LnC_6N_7(NCN)_3 \cdot xH_2O$ (Ln = La, Ce, Pr, Nd, Sm, Eu, Tb; x = 8-12) were synthesized by metathesis reactions in aqueous solution from ammonium melonate and the respective $LnCl_3 \cdot xH_2O$ (all Alfa Aesar, 99.9 %). Ammonium melonate was prepared by ion exchange from potassium melonate pentahydrate, which can be easily obtained in large quantities.[12] Melon was synthesized in preparative amounts according to the procedure described by *Sattler* et al. by heating melamine (Fluka, purum) in an open porcelain crucible at 490 °C for 4 days.[22]

Potassium Melonate Pentahydrate: Melon (10.0 g, 49.7 mmol) was added in small portions to a melt of KSCN (20.0 g, 206 mmol, Acros, ≥ 99 %). After heating for 1 h, the reaction was quenched, the solid obtained was dissolved in boiling H_2O (100 mL), and the mixture was filtered. On cooling to room temperature, a yellow solid crystallized from the filtrate. The crude product was recrystallized from water three times for purification. After drying at 75 °C, potassium melonate pentahydrate (8.32 g, 16.7 mmol, 34 %) was obtained as colorless needles. $K_3C_9N_{13} \cdot 5H_2O$ (497.56) calcd. C 21.73, H 2.03, N 36.60, K 23.57; found C 23.02, H 1.59, N 39.24, K 25.96.

Ammonium Melonate: Ammonium melonate was prepared by ion exchange in aqueous solution at room temperature. A solution of potassium melonate pentahydrate (500 mg, 1.00 mmol, 0.02 M) was poured on to a column containing a strongly acidic ion exchange resin (55 mL, Amberlyst 15, Fluka, ion exchange capacity 1.8 mmol mL^{-1}). The eluate was dropped into an aqueous ammonia solution (25 mL, 10 wt.-%). After removing the solvent by vacuum evaporation, ammonium melonate was obtained as a colorless powder.

$LnC_6N_7(NCN)_3 \cdot xH_2O$: A solution of $LnCl_3 \cdot xH_2O$ (100 mg) in water (30 mL) was added dropwise to a solution of ammonium melonate (100 mg) in water (30 mL) (molar ratio ≈ 1:1). The amount of crystal water in the obtained samples depended on synthesis temperature. For the preparation of $LnC_6N_7(NCN)_3 \cdot 8H_2O$ (Ln = La, Ce), $LnC_6N_7(NCN)_3 \cdot 12H_2O$ (Ln = Pr, Nd, Sm, Eu), and $TbC_6N_7(NCN)_3 \cdot 9H_2O$, the ammonium melonate solution was kept at room temperature. For the preparation of $LnC_6N_7(NCN)_3 \cdot 8H_2O$ (Ln = Pr, Nd), the ammonium melonate solution was warmed to ca. 80 °C. Crystalline $SmC_6N_7(NCN)_3 \cdot 8H_2O$ was obtained under hydrothermal conditions at 120 °C and an approximate pressure of $2 \cdot 10^5$ Pa: a suspension of as-synthesized $SmC_6N_7(NCN)_3 \cdot 12H_2O$ (30 mg) in water (4 mL) was put in a 12 mL Teflon-lined steel autoclave and heated to 120 °C over 30 min, held at this temperature for 4 h, and cooled to room temperature by turning off the furnace. Single crystals of **7a** were grown by gel crystallization in 1 wt.-% agar gels in U-tubes using 0.01 M solutions of ammonium melonate and $LaCl_3 \cdot 7H_2O$. **7a**: $LaC_9N_{13} \cdot 8H_2O$ (573.21): calcd. C 18.86, H 2.81, N 31.77, La 24.23; found C 19.01, H 2.82, N 32.06, La 24.90. **7b**: $CeC_9N_{13} \cdot 8H_2O$ (574.43): calcd. C 18.82, H 2.81, N 31.70, Ce 24.39; found C 18.82, H 2.81, N 31.72 31.70, Ce 24.39. **7c**: $PrC_9N_{13} \cdot 8H_2O$ (575.22): calcd. C 18.78, H 2.80, N 31.64, Pr 24.5; found C 18.66, H 3.25, N 31.47, Pr 26.99. $PrC_9N_{13} \cdot 12H_2O$ (647.28): calcd. C 16.70, H 3.74, N 28.13, Pr 21.77; found C 16.50, H 3.67, N 28.06, Pr 21.56. **7d**: $NdC_9N_{13} \cdot 8H_2O$ (578.55): calcd. C 18.68, H 2.79, N 31.47, Nd 24.93; found C 18.75, H 2.81, N 31.49, Nd 24.32. $NdC_9N_{13} \cdot 12H_2O$ (650.61): calcd. C 16.61, H 3.72, N 27.99, Nd 22.17; found C 16.37, H 3.66, N 27.75, Nd 22.01. **7e**: $SmC_9N_{13} \cdot 8H_2O$ (584.67): calcd. C 18.49, H 2.76, N 31.15, Sm 25.72; found C 17.45, H 2.82, N 29.42, Sm 20.71. $SmC_9N_{13} \cdot 12H_2O$ (656.73): calcd. C 16.46, H 3.68, N 27.73, Sm 22.90; found C 16.67, H 3.40, N 27.62, Sm 20.97. **7f**: $EuC_9N_{13} \cdot 12H_2O$ (658.33): calcd. C 16.42, H 3.67, N 27.66, Eu 23.08; found C 16.57, H 3.47, N 27.54, Eu 25.43. **7g**: $TbC_9N_{13} \cdot 9H_2O$ (611.25): calcd. C 17.68, H 2.97, N 29.79, Tb 26.00; found C 17.70, H 2.94, N 29.43, Tb 24.33.

X-ray Structure Determination

Single-crystal XRD data for **7a** were collected at 293 K with a Kappa CCD diffractometer (Mo-K_α radiation, λ = 71.073 pm, Table 2). Diffraction intensities were scaled using the SCALEPACK[23] software package, and the SADABS[24] program was used for absorption correction. The crystal structure was solved by direct methods (SHELXS-97) and refined against F^2 by applying the full-matrix least-squares method (SHELXL-97).[25] Hydrogen atom positions of the crystal water molecules could not be unequivocally determined from difference Fourier syntheses and were therefore omitted. All non-hydrogen atoms were refined anisotropically.

Powder XRD measurements were carried out in transmission geometry with a Huber G670 Guinier Imaging Plate diffractometer using Ge(111)-monochromated Cu-$K_{\alpha 1}$ radiation (λ = 154.06 pm). Rietveld refinements of the powder XRD data for **7b**–**7e** were performed with the program TOPAS[26] using the lattice constants and atomic coordinates of **7a** as starting values. During the refinements, the melonate units were fixed as rigid bodies and only the translation and rotation of these fragments were refined, excluding the bond lengths and angles within these entities.

Table 2. Crystallographic data and details of the structure refinement of **7a**.

Molar mass /g mol^{-1}	573.21
Crystal system	monoclinic
Space group	*C*2 (no. 5)
T /K	293
Diffractometer	Nonius Kappa-CCD
Radiation (Mo-K_α), λ /pm	71.073
a /pm	1666.2(3)
b /pm	669.04(13)
c /pm	1751.0(4)
β /°	108.74(3)
V /10^6 pm^3	1848.4(6)
Z	4
Calculated density /g cm^{-3}	2.002
Flack parameter	0.05(2)
Crystal size /mm^3	0.11 x 0.09 x 0.03
Absorption coefficient /mm^{-1}	2.384
Absorption correction	multi-scan
Min. / max. transmission	0.6194 / 0.8633
Diffraction range	$3.20^\circ \leq \theta \leq 25.45^\circ$
Index range	$-19 \leq h \leq 20$, $-7 \leq k \leq 8$, $-20 \leq l \leq 21$
Parameters / restraints	281 / 1
Total reflections	12495
Independent reflections	3345
Observed reflections	3095
Min./max. resid. electron density /e 10^{-6} pm^{-3}	-0.507 / +0.624
GooF	1.095
Final *R* indices [$I > 2\sigma(I)$]	$R1$ = 0.0289; $wR2$ = 0.0694[a]
Final *R* indices (all data)	$R1$ = 0.0338; $wR2$ = 0.0714[a]

[a] $w = [\sigma^2(F_0^2) + (0.0291P)^2 + 3.1965P]^{-1}$, with $P = (F_0^2 + 2\,F_c^2)/3$

Further details on the crystal structure investigations may be obtained from the Fachinformationszentrum Karlsruhe, 76344 Eggenstein-Leopoldshafen, Germany (fax: +49-7247-808-666; e-mail: crysdata@fiz-karlsruhe.de), on quoting the depository numbers CSD-423756 (for **7a**), -423757 (for **7b**), -423758 (for **7c**), -423759 (for **7d**), and -423760 (for **7e**).

Thermal Analysis

Thermoanalytical measurements were performed with a Thermoanalyzer TG-DTA92 (Setaram). The samples were heated in alumina crucibles under an inert atmosphere (He) from room temperature to 800 °C with a heating rate of 5 K min^{-1}.

Photoluminescence Studies

Diffuse reflectance spectra were measured with a Varian Cary 500 spectrometer between 240 and 780 nm. Excitation and emission spectra were recorded with a FL900 spectrofluorimeter (Edinburgh Instruments) fitted with a Hamamatsu photomultiplier using a Xe lamp as the light source.

General Techniques

FTIR spectra were recorded with a Spektrum BX II FTIR spectrometer (Perkin–Elmer) equipped with a DuraSampler diamond ATR device. Measurements were conducted at ambient conditions between 600 and 4000 cm^{-1}. Elemental analyses for C, H, and N were performed with the elemental analyzer systems Vario EL and Vario Micro (Elementar Analysensysteme GmbH) and for the rare-earth elements by atomic emission spectroscopy with inductively coupled plasma using a Varian-Vista simultaneous spectrometer.

Supporting Information (see footnote on the first page of this article): Plots of Rietveld refinements for **7c**–**e**; TG and DTA curves of **7b**–**e**.

Acknowledgments

The authors would like to thank the Deutsche Forschungsgemeinschaft (DFG) (project SCHN 377/15) and the Fonds der Chemischen Industrie (FCI) for financial support, Petra Huppertz and Detlef Wiechert (Philips Technologie) for recording the photoluminescence spectra, and Dr. Peter Mayer (Department Chemie, LMU, München) for the single-crystal XRD data collection.

3.5 Bibliography

[1] For recent reviews, see: a) G. Goglio, D. Foy, G. Demazeau, *Mater. Sci. Eng. R* **2008**, *58*, 195-227; b) E. Kroke, M. Schwarz, *Coord. Chem. Rev.* **2004**, *248*, 493-532; c) A. Thomas, A. Fischer, F. Goettmann, M. Antonietti, J.-O. Müller, R. Schlögl, J. M. Carlsson, *J. Mater. Chem.* **2008**, *18*, 4893-4908.

[2] See, for example: a) F. Goettmann, A. Fischer, M. Antonietti, A. Thomas, *Angew. Chem.* **2006**, *118*, 4579-4583; *Angew. Chem. Int. Ed.* **2006**, *45*, 4467-4471; b) F. Goettmann, A. Thomas, M. Antonietti, *Angew. Chem.* **2007**, *119*, 2773-2776; *Angew. Chem. Int. Ed.* **2007**, *46*, 2717-2720; c) H. Grueger, C. Kunath, European Patent *EP1436607*; d) H. Sugimura, Y. Sato, N. Tajima, O. Takai, *Surface Coating Technol.* **2001**, *142-144*, 714-718; e) X. Wang, K. Maeda, A. Thomas, K. Takanabe, G. Xin, J. M. Carlsson, K. Domen, M. Antonietti, *Nat. Mater.* **2009**, *8*, 76-80; f) Z. B. Zhou, R. Q. Cui, Q. J. Pang, G. M. Hadi, Z. M. Ding, W. Y. Li, *Solar Energy Mater. Solar Cells* **2002**, *70*, 487-493.

[3] Numerous cyanides, cyanamides and dicyanamides have been reported. See, for example: a) S. R. Batten, K. S. Murray, *Coord. Chem. Rev.* **2003**, *246*, 103-130; b) U. Berger, W. Schnick, *J. Alloys Compd.* **1994**, *206*, 179-184; c) J. Černák, M. Orendáč, I. Potočňák, J. Chomič, A. Orendáčová, J. Skoršepa, A. Feher, *Coord. Chem. Rev.* **2002**, *224*, 51-66; d) R. Gheorghe, P. Cucos, M. Andruh, J.-P. Costes, B. Donnadieu, S. Shova, *Chem. Eur. J.* **2006**, *12*, 187-203; e) B. Jürgens, E. Irran, W. Schnick, *J. Solid State Chem.* **2001**, *157*, 241-249; f) B. Jürgens, E. Irran, W. Schnick, *J. Solid State Chem.* **2005**, *178*, 72-78; g) J. S. Miller, J. L. Manson, *Acc. Chem. Res.* **2001**, *34*, 563-570; h) A. Nag, W. Schnick, *Z. Anorg. Allg. Chem.* **2006**, *632*, 609-614; i) M. Verdaguer, A. Bleuzen, V. Marvaud, J. Vaissermann, M. Seuleiman, C. Desplanches, A. Scuiller, C. Train, R. Garde, G. Gelly, C. Lomenech, I. Rosenman, P. Veillet, C. Cartier, F. Villain, *Coord. Chem. Rev.* **1999**, *190-192*, 1023-1047; j) M. S. Wickleder, *Chem. Rev.* **2002**, *102*, 2011-2088; k) A. Williams, I. T. Ibrahim, *Chem. Rev.* **1981**, *81*, 589-636; l) A.-Q. Wu, F.-K. Zheng, W.-T. Chen, L.-Z. Cai, G.-C. Guo, J.-S. Huang, Z.-C. Dong, Y. Takano, *Inorg. Chem.* **2004**, *43*, 4839-4845.

[4] a) E. Irran, B. Jürgens, W. Schnick, *Chem. Eur. J.* **2001**, *7*, 5372–5381; b) B. Jürgens, E. Irran, J. Schneider, W. Schnick, *Inorg. Chem.* **2000**, *39*, 665-670.

[5] A. Nag, P. J. Schmidt, W. Schnick, *Chem. Mater.* **2006**, *18*, 5738-5745.

[6] a) B. F. Abrahams, S. J. Egan, B. F. Hoskins, R. Robson, *Chem. Commun.* **1996**, *10*, 1099-1100; b) J. L. Hoard, *J. Am. Chem. Soc.* **1938**, *60*, 1194-1198; c) E. Irran, B. Jürgens, W. Schnick, *Solid State Sci.* **2002**, *4*, 1305-1311; d) B. Jürgens, H. A. Höppe, W. Schnick, *Z. Anorg. Allg. Chem.* **2004**, *630*, 35-40; e) B. V. Lotsch, W. Schnick, *Z. Anorg. Allg. Chem.* **2007**, *633*, 1435-1441.

[7] B. Jürgens, W. Milius, P. Morys, W. Schnick, *Z. Anorg. Allg. Chem.* **1998**, *624*, 91-97.

[8] B. V. Lotsch, W. Schnick, *Chem. Mater.* **2006**, *18*, 1891-1900.

[9] A. Nag, B. V. Lotsch, J. Schmedt a. d. Günne, O. Oeckler, P. J. Schmidt, W. Schnick, *Chem. Eur. J.* **2007**, *13*, 3512-3524.

[10] C. Clauss, H. Schmidt, A. Schwarzer, E. Kroke, *Z. Anorg. Allg. Chem.* **2011**, *637*, 2246-2251.

[11] a) C. Clauss, J. Wagler, M. Schwarz, A. Schwarzer, E. Kroke, *Z. Anorg. Allg. Chem.* **2010**, *636*, 196-200; b) S. J. Makowski, W. Schnick, *Z. Anorg. Allg. Chem.* **2009**, *635*, 2197-2202.

[12] E. Horvath-Bordon, E. Kroke, I. Svoboda, H. Fuess, R. Riedel, *New J. Chem.* **2005**, *29*, 693-699.

[13] S. J. Makowski, D. Gunzelmann, J. Senker, W. Schnick, *Z. Anorg. Allg. Chem.* **2009**, *635*, 2434-2439.

[14] A. Sattler, W. Schnick, *Eur. J. Inorg. Chem.* **2009**, 4972-4981.

[15] B. V. Lotsch, W. Schnick, *Chem. Mater.* **2005**, *17*, 3976-3982.

[16] See, for example: a) C. Clauss, M. Schwarz, E. Kroke, *Carbon* **2010**, *48*, 1137-1145; b) A. Finkelstein, L. Finkelstein, E. Eliyahu, PCT Int. Appl., *WO 2000032837*; c) A. Kreipl, N. Boege, PCT Int. Appl., *WO 2010128166*; d) M. Schwarz, C. Clauss, E. Voigt, E. Kroke, Ger. Offen., *DE 102008045742*; e) N. I. Zhogrova, N. V. Spiridonova, A. I. Finkel'shtein, *Zhurnal Prikladnoi Spektroskopii* **1973**, *19*, 153-154.

[17] A. Sattler, M. R. Budde, W. Schnick, *Z. Anorg. Allg. Chem.* **2009**, *635*, 1933-1939.

[18] L. Gmelin, *Ann. Pharm.* **1835**, *15*, 252-258.

[19] L. Pauling, J. H. Sturdivant, *Proc. Natl. Acad. Sci. U.S.A.* **1937**, *23*, 615-620.

[20] R. D. Shannon, *Acta Crystallogr., Sect. A* **1976**, *32*, 751-767.

[21] E. Horvath-Bordon, E. Kroke, I. Svoboda, H. Fueß, R. Riedel, S. Neeraj, A. K. Cheetham, *Dalton Trans.* **2004**, 3900-3908.

[22] A. Sattler, W. Schnick, *Z. Anorg. Allg. Chem.* **2006**, *632*, 1518-1523.

[23] Z. Otwinowski, W. Minor, *Methods Enzymol.* **1997**, *276*, 307-326.

[24] G. M. Sheldrick, *SADABS, Version 2* **2001**.

[25] a) G. M. Sheldrick, *Acta Crystallogr., Sect. A* **2008**, *64*, 112-122; b) G. M. Sheldrick, *SHELXS-97, Program for the Solution of Crystal Structures,* Universität Göttingen **1997**; c) G. M. Sheldrick, *SHELXL-97, Program for the Refinement of Crystal Structures,* Universität Göttingen **1997**.

[26] A. Coelho, *TOPAS Academic, Version 4.1* **2007**.

4. Triazine Tricarboxylates

Melonates, which have been described in the previous chapter, can be assigned to a group of anions which comprise only carbon and nitrogen in an alternating arrangement, namely cyanides $(CN)^-$, cyanamides $(CN_2)^{2-}$, dicyanamides $(N(CN)_2)^-$ and tricyanomelaminates $(C_3N_3(NCN)_3)^{3-}$. In contrast to such compounds several ligands are known in which *s*-triazine and *s*-heptazine rings are combined with further aromatic cycles, e. g. *s*-triazine-tris(4-pyridyl), *s*-triazine tribenzoate or *s*-heptazine tribenzoate. The triazine tricarboxylate unit $(C_3N_3(CO_2)_3)^{3-}$ can be regarded as intermediate between these two groups, because it comprises carbon-carbon bonds next to carbon-nitrogen bonds and contains only the *s*-triazine core but not any additional hydrocarbon cycles. Employment of triazine tricarboxylate as a building block in molecular salts or coordination compounds has been performed only very rarely prior to this work although this ligand appears to be a promising linker for metal organic frameworks (MOFs). Triazine tricarboxylate represents the *s*-triazine analog to benzene tricarboxylate $(C_6H_3(CO_2)_3)^{3-}$, a compound that has already successfully been applied for the construction of such frameworks. In this chapter, synthesis and crystal structures of a number of alkali and alkaline earth triazine tricarboxylates are described, thereby providing an overview of structural features in this class of compounds. Moreover, the suitability of triazine tricarboxylate to be employed as linker in MOFs is investigated by examining its thermal stability and its chemical stability in solutions of transition metal salts.

4.1 Alkali Triazine Tricarboxylates

4.1.1 Potassium Triazine Tricarboxylate Dihydrate

$K_3[C_3N_3(COO)_3]\cdot 2H_2O$ – Crystal Structure of a New Alkali Derivative of the Multidentate Ligand Triazine Tricarboxylate

Sophia J. Makowski, Michael Hörmannsdorfer, and Wolfgang Schnick

published in: *Z. Anorg. Allg. Chem.* **2010**, *636*, 2584. DOI: 10.1002/zaac.201000245

Keywords: *s*-Triazine; Potassium; Carboxylate ligands; Structure elucidation; Metal-organic frameworks

Abstract. Potassium-1,3,5-triazine-2,4,6-tricarboxylate dihydrate $K_3[C_3N_3(COO)_3]\cdot 2H_2O$ was obtained by saponification of the respective ethyl ester in aqueous solution under mild conditions and subsequent crystallization at 4 °C. The crystal structure of the molecular salt was elucidated by single-crystal X-ray diffraction [$P\ \bar{1}$, a = 696.63(14), b = 1748.5(3), c = 1756.0(3) pm, α = 119.73(3), β = 91.96(3), γ = 93.84(3)°, V = 1847.6(6)·10^6 pm^3, Z = 6, T = 200 K]. Perpendicular to [100] the triazine tricarboxylate and potassium ions are arranged in layers alternating with layers of crystal water molecules. Two thirds of the triazine tricarboxylate units form hexagonal channels being filled with the remaining triazine tricarboxylate molecules. $K_3[C_3N_3(COO)_3]\cdot 2H_2O$ was additionally investigated by means of FTIR spectroscopy, TG and DTA measurements.

4.1.1.1 Introduction

Research in the field of carbon nitrides is mainly focused on the synthesis of two- and three-dimensional networks, which can serve as functional materials for a wide field of applications such as catalysis or optoelectronic uses.[1-3] A common approach towards multidimensional networks is the pyrolysis of *s*-triazine (C_3N_3) or *s*-heptazine (C_6N_7) based precursors to induce condensation and thereby generating covalently bound products. A variety of precursors with different functional groups has been utilized in this regard (cf. Scheme 1, **1a-d** and **2a-d**).[4-8]

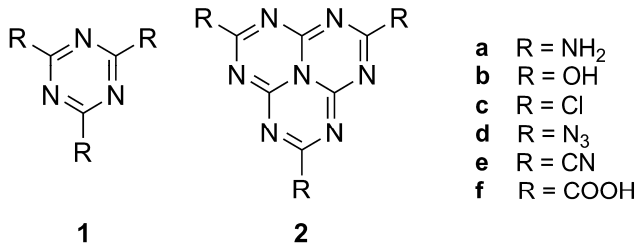

Scheme 1. Molecular precursors for carbon nitride networks comprising the *s*-triazine (**1**) or *s*-heptazine (**2**) core.

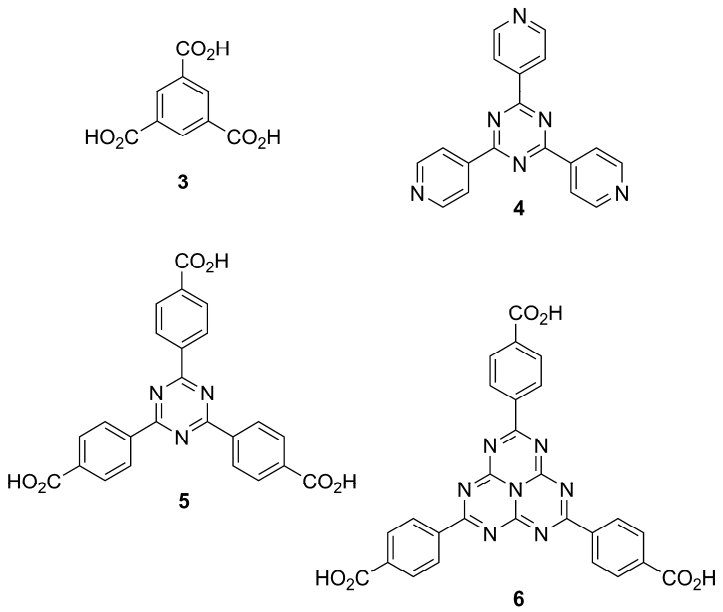

Scheme 2. Multidentate ligands, which are commonly employed as linkers in metal organic frameworks.

In general, molecules containing residues that are bound to the *s*-triazine or *s*-heptazine core via C–C bonds (cf. Scheme 1, **1e-f** and **2e-f**) are adverse in this regard. This is due to the strength of the C–C bonds impeding a successful condensation. Furthermore, the synthesis of carbon nitrides necessitates an alternating sequence of carbon and nitrogen both in the precursor and in the resulting polymeric network. Even though such compounds are no suitable precursors for the synthesis of covalently bound true carbon nitrides by condensation reactions they can be regarded as promising linkers in coordination polymers. Metal organic frameworks (MOFs) have been extensively studied in the last years due to their potential applications, e. g. as

materials for ion exchange, separation, catalysis or gas storage.[9,10] Whereas numerous MOFs are known in which a hydrocarbon cycle functionalized with several carboxylate groups, e. g. trimesic acid **3** (cf. Scheme 2),[11-13] serves as the linker between inorganic atoms or clusters, the analog *s*-triazine or *s*-heptazine compounds **1f** and **2f** have not been employed for this purpose so far.

In known *s*-triazine and *s*-heptazine based linkers such as *s*-triazine-2,4,6-tris(4-pyridyl) **4**,[14,15] *s*-triazine-2,4,6-triyl-tribenzoic acid **5**,[16-20] or *s*-heptazine-2,5,8-triyl-tribenzoic acid **6**[20,21] (cf. Scheme 2), the *s*-triazine or *s*-heptazine cores, respectively, only provide the threefold symmetry but do not contribute to metal coordination. In contrast, in compounds **1f** and **2f** both the carboxylate groups and the nitrogen atoms of the ring can be regarded as coordination positions. The *s*-heptazine compound **2f** has not been mentioned in the literature so far, whereas the synthesis of **1f** by a multistep reaction via the respective ethyl ester and potassium salt has already been described over 50 years ago.[22] However, no structural characterization of the product or any intermediate was performed and since then only very little research regarding triazine tricarbonic acid or its salts has been carried out until 2002 when *Dunbar* et al. reported the crystal structure and magnetic properties of K{Fe(1,3,5-triazine-2,4,6-tricarboxylate)$(H_2O)_2$}$\cdot 2H_2O$.[23]

To the best of our knowledge no crystal structure of any other salt of triazine tricarbonic acid has been described so far. However, regarding the potential application of triazine tricarboxylate as a multidentate ligand, a deeper understanding of its coordination behavior towards various metal ions is of great interest. In this contribution we report on synthesis and crystal structure of potassium triazine tricarboxylate dihydrate $K_3[C_3N_3(COO)_3]\cdot 2H_2O$ as a further example of a structurally characterized triazine tricarboxylate and thereby providing further insight into the coordination properties of this linker.

4.1.1.2 Results and Discussion

Crystal Structure

Potassium triazine tricarboxylate crystallizes as a dihydrate in the triclinic space group $P\,\overline{1}$ with six formula units in the unit cell. Crystallographic data and details of the structure refinement are summarized in Table 1. The crystal structure comprises triazine tricarboxylate $[C_3N_3(COO)_3]^{3-}$ and

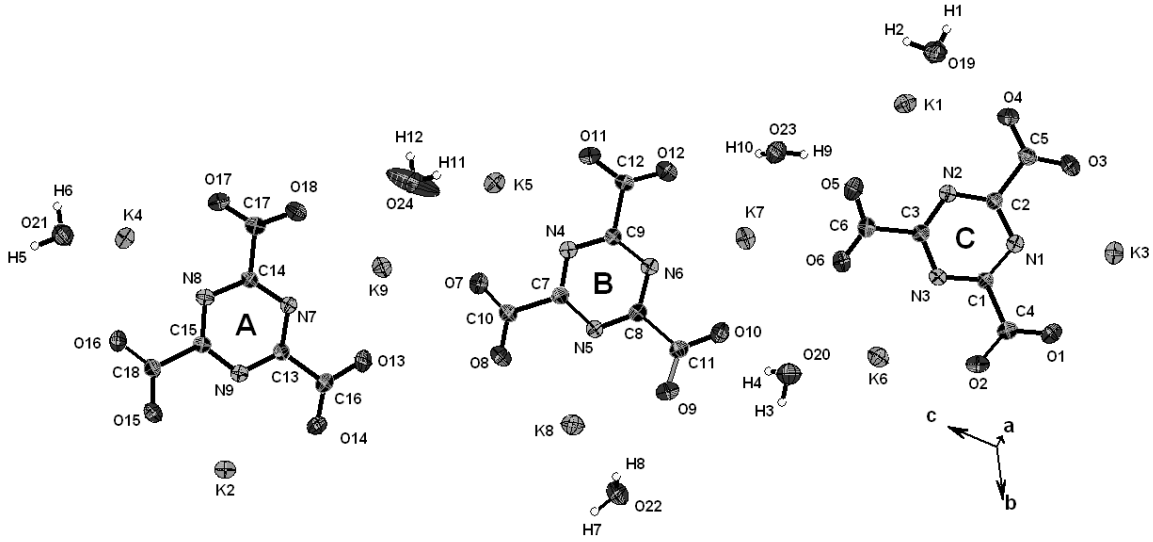

Figure 1. Representation of one formula unit of $K_3[C_3N_3(COO)_3]\cdot 2H_2O$. The three triazine tricarboxylate entities present in the crystal structure are labeled A-C. Thermal ellipsoids (except for hydrogen) are drawn at the 50 % probability level.

potassium ions and crystal water molecules (cf. Figure 1). The triazine tricarboxylate ions are nearly planar with only the carboxylate groups being slightly rotated out of plane so that the anions exhibit molecular symmetry C_3. The substituents cause an increase of the adjacent angles (N1–C1–N3 = 124.5°), whereas the remaining angles of the *s*-triazine core are accordingly reduced (C1–N1–C2 = 115.5°). In accordance with expectation, the bond lengths of both the C–N bonds within the ring (133–134 pm) and the C–O bonds of the carboxylate groups (124-125 pm) correspond to conjugated double bonds, whereas the C–C bond lengths of 153-154 pm resemble those of single bonds (cf. Table 2).

The triazine tricarboxylate ions, the potassium atoms, and water molecules are arranged in an AA'BB' type stacking pattern perpendicular to [100] (cf. Figure 2) with the A and A' layers consisting of the triazine tricarboxylate and potassium ions and the crystal water molecules being located in the intermediate B and B' layers. Within the A and A' layers the triazine tricarboxylate ions are not coplanar but are slightly tilted out of the *bc*-plane. Perpendicular to [100] the triazine tricarboxylate units form two different kinds of columns. One third of the columns consist solely of molecules B (cf. Figure 1) with the molecules of two adjacent layers A and A' being rotated by 60° within the plane. In the remaining columns molecules A and C alternate and are rotated by 30°. These columns form hexagonal channels around the B columns (cf. Figure 3).

Table 1. Crystallographic data and details of the structure refinement for $K_3[C_3N_3(COO)_3]\cdot 2H_2O$.

molar mass / g·mol^{-1}	363.41
crystal system	triclinic
space group	$P\bar{1}$ (no. 2)
T / K	200
diffractometer	Nonius Kappa-CCD
radiation, λ / pm	Mo-K_α, 71.073
a / pm	696.63(14)
b / pm	1748.5(3)
c / pm	1756.0(3)
α / deg	119.73(3)
β / deg	91.96(3)
γ / deg	93.84(3)
V / 10^6 pm^3	1847.6(8)
Z	6
calculated density / g·cm^{-3}	1.960
crystal size / mm^3	0.70 x 0.07 x 0.05
absorption coefficient / mm^{-1}	1.150
diffraction range	$3.26^\circ \leq \theta \leq 27.54^\circ$
index range	$-8 \leq h \leq 9$, $-22 \leq k \leq 22$, $-22 \leq l \leq 22$
parameters / restraints	577 / 16
total no. of reflections	14291
no. of independent reflections	8452
no. of observed reflections	5617
min./max. residual electron density / e 10^{-6} pm^{-3}	-0.679/ +0.984
GooF	1.047
final R indices [$I > 2\sigma(I)$]	$R1$ = 0.0513, $wR2$ = 0.1068 [a)]
final R indices (all data)	$R1$ = 0.0868, $wR2$ = 0.1228 [a)]

a) $w = [\sigma^2(F_0^2) + (0.0389P)^2 + 1.6956P]^{-1}$, with $P = (F_0^2 + 2F_c^2)/3$

The interlayer distance of 347 pm between two triazine tricarboxylate layers is in the expected range for molecular *s*-triazine derivatives.[1,24,25] Between the layers the triazine tricarboxylate units are interconnected by a network of medium strong[26] hydrogen bonds (cf. Table 3) by the carboxylate groups. All crystal water molecules are part of the hydrogen bonding network although due to the strong disorder of one oxygen atom (O24) no hydrogen bond can be clearly assigned to the linked hydrogen atom H11. The potassium ions are coordinated in the form of irregular polyhedrons by four to six oxygen atoms of water molecules and carboxylate groups and by one nitrogen atom of the triazine rings. The triazine tricarboxylate units serve as tridentate ligands and coordinate the K^+ atoms

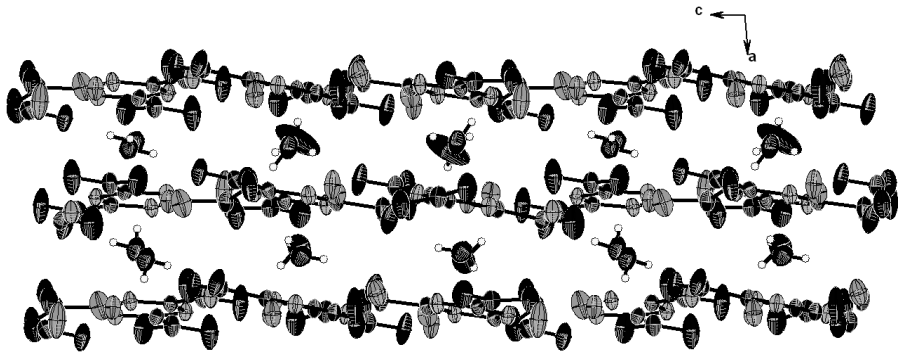

Figure 2. Crystal structure of $K_3[C_3N_3(COO)_3]\cdot 2H_2O$ representing the layered structure perpendicular to [100]. Thermal ellipsoids (except for hydrogen) are drawn at the 50 % probability level.

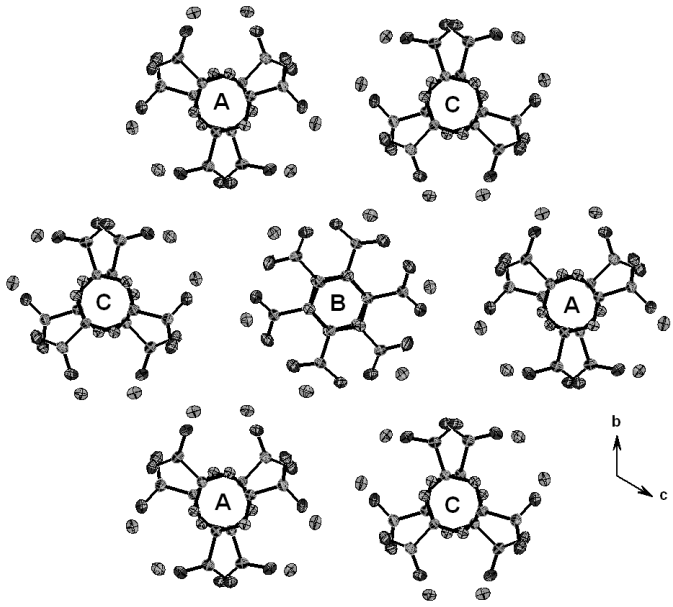

Figure 3. Crystal structure of $K_3[C_3N_3(COO)_3]\cdot 2H_2O$ representing the stacked arrangement of the triazine tricarboxylate entities. Crystal water molecules are omitted for clarity. The labels A-C refer to Figure 1, indicating which triazine tricarboxylate unit lies on top of the respective column. Thermal ellipsoids are drawn at the 50 % probability level.

through the O–N–O entities (cf. Figure 1) with the K^+ atom being slightly shifted towards one of the oxygen atoms.

The coordination sphere is completed by the oxygen atoms of further triazine tricarboxylate units and water molecules. The K–O distances (273–297 pm) are in accordance with the sum of the ionic radii,[27] whereas the K–N distances (278–282 pm) are relatively short compared to the potassium salts of other *s*-triazine or *s*-heptazine compounds.[28-30] In K{Fe(1,3,5-triazine-2,4,6-tricarboxylate)$(H_2O)_2$}$\cdot 2H_2O$, the iron atoms are coordinated by an O–N–O unit in a similar way as in the title compound with a short Fe–N distance of 212 pm, whereas the potassium ions are coordinated solely by oxygen atoms and the K–O distances are comparable in both compounds. Hence, in both triazine tricarboxylate salts a strong

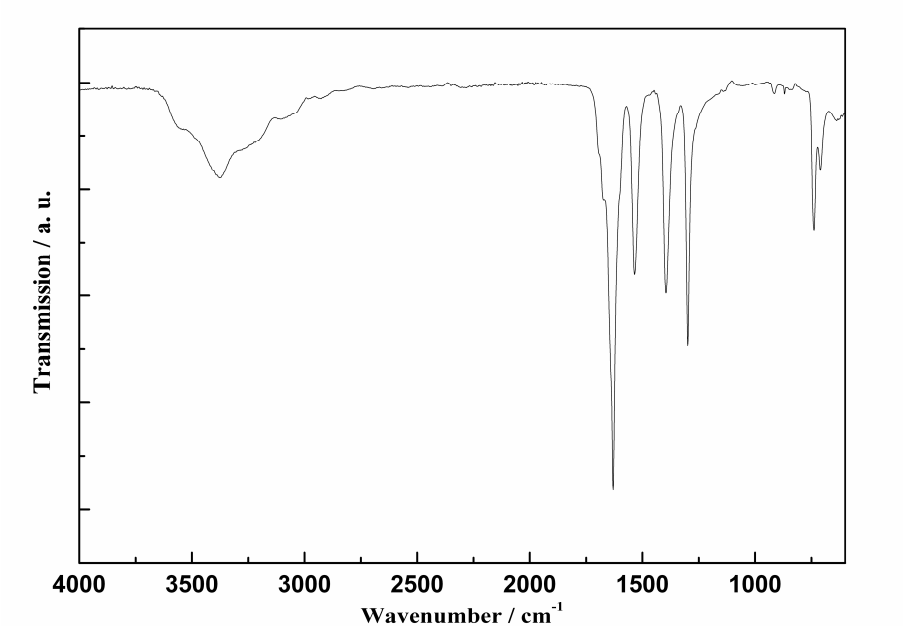

Figure 4. FTIR spectrum of $K_3[C_3N_3(COO)_3]\cdot 2H_2O$.

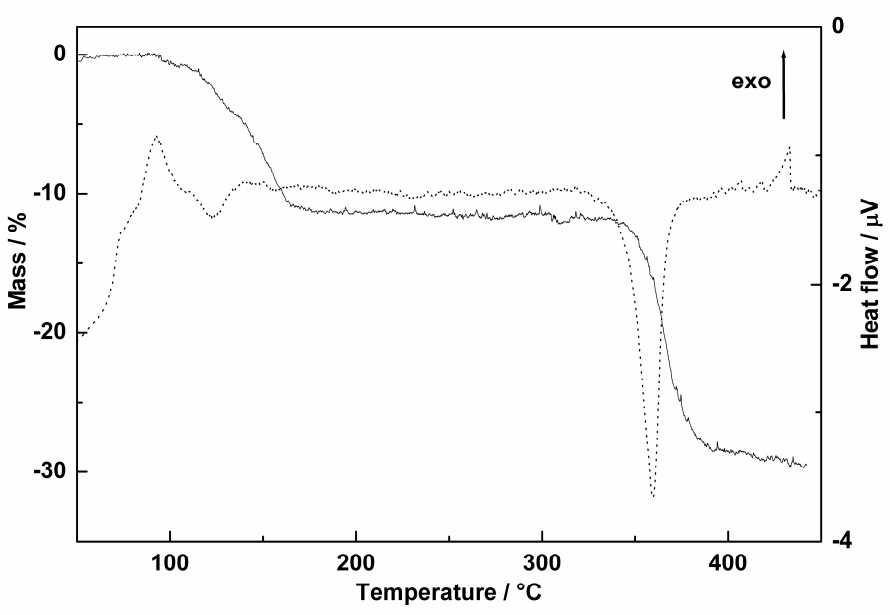

Figure 5. TG (solid) and DTA (dotted) curves of $K_3[C_3N_3(COO)_3]\cdot 2H_2O$, recorded with a heating rate of 5 °C·min^{-1}.

Table 2. Selected bond lengths /pm and angles /° in $K_3[C_3N_3(COO)_3]\cdot 2H_2O$, standard deviations in parentheses.

K1 - O4	292.6(3)	K4 - O17	286.5(3)	K8 - O4	278.7(3)	C2 - N1 - C1	115.4(3)
K1 - O5	281.7(3)	K4 - O21	273.4(3)	K8 - O8	284.0(3)	C2 - N2 - C3	115.4(3)
K1 - O14	279.1(3)	K4 - O22	279.3(3)	K8 - O9	296.2(3)	C3 - N3 - C1	115.7(3)
K1 - O14	284.6(3)	K4 - N8	281.8(3)	K8 - O22	278.2(3)	N3 - C1 - N1	124.3(3)
K1 - O19	280.3(3)	K5 - O1	280.5(3)	K8 - N5	279.7(3)	N2 - C2 - N1	124.7(3)
K1 - N2	278.6(3)	K5 - O7	291.3(3)	K9 - O7	274.4(3)	N3 - C3 - N2	124.5(3)
K2 - O4	286.3(3)	K5 - O11	277.1(3)	K9 - O13	274.0(3)	N1 - C1 - C4	117.9(3)
K2 - O12	281.2(3)	K5 - O24	280.0(5)	K9 - O18	297.1(3)	N3 - C1 - C4	117.8(3)
K2 - O14	284.4(3)	K5 - N4	278.2(3)	K9 - O20	275.7(3)	N1 - C2 - C5	117.4(3)
K2 - O15	283.0(3)	K6 - O2	278.6(3)	K9 - O24	274.0(4)	N2 - C2 - C5	117.9(3)
K2 - O19	275.7(3)	K6 - O6	287.2(3)	K9 - N7	281.8(3)	N2 - C3 - C6	118.2(3)
K2 - O23	273.4(3)	K6 - O18	280.0(3)	N1 - C1	133.8(4)	N3 - C3 - C6	117.3(3)
K2 - N9	280.7(3)	K6 - O18	293.0(3)	N1 - C2	133.4(4)	O1 - C4 - O2	127.5(3)
K3 - O1	287.6(3)	K6 - O20	285.4(4)	N2 - C2	133.1(4)	O4 - C5 - O3	127.8(3)
K3 - O3	281.1(3)	K6 - O24	284.7(4)	N2 - C3	133.9(4)	O6 - C6 - O5	128.5(4)
K3 - O16	281.0(3)	K6 - N3	279.3(3)	N3 - C1	133.6(4)	O1 - C4 - C1	117.5(3)
K3 - O16	283.7(3)	K7 - O6	277.8(3)	N3 - C3	132.9(4)	O2 - C4 - C1	115.0(3)
K3 - O21	282.2(3)	K7 - O10	276.2(3)	C4 - O1	123.9(4)	O3 - C5 - C2	115.2(3)
K3 - N1	279.7(3)	K7 - O12	291.8(3)	C4 - O2	125.0(4)	O4 - C5 - C2	117.0(3)
K4 - O1	287.5(3)	K7 - O19	295.5(3)	C1 - C4	153.0(4)	O5 - C6 - C3	115.3(3)
K4 - O9	276.9(3)	K7 - O23	285.2(3)	C2 - C5	154.2(5)	O6 - C6 - C3	116.1(3)
K4 - O16	290.3(3)	K7 - N6	279.1(3)	C3 - C6	153.0(5)		

contribution of the *s*-triazine core to metal coordination is observed so that the triazine tricarboxylate unit can be regarded as an interesting linker for coordination networks potentially allowing other linkage motifs than those observed in MOFs, which contain trimesic acid as the organic linker.

Vibrational Spectroscopy

Potassium triazine tricarboxylate dihydrate was analyzed by FTIR spectroscopy. All signals in the spectrum can be attributed to vibrations of the triazine tricarboxylate entities and water molecules, respectively (cf. Figure 4). The bending and stretching vibrations of the *s*-triazine ring lead to a

characteristic absorption band at 740 cm^{-1} and a group of signals at 1300–1660 cm^{-1}, respectively. In the range between 1300 and 1660 cm^{-1}, the stretching vibrations of the carboxylate groups can be observed as well. The broad band at 3000–3600 cm^{-1} can be attributed to the OH stretching vibrations of the crystal water molecules and in accordance with the crystal structure the redshift of the ν(OH) signals corresponds to medium strong hydrogen bonds.[26]

Table 3. Donor-acceptor distances /pm and donor-hydrogen-acceptor angles /° for the hydrogen bonding network in $K_3[C_3N_3(COO)_3]\cdot 2H_2O$.

D-H···A	D···A	<D-H···A	D-H···A	D···A	<D-H···A
O19-H1···O8	283.9	154.79	O22-H7···O15	266.5	173.09
O19-H2···O5	272.0	159.35	O22-H8···O11	292.8	176.50
O20-H3···O2	277.5	152.52	O23-H9···O13	269.0	157.25
O20-H4···O10	279.6	166.63	O23-H10···O8	290.1	167.27
O21-H5···O3	270.6	160.13	O24-H12···O17	266.6	155.49
O21-H6···O11	281.4	169.61			

Thermal Behavior

TG and DTA curves of potassium triazine tricarboxylate dihydrate are displayed in Figure 5. In the temperature range between 65 and 150 °C, the crystal water molecules are released (mass loss observed: 10.9 %, calculated: 9.9 %) and the so obtained dehydrated compound is thermally stable up to 325 °C. The decomposition of the sample starts with a mass loss of 17 % accompanied by a sharp endothermic signal at 325–390 °C, probably due to a partial decarboxylation, and proceeds with a slow and steady mass loss at higher temperatures.

4.1.1.3 Conclusions

We have reported on the crystal structure and thermal behavior of potassium triazine tricarboxylate dihydrate. Triazine tricarboxylate represents a multidentate ligand, which can be regarded as the *s*-triazine analog of trimesic acid and hence as a promising linker for metal organic frameworks but only one triazine tricarboxylate salt has been structurally characterized so far. This study has expanded

the investigations of this class of compounds to a new salt and thereby provides further insight into the coordination properties of triazine tricarboxylate. The presented crystal structure shows that the nitrogen atoms of the *s*-triazine cycle exhibit a strong interaction with the potassium ions and that the coordination of metal ions via the O–N–O units of the triazine tricarboxylate entities is a recurring binding motif for this ligand. Because of the differing coordination properties compared to trimesic acid, triazine tricarboxylate seems to be an interesting linker for coordination networks and with the observed high thermal stability of $K_3[C_3N_3(COO)_3]$ an important condition for syntheses of three-dimensional networks at elevated temperatures is fulfilled.

4.1.1.4 Experimental Section

Syntheses

Potassium triazine tricarboxylate dihydrate was synthesized according to the procedure described in the literature[22,31] by saponification of the respective triethyl ester. To prepare the triethyl ester, dry HCl was conducted through ethyl cyanoformate (20.0 g, 202 mmol, Aldrich, 99 %) under argon until the trimerization product started to precipitate. Afterwards, the conversion was completed by cooling the reaction mixture to 4 °C overnight. The product was filtered, washed with cold water and dried at 75 °C to yield 7.15 g (24.1 mmol, 36 %) triethyl-*s*-triazine-2,4,6-tricarboxylate as colorless needles.

Elemental analysis: N 14.22 (calcd. 14.13), C 47.20 (calcd. 48.47), H 4.88 (calcd. 5.08) %.

Small amounts of the triethyl ester (100 mg, 0.34 mmol) were added to KOH (3.5 mL of a 1 M aqueous solution), while cooling with an ice bath. The reaction was stirred until the ester was completely dissolved. Afterwards, ethanol (25 mL) was poured into the solution to precipitate the potassium salt. The product was filtered, washed with ethanol and dried at 75 °C to obtain potassium-1,3,5-triazine-2,4,6-tricarboxylate dihydrate (103 mg, 0.28 mmol) as colorless needles. Yield 83 %. Single crystals suitable for single-crystal X-ray diffraction were obtained by repeated recrystallization from aqueous solution at 4 °C.

Elemental analysis: N 11.60 (calcd. 11.56), C 20.45 (calcd. 19.83), H 0.64 (calcd. 1.11) %.

X-ray Structure Determination

Single-crystal X-ray diffraction data of $K_3[C_3N_3(COO)_3]\cdot 2H_2O$ were collected at 200 K on a Kappa CCD diffractometer using monochromated Mo-K_α radiation (λ = 71.073 pm). The diffraction intensities were scaled using the SCALEPACK software package[32] and no additional absorption correction was applied. The crystal structure was solved by direct methods using the software package SHELXS-97[33] and refined against F^2 by applying the full-matrix least-squares method (SHELXL-97).[34] The hydrogen positions could be determined from difference Fourier syntheses and were refined isotropically using restraints for oxygen-hydrogen distances. All non-hydrogen atoms were refined anisotropically.

CCDC-784049 contains the supplementary crystallographic data for this paper. These data can be obtained free of charge via http://www.ccdc.cam.ac.uk/data_request/cif, or from the Cambridge Crystallographic Data Centre, 12 Union Road, Cambridge CB2 1EZ, UK (Fax: +44-1223-336-033; or E-Mail: deposit@ccdc.cam.ac.uk).

FT-Infrared Spectroscopy

A FTIR spectrum was recorded at ambient conditions between 600 and 4500 cm^{-1} on a Spektrum BX II FTIR spectrometer (Perkin Elmer) equipped with a DuraSampler diamond ATR device.

Thermal Analysis

Thermoanalytical measurements were performed with a Thermoanalyzer TG-DTA92 (Setaram) under inert atmosphere (helium). The sample was heated in an alumina crucible from room temperature to 500 °C with a heating rate of 5 °C·min^{-1}.

Acknowledgments

The authors thank the *Deutsche Forschungsgemeinschaft* (DFG) (project SCHN 377/12) and the *Fonds der Chemischen Industrie* (FCI) for financial support and *Dr. Peter Mayer* (Department Chemie, LMU München) for the single-crystal data collection.

4.1.1.5 Bibliography

[1] G. Goglio, D. Foy, G. Demazeau, *Mater. Sci. Eng. R* **2008**, *58*, 195.

[2] E. Kroke, M. Schwarz, *Coord. Chem. Rev.* **2004**, *248*, 493.

[3] A. Thomas, A. Fischer, F. Goettmann, M. Antonietti, J.-O. Müller, R. Schlögl, J. M. Carlsson, *J. Mater. Chem.* **2008**, *18*, 4893.

[4] E. G. Gillan, *Chem. Mater.* **2000**, *12*, 3906.

[5] T. Komatsu, *J. Mater. Chem.* **2001**, *11*, 799.

[6] E. Kroke, M. Schwarz, E. Horath-Bordon, P. Kroll, B. Noll, A. D. Norman, *New J. Chem.* **2002**, *26*, 508.

[7] B. V. Lotsch, M. Döblinger, J. Sehnert, L. Seyfarth, J. Senker, O. Oeckler, W. Schnick, *Chem. Eur. J.* **2007**, *13*, 4969.

[8] D. R. Miller, J. R. Holst, E. G. Gillan, *Inorg. Chem.* **2007**, *46*, 2767.

[9] A. U. Czaja, N. Trukhan, U. Müller, *Chem. Soc. Rev.* **2009**, *38*, 1284.

[10] R. J. Kuppler, D. J. Timmons, Q.-R. Fang, J.-R. Li, T. A. Makal, M. D. Young, D. Yuan, D. Zhao, W. Zhuang, H.-C. Zhou, *Coord. Chem. Rev.* **2009**, *253*, 3042.

[11] S. S.-Y. Chui, S. M.-F. Lo, J. P. H. Charmant, A. G. Orpen, I. D. Williams, *Science* **1999**, *283*, 1148.

[12] J. Kim, B. Chen, T. M. Reineke, H. Li, M. Eddaoudi, D. B. Moler, M. O'Keeffe, O. M. Yaghi, *J. Am. Chem. Soc.* **2001**, *123*, 8239.

[13] O. M. Yaghi, G. Li, H. Li, *Nature* **1995**, *378*, 703.

[14] D. N. Dybtsev, H. Chun, K. Kim, *Chem. Commun.* **2004**, 1594.

[15] M.-X. Li, Z.-X. Miao, M. Shao, S.-W. Liang, S.-R. Zhu, *Inorg. Chem.* **2008**, *47*, 4481.

[16] D. Sun, S. Ma, Y. Ke, T. M. Petersen, H.-C. Zhou, *Chem. Commun.* **2005**, 2663.

[17] Y. K. Park, S. B. Choi, H. Kim, K. Kim, B.-H. Won, K. Choi, J.-S. Choi, W.-S. Ahn, N. Won, S. Kim, D. H. Jung, S.-H. Choi, G.-H. Kim, S.-S. Cha, Y. H. Jhon, J. K. Yang, J. Kim, *Angew. Chem.* **2007**, *119*, 8378; *Angew. Chem. Int. Ed.* **2007**, *46*, 8230.

[18] S. Ma, X.-S. Wang, D. Yuan, H.-C. Zhou, *Angew. Chem.* **2008**, *120*, 4198; *Angew. Chem. Int. Ed.* **2008**, *47*, 4130.

[19] D. Sun, S. Ma, Y. Ke, D. J. Collins, H.-C. Zhou, *J. Am. Chem. Soc.* **2006**, *1258*, 3896.

[20] S. Ma, D. Sun, M. Ambrogio, J. A. Fillinger, S. Parkin, H.-C. Zhou, *J. Am. Chem. Soc.* **2007**, *129*, 1858.

[21] Y. Ke, D. J. Collins, D. Sun, H.-C. Zhou, *Inorg. Chem.* **2006**, *45*, 1897.

[22] C. Grundmann, E. Kober, *J. Org. Chem.* **1956**, *21*, 1392.

[23] J.-R. Galán-Mascarós, J.-M. Clemente-Juan, K. R. Dunbar, *J. Chem. Soc., Dalton Trans.* **2002**, *13*, 2710.

[24] S.-J. Chen, U. Behrens, E. Fischer, R. Mews, F. Pauer, G. M. Sheldrick, D. Stalke, W.-D. Stohrere, *Chem. Ber.* **1993**, *126*, 2601.

[25] B. V. Lotsch, W. Schnick, *Chem. Mater.* **2006**, *18*, 1891.

[26] T. Steiner, *Angew. Chem.* **2002**, *114*, 50; *Angew. Chem. Int. Ed.* **2002**, *41*, 48.

[27] R. D. Shannon, *Acta Crystallogr., Sect. A* **1976**, *32*, 751.

[28] E. Horvath-Bordon, E. Kroke, I. Svoboda, H. Fueß, R. Riedel, S. Neeraj, A. K. Cheetham, *Dalton Trans.* **2004**, 3900.

[29] E. Irran, B. Jürgens, W. Schnick, *Chem. Eur. J.* **2001**, *7*, 5372.

[30] A. Sattler, W. Schnick, *Eur. J. Inorg. Chem.* **2009**, 4972.

[31] E. Ott, *Ber. Dtsch. Chem. Ges.* **1919**, *52*, 656.

[32] Z. Otwinowski, W. Minor, *Methods Enzymol.* **1997**, *276*, 307.

[33] G. M. Sheldrick, *SHELXS-97, Program for the Solution of Crystal Structures*, Universität Göttingen, Germany **1997**.

[34] G. M. Sheldrick, *SHELXL-97, Program for the Refinement of Crystal Structures*, Universität Göttingen, Germany **1997**.

4.1.2 Lithium, Rubidium and Cesium Triazine Tricarboxylate

Novel Alkali Triazine Tricarboxylates $Li_3[C_3N_3(CO_2)_3]\cdot 4H_2O$, $Rb_3[C_3N_3(CO_2)_3]\cdot 2H_2O$ and $Cs_3[C_3N_3(CO_2)_3]\cdot 2H_2O$ – Synthesis, Crystal Structure and Thermal Behavior

Sophia J. Makowski, Evelyn Calta, and Wolfgang Schnick

published in: *Z. Anorg. Allg. Chem.* **2011**, *637*, 2142. DOI: 10.1002/zaac.201100311

Keywords: Alkali salts; Carboxylate ligands; Crystal structure; *s*-Triazine

Abstract. The alkali 1,3,5-triazine-2,4,6-tricarboxylates $Li_3[C_3N_3(CO_2)_3]\cdot 4H_2O$, $Rb_3[C_3N_3(CO_2)_3\cdot 2H_2O$ and $Cs_3[C_3N_3(CO_2)_3]\cdot 2H_2O$ were synthesized by saponification of the respective triethyl ester in aqueous solution. In the crystal structure, the triazine tricarboxylate (TTC) units and metal ions are arranged in layers alternating with layers of crystal water molecules. Within the layers the triazine tricarboxylate entities form either strands in $Li_3[C_3N_3(CO_2)_3]\cdot 4H_2O$ or a hexagonal arrangement in $Rb_3[C_3N_3(CO_2)_3]\cdot 2H_2O$ and $Cs_3[C_3N_3(CO_2)_3]\cdot 2H_2O$. Perpendicular to the layers, the triazine cores exhibit varying degrees of π-π stacking dependent on the metal ions resulting in the formation of rods in $Rb_3[C_3N_3(CO_2)_3]\cdot 2H_2O$ and $Cs_3[C_3N_3(CO_2)_3]\cdot 2H_2O$. Additionally, the thermal behavior of the alkali triazine tricarboxylates was investigated by means of FT-IR spectroscopy, TG and DTA measurements. Differences and similarities regarding structural features and thermal behavior are discussed for the obtained novel alkali triazine tricarboxylates and potassium triazine tricarboxylate dihydrate.

4.1.2.1 Introduction

Molecules containing the *s*-triazine core (C_3N_3) are widely applied as building units for functional materials. Examples are covalent triazine frameworks (CTFs)[1] and polymeric carbon nitride networks,[2] which are employed for catalysis or optoelectronic uses, or metal organic frameworks (MOFs) comprising triazine based linkers which are utilized e. g. as materials for catalysis, ion exchange, separation, and gas storage.[3] In this regard e. g. *s*-triazine-2,4,6-tris(4-pyridyl) (**1a**) or *s*-triazine-2,4,6-triyl-tribenzoic acid (**1b**) are commonly used as linkers (see Scheme 1).[4] In contrast, *s*-triazine-2,4,6-tricarbonic acid (**2**) has not been utilized as linker so far. However, since **2** can be regarded the *s*-triazine analog to trimesic acid (**3**) (see Scheme 1), a compound that has already been applied as linker in numerous MOFs,[5] it represents a potential multidentate ligand for coordination networks. In comparison to trimesic acid (**3**) triazine tricarbonic acid (**2**) provides not only the carbonyl groups but also the nitrogen atoms of the *s*-triazine core as potential coordination sites.

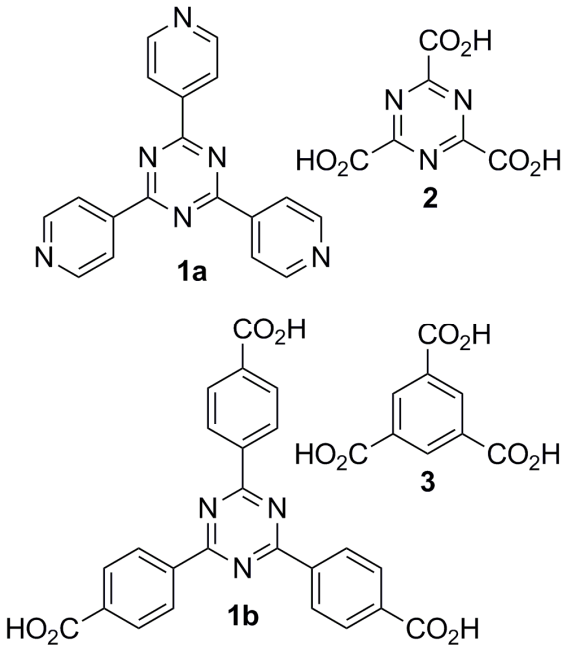

Scheme 1. Threefold multidentate ligands as building units for metal organic frameworks.

The synthesis of triazine tricarbonic acid (**2**) via the respective ethyl ester and potassium salt **4c** has already been described by *Grundmann* et al. in 1956 but a structural characterization has been performed neither for the product nor any intermediate.[6] The first crystal structure of a salt of triazine tricarbonic acid **2**, K{Fe(1,3,5-triazine-2,4,6-tricarboxylate)$(H_2O)_2$}·$2H_2O$ (**5**), was reported by *Dunbar* et al. together with an investigation of the magnetic properties.[7] Additionally, we were able to elucidate the structure of the potassium salt **4c** recently.[8] In both **4c** and **5** the tridentate coordination of metal ions via two carboxylate groups and one nitrogen atom of the triazine ring can be observed as a recurring binding motif indicating a strong interaction between the *s*-triazine core and the metal ions. So far neither the crystal structure of any other salts of triazine tricarbonic acid **2** nor the synthesis of MOFs containing triazine tricarboxylate

(TTC) as a linker has been described. During our attempts to prepare such MOFs we observed that the stability of the triazine tricarboxylate unit in solution strongly depends on the nature of the counterions as will be discussed in a forthcoming paper.[9] Furthermore, the influence of the counterions on structural features and thermal behavior of triazine tricarboxylate salts has not been examined so far due to the limited number of known triazine tricarboxylate salts. In order to gain a better understanding of the coordination and thermal properties of triazine tricarboxylates it is desirable to synthesize and characterize various novel salts.

In this contribution, we report on the synthesis, crystal structure and thermal characterization of three novel alkali salts of triazine tricarbonic acid, namely $Li_3[C_3N_3(CO_2)_3]\cdot 4H_2O$ ($LiTTC\cdot 4H_2O$) (**4a**), $Rb_3[C_3N_3(CO_2)_3]\cdot 2H_2O$ ($RbTTC\cdot 2H_2O$) (**4d**) and $Cs_3[C_3N_3(CO_2)_3]\cdot 2H_2O$ ($CsTTC\cdot 2H_2O$) (**4e**), thereby providing further insight into the coordination properties of this linker and emphasizing recurring binding and stacking motifs in triazine tricarboxylates.

4.1.2.2 Results and Discussion

Crystal Structure

Lithium triazine tricarboxylate tetrahydrate $Li_3[C_3N_3(CO_2)_3]\cdot 4H_2O$ (**4a**) crystallizes in the triclinic space group $P\ \bar{1}$, rubidium triazine tricarboxylate dihydrate $Rb_3[C_3N_3(CO_2)_3]\cdot 2H_2O$ (**4d**) in the monoclinic space group $P2_1/n$ and cesium triazine tricarboxylate dihydrate $Cs_3[C_3N_3(CO_2)_3]\cdot 2H_2O$ (**4e**) in the orthorhombic space group *Cmcm*. Crystallographic data and details of the structure refinements are summarized in Table 1. In order to accentuate common structural features in the different alkali triazine tricarboxylates and gradual changes with increasing cation radius the crystal structure of **4c**[8] will be briefly included in the following discussion. The analogous sodium salt of triazine tricarboxylate can be synthesized in a similar way as the remaining alkali salts but so far no sample of sodium triazine tricarboxylate crystalline enough for an elucidation of its structure could be obtained. The crystal structures of **4a**, **c**, **d**, **e** comprise alkali ions, triazine tricarboxylate units $(C_3N_3(CO_2)_3)^{3-}$ and crystal water molecules in layer like arrangements. In **4a**, **c**, **d** the carboxylate groups of the anions are slightly tilted out of plane resulting in the molecular symmetry C_3 of the triazine tricarboxylates, whereas in **4e** the triazine tricarboxylates are planar with molecular symmetry C_{3h}. In all salts the C–N bond lengths in the triazine rings (133-134 pm) and the C–O bond lengths in

Table 1. Crystallographic data and details of the structure refinement for $Li_3[C_3N_3(CO_2)_3]\cdot 4H_2O$ (**4a**), $Rb_3[C_3N_3(CO_2)_3]\cdot 2H_2O$ (**4d**) and $Cs_3[C_3N_3(CO_2)_3]\cdot 2H_2O$ (**4e**).

	4a	**4d**	**4e**
molar mass /g·mol^{-1}	302.97	502.53	644.85
crystal system	triclinic	monoclinic	orthorhombic
space group	$P\bar{1}$ (no. 2)	$P2_1/n$ (no. 14)	*Cmcm* (no. 63)
T /K	293	293	293
diffractometer	Nonius Kappa-CCD	Nonius Kappa-CCD	Stoe IPDS
radiation, λ /pm	Mo-K_α, 71.073	Mo-K_α, 71.073	Ag-K_α, 56.087
a /pm	655.10(13)	1038.1(2)	2043.3(4)
b /pm	939.84(19)	687.44(14)	967.51(19)
c /pm	1025.2(2)	1807.9(4)	726.54(15)
α /°	102.81(3)	90	90
β /°	106.56(3)	92.47(3)	90
γ /°	91.38(3)	90	90
V /10^6 pm^3	587.4(2)	1289.0(5)	1436.3(5)
Z	2	4	4
calculated density /g·cm^{-3}	1.713	2.507	2.982
crystal size /mm^3	0.14 x 0.09 x 0.05	0.35 x 0.07 x 0.07	0.08 x 0.05 x 0.05
absorption coefficient /mm^{-1}	0.158	11.386	4.032
F(000)	308	944	1160
absorption correction	none	multi-scan	numerical
min. / max. transmission		0.1334 / 0.3160	0.6187 / 0.6609
diffraction range	$3.26^o \le \theta \le 29.98^o$	$3.17^o \le \theta \le 27.56^o$	$2.88^o \le \theta \le 30.45^o$
index range	$-9 \le h \le 9$	$-13 \le h \le 13$	$-36 \le h \le 36$
	$-13 \le k \le 12$	$-8 \le k \le 8$	$-17 \le k \le 16$
	$-14 \le l \le 14$	$-23 \le l \le 23$	$-13 \le l \le 11$
parameters / restraints	223 / 8	193 / 4	68 / 1
total no. of reflections	6297	19647	15268
no. of independent reflections	3349	2963	2364
no. of observed reflections	2467	2203	1481
min./max. residual electron density /e 10^{-6} pm^{-3}	-0.278 / +0.300	-0.569 / +0.527	-2.654 / +2.054
GooF	1.049	1.049	1.071
final R indices [$I > 2\sigma(I)$]	$R1$ = 0.0429	$R1$ = 0.0342	$R1$ = 0.0442
	$wR2$ = 0.1067 [a)]	$wR2$ = 0.0615 [b)]	$wR2$ = 0.1065 [c)]
final R indices (all data)	$R1$ = 0.0632	$R1$ = 0.0595	$R1$ = 0.0801
	$wR2$ = 0.1170 [a)]	$wR2$ = 0.0697 [b)]	$wR2$ = 0.1293 [c)]

a) $w = [\sigma^2(F_0^2) + (0.0533P)^2 + 0.1410P]^{-1}$, with $P = (F_0^2 + 2F_c^2)/3$

b) $w = [\sigma^2(F_0^2) + (0.0000P)^2 + 1.5124P]^{-1}$, with $P = (F_0^2 + 2F_c^2)/3$

c) $w = [\sigma^2(F_0^2) + (0.0595P)^2 + 3.1384P]^{-1}$, with $P = (F_0^2 + 2F_c^2)/3$

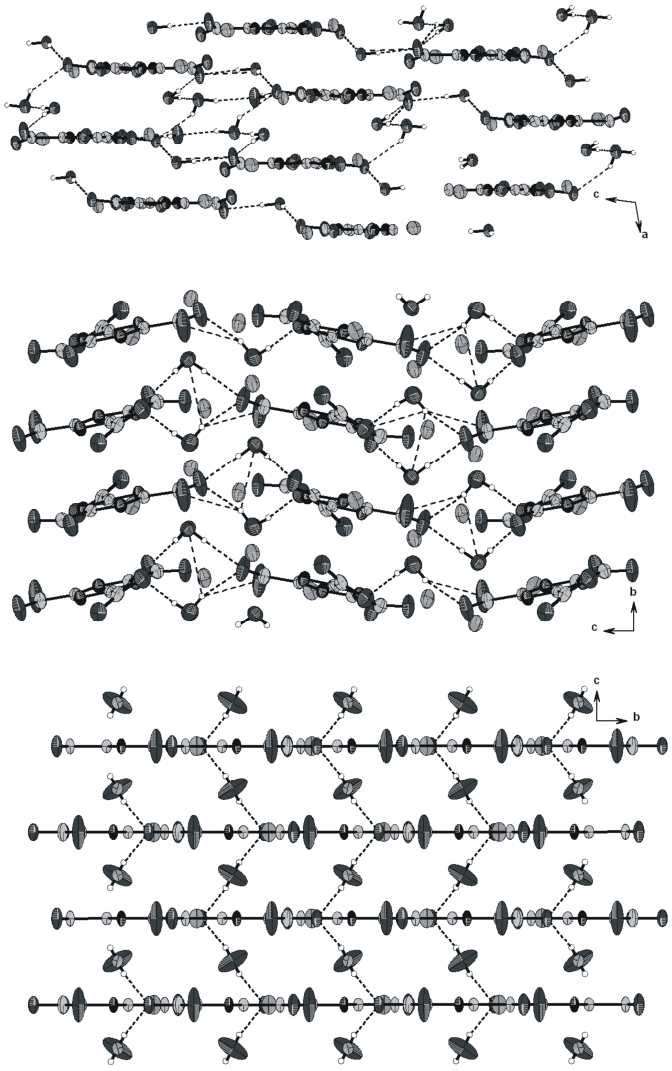

Figure 1. Layered arrangement of triazine tricarboxylate units in the crystal structure of LiTTC·4H_2O (**4a)** (top), RbTTC·2H_2O (**4d**) (middle) and CsTTC·2H_2O (**4e**) (bottom). Dashed lines represent hydrogen bonds. Thermal ellipsoids (except for hydrogen) are drawn at the 50 % probability level.

the carboxylate groups (122-128 pm) resemble those of conjugated double bonds and the C–C bond lengths of 153-154 pm correspond to single bonds. Within the triazine rings the C–N–C angles range between 114-116°, whereas the N–C–N angles are widened to 124-127° due to the carboxylate substituents bound to the carbon atoms of the ring.

The triazine tricarboxylate ions are arranged in layers with interlayer distances of 328 pm (**4a**), 347 pm (**4c**), 345 pm (**4d**) and 363 pm (**4e**), respectively. In **4d** the layers are slightly corrugated, whereas in the remaining salts the layers exhibit a coplanar arrangement (see Figure 1). The metal ions and some of the crystal water molecules are located in the triazine tricarboxylate layers and the remaining water molecules are situated between these layers. All crystal water molecules are part of a hydrogen bonding network in which oxygen atoms of the carboxylate groups and of other water molecules as well as triazine nitrogen atoms act as acceptors. With donor-acceptor distances of 267-295 pm and donor-hydrogen-acceptor angles between 116 and 179° the hydrogen bonds can be classified as medium strong.[10] In **4a**, **4c**, and **4e** hydrogen bonds are formed both within and between the layers, whereas in rubidium triazine tricarboxylate dihydrate **4d**

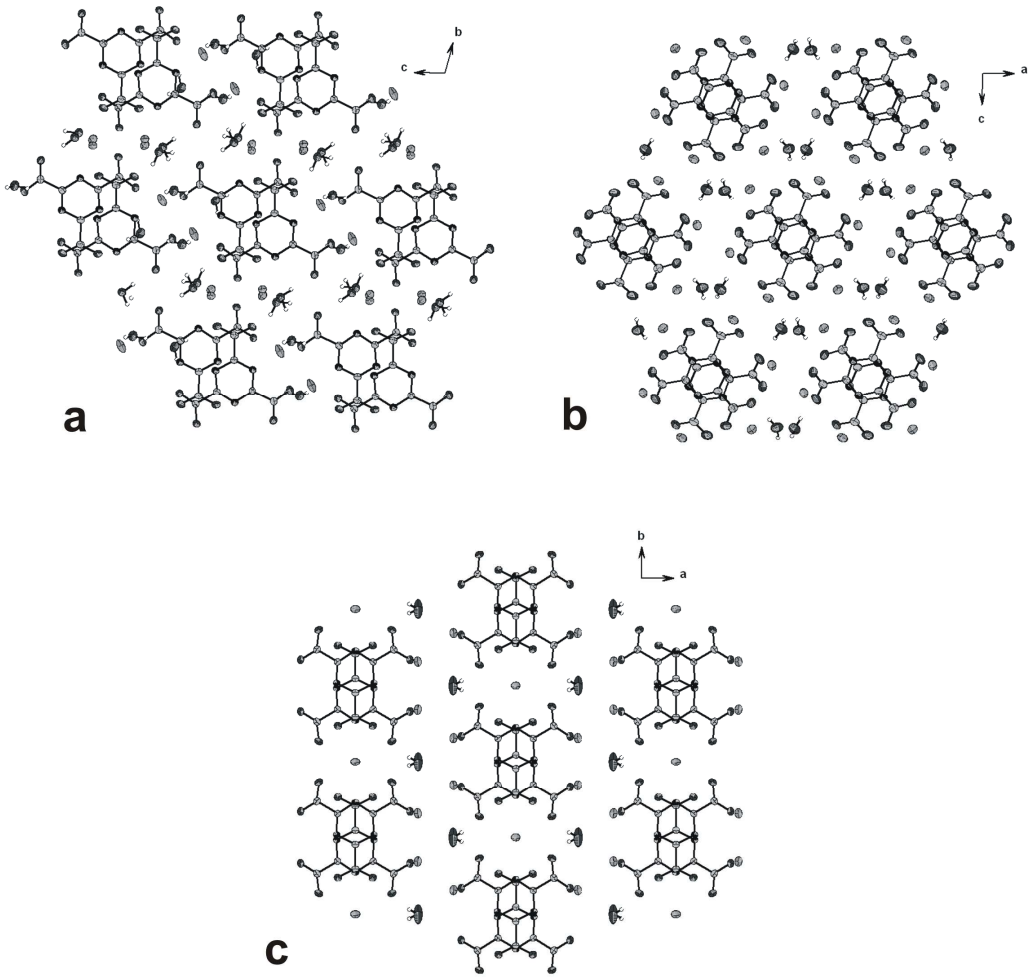

Figure 2. Crystal structure of a) $LiTTC \cdot 4H_2O$ (**4a**), b) $RbTTC \cdot 2H_2O$ (**4d**) and c) $CsTTC \cdot 2H_2O$ (**4e**), representing the varying degrees of stacking between the triazine cores and the strand like (**4a**) or hexagonal arrangement (**4d, e**) of triazine tricarboxylate columns, respectively. Thermal ellipsoids (except for hydrogen) are drawn at the 50 % probability level.

no hydrogen bonds occur that connect adjacent layers (see Figure 1). In this salt the cohesion between the layers is mainly achieved by coordinative interactions and dispersive stacking interactions between the triazine cores. When the structures are viewed perpendicular to the layer planes (see Figure 2) it becomes evident that these stacking interactions are indeed strongest in **4d**. Whereas in **4a** no overlapping between the triazine rings of adjacent layers occurs, the triazine cores overlap half in **4e** and completely in **4d**. The rods of stacked triazine tricarboxylate units are arranged in parallel strands

in **4a** and in a hexagonal pattern in **4d-e** (see Figure 2). A hexagonal arrangement of triazine tricarboxylate columns also occurs in the potassium salt **4c** and merely the alignment of the anions within the columns varies for each salt **4c**-**e**.

The alkali ions are coordinated in the form of irregular polyhedrons by nitrogen atoms of the triazine rings and by oxygen atoms of the crystal water molecules and the carboxylate groups. The coordination number of the alkali ions amounts to 4-5 (**4a**), 5-7 (**4c**), 7 (**4d**) or 10 (**4e**), respectively. In all salts the triazine tricarboxylate units act as tridentate ligands and coordinate the metal ions via two adjacent carboxylate groups and the intermediate nitrogen atom of the ring. In **4c** and **4d** each triazine nitrogen atom is involved in metal coordination so that the triazine tricarboxylates are surrounded symmetrically by three potassium and rubidium atoms, respectively. In contrast, in **4a** and **4e** only one and two thirds of triazine nitrogen atoms, respectively, serve as coordination sites, leading to a strand-like arrangement of triazine tricarboxylates (see Figure 3). The *M*–O distances (Li: 190-251 pm, Rb: 291-355 pm, Cs: 304-378 pm) are

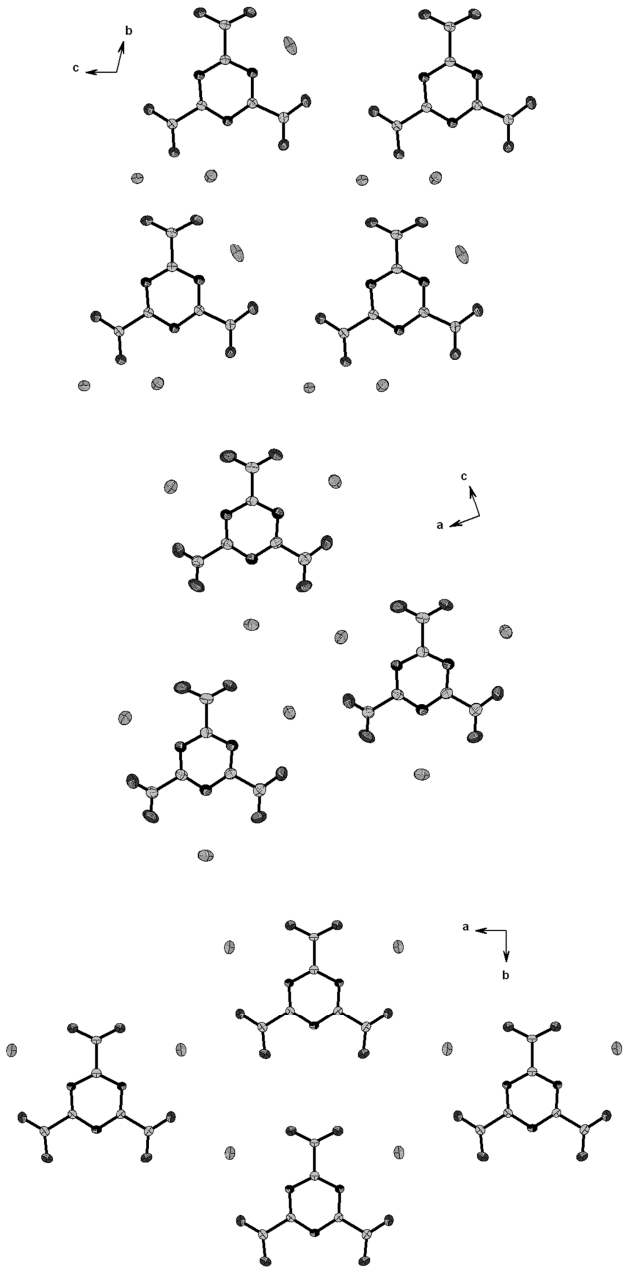

Figure 3. Coordination of alkali metal ions by the triazine tricarboxylate units in $LiTTC \cdot 4H_2O$ (**4a**) (top), $RbTTC \cdot 2H_2O$ (**4d**) (middle) and $CsTTC \cdot 2H_2O$ (**4e**) (bottom). Crystal water molecules are omitted for clarity. Thermal ellipsoids are drawn at the 50 % probability level.

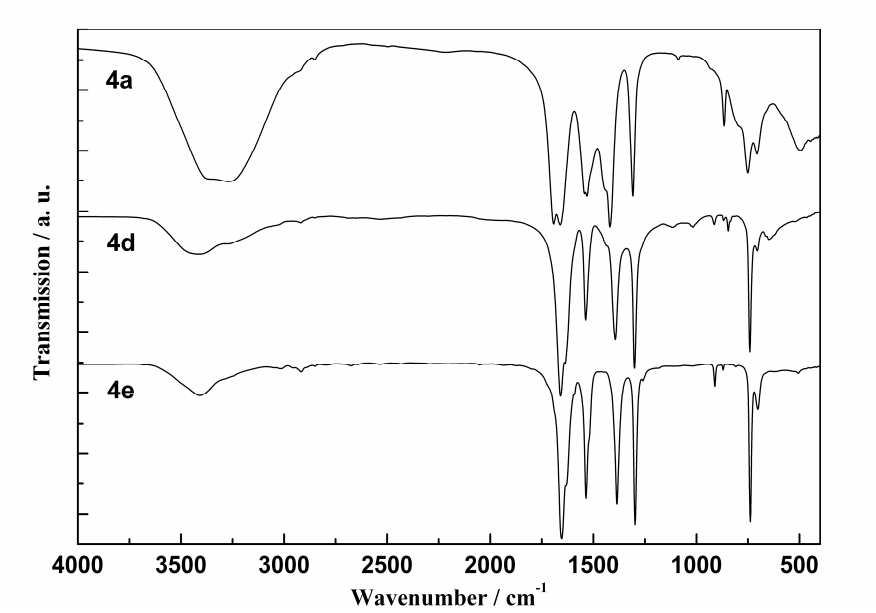

Figure 4. FT-IR spectra of LiTTC·4H_2O (**4a**) (top), RbTTC·2H_2O (**4d**) (middle) and CsTTC·2H_2O (**4e**) (bottom).

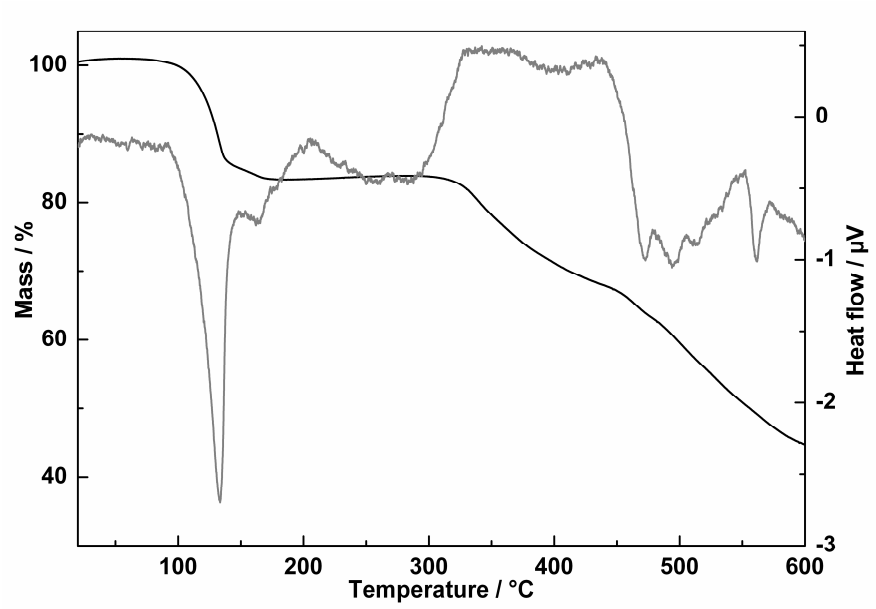

Figure 5. TG (black) and DTA (gray) curves of LiTTC·4H_2O (**4a**), recorded with a heating rate of 5 K·min^{-1}.

in accordance with the ionic radii sums,[11] whereas the *M*–N distances (Li: 204-252 pm, Rb: 295-299 pm, Cs: 320-326 pm) are partially rather short, which indicates a strong contribution of the *s*-triazine cores to metal coordination.

Vibrational Spectroscopy and Thermal Behavior

The alkali triazine tricarboxylates **4a**, **4d**, and **4e** were analyzed by FT-IR spectroscopy. All observed signals can be attributed to vibration modes of the triazine tricarboxylate units and water molecules (see Figure 4). The bending and stretching vibrations of the *s*-triazine core lead to a characteristic signal around 740 cm^{-1} and a group of absorption bands at 1300-1600 cm^{-1}, respectively. The stretching vibrations of the carboxylate groups lead to further signals between 1400 and 1760 cm^{-1} and the OH stretching vibrations of the crystal water molecules to a broad band at 2900-3650 cm^{-1}. The red-shift of these signals to values below 3650 cm^{-1} is in accordance with the crystal structure indicating the presence of medium strong hydrogen bonds.

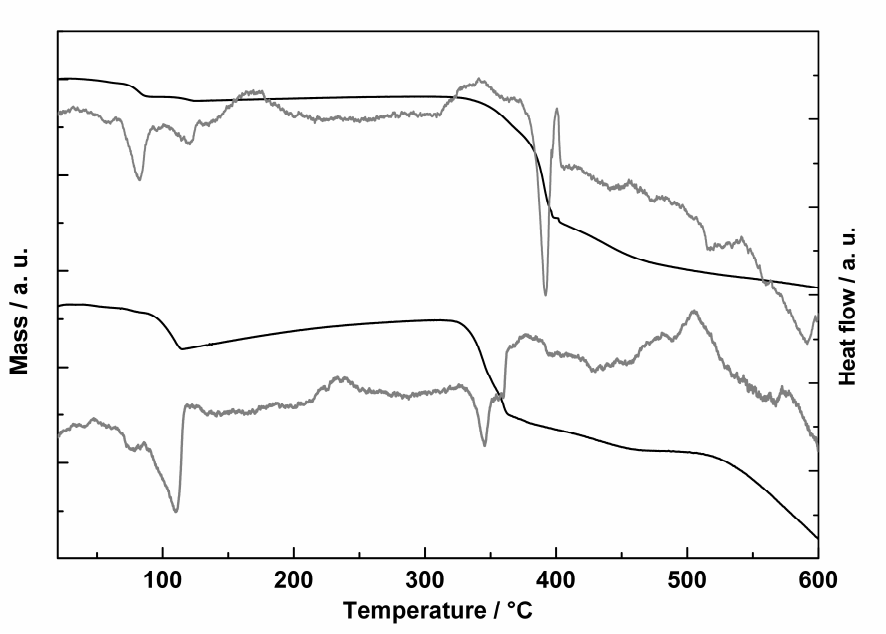

Figure 6. TG (black) and DTA (gray) curves of $RbTTC{\cdot}2H_2O$ (**4d**) (top) and $CsTTC{\cdot}2H_2O$ (**4e**) (bottom), recorded with a heating rate of 5 $K{\cdot}min^{-1}$.

To investigate dehydration and decomposition processes in the alkali triazine tricarboxylates TG and DTA measurements were performed. The obtained TG and DTA curves are displayed in Figure 5 and Figure 6. In all salts the crystal water is released between 70 and 150 °C and the dehydrated compounds are thermally stable up to 300 °C (**4a**) and 320 °C (**4c-e**), respectively. Above these temperatures LiTTC·4H_2O (**4a**) decomposes continuously whereas for RbTTC·2H_2O (**4d**) and CsTTC·2H_2O (**4e**) first a partial mass loss accompanied by a sharp endothermic signal occurs and during further heating the mass loss proceeds slowly and continuously. A similar curve progression was observed for KTTC·2H_2O (**4c**)[8] indicating a comparable thermal behavior and stability for the salts **4c-e**. To examine if the endothermic mass loss in these compounds around 350 °C is caused by a decomposition of the samples or rather indicates a condensation reaction as in other *s*-triazine compounds such as melamine, samples of **4a-e** were heated to 350 °C in closed ampoules. The obtained brownish, X-ray amorphous products were analyzed by FTIR spectroscopy (see Figure 7).

In comparison to the starting materials for **4c-e** an additional absorption band around 2170 cm^{-1} is observed that can be attributed to C≡N stretching vibrations. Furthermore, the intensity of the characteristic bending vibration of the *s*-triazine ring at around 740 cm^{-1} clearly decreases. Therefore it can be assumed that heating of the alkali triazine tricarboxylates does not lead to any cross-linking

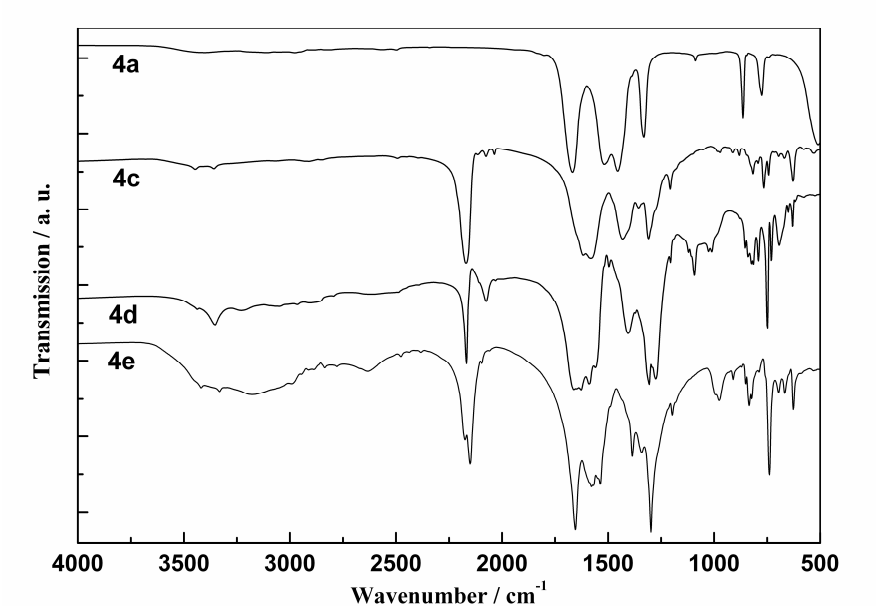

Figure 7. FT-IR spectra of samples obtained by heating LiTTC·4H_2O (**4a**), KTTC·2H_2O (**4c**), RbTTC·2H_2O (**4d**) and CsTTC·2H_2O (**4e**) to 350 °C.

or condensation reactions but that around 350 °C the decomposition of the samples commences, probably via a partial decarboxylation, which is accompanied by a cleavage of the ring. In comparison, in the FT-IR spectrum of a sample of LiTTC·4H_2O (**4a**) heated to 350 °C (see Figure 7) no absorption bands of nitrile stretching vibrations that indicate a cleavage of the ring can be observed. Whereas the thermal decomposition is similar for **4c-e** lithium triazine tricarboxylate tetrahydrate **4a** not only differs from its higher homologues regarding structural motifs but also with respect to its thermal behavior. This observation may be due to the more covalent interaction of the Li^+ ions.

4.1.2.3 Conclusions

We have reported on the synthesis, crystal structure and thermal behavior of three novel alkali triazine tricarboxylates. The multidentate symmetric ligand triazine tricarboxylate represents an interesting linker for coordination networks but only very few examples of its salts have been synthesized and characterized so far. With this contribution we provide the first overview of a series of triazine tricarboxylates and depict similarities as well as gradual changes in the alkali triazine tricarboxylates regarding structural features and thermal behavior. The formation of symmetric structures reflecting the threefold symmetry of the ligand demonstrates the potential of triazine tricarboxylate to be employed as a linker for further symmetric coordination networks.

4.1.2.4 Experimental Section

Syntheses

The alkali triazine tricarboxylates **4a**, **4d**, and **4e** were synthesized in analogy to the procedure described for the potassium salt[6,12] from the respective triethyl ester. The triethyl ester was prepared by the trimerization of ethyl cyanoformate. Dry HCl gas was piped through ethyl cyanoformate (20.0 g, 202 mmol, Aldrich, 99 %) under argon until the product started to precipitate. Afterwards, the conversion was completed by cooling the reaction to 4 °C for 12. The product was filtered, washed with cold water and dried at 75 °C yielding 7.15 g (24 mmol, 36 %) triethyl-*s*-triazine-2,4,6-tricarboxylate as colorless needles. Small amounts of the triethyl ester (250 mg, 0.85 mmol) were treated with a 1 M aqueous solution (ABCR, 99 %) of *M*OH (*M* = Li, Rb, Cs, 10 mL) and the reaction

mixture was stirred at room temperature until the ester was completely dissolved. Afterwards, ethanol (200 mL) was poured into the solution to precipitate the alkali salts. The products were filtered, washed with ethanol and dried at 75 °C to obtain 165 mg (0.54 mmol, 64 %) lithium-1,3,5-triazine-2,4,6-tricarboxylate tetrahydrate (**4a**), 322 mg (0.64 mmol, 75 %) rubidium-1,3,5-triazine-2,4,6-tricarboxylate dihydrate (**4d**) or 396 mg (0.62 mmol, 73 %) cesium-1,3,5-triazine-2,4,6-tricarboxylate dihydrate (**4e**) as colorless powders. Single crystals suitable for X-ray diffraction analyses were obtained by repeated recrystallization of the raw products from aqueous solution at 4 °C.

Elemental analysis (wt. %): $C_3N_3(CO_2Et)_3$: N 14.22 (calcd. 14.13), C 47.20 (calcd. 48.47), H 4.88 (calcd. 5.08); **4a**: Li 7.47 (calcd. 6.87), N 10.26 (calcd. 13.87), C 20.03 (calcd. 23.79), H 2.32 (calcd. 2.66); **4d**: Rb 47.24 (calcd. 51.02), N 6.50 (calcd. 8.36), C 12.14 (calcd. 14.34), H 0.74 (calcd. 0.80); **4e**: N 6.40 (calcd. 6.52), C 10.94 (calcd. 11.18), H 0.58 (calcd. 0.62).

For the thermal treatment of alkali triazine tricarboxylates 30 mg of the respective sample was placed in a dried duran glass tube ($ø_{ext.}$ = 10 mm, $ø_{int.}$ = 8 mm). The tube was filled with argon, sealed at a length of 12 cm and placed in an inclined tube furnace. The samples were heated at 2 $K \cdot min^{-1}$ to 350 °C, held at this temperature for 12 h and cooled to room temperature at 2 $K \cdot min^{-1}$.

X-ray Structure Determination

Single-crystal X-ray diffraction data of **4a** and **4d** were collected at 293 K with a Kappa CCD diffractometer (Mo-K_α radiation, λ = 71.073 pm). The diffraction intensities were scaled using the SCALEPACK[13] software package. For **4a** no additional absorption correction was applied, for **4d** an absorption correction was performed using the program SADABS.[14] Single-crystal X-ray diffraction data of **4e** were collected at 293 K with a Stoe IPDS diffractometer (Ag-K_α radiation, λ = 56.087 pm). For an absorption correction the program XSHAPE[15] (based on the program HABITUS[16]) was used. All crystal structures were solved by direct methods using the software package SHELXS-97 and refined against F^2 by applying the full-matrix least-squares method (SHELXL-97).[17] The hydrogen positions could be determined from difference Fourier syntheses and were refined isotropically using restraints for oxygen-hydrogen distances. All non-hydrogen atoms were refined anisotropically.

CCDC 827795-827797 contain the supplementary crystallographic data for this paper. These data can be obtained free of charge from The Cambridge Crystallographic Data Centre via www.ccdc.cam.ac.uk/data_request/cif.

General Techniques

FT-IR spectra were recorded at ambient conditions between 400 and 4000 cm^{-1} on a Bruker IFS 66v/S spectrometer. The samples were measured as KBr pellets in an evacuated cell. Thermoanalytical measurements were performed under inert atmosphere (He) with a Thermoanalyzer TG-DTA92 (Setaram). The samples were heated in an alumina crucible from room temperature to 600 °C with a heating rate of 5 $K \cdot min^{-1}$. Elemental analyses for C, H and N were performed with the elemental analyzer systems Vario EL and Vario Micro (Elementar Analysensysteme GmbH). The amounts of alkali metals were ascertained by atomic emission spectroscopy with inductively coupled plasma (ICP-AES) using a Varian-Vista simultaneous spectrometer.

Acknowledgments

The authors thank the *Deutsche Forschungsgemeinschaft* (DFG) (project SCHN 377/15) and the *Fonds der Chemischen Industrie* (FCI) for financial support and *Sandra Albrecht*, *Dr. Peter Mayer* and *Thomas Miller* (all Department Chemie, LMU München) for the single-crystal data collection.

4.1.2.5 Bibliography

[1] a) P. Kuhn, M. Antonietti, A. Thomas, *Angew. Chem.* **2008**, *120*, 3499; *Angew. Chem. Int. Ed.* **2008**, *47*, 3450; b) P. Kuhn, A. Forget, D. Su, A. Thomas, M. Antonietti, *J. Am. Chem. Soc.* **2008**, *130*, 13333; c) P. Kuhn, A. Thomas, M. Antonietti, *Macromolecules* **2009**, *42*, 319.

[2] For reviews, see: a) G. Goglio, D. Foy, G. Demazeau, *Mater. Sci. Eng. R* **2008**, *58*, 195; b) E. Kroke, M. Schwarz, *Coord. Chem. Rev.* **2004**, *248*, 493; c) A. Thomas, A. Fischer, F. Goettmann, M. Antonietti, J.-O. Müller, R. Schlögl, J. M. Carlsson, *J. Mater. Chem.* **2008**, *18*, 4893.

[3] For reviews, see, for example: a) A. U. Czaja, N. Trukhan, U. Müller, *Chem. Soc. Rev.* **2009**, *38*, 1284; b) R. J. Kuppler, D. J. Timmons, Q.-R. Fang, J.-R. Li, T. A. Makal, M. D. Young, D. Yuan, D. Zhao, W. Zhuang, H.-C. Zhou, *Coord. Chem. Rev.* **2009**, *253*, 3042.

[4] See, for example: a) D. N. Dybtsev, H. Chun, K. Kim, *Chem. Commun.* **2004**, 1594; b) M.-X. Li, Z.-X. Miao, M. Shao, S.-W. Liang, S.-R. Zhu, *Inorg. Chem.* **2008**, *47*, 4481; c) S. Ma, D. Sun, M. Ambrogio, J. A. Fillinger, S. Parkin, H.-C. Zhou, *J. Am. Chem. Soc.* **2007**, *129*, 1858; d) S. Ma, X.-S. Wang, D. Yuan, H.-C. Zhou, *Angew. Chem.* **2008**, *120*, 4198; *Angew. Chem. Int. Ed.* **2008**, *47*, 4130; e) Y. K. Park, S. B. Choi, H. Kim, K. Kim, B.-H. Won, K. Choi, J.-S. Choi, W.-S. Ahn, N. Won, S. Kim, D. H. Jung, S.-H. Choi, G.-H. Kim, S.-S. Cha, Y. H. Jhon, J. K. Yang, J. Kim, *Angew. Chem.* **2007**, *119*, 8378; *Angew. Chem. Int. Ed.* **2007**, *46*, 8230; f) D. Sun, S. Ma, Y. Ke, D. J. Collins, H.-C. Zhou, *J. Am. Chem. Soc.* **2006**, *128*, 3896; g) D. Sun, S. Ma, Y. Ke, T. M. Petersen, H.-C. Zhou, *Chem. Commun.* **2005**, 2663.

[5] See, for example: a) S. S.-Y. Chui, S. M.-F. Lo, J. P. H. Charmant, A. G. Orpen, I. D. Williams, *Science* **1999**, *283*, 1148; b) J. Kim, B. Chen, T. M. Reineke, H. Li, M. Eddaoudi, D. B. Moler, M. O'Keeffe, O. M. Yaghi, *J. Am. Chem. Soc.* **2001**, *123*, 8239; c) O. M. Yaghi, G. Li, H. Li, *Nature* **1995**, *378*, 703.

[6] C. Grundmann, E. Kober, *J. Org. Chem.* **1956**, *21*, 1392.

[7] J.-R. Galán-Mascarós, J.-M. Clemente-Juan, K. R. Dunbar, *J. Chem. Soc., Dalton Trans.* **2002**, *13*, 2710.

[8] S. J. Makowski, M. Hörmannsdorfer, W. Schnick, *Z. Anorg. Allg. Chem.* **2010**, *636*, 2584.

[9] S. J. Makowski, E. Calta, M. Hörmannsdorfer, W. Schnick, *in preparation*.

[10] T. Steiner, *Angew. Chem.* **2002**, *114*, 50; *Angew. Chem. Int. Ed.* **2002**, *41*, 48.

[11] R. D. Shannon, *Acta Crystallogr., Sect. A* **1976**, *32*, 751.

[12] E. Ott, *Ber. Dtsch. Chem. Ges.* **1919**, *52*, 656.

[13] Z. Otwinowski, W. Minor, *Methods Enzymol.* **1997**, *276*, 307.

[14] G. M. Sheldrick, *SADABS, Version 2* **2001**.

[15] XSHAPE, *Crystal Optimisation for Numerical Absorption Correction*, v1.05, Stoe & Cie GmbH Darmstadt **1999**.

[16] W. Herrendorfer, H. Bärninghausen, *HABITUS, A Programm for Crystal Shape Optimization and Numerical Absorption Correction*, Universitäten Gießen und Karlsruhe **1996**.

[17] a) G. M. Sheldrick, *SHELXS-97, Program for the Solution of Crystal Structures*, Universität Göttingen, Germany **1997**; b) G. M. Sheldrick, *SHELXL-97, Program for the Refinement of Crystal Structures*, Universität Göttingen, Germany **1997**; c) G. M. Sheldrick, *Acta Crystallogr., Sect. A* **2008**, *64*, 112.

4.2 Triazine Tricarboxylates with Divalent Cations

Investigation of the Hydrolysis Stability of Triazine Tricarboxylate in the Presence of Transition Metal(II) Ions and Synthesis and Crystal Structure of the Alkaline Earth Triazine Tricarboxylates $M_3[C_3N_3(CO_2)_3]_2 \cdot 12H_2O$ (M = Sr, Ba)

Sophia J. Makowski, Evelyn Calta, Michael Hörmannsdorfer, and Wolfgang Schnick

published in: *Z. Anorg. Allg. Chem.* **2012**, *638*, 345. DOI: 10.1002/zaac.201100377

Keywords: Alkaline earth metals; Crystal structure; Hydrolysis; Reaction mechanism; *s*-Triazine

Abstract. The stability against hydrolysis of triazine tricarboxylate (TTC) in the presence of divalent transition metal and alkaline earth ions was investigated by means of X-ray diffraction and FTIR spectroscopy. Depending on the size of the cation either formation of the respective triazine tricarboxylate salts or hydrolysis of TTC yielding oxalate was observed. The hydrolysis of TTC induced by transition metal ions could be explained in analogy to the hydrolysis of triazine tris(2-pyrimidyl) as a result of ring tension caused by the coordination of these ions. By the reaction of potassium triazine tricarboxylate with alkaline earth salts in aqueous solution the alkaline earth triazine tricarboxylates $M_3[C_3N_3(CO_2)_3]_2 \cdot 12H_2O$ (M = Sr, Ba) were obtained and analyzed by single-crystal X-ray diffraction. The isotypic salts represent the first examples of alkaline earth triazine tricarboxylates and the first TTC salts comprising solely divalent cations.

4.2.1 Introduction

The *s*-triazine core (C_3N_3) is widely employed as building unit in various fields, such as polymer, organic, solid-state or coordination chemistry. In coordination compounds, *s*-triazine based ligands are of interest because next to functional groups bound to the *s*-triazine core also the nitrogen atoms of the ring can act as coordination sites. Ligands which are commonly used for the synthesis of coordination networks and metal organic frameworks (MOFs) mostly comprise aromatic hydrocarbon rings bound to the *s*-triazine core, for instance *s*-triazine-2,4,6-tris(4-pyridyl) (**1a**), *s*-triazine-2,4,6-tris(3-pyridyl) (**1b**) or *s*-triazine-2,4,6-triyl-tribenzoic acid (**1c**) (see Scheme 1).[1] Contrary, further *s*-triazine derivatives capable of metal coordination which mainly consist of carbon and nitrogen (e. g. tri-cyanomelaminates, **2**)[2] are rather considered as solid-state precursors for covalent carbon nitride networks and not as ligands for coordination networks. The only *s*-triazine compound that is frequently employed as ligand in coordination networks which does not comprise any hydrocarbon cycles is cyanuric acid **3**.[3]

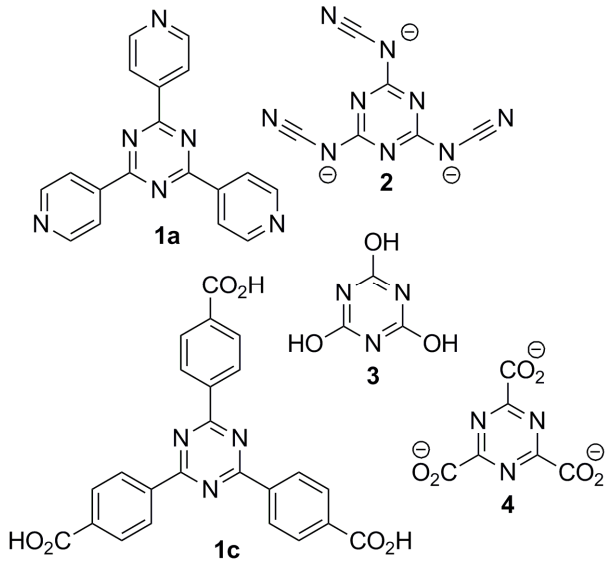

Scheme 1. *s*-Triazine compounds: *s*-triazine-2,4,6-tris(4-pyridyl) (**1a**), *s*-triazine-2,4,6-triyl-tribenzoic acid (**1c**), tricyanomelaminate (**2**), cyanuric acid (**3**) and triazine tricarboxylate **(4)**.

However, further extension of coordination chemistry to such *s*-triazine compounds might facilitate the access to several new coordination networks possibly featuring interesting properties. In this regard we are especially interested in *s*-triazine containing ligands that can be regarded as intermediates between organic *s*-triazine ligands such as **1a-c** and pure carbon nitrides such as **2**. A ligand we have started to study in detail in this context is triazine tricarboxylate (**4**, TTC) (see Scheme 1). The first synthesis of a triazine tricarboxylate salt was already published in 1956[4] but a detailed characterization of structures and properties of triazine tricarboxylates was conducted only recently.[5,6] Interestingly, although TTC appears to be a suitable multi-dentate ligand for MOFs due to its structural similarity to benzene tricarboxylate (**5**), a compound that has already been applied as

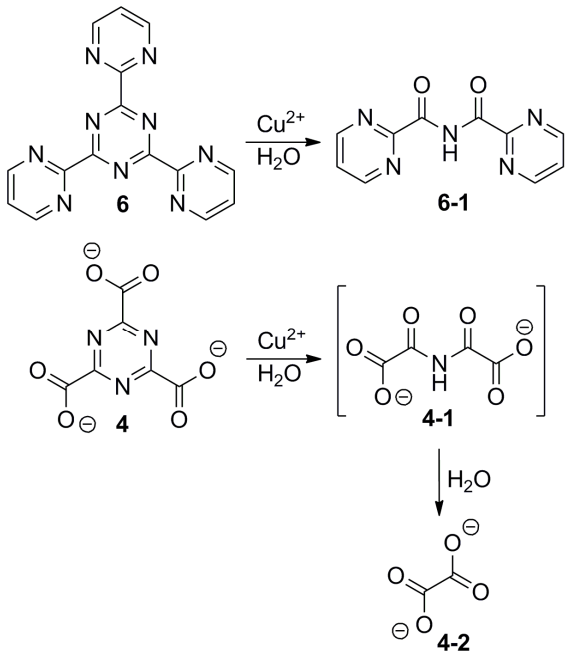

Scheme 2. Hydrolysis of triazine tris(2-pyrimidyl) (**6**) to bis(2-pyrimidylcarbonyl)amine (**6-1**) and of triazine tricarboxylate (**4**) to oxalate (**4-2**).

linker in numerous MOFs,[7] no three-dimensional coordination networks of TTC have been reported so far.[8] In fact, only one TTC compound with multivalent cations is known, namely K{Fe(1,3,5-triazine-2,4,6-tricarboxylate)$(H_2O)_2$}·$2H_2O$ (KFeTTC·$4H_2O$) (**4a**) comprising one-dimensional chains of Fe^{2+} and TTC. A potential analogous reaction with other divalent transition metals is mentioned in the same publication but difficulties in obtaining crystalline products sufficient for a structural characterization have been reported.[5] During our attempts to prepare novel triazine tricarboxylates of various transition metals, we had to focus similar problems. Efforts to increase the crystallinity of products by slow diffusion reactions or hydrothermal treatment eventually resulted in the formation of crystalline products which, however, appeared to be only decomposition products of TTC. Due to this observation we started to study the reaction of TTC and divalent metal ions in more detail.

In this contribution we present a systematic investigation of the stability of triazine tricarboxylate towards hydrolysis in the presence of divalent metal ions. The dependence of stability on the size of the counterion and with it attributed sterical reasons is discussed and compared with other *s*-triazine based linkers. Furthermore, synthesis and crystal structures of the first alkaline earth triazine tricarboxylates $M_3[C_3N_3(CO_2)_3]_2 \cdot 12H_2O$ (M = Sr, Ba) are presented. Thereby, this study leads to a better understanding of the coordination properties of the linker triazine tricarboxylate and emphasizes possibilities and limitations for the synthesis of novel divalent triazine tricarboxylates.

4.2.2 Results and Discussion

The Reaction of Triazine Tricarboxylate with Transition Metal(II) Salts

For the attempted synthesis of TTC salts of divalent transition metals via metathesis reactions aqueous solutions of potassium triazine tricarboxylate dihydrate $K_3[C_3N_3(CO_2)_3]\cdot 2H_2O$ (**4b**, K-TTC·$2H_2O$) were combined with aqueous solutions of different transition metal chlorides MCl_2 (*M* = Mn, Co, Ni, Cu, Zn). The poorly soluble products that precipitated immediately were filtered, washed and dried.

To increase the crystallinity of products the reactions were additionally conducted under hydrothermal conditions or by slow diffusion reactions using agar gels. In most cases, crystalline products were identified by single-crystal and powder X-ray diffraction as the respective transition metal oxalates. The formation of oxalates can be explained by hydrolytic decomposition of triazine tricarboxylate as shown in Scheme 2. To rule out that this decomposition occurs only due to the elevated temperatures during hydrothermal reactions or as a result of the usage of agar gels we additionally examined the poorly crystalline materials obtained by metathesis reactions in solution at room temperature.

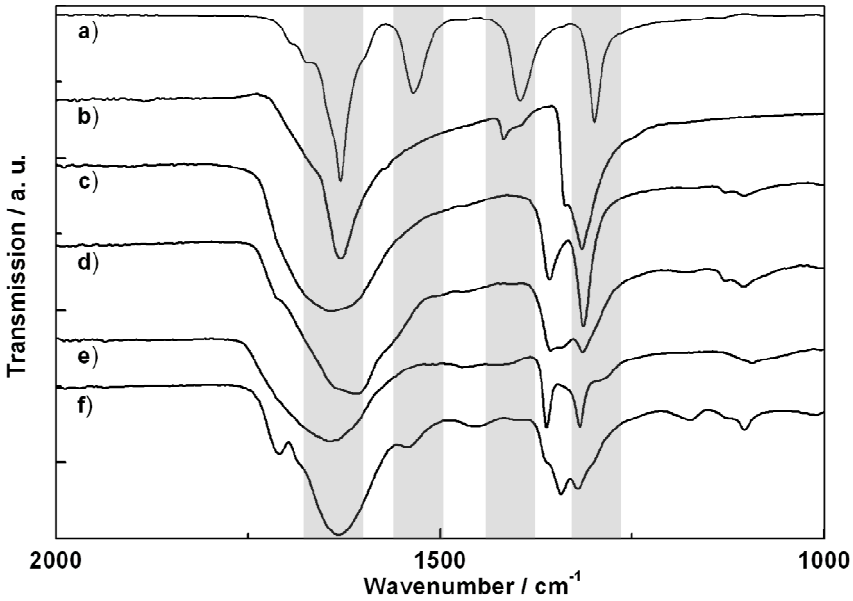

Figure 1. FTIR spectra of a) K-TTC·$2H_2O$ (**4b**), b) sodium oxalate and c)-f) of the products obtained by the reaction of K-TTC·$2H_2O$ (**4b**) with c) $CoCl_2$, d) $NiCl_2$, e) $CuCl_2$ and f) $ZnCl_2$. Gray areas highlight the characteristic absorption bands of triazine tricarboxylate.

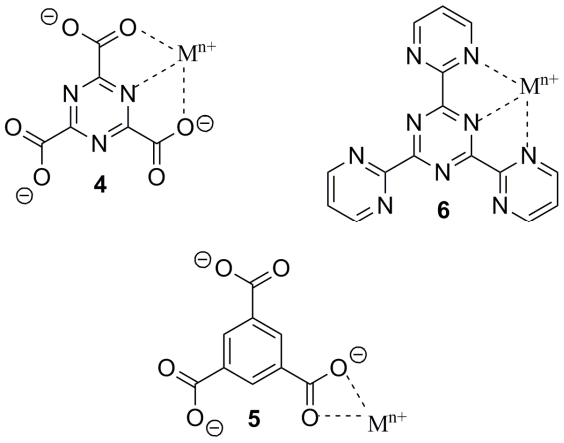

Scheme 3. Coordination of metal ions by triazine tricarboxylate (**4**), benzene tricarboxylate (**5**) and triazine tris(2-pyrimidyl) (**6**).

These samples were analyzed by FTIR spectroscopy, a method that allows for a reliable distinction between triazine tricarboxylate and oxalate units. The obtained IR spectra in comparison to the IR spectra of the triazine tricarboxylate salts **4a** and **4b** and of sodium oxalate are shown in Figures 1 and 2. Between 1200 and 1700 cm^{-1} the TTC unit leads to four characteristic absorption bands which can be attributed to the stretching vibrations of the carbonyl groups and the *s*-triazine ring. Based on the presence or absence of these signals it can be analyzed if the samples contain TTC units. It was observed that the TTC units are decomposed to oxalates in the presence of Co^{2+}, Ni^{2+}, Cu^{2+} and Zn^{2+} (see Figure 1) but not in the presence of Fe^{2+} and Mn^{2+} (see Figure 2).[5] To elucidate the reason for the differing stability of TTC

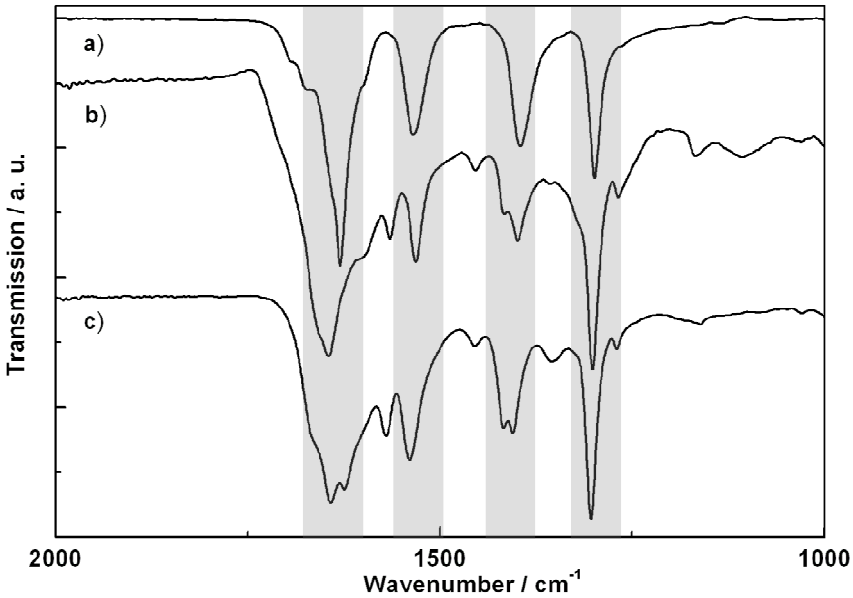

Figure 2. FTIR spectra of a) K-TTC·$2H_2O$ (**4b**), b) KFe-TTC·$4H_2O$ (**4a**) and c) product obtained by the reaction of K-TTC·$2H_2O$ (**4b**) and $MnCl_2$ in aqueous solution. Gray areas highlight the characteristic absorption bands of triazine tricarboxylate.

dependent on the transition metal we beheld the coordination motifs in different structurally characterized triazine tricarboxylates more closely. Both in KFe-TTC·4H_2O (**4a**) and in all known alkali triazine tricarboxylates metal ions are coordinated by the TTC units via two adjacent carboxylate groups and the intermediate nitrogen atom of the ring.[5,6] In contrast, the analogous hydrocarbon compound benzene tricarboxylate (**5**) coordinates merely via the carboxylate groups so that metal ions are bound less tight to **5** than to TTC. The coordination motif observed for TTC resembles rather that of *s*-triazine-2,4,6-tris(2-pyrimidyl) (**6**, TPymT) (see Scheme 3). Whereas benzene tricarboxylate (**5**) is indeed stable against aqueous solutions of transition metal ions even under hydrothermal conditions [7] for TPymT (**6**) hydrolysis in aqueous solutions of Cu^{2+} salts is a commonly observed reaction.[9,10] The hydrolysis of TPymT leads to the formation of bis(2-pyrimidyl-carbonyl)amine **6-1**. The hydrolytic decomposition of TTC (**4**) to oxalate **4-2** can be explained by an analogous mechanism (see Scheme 2). However, whereas the intermediate **4-1** cannot be isolated the respective compound **6-1** represents the final reaction product allowing a detailed investigation of bond lengths and angles in the crystal. *Lerner* et al. explained the decomposition of **6** as a result of destabilization of the *s*-triazine ring upon coordination: Binding of copper ions causes the involved pyrimidyl rings to move

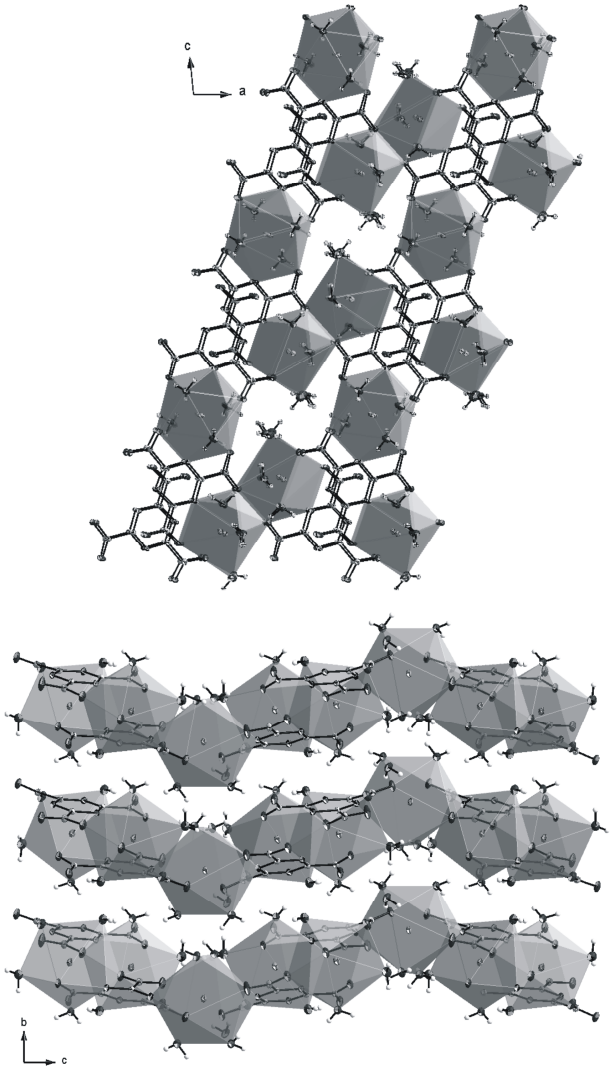

Figure 3. Metal coordination in the crystal structure of Sr-TTC·6H_2O (**8a**) and Ba-TTC·6H_2O (**8b**). Thermal ellipsoids (except for hydrogen) are drawn at the 50 % probability level.

Table 1. Crystallographic data and details of the structure refinement for $Sr_3[C_3N_3(CO_2)_3]_2 \cdot 12H_2O$ (**8a**) and $Ba_3[C_3N_3(CO_2)_3]_2 \cdot 12H_2O$ (**8b**).

	$Sr_3[C_3N_3(CO_2)_3]_2 \cdot 12H_2O$	$Ba_3[C_3N_3(CO_2)_3]_2 \cdot 12H_2O$
molar mass /g·mol^{-1}	899.23	1048.36
crystal system	monoclinic	monoclinic
space group	$P2_1/n$ (no. 14)	$P2_1/n$ (no. 14)
T /K	173	173
diffractometer	Nonius Kappa-CCD	Nonius Kappa-CCD
radiation, λ /pm	Mo-K_α, 71.073	Mo-K_α, 71.073
a /pm	1005.4(2)	1020.9(2)
b /pm	1302.7(3)	1337.4(3)
c /pm	2107.2(4)	2139.5(4)
β /°	97.36(3)	95.71(3)
V /10^6 pm^3	2737.1(10)	2906.6(10)
Z	4	4
calculated density /g·cm^{-3}	2.182	2.396
crystal size /mm^3	0.14 x 0.11 x 0.10	0.09 x 0.07 x 0.04
absorption coefficient /mm^{-1}	5.941	4.129
F(000)	1776	1992
absorption correction	multi-scan	multi-scan
min. / max. transmission	0.4270 / 0.5433	0.6322 / 0.7876
diffraction range	$3.28^o \leq \theta \leq 27.58^o$	$3.19^o \leq \theta \leq 27.49°$
index range	$-13 \leq h \leq 13$, $-16 \leq k \leq 16$	$-13 \leq h \leq 13$, $-16 \leq k \leq 17$
	$-27 \leq l \leq 27$	$-27 \leq l \leq 27$
parameters / restraints	478 / 24	478 / 24
total no. of reflections	44575	52024
no. of independent reflections	6286	6665
no. of observed reflections	4809	5596
min./max. res. electron dens. /e 10^{-6} pm^{-3}	-0.656 / +1.148	-0.980 / +0.942
GooF	1.017	1.107
final R indices [$I > 2\sigma(I)$]	$R1 = 0.0303$, $wR2 = 0.0611$ [a)]	$R1 = 0.0227$, $wR2 = 0.0463$ [b)]
final R indices (all data)	$R1 = 0.0502$, $wR2 = 0.0682$ [a)]	$R1 = 0.0321$, $wR2 = 0.0499$ [b)]

a) $w = [\sigma^2(F_0^2) + (0.0251P)^2 + 3.5914P]^{-1}$, with $P = (F_0^2 + 2\,F_c^2)/3$

b) $w = [\sigma^2(F_0^2) + (0.0154P)^2 + 3.7650P]^{-1}$, with $P = (F_0^2 + 2\,F_c^2)/3$

closer to each other and hence decreases the N–C–C angles at the carbon atoms of the *s*-triazine ring from ideal 120° close to 110°. This angular strain in the *s*-triazine ring facilitates hydrolysis leading to the formation of **6-1**.[10] These mechanistic considerations can be transferred to the decomposition of TTC (**4**) matching very well the observed differences in stability against hydrolysis dependent on the metal ions when the ionic radii are compared. For Mn^{II}, Fe^{II} and Co^{II} the values for high-spin complexes were taking into account because magnetic measurements of KFe-TTC·4H_2O (**4a**) revealed

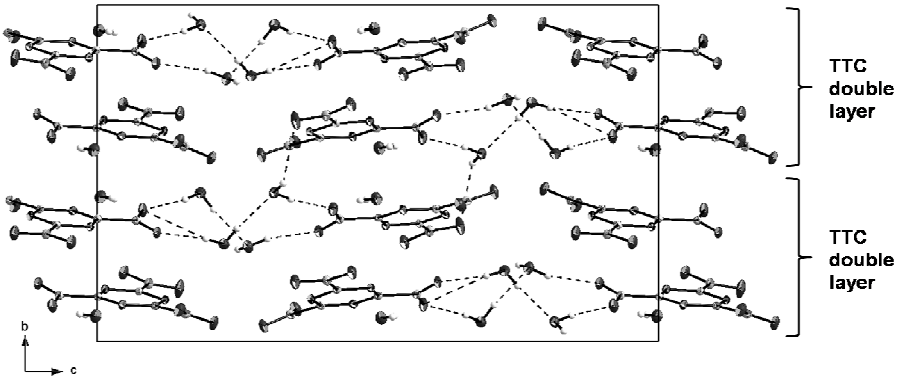

Figure 4. Exemplary illustration of the superstructure along *b* in the crystal structure of Sr-TTC·6H_2O (**8a**) and Ba-TTC·6H_2O (**8b**) caused by differences in the hydrogen bonding network (dashed lines). Further hydrogen bonds and metal ions are omitted for clarity. Thermal ellipsoids (except for hydrogen) are drawn at the 50 % probability level.

a high-spin state of Fe^{II} ions.[5] The ionic radii (CN = 6, in Å) of M^{II} ions are as follows:[11] 0.97 (Mn), 0.92 (Fe), 0.89 (Co), 0.83 (Ni), 0.87 (Cu), 0.88 (Zn). Hence the ionic radii of metal ions and consequently the *M*–O and *M*–N bond lengths in the crystal are largest for Mn^{II} and Fe^{II}. According to the above considerations for Co^{II}, Ni^{II} and Cu^{II} a decrease in *M*–O and *M*–N bond lengths between metal ions and TTC increases the angular strain in the *s*-triazine ring and therefore facilitates a hydrolytic cleavage of TTC.

Table 2. N–C–C angles (in °) of the triazine tricarboxylate units in Sr-TTC·6H_2O (**8a**), Ba-TTC·6H_2O (**8b**) and KFe-TTC·4H_2O (**4a**).[5] The assignment of angles is given in Figure 5.

	Sr-TTC·6H_2O (**8a**)	Ba-TTC·6H_2O (**8b**)	KFe-TTC·4H_2O (**4a**)
$\alpha 1$	115.1	115.1	114.5
$\alpha 2$	117.0	117.2	114.5
$\beta 1$	119.5	119.5	121.0
$\beta 2$	118.3	118.4	121.0
$\gamma 1$	118.8	118.3	117.1
$\gamma 2$	116.7	116.8	117.1

These results indicate that as for TPymT the number of accessible TTC coordination compounds is probably limited and allow for an improved planning of syntheses. We assume that it might be possible to prepare coordination networks comprising triazine tricarboxylate units avoiding the hydrolysis by one of the methods that have already successfully been employed for the synthesis of TPymT complexes:[12] (I) the use of large metal ions like Pb^{2+} that form long and weak bonds to the triazine ring, (II) the addition of a second strongly coordinating ligand which prevents a tight binding of metal ions to TTC, (III) syntheses under anhydrous conditions. Although

the starting material potassium triazine tricarboxylate dihydrate (**4b**) is insoluble in common organic solvents the use of polar ionic liquids might enable anhydrous syntheses.

The Reaction of Triazine Tricarboxylate with Alkaline Earth Salts

In analogy to the reaction with transition metal salts potassium triazine tricarboxylate dihydrate (**4b**) was also reacted with $MCl_2 \cdot xH_2O$ (M = Mg, Ca, Sr, Ba) in aqueous solution. Analysis of the obtained insoluble poorly crystalline powders by FTIR spectroscopy and elemental analysis indicated the presence of alkaline earth TTC salts as could be expected due to the rather large size of the alkaline earth ions. Metathesis reactions in agar gels yielded single crystals of strontium triazine tricarboxylate hexahydrate $Sr_3[C_3N_3(CO_2)_3]_2 \cdot 12H_2O$ (Sr-TTC·$6H_2O$) (**8a**) and barium triazine tricarboxylate hexahydrate $Ba_3[C_3N_3(CO_2)_3]_2 \cdot 12H_2O$ (Ba-TTC·$6H_2O$) (**8b**). Both salts are isotypic and crystallize in the monoclinic space group $P2_1/n$. Crystallographic data and details of the structure refinements are summarized in Table 1. In the crystal the triazine tricarboxylate ions are arranged in layers perpendicular to [010] with interlayer distances of 328 pm (**8a**) and 337 pm (**8b**), respectively. Within the layers the TTC units are not coplanar but are slightly tilted out of the *ca*-plane forming corrugated layers. Crystal water molecules are located both within and between these layers and connect the TTC units via medium strong hydrogen bonds.[13] The triazine

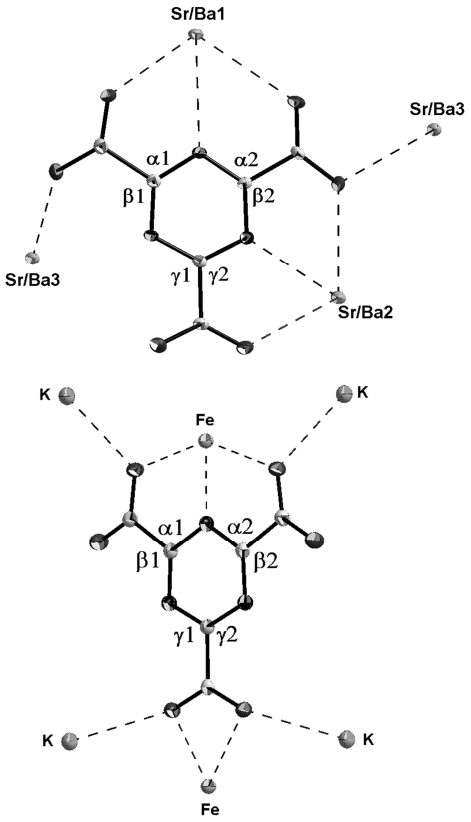

Figure 5. Representation of the coordination of metal ions by triazine tricarboxylate in Sr-TTC·$6H_2O$ (**8a**) and Ba-TTC·$6H_2O$ (**8b**), respectively (top) and in KFe-TTC·$4H_2O$ (**4a**) (bottom) and labeling of N–C–C angles referring to Table 2. The bottom picture was drawn using the electronic cif-file provided as supplementary data for **4a**.[5]

Table 3. *M*–O and *M*–N distances (in pm) in Sr-TTC·6H_2O (**8a**) and Ba-TTC·6H_2O (**8b**), standard deviations in parentheses.

Sr1	- O13	260.6(2)	Ba1	- O5	278.2(2)
Sr1	- O14	262.6(2)	Ba1	- O13	280.0(2)
Sr1	- O5	265.2(2)	Ba1	- O14	280.2(2)
Sr1	- O12	272.5(2)	Ba1	- O12	282.3(2)
Sr1	- O22	272.7(2)	Ba1	- O7	286.1(2)
Sr1	- O7	273.4(2)	Ba1	- O24	288.5(2)
Sr1	- O24	276.4(2)	Ba1	- O22	289.3(2)
Sr1	- O4	286.1(2)	Ba1	- O4	293.3(2)
Sr1	- N4	271.9(2)	Ba1	- N4	287.2(2)
Sr1	- N2	275.8(2)	Ba1	- N2	290.6(2)
Sr2	- O8	255.1(2)	Ba2	- O11	271.7(2)
Sr1	- O11	257.0(2)	Ba2	- O8	274.1(2)
Sr2	- O19	260.0(2)	Ba2	- O16	278.3(3)
Sr2	- O20	261.2(2)	Ba2	- O3	278.7(2)
Sr2	- O16	262.6(2)	Ba2	- O19	278.9(2)
Sr2	- O2	271.8(2)	Ba2	- O20	279.7(2)
Sr2	- O3	278.0(2)	Ba2	- O2	289.3(2)
Sr2	- N1	268.0(2)	Ba2	- N1	286.3(2)
Sr3	- O18	256.8(2)	Ba3	- O6	273.2(2)
Sr3	- O3	256.9(2)	Ba3	- O3	274.4(2)
Sr3	- O15	258.7(2)	Ba3	- O18	276.7(2)
Sr2	- O6	259.2(2)	Ba3	- O15	277.1(3)
Sr2	- O17	263.3(2)	Ba3	- O17	281.3(2)
Sr3	- O9	268.9(2)	Ba3	- O8	284.7(2)
Sr3	- O8	292.6(2)	Ba3	- O9	289.0(2)
Sr3	- N5	273.7(2)	Ba3	- N5	289.7(2)

cores of TTC entities of adjacent layers do not overlap but are shifted against each other and alternately rotated by 180°. The so formed double columns of TTC units are arranged in strands (see Figure 3 top). Alkaline earth ions are located between these strands and coordinated by the TTC units and crystal water molecules. Within the TTC strands each metal ion is coordinated by two adjoining TTC entities (CN = 10) and between the strands four TTC units of two adjacent layers together coordinate two metal ions (CN = 8) (see Figure 3 top). Between these TTC double layers no metal ions are located (see Figure 3 bottom). Along *b* adjacent double layers differ only with respect to the orientation of crystal water molecules and slight variations in torsion of the carboxyl groups. This superstructure can be explained by small differences regarding the formation of preferred hydrogen bonds. Because the water molecules are part of an extended hydrogen bonding network there is a relation between the orientation of all water molecules and carboxyl groups. As is exemplary shown in Figure 4 rotation of one water molecule requires also the reorientation of adjacent water molecules and carboxyl groups so that these can serve most suitable as donors and acceptors, respectively, for hydrogen bonds.

Each triazine tricarboxylate coordinates two metal ions closely via two carboxylate groups and the intermediate nitrogen atom of the *s*-triazine ring, whereas further metal ions are coordinated solely via the carboxylate groups but without short *M*–N contacts. The coordination motifs in Sr-TTC·6H_2O (**8a**) and Ba-TTC·6H_2O (**8b**), respectively, and KFe-TTC·4H_2O (**4a**)[5] are shown in Figure 5. A comparison of the labeled N–C–C angles (see Table 2) demonstrates that coordination of Sr^{2+} and Ba^{2+}

causes less distortion of TTC than coordination of Fe^{2+}. Consistently, each TTC unit in **8a** and **8b** can coordinate closely two alkaline earth atoms without being hydrolyzed. Both *M*–O distances (Sr: 255-293 pm, Ba: 272-293 pm) and *M*–N distances (Sr: 268-276 pm, Ba: 286-291 pm) (see Table 3) are in accordance with the ionic radii sums.[11] The C–N bond lengths of the *s*-triazine rings (133-135 pm) and the C–O bond lengths of the carboxylate groups (123-126 pm) resemble those of conjugated double bonds, whereas the C–C bond lengths (153-155 pm) correspond to single bonds.

4.2.3 Conclusions

Due to the structural similarity with benzene tricarboxylate the multidentate ligand triazine tricarboxylate TTC appears to be a promising linker for coordination frameworks. However, to be employed as linker in the synthesis of such frameworks a sufficient thermal and chemical stability under the respective reaction conditions is a required prerequisite. In this contribution we have studied the stability of TTC against hydrolysis in the presence of divalent alkaline earth and transition metal ions. We have reported on the crystal structures of strontium and barium triazine tricarboxylate hexahydrate thereby presenting the first structurally characterized alkaline earth triazine tricarboxylates. Furthermore, we have demonstrated that the coordination motifs of TTC and triazine tris(2-pyrimidyl) are alike and that the tendency towards hydrolysis in the presence of transition metal ions due to tension in the triazine ring which is well known for triazine tris(2-pyrimidyl) also occurs for TTC. We have discussed a correlation between size of the metal ion and stability of TTC in aqueous solution and have drawn conclusions regarding limitations in the synthesis of TTC frameworks with respect to possible solvents and metal ions.

4.2.4 Experimental Section

Syntheses

Potassium triazine tricarboxylate dihydrate (**4b**) was synthesized from the respective triethyl ester.[4,14] To prepare the triethyl ester dry HCl gas was piped through ethyl cyanoformate (20.0 g, 202 mmol, Aldrich, 99 %) under argon until the trimerization product started to precipitate. The conversion was completed by cooling the reaction to 4 °C overnight and then the product was filtered, washed with

cold water and dried at 75 °C yielding 7.15 g (24 mmol, 36 %) triethyl-*s*-triazine-2,4,6-tricarboxylate as colorless needles. The triethyl ester (250 mg, 0.85 mmol) was stirred in an aqueous solution of KOH (10 mL, 1 M, Acros, p. a.) at room temperature until the ester was completely dissolved. The product was precipitated by the addition of ethanol (200 mL), filtered, washed with ethanol and dried at 75 °C to obtain 258 mg (0.71 mmol, 83 %) potassium-1,3,5-triazine-2,4,6-tricarboxylate dihydrate (**4b**) as colorless powder.

Metathesis reactions for the attempted syntheses of transition metal triazine tricarboxylates were performed in concentrated aqueous solutions at room temperature.[5] The potassium salt (**4b**) and the transition metal salts $MnCl_2 \cdot 4H_2O$ (Merck, p. a.), $Fe(NH_4)_2(SO_4)_2 \cdot 6H_2O$ (Grüssing, p. a.), $CoCl_2 \cdot 6H_2O$ (Merck, p. a.), $NiCl_2 \cdot 6H_2O$ (Fluka, p. a.), $CuCl_2 \cdot 2H_2O$ (Merck, p. a.) and $ZnCl_2 \cdot 4H_2O$ (Alfa Aesar, p. a.), respectively, were reacted in a molar ratio of 2:3. The precipitated products were filtered, washed with water and dried at 75 °C.

To prepare the alkaline earth triazine tricarboxylates **8a** and **8b** a solution of the potassium salt **4b** (80.0 mg, 0.22 mmol) in H_2O (3 mL) was added to a solution of $SrCl_2 \cdot 6H_2O$ (39.0 mg, 0.15 mmol, Merck, p. a.) or $BaCl_2 \cdot 2H_2O$ (36.0 mg, 0.15 mmol, Merck, p. a.) in H_2O (12 mL), respectively. The precipitated products were filtered, washed with water and dried at 75 °C. Single crystals of **8a** and **8b** were grown by gel crystallization in 1 % agar gels in U-tubes using 0.1 M solutions of **4b** and $SrCl_2 \cdot 6H_2O$ or $BaCl_2 \cdot 2H_2O$, respectively.

Elemental analysis (wt. %): $C_3N_3(CO_2Et)_3$: N 14.22 (calcd. 14.13), C 47.20 (calcd. 48.47), H 4.88 (calcd. 5.08); $K_3C_3N_3(CO_2)_3 \cdot 2H_2O$ **4b**: N 11.60 (calcd. 11.56), C 20.45 (calcd. 19.84), H 0.64 (calcd. 1.10); $Sr_3[C_3N_3(CO_2)_3]_2 \cdot 12H_2O$ **8a**: Sr 29.99 (calcd. 29.23), N 8.70 (calcd. 9.35), C 15.70 (calcd. 16.03), H 2.49 (calcd. 2.69); $Ba[C_3N_3(CO_2)_3]_2 \cdot 12H_2O$ **8b**: Ba 40.86 (calcd. 39.30), N 7.47 (calcd. 8.02), C 13.38 (calcd. 13.75), H 2.13 (calcd. 2.31).

X-ray Structure Determination

Single-crystal X-ray diffraction data of **8a** and **8b** were collected at 173 K with a Kappa CCD diffractometer (Mo-K_α radiation, λ = 71.073 pm). Diffraction intensities were scaled using the SCALEPACK[15] software package and an absorption correction was performed using the program SADABS.[16] The crystal structures were solved by direct methods (SHELXS-97) and refined against F^2 by applying the full-matrix least-squares method (SHELXL-97).[17] Hydrogen positions could be determined from difference Fourier syntheses and were refined isotropically using restraints for

oxygen-hydrogen distances. All non-hydrogen atoms were refined anisotropically. CCDC 834692-834693 contain the supplementary crystallographic data for this paper. These data can be obtained free of charge from The Cambridge Crystallographic Data Centre via www.ccdc.cam.ac.uk/data_ request/ cif.

General Techniques

FTIR spectra were recorded at ambient conditions between 600 and 4000 cm^{-1} on a Spektrum BX II FTIR spectrometer (Perkin Elmer) equipped with a DuraSampler diamond ATR device. Elemental analyses for C, H and N were performed with the elemental analyzer systems Vario EL and Vario Micro (Elementar Analysensysteme GmbH). The amounts of alkaline earth metals were ascertained by atomic emission spectroscopy with inductively coupled plasma (ICP-AES) using a Varian-Vista simultaneous spectrometer.

Acknowledgments

The authors thank the *Deutsche Forschungsgemeinschaft* (DFG) (project SCHN 377/15) and the *Fonds der Chemischen Industrie* (FCI) for financial support, *Dr. Peter Mayer* for the single-crystal data collection and *PD Dr. Oliver Oeckler* for fruitful discussions (all Department Chemie, LMU München).

4.2.5 Bibliography

[1] See, for example: a) D. N. Dybtsev, H. Chun, K. Kim, *Chem. Commun.* **2004**, 1594; b) M.-X. Li, Z.-X. Miao, M. Shao, S.-W. Liang, S.-R. Zhu, *Inorg. Chem.* **2008**, *47*, 4481; c) S. Ma, D. Sun, M. Ambrogio, J. A. Fillinger, S. Parkin, H.-C. Zhou, *J. Am. Chem. Soc.* **2007**, *129*, 1858; d) S. Ma, X.-S. Wang, D. Yuan, H.-C. Zhou, *Angew. Chem.* **2008**, *120*, 4198; *Angew. Chem. Int. Ed.* **2008**, *47*, 4130; e) Y. K. Park, S. B. Choi, H. Kim, K. Kim, B.-H. Won, K. Choi, J.-S. Choi, W.-S. Ahn, N. Won, S. Kim, D. H. Jung, S.-H. Choi, G.-H. Kim, S.-S. Cha, Y. H. Jhon, J. K. Yang, J. Kim, *Angew. Chem.* **2007**, *119*, 8378; *Angew. Chem. Int. Ed.* **2007**, *46*, 8230; f) D. Sun, S. Ma, Y. Ke, D. J. Collins, H.-C. Zhou, *J. Am. Chem. Soc.* **2006**, *128*, 3896; g) D. Sun, S. Ma, Y. Ke, T. M. Petersen, H.-C. Zhou, *Chem. Commun.* **2005**, 2663.

[2] a) E. Irran, B. Jürgens, W. Schnick, *Chem. Eur. J.* **2001**, *7*, 5372; b) E. Irran, B. Jürgens, W. Schnick, *Solid State Sci.* **2002**, *4*, 1305; c) B. Jürgens, H. A. Höppe, W. Schnick, *Z. Anorg. Allg. Chem.* **2004**, *630*, 35; d) B. Jürgens, E. Irran, J. Schneider, W. Schnick, *Inorg. Chem.* **2000**, *39*, 665; e) B. V. Lotsch, W. Schnick, *Chem. Mater.* **2006**, *18*, 1891; f) B. V. Lotsch, W. Schnick, *Z. Anorg. Allg. Chem.* **2007**, *633*, 1435; g) A. Nag, B. V. Lotsch, J. Schmedt a. d. Günne, O. Oeckler, P. J. Schmidt, W. Schnick, *Chem. Eur. J.* **2007**, *13*, 3512.

[3] See, for example: a) S. Aoki, M. Shiro, T. Koike, E. Kimura, *J. Am. Chem. Soc.* **2000**, *122*, 576; b) L. R. Falvello, M. A. Hitchman, F. Palacio, I. Pascual, A. J. Schultz, H. Stratemeier, M. Tomás, E. P. Urriolabeitia, D. M. Young, *J. Am. Chem. Soc.* **1999**, *121*, 2808; c) L. R. Falvello, I. Pascual, M. Tomás, *Inorg. Chim. Acta* **1995**, *229*, 135; d) L. R. Falvello, I. Pascual, M. Tomás, E. P. Urriolabeitia, *J. Am. Chem. Soc.* **1997**, *119*, 11894; e) X.-C. Huang, W. Luo, Y.-F. Shen, X.-J. Lin, D. Li, *Chem. Commun.* **2008**, 3995; f) J. Server-Carrió, E. Escrivà, J.-V. Folgado, *Polyhedron* **1998**, *17*, 1495.

[4] C. Grundmann, E. Kober, *J. Org. Chem.* **1956**, *21*, 1392.

[5] J.-R. Galán-Mascarós, J.-M. Clemente-Juan, K. R. Dunbar, *J. Chem. Soc., Dalton Trans.* **2002**, *13*, 2710.

[6] a) S. J. Makowski, E. Calta, M. Lacher, W. Schnick, *Z. Anorg. Allg. Chem.* **2011**, *637*, *in press*; S. J. Makowski, E. Calta, W. Schnick, *Z. Anorg. Allg. Chem.* **2011**, *637*, *in press*; S. J. Makowski, M. Hörmannsdorfer, W. Schnick, *Z. Anorg. Allg. Chem.* **2010**, *636*, 2584.

[7] See, for example: a) S. S.-Y. Chui, S. M.-F. Lo, J. P. H. Charmant, A. G. Orpen, I. D. Williams, *Science* **1999**, *283*, 1148; b) J. Kim, B. Chen, T. M. Reineke, H. Li, M. Eddaoudi, D. B. Moler, M. O'Keeffe, O. M. Yaghi, *J. Am. Chem. Soc.* **2001**, *123*, 8239; c) O. M. Yaghi, G. Li, H. Li, *Nature* **1995**, *378*, 703.

[8] X.-C. Zhang, L. Xu, W.-G. Liu, B. Liu, *Bull. Korean Chem. Soc.* **2011**, *32*, 1349. The structure of a 3D Zn triazine tricarboxylate framework obtained under hydrothermal conditions has been reported (CCDC-675915). However, since both cell parameters and atomic positions exactly match those of the respective Zn benzene tricarboxylate framework (CCDC-664416) it can be assumed that in this publication by mistake the data of a benzene tricarboxylate framework and not of a triazine tricarboxylate framework have been used.

[9] a) T. Glaser, H. Theil, I. Liratzis, T. Weyhermüller, E. Bill, *Inorg. Chem.* **2006**, *45*, 4889; b) D. C. d. Castro Gomes, H. O. Stumpf, F. Lloret, M. Julve, V. González, H. Adams, J. A. Thomas, *Inorg. Chim. Acta* **2005**, *358*, 1113.

[10] a) E. I. Lerner, S. J. Lippard, *J. Am. Chem. Soc.* **1976**, *98*, 5397; b) E. I. Lerner, S. J. Lippard, *Inorg. Chem.* **1977**, *16*, 1546.

[11] R. D. Shannon, *Acta Crystallogr., Sect. A* **1976**, *32*, 751.

[12] a) A. M. Garcia, D. M. Bassani, J.-M. Lehn, G. Baum, D. Fenske, *Chem. Eur. J.* **1999**, *5*, 1234; b) E. I. Lerner, S. J. Lippard, *Inorg. Chem.* **1977**, *16*, 1537; c) C. Metcalfe, S. Spey, H. Adams, J. A. Thomas, *Dalton Trans.* **2002**, 4732.

[13] T. Steiner, *Angew. Chem.* **2002**, *114*, 50; *Angew. Chem. Int. Ed.* **2002**, *41*, 48.

[14] E. Ott, *Ber. Dtsch. Chem. Ges.* **1919**, *52*, 656.

[15] Z. Otwinowski, W. Minor, *Methods Enzymol.* **1997**, *276*, 307.

[16] G. M. Sheldrick, *SADABS, Version 2* **2001**.

[17] a) G. M. Sheldrick, *Acta Crystallogr., Sect. A* **2008**, *64*, 112; b) G. M. Sheldrick, *SHELXS-97, Program for the Solution of Crystal Structures*, Universität Göttingen, Germany **1997**; c) G. M. Sheldrick, *SHELXL-97, Program for the Refinement of Crystal Structures*, Universität Göttingen, Germany **1997**.

5. Cocrystals of Alkali Triazine Tricarboxylates and Cyanuric Acid

Crystal structure analysis of several triazine tricarboxylate salts in the previous chapter has shown that in these compounds numerous interactions are present. Next to Coulomb forces between triazine tricarboxylate and metal ions also hydrogen bonds between crystal water and triazine tricarboxylate, and dispersive interactions between triazine tricarboxylate units determine the observed assemblies of building units in the structures. Understanding the interplay between these different types of interactions is an inevitable prerequisite for a more directed synthesis of such compounds. Whereas several *s*-triazine based salts and coordination compounds as well as metal free supramolecular structures of *s*-triazine derivatives have been studied in this regard, so far no example is known in which both different *s*-triazine compounds and metal ions are present. In order to obtain materials in which noncovalent interactions between different *s*-triazine derivatives, Coulomb interactions between those *s*-triazine units and metal ions, and their mutual influence can be studied, alkali triazine tricarboxylates have been reacted with cyanuric acid $C_3N_3O_3H_3$. Synthesis, crystal structures and thermal characterization of obtained cocrystals are reported in this chapter.

Formation of Cocrystals between Alkali Triazine Tricarboxylates and Cyanuric Acid – Reactivity Considerations and Structural Characterization of the Adduct Phases $M_3[C_3N_3(CO_2)_3][C_3N_3O_3H_3]\cdot H_2O$ (M = K, Rb)

Sophia J. Makowski, Evelyn Calta, Monika Lacher, and Wolfgang Schnick

published in: *Z. Anorg. Allg. Chem.* **2012**, *638*, 88. DOI: 10.1002/zaac.201100316

Keywords: Alkali salts; Carbon nitrides; Cocrystals; Crystal structure; *s*-Triazine

Abstract. The reactivity of cyanuric acid towards alkali triazine tricarboxylates was investigated and the first triazine–triazine adduct phases comprising alkali metal ions were synthesized and characterized by single-crystal X-ray diffraction and thermal analysis. An investigation of the reaction between the alkali triazine tricarboxylates $M_3[C_3N_3(CO_2)_3]\cdot xH_2O$ (M = Li, Na, K, Rb, Cs) and cyanuric acid showed that the degree of ion transfer from triazine tricarboxylate to cyanuric acid increases gradually from the lithium to the cesium salt reflecting an increasing basicity of the triazine tricarboxylates. The reaction of potassium and rubidium triazine tricarboxylate dihydrate with cyanuric acid yielded the novel co-crystals $K_3[C_3N_3(CO_2)_3][C_3N_3O_3H_3]\cdot H_2O$ (**3a**) and $Rb_3[C_3N_3(CO_2)_3][C_3N_3O_3H_3]\cdot H_2O$ (**3b**). In comparison to metal free triazine–triazine adduct phases in these compounds the assembly of molecules in the crystal is mainly determined by Coulomb interactions and only to a certain degree by hydrogen bonds and dispersive interactions. In the crystal the *s*-triazine units exhibit a layered structure with triazine tricarboxylate and isocyanuric acid being arranged in zigzag strands within the layers and stacked in columns perpendicular to the layers. Thermal analysis revealed a rather weak cohesion between triazine tricarboxylate and cyanuric acid upon heating.

5.1 Introduction

In the last decades the concept of crystal engineering for the rational design of new solid materials with desired physical and chemical properties has attracted considerable interest.[1] For the directed preparation of solids with specific architecture and properties a detailed understanding of the factors that affect the arrangement of molecular building blocks in the solid state is an indispensable prerequisite. The assembly of molecules and ions in the crystal is determined by several types of non covalent interactions such as hydrogen bonding, coordination interactions or π-π stacking interactions.[1,2] In this regard we are especially interested in such non covalent interactions between molecular carbon nitride compounds. Even though recent research in the field of carbon nitrides is mainly focused on synthesis, characterization and application of covalently bound frameworks[3] also several adduct phases, in which the cohesion between molecular carbon nitrides is solely achieved by various types of non covalent interactions, were investigated.[4-7] The most prominent example is probably the adduct between the *s*-triazine compounds melamine and cyanuric acid, in which the self-assembly of two molecules with a threefold symmetry leads to the formation of a highly symmetric rosette-like arrangement.[4,6] Further adduct phases of *s*-triazine (C_3N_3) and *s*-heptazine (C_6N_7) compounds were obtained from solutions comprising both building blocks[5] or under solvent free conditions as intermediates during the thermal condensation of *s*-triazine precursors.[7] However, to the best of our knowledge no structurally characterized compound is known so far, in which two different *s*-triazine molecules are present together with metal ions. In contrast to the above mentioned adduct phases in such systems not only hydrogen bonds and dispersive interactions but also Coulomb and coordination interactions will determine the assembly of molecules in the crystal.

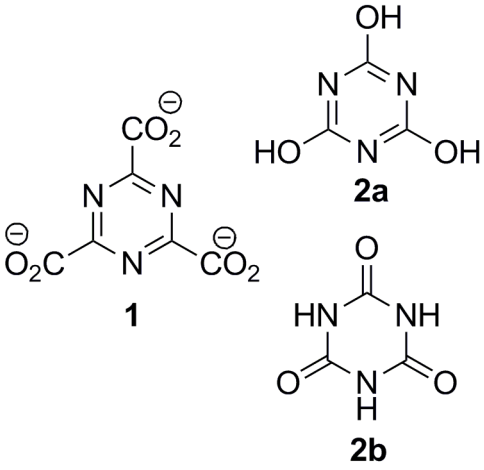

Scheme 1. Triazine tricarboxylate TTC (**1**), the enol form of cyanuric acid (**2a**) and its keto form isocyanuric acid (**2b**).

In order to obtain a system in which the effect of various types of non covalent interactions on the arrangement of *s*-triazine molecules as well as the mutual influence of these diverse types of

interactions can be studied we tried to combine *s*-triazine based salts with further *s*-triazine compounds capable of metal coordination. For this purpose we used alkali triazine tricarboxylates $M_3[C_3N_3(CO_2)_3]$ (*M* = Li, Na, K, Rb, Cs), an interesting class of compounds that has been studied in detail only recently,[8,9] as molecular *s*-triazine based salts and cyanuric acid as further ligand (see Scheme 1). In this contribution the reactivity of different alkali triazine tricarboxylates (TTC) towards cyanuric acid is investigated and the synthesis and crystal structure of the co-crystals $K_3[C_3N_3(CO_2)_3]$-$[C_3N_3O_3H_3]\cdot H_2O$ (**3a**) and $Rb_3[C_3N_3(CO_2)_3][C_3N_3O_3H_3]\cdot H_2O$ (**3b**) is presented. The influence of hydrogen bonding and π-π stacking interactions in comparison to Coulomb interactions on the arrangement of the *s*-triazine building blocks in these adduct phases is discussed and the strength of the cohesion by non covalent interactions is further examined by thermal analysis.

5.2 Results and Discussion

Reactivity

The alkali triazine tricarboxylates $M_3[C_3N_3(CO_2)_3]\cdot xH_2O$ (*M* = Li, Na, K, Rb, Cs) (**1a-e**) were combined with cyanuric acid $C_3N_3O_3H_3$ (**2**) in an attempt to prepare metal comprising *s*-triazine adduct phases. Both starting materials represent *s*-triazine based tridentate ligands with threefold symmetry and sufficient solubility in water. Aqueous solutions of the respective alkali triazine tricarboxylate and cyanuric acid were mixed and hold at room temperature until the evaporation of solvent caused the precipitation of the product. A characterization of the products by X-ray diffraction revealed a dependency of the reactivity on the alkali ions. For the combination of lithium and sodium triazine tricarboxylate with cyanuric acid no co-crystallization occurred but the starting materials crystallized separately. In the case of potassium and rubidium triazine tricarboxylate co-crystals with cyanuric acid were obtained but only the combination of potassium triazine tricarboxylate and

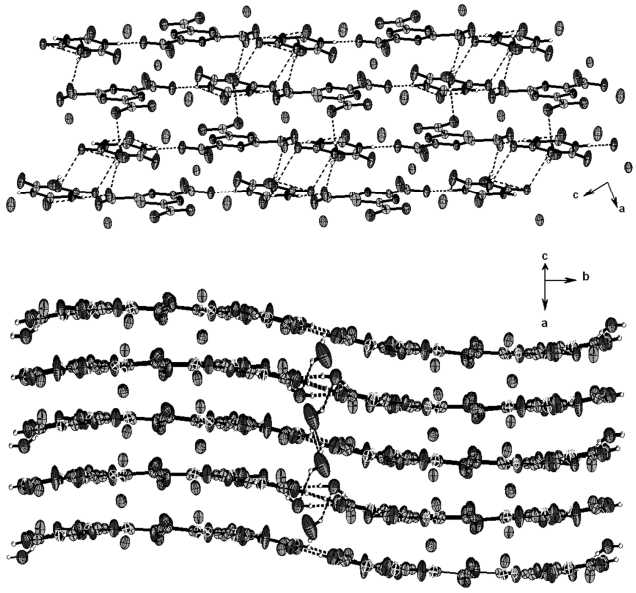

Figure 1. Layered structures of K-TTC-CA·H_2O (**3a**) (top) and Rb-TTC-CA·H_2O (**3b**) (bottom). Dashed lines represent hydrogen bonds. Thermal ellipsoids (except for hydrogen) are drawn at the 50 % probability level.

cyanuric acid yielded a phase pure sample of the adduct $K_3[C_3N_3(CO_2)_3][C_3N_3O_3H_3]\cdot H_2O$ (K-TTC-CA·H_2O) (**3a**). The reaction of rubidium triazine tricarboxylate with cyanuric acid resulted in a reaction mixture comprising single-crystals of the adduct $Rb_3[C_3N_3(CO_2)_3][C_3N_3O_3H_3]\cdot H_2O$ (Rb-TTC-CA·H_2O) (**3b**), single-crystals of rubidium cyanurate and further unidentified phases. From the reaction product of cesium triazine tricarboxylate and cyanuric acid only cesium cyanurate could be isolated. Hence from **1a** to **1e** the tendency of a transfer of the alkali ions from triazine tricarboxylate to cyanuric acid increases gradually.

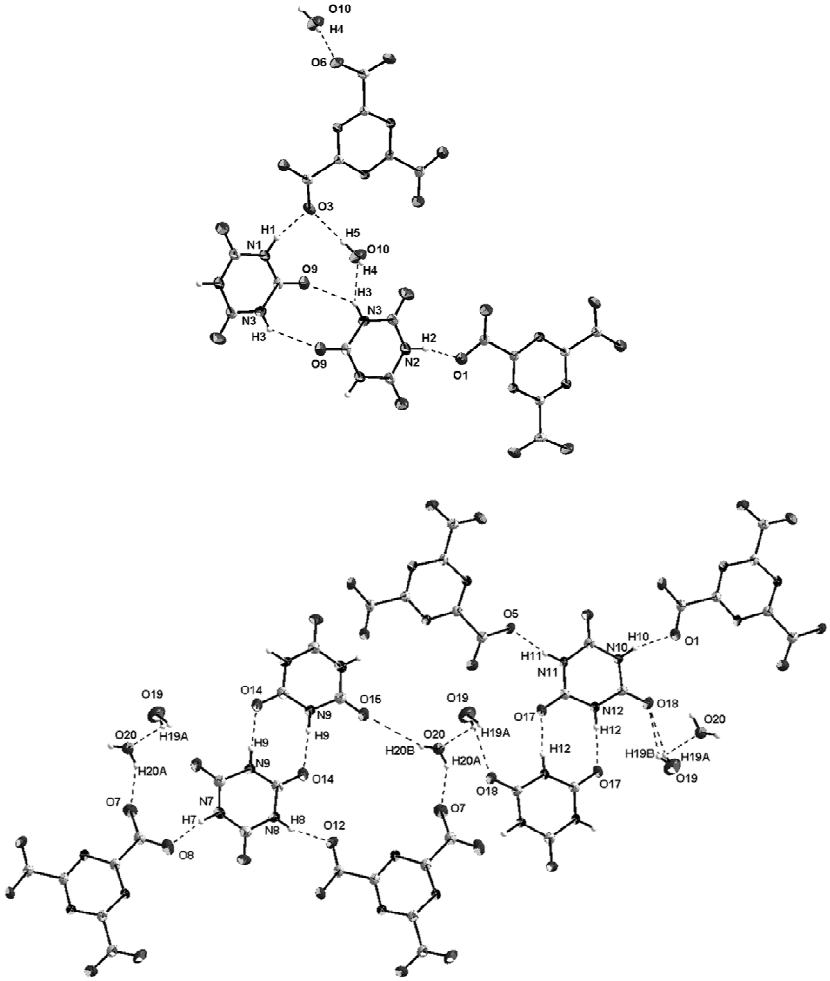

Figure 2. Hydrogen bonding interactions in K-TTC-CA·H_2O (**3a**) (top) and Rb-TTC-CA·H_2O (**3b**) (bottom). Thermal ellipsoids (except for hydrogen) are drawn at the 50 % probability level.

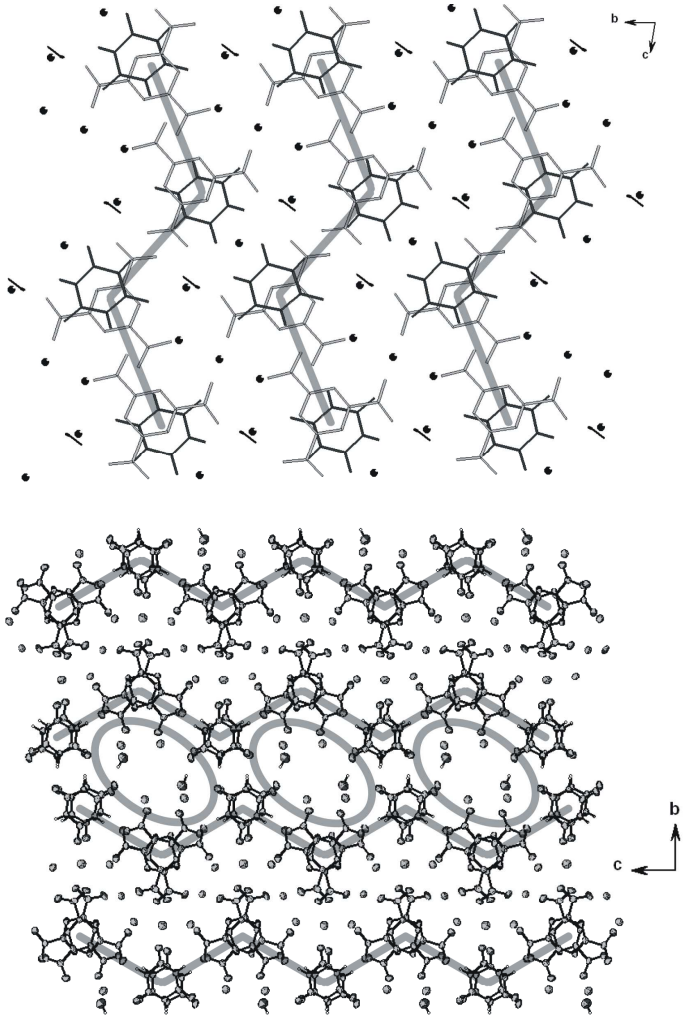

Figure 3. Crystal structures of the adduct phases K-TTC-CA·H_2O (**3a**) (top) and Rb-TTC-CA·H_2O (**3b**) (bottom), representing the arrangement of triazine tricarboxylate and cyanuric acid rods in zigzag strands and the formation of voids between two double strands in **3b**. Triazine tricarboxylate units are displayed in light gray and isocyanuric acid units in dark gray.

The lithium and sodium ions remain bound to triazine tricarboxylate, the potassium ions are coordinated by triazine tricarboxylate and cyanuric acid simultaneously, the rubidium ions are partially shared between both ligands and are partially transferred to cyanuric acid, and the cesium ions are eventually completely transferred from triazine tricarboxylate to cyanuric acid. Aqueous solutions of **1d** and **1e** are basic enough to deprotonate cyanuric acid resulting in the formation of the alkali cyanurates $M_3[C_3N_3O_3]\cdot xH_2O$ (M = Rb, Cs). This observation is also in accordance with expectation due to the HSAB concept. Metal ions are coordinated by triazine tricarboxylate via two carboxylate groups and the intermediate nitrogen atom of the *s*-triazine ring. In contrast to these hard coordination sites the keto oxygen atoms of isocyanuric acid can be regarded as rather soft. The binding strength between the hard triazine tricarboxylate units and alkali metal ions decreases from hard Li^+ to soft Cs^+, whereas the trend is just vice versa for isocyanuric acid. The formation of co-crystals between triazine tricarboxylate and cyanuric acid can only be achieved for potassium and rubidium, where the coordination strength of both ligands for the respective metal cation is comparable.

Table 1. Crystallographic data and details of the structure refinement for $K_3[C_3N_3(CO_2)_3][C_3N_3O_3H_3]\cdot H_2O$ (**3a**) and $Rb_3[C_3N_3(CO_2)_3][C_3N_3O_3H_3]\cdot H_2O$ (**3b**).

	3a	**3b**
Molar mass /g·mol^{-1}	474.49	613.58
Crystal system	triclinic	monoclinic
Space group	$P\bar{1}$ (no. 2)	$P2_1/c$ (no. 14)
T /K	293	293
Diffractometer	Nonius Kappa-CCD	Nonius Kappa-CCD
Radiation, λ /pm	Mo-K_α, 71.073	Mo-K_α, 71.073
a /pm	709.66(14)	720.01(14)
b /pm	964.97(19)	3756.4(8)
c /pm	1279.1(3)	1256.9(3)
α /°	75.83(3)	90
β /°	75.38(3)	101.81(3)
γ /°	70.88(3)	90
V /10^6 pm^3	788.1(3)	3327.5(11)
Z	2	4
Calculated density /g·cm^{-3}	1.911	2.450
Crystal size /mm^3	0.33 x 0.23 x 0.20	0.27 x 0.13 x 0.11
Absorption coefficient /mm^{-1}	0.930	8.859
F(000)	450	2336
Absorption correction	none	multi-scan
Min. / max. transmission		0.1889 / 0.3084
Diffraction range	$3.23^o \le \theta \le 34.41^o$	$3.18^o \le \theta \le 26.42°$
Index range	$-11 \le h \le 11$, $-15 \le k \le 15$	$-7 \le h \le 8$, $-46 \le k \le 45$
	$-20 \le l \le 20$	$-15 \le l \le 15$
Parameters / restraints	271 / 5	517 / 4
Total no. of reflections	11999	44111
No. of independent reflections	6608	6796
No. of observed reflections	5053	5128
Min./max. residual electron density /e 10^{-6} pm^{-3}	-0.472 / +0.563	-2.026 / +0.849
GooF	0.935	1.055
Final R indices [$I > 2\sigma(I)$]	$R1 = 0.0407$, $wR2 = 0.1008$ [a)]	$R1 = 0.0473$, $wR2 = 0.1195$ [b)]
Final R indices (all data)	$R1 = 0.0570$, $wR2 = 0.1123$ [a)]	$R1 = 0.0712$, $wR2 = 0.1318$ [b)]

a) $w = [\sigma^2(F_0^2) + (0.0483P)^2 + 0.5488P]^{-1}$, with $P = (F_0^2 + 2\,F_c^2)/3$

b) $w = [\sigma^2(F_0^2) + (0.0606P)^2 + 14.1010P]^{-1}$, with $P = (F_0^2 + 2\,F_c^2)/3$

Crystal Structure

Potassium triazine tricarboxylate isocyanuric acid hydrate $K_3[C_3N_3(CO_2)_3][C_3N_3O_3H_3]\cdot H_2O$ (**3a**) crystallizes in the triclinic space group $P\ \bar{1}$ and rubidium triazine tricarboxylate isocyanuric acid hydrate $Rb_3[C_3N_3(CO_2)_3][C_3N_3O_3H_3]\cdot H_2O$ (**3b**) in the monoclinic space group $P2_1/c$. Crystallographic data and details of the structure refinements are summarized in Table 1. In both compounds the alkali ions are coordinated by triazine tricarboxylate and cyanuric acid simultaneously. Cyanuric acid is present in its keto form isocyanuric acid, thereby providing three carbonyl groups as coordination sites, whereas the nitrogen atoms of the triazine ring are protonated and hence do not participate in metal coordination. Each triazine tricarboxylate unit coordinates three K^+ or Rb^+ atoms, respectively, via two carboxylate groups and the intermediate *s*-triazine nitrogen atom as in the respective triazine tricarboxylate salts. The coordination sphere is completed by the carboxyl groups of other triazine tricarboxylates and the oxygen atoms of isocyanuric acid and water molecules amounting to coordination numbers of 5-8 for **3a** and 7-9 for **3b**. The *M*–O distances (K: 258-295 pm, Rb: 276-364 pm) are comparable with the distances observed in the respective triazine tricarboxylate salts[9] and are in accordance with the ionic radii sums.[10] On contrast, the *M*–N distances (K: 281-290 pm, Rb: 301-303 pm) are on average 5 pm longer than in the triazine tricarboxylate salts, indicating a less tighter binding of the alkali ions to the triazine core as can be expected due to the additional coordination by isocyanuric acid. Both adduct phases form layered structures typically for *s*-triazine systems (cf. Figure 1). The interlayer distances amount to 355 pm in **3a** and 360 pm in **3b** and hence are slightly larger than in the respective triazine tricarboxylate salts. Hydrogen bonds are mainly present within the layers and especially in **3b** only to a small amount also between the layers.

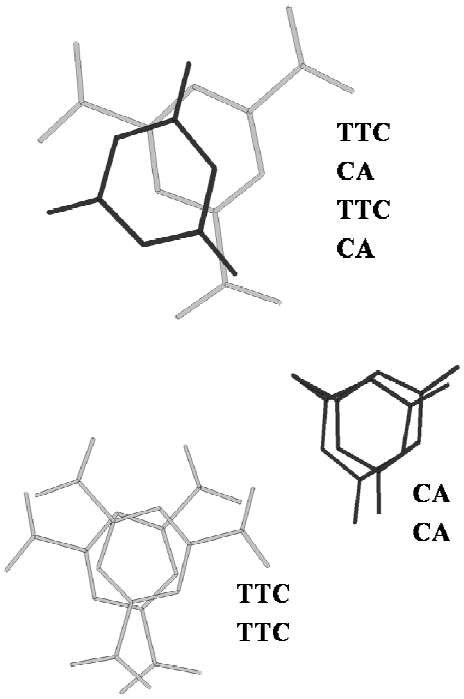

Figure 4. Stacking of the ligands triazine tricarboxylate (TTC) and cyanuric acid (CA) in the adduct phases K-TTC-CA·H_2O (**3a**) (top) and Rb-TTC-CA·H_2O (**3b**) (bottom). Triazine tricarboxylate units are displayed in light gray and isocyanuric acid units in dark gray.

As is illustrated in Figure 2, each two isocyanuric acid (CA) units are interconnected by a double N-H···O hydrogen bridge. Additionally, each CA entty forms a strong hydrogen bond to a carboxylate group of triazine tricarboxylate (TTC). Further hydrogen bonding interactions connect crystal water molecules with both CA and TTC units, with all hydrogen atoms of H_2O being involved in the hydrogen bonding network. Hydrogen bonds in **3a** and **3b** can be classified as medium strong with donor-acceptor distances of 267-299 pm (**3a**) and 264-301 pm (**3b**) and donor-hydrogen-acceptor angles of 121-166° (**3a**) and 113-173° (**3b**) (see Table 2).[11]

The ligands triazine tricarboxylate and isocyanuric acid are stacked in columns perpendicular to [100] (cf. Figure 3). In **3b** these columns form single zigzag strands along *c*, whereas the crystal structure of **3b** comprises double strands along *c* which surround hexangular voids that are filled with crystal water molecules and rubidium ions. The remaining rubidium ions in **3b** and all potassium ions in **3a** are located between the zigzag strands of ligands forming corrugated bands. The composition of the columns is different for both adduct phases. In **3a** only one type of columns is present, in which triazine tricarboxylate TTC and isocyanuric acid CA units are alternately stacked with a partial overlap of the *s*-triazine cores. In contrast, in **3b** the columns comprise either TTC or CA and show a complete overlap of the *s*-triazine cores (cf. Figure 4). Hence in **3b** the two ligands TTC and CA are merely connected via shared metal coordination and hydrogen bonds, whereas in **3a** additionally weak dispersive interactions between the *s*-triazine cores of both ligands are present.

Table 2. Donor-acceptor distances and donor-hydrogen-acceptor angles /pm, ° for the hydrogen bonding network in K-TTC-CA·H_2O (**3a**) and Rb-TTC-CA·H_2O (**3b**).

D-H···A	D···A	<D-H···A
K-TTC-CA·H_2O **3a**		
N1-H1···O3	264.6	165.11
N2-H2···O1	266.9	165.61
N3-H3···O10	294.3	151.06
N3-H3···O9	298.5	120.55
O10-H4···O6	276.7	151.79
O10-H5···O3	288.9	153.75
Rb-TTC-CA·H_2O **3b**		
N7-H7···O8	264.1	167.17
N8-H8···O12	266.2	161.79
N9-H9···O14	279.2	172.98
N10-H10···O1	265.5	164.76
N11-H11···O5	266.4	170.48
N12-H12···O17	282.0	172.96
O19-H19A···O18	286.1	124.91
O19-H19A···O20	300.2	120.89
O19-H19B···O18	286.1	118.41
O20-H20A···O7	268.7	140.79
O20-H20B···O20	300.6	112.73

Interestingly, in the metal free adduct melamine·cyanuric acid M·CA an alternative assembly M–CA–M–CA is the most stable stacking arrangement,[6] whereas in **3a** and **3b** a homogeneous CA–CA and TTC–TTC stacking is preferred to an alternating TTC–CA–TTC–CA stacking as the varying degrees

of overlap show. The observation that homogeneous CA–CA stacks are favored over CA–TTC stacks in **3a** and **3b** but not over CA–M stacks in M·CA might be explained by the influence of the rather strong Coulomb interactions in **3a** and **3b** impeding a complete overlap of TTC and CA. In contrast to metal free triazine–triazine adduct phases, where π-π stacking interactions – next to strong hydrogen bonds – are essentially determining the arrangement of molecules in the crystal, these interactions become less important in the presence of strong Coulomb interactions.

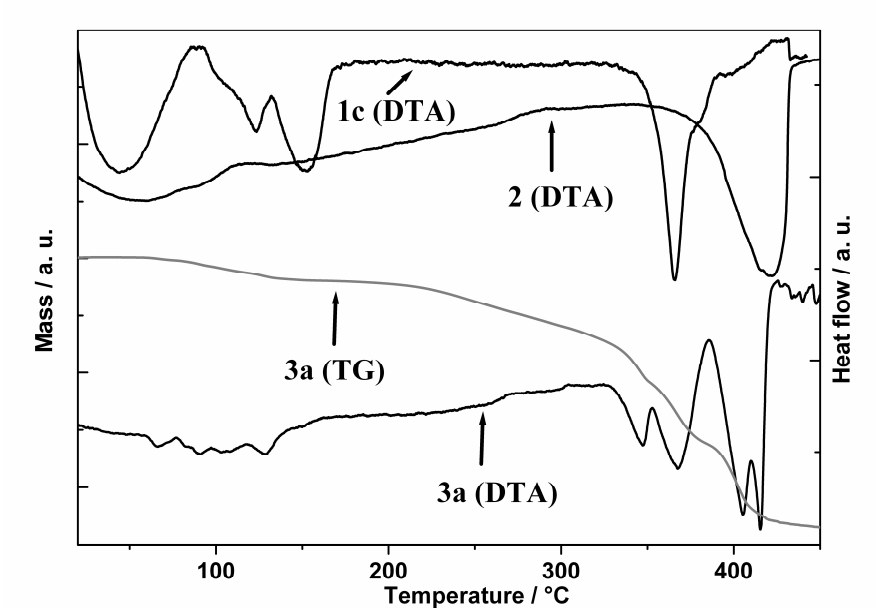

Figure 5. DTA curves (black) of K-TTC·2H_2O (**1c**), cyanuric acid (**2**) and K-TTC-CA·H_2O (**3a**) and TG curve (gray) of K-TTC-CA·H_2O (**3a**), recorded with a heating rate of 5 K·min^{-1}.

Thermal Behavior

The thermal behavior of the adduct phase K-TTC-CA·H_2O (**3a**) was compared with that of the starting materials K-TTC·2H_2O (**1c**) and cyanuric acid (**2**) (see Figure 5). The potassium salt **1c** is dehydrated below 200 °C and starts to decompose around 350 °C. Cyanuric acid **2** completely transforms into gaseous isocyanic acid HNCO around 400 °C.[12] TG and DTA curves of the adduct phase **3a** show a release of crystal water at low temperatures and subsequent a slow decomposition of the dehydrated compound starting around 200 °C. Hence the adduct phase **3a** exhibits a lower thermal stability than its components. The main mass loss occurs stepwise between 320 and 420 °C accompanied by three

exothermic signals in the DTA curve. Two of these signals closely match the decomposition temperatures of K-TTC·$2H_2O$ (**1c**) and cyanuric acid (**2**). This indicates that the cohesion between the ligands TTC and CA seems to be broken up while heating, so that the thermal decomposition of the two individual compounds TTC and CA can be observed.

5.3 Conclusions

We have reported on the synthesis, crystal structure, and thermal behavior of two co-crystals of alkali triazine tricarboxylates and isocyanuric acid. $M_3[C_3N_3(CO_2)_3][C_3N_3O_3H_3]\cdot H_2O$ (M = K, Rb) represent the first examples of metal containing adduct phases between two different *s*-triazine molecules. This demonstrates a further possibility to construct layered *s*-triazine materials by combining diverse *s*-triazine ligands in a single compound. It was discussed how the formation of such co-crystals depends on the relative coordination strength of both ligands for the respective metal cation. Furthermore, the role of different types of non covalent interactions on the assembly of molecules and ions in the crystal was investigated and compared to metal free triazine–triazine adduct phases. These findings add to a deeper understanding of the factors that determine the assembly of different *s*-triazine molecules in the solid state and might contribute to a rational preparation of specific carbon nitride materials by crystal engineering in the future.

5.4 Experimental Section

Syntheses

The alkali triazine tricarboxylates **1a-e** were synthesized according to the procedure described for the potassium salt by saponification of the respective triethyl ester.[13] To prepare the ester dry HCl was piped through ethyl cyanoformate (20.0 g, 202 mmol, Aldrich, 99 %) in argon until the trimerization product started to precipitate. After cooling the reaction to 4 °C overnight the product was filtered, washed with cold water, and dried at 75 °C. Small amounts of the triethyl ester (250 mg, 0.85 mmol) were treated with 10 mL of a 1 M aqueous solution of *M*OH (ABCR, 99 %, M = Li, Na, K, Rb, Cs). The reaction was stirred at room temperature until the ester was completely dissolved. Afterwards,

200 mL ethanol was poured into the solution to precipitate the alkali salts. The products were filtered, washed with ethanol, and dried at 75 °C.

To prepare the adduct phases **3a** and **3b** equimolar amounts (0.15 mmol) of cyanuric acid **2** (20.0 mg, Aldrich, ≥ 98 %) and potassium or rubidium triazine tricarboxylate dihydrate **1c** (56.3 mg) and **1d** (77.9 mg), respectively, were dissolved in water (50 mL) and mixed for 48 h at room temperature. By slow evaporation of the solvent at room temperature the product **3a** in the form of colorless block-like crystals or a mixture of several phases containing single-crystals of **3b** were obtained.

Elemental analysis for **3a**: N 15.16 (calcd. 17.71), C 20.83 (calcd. 22.78), H 1.41 (calcd. 1.06) %.

X-ray Structure Determination

Single-crystal X-ray diffraction data of **3a** and **3b** were collected with a Kappa CCD diffractometer (293 K, Mo-K_α radiation, λ = 71.073 pm). The diffraction intensities were scaled using the SCALEPACK software package.[14] For **3a** no additional absorption correction was applied and for **3b** an absorption correction was performed using the program SADABS.[15] The crystal structures were solved by direct methods using the software package SHELXS-97 and refined against F^2 by applying the full-matrix least-squares method (SHELXL-97).[16] The hydrogen positions could be determined from difference Fourier syntheses and were refined isotropically using restraints for oxygen-hydrogen distances. All non-hydrogen atoms were refined anisotropically.

Crystallographic data (excluding structure factors) for the structures in this paper have been deposited with the Cambridge Crystallographic Data Centre, CCDC, 12 Union Road, Cambridge CB21EZ, UK. Copies of the data can be obtained free of charge on quoting the depository numbers CCDC-834102 and CCDC-834103 (Fax: +44-1223-336-033; E-Mail: deposit@ccdc.cam.ac.uk, http://www.ccdc.cam.ac.uk).

General Techniques

Powder X-ray diffraction data were collected in transmission geometry with a Huber G670 Guinier Imaging Plate diffractometer (Cu-K_α radiation, λ = 154.06 pm) and analyzed with the software WinXPOW.[17] Thermoanalytical measurements were performed in an inert atmosphere (He) with a Thermoanalyzer TG-DTA92 (Setaram). The samples were heated in an alumina crucible from room temperature to 450 °C with a heating rate of 5 $K \cdot min^{-1}$. Elemental analyses for C, H, and N were

performed with the elemental analyzer systems Vario EL and Vario Micro (Elementar Analysensysteme GmbH).

Acknowledgments

The authors thank the *Deutsche Forschungsgemeinschaft* (DFG) (project SCHN 377/15) and the *Fonds der Chemischen Industrie* (FCI) for financial support and *Dr. Peter Mayer* (Department Chemie, LMU München) for the single-crystal data collection.

5.5 Bibliography

[1] For recent reviews see, for example: a) C. B. Aakeröy, N. R. Champness, C. Janiak, *CrystEngComm* **2010**, *12*, 22; b) R. Custelcean, *Chem. Commun.* **2008**, 295; c) G. R. Desiraju, *Angew. Chem.* **2007**, *119*, 8492; *Angew. Chem. Int. Ed.* **2007**, *46*, 8342; d) K. Merz, V. Vasylyeva, *CrystEngComm* **2010**, *12*, 3989; e) C. M. Reddy, G. R. Krishna, S. Ghosh, *CrystEngComm* **2010**, *12*, 2296.

[2] a) S. Grimme, *Angew. Chem.* **2008**, *120*, 3478; *Angew. Chem. Int. Ed.* **2008**, *47*, 3430; b) C. Janiak, *Dalton Trans.* **2000**, 3885.

[3] For reviews, see: a) G. Goglio, D. Foy, G. Demazeau, *Mater. Sci. Eng. R* **2008**, *58*, 195; b) E. Kroke, M. Schwarz, *Coord. Chem. Rev.* **2004**, *248*, 493; c) A. Thomas, A. Fischer, F. Goettmann, M. Antonietti, J.-O. Müller, R. Schlögl, J. M. Carlsson, *J. Mater. Chem.* **2008**, *18*, 4893.

[4] See, for example: a) I. S. Choi, X. Li, E. E. Simanek, R. Akaba, G. M. Whitesides, *Chem. Mater.* **1999**, *11*, 684; b) K. Damodaran, G. J. Sanjayan, P. R. Rajamohanan, S. Ganapathy, K. N. Ganesh, *Org. Lett.* **2001**, *3*, 1921; c) C. T. Seto, G. M. Whitesides, *J. Am. Chem. Soc.* **1990**, *112*, 6409; d) G. M. Whitesides, J. P. Mathias, C. T. Seto, *Science* **1991**, *254*, 1312.

[5] B. V. Lotsch, W. Schnick, *Chem. Mater.* **2006**, *18*, 1891.

[6] A. Ranganathan, V. R. Pedireddi, C. N. R. Rao, *J. Am. Chem. Soc.* **1999**, *121*, 1752.

[7] a) A. Sattler, S. Pagano, M. Zeuner, A. Zurawski, D. Gunzelmann, J. Senker, K. Müller-Buschbaum, W. Schnick, *Chem. Eur. J.* **2009**, *15*, 13161; b) S. Tragl, K. Gibson, H.-J. Meyer, *Z. Anorg. Allg. Chem.* **2004**, *630*, 2373.

[8] a) J.-R. Galán-Mascarós, J.-M. Clemente-Juan, K. R. Dunbar, *J. Chem. Soc., Dalton Trans.* **2002**, *13*, 2710; b) X.-C. Zhang, L. Xu, W.-G. Liu, B. Liu, *Bull. Korean Chem. Soc.* **2011**, *32*, 1349.

[9] a) S. J. Makowski, E. Calta, W. Schnick, *Z. Anorg. Allg. Chem.* **2011**, *accepted*; b) S. J. Makowski, M. Hörmannsdorfer, W. Schnick, *Z. Anorg. Allg. Chem.* **2010**, *636*, 2584.

[10] R. D. Shannon, *Acta Crystallogr., Sect. A* **1976**, *32*, 751.

[11] T. Steiner, *Angew. Chem.* **2002**, *114*, 50; *Angew. Chem. Int. Ed.* **2002**, *41*, 48.

[12] A. F. Holleman, E. Wiberg, N. Wiberg *Lehrbuch der Anorganischen Chemie*; Walter de Gruyter: Berlin, New York, **2007**.

[13] a) C. Grundmann, E. Kober, *J. Org. Chem.* **1956**, *21*, 1392; b) E. Ott, *Ber. Dtsch. Chem. Ges.* **1919**, *52*, 656.

[14] Z. Otwinowski, W. Minor, *Methods Enzymol.* **1997**, *276*, 307.

[15] G. M. Sheldrick, *SADABS, Version 2* **2001**.

[16] a) G. M. Sheldrick, *Acta Crystallogr., Sect. A* **2008**, *64*, 112; b) G. M. Sheldrick, *SHELXS-97, Program for the Solution of Crystal Structures,* Universität Göttingen, Germany **1997**; c) G. M. Sheldrick, *SHELXL-97, Program for the Refinement of Crystal Structures,* Universität Göttingen, Germany **1997**.

[17] WinXPOW, Version 2.12, Stoe & Cie GmbH, Darmstadt, **2005**.

6. Melem Hydrate

In the previous chapter, the impact of different types of interactions on the assembly of building blocks in cocrystals between alkali triazine tricarboxylates and cyanuric acid has been investigated. Comparing the arrangement of *s*-triazine units in these materials has revealed that according to expectation Coulomb forces and hydrogen bridges have a strong influence on the structure, whereas dispersive interactions between *s*-triazine units are only weak. The importance of hydrogen bonds for self-assembly of molecules into a specific structure becomes even more evident in metal free materials. For supramolecular structures which comprise *s*-triazine units this influence has been studied in detail by several groups, whereas *s*-heptazine derivatives have been employed only rarely in supramolecular compounds so far. The reason for this is probably the poor solubility of uncharged *s*-heptazine derivatives in common solvents. However, for several *s*-heptazine compounds such as melem $C_6N_7(NH_2)_3$ or cyameluric acid $C_6N_7O_3H_3$, formation of hydrates has been reported, indicating that interactions between *s*-heptazine units and solvent molecules occur, even though these forces are not strong enough to actually dissolve the materials. Whereas the crystal structure of cyameluric acid hydrate has been studied in detail prior to this work, the structure of melem hydrate has not been known yet. In this chapter, elucidation of the crystal structure of melem hydrate is reported, including a comprehensive investigation of the influence of hydrogen bonds on the self-assembly of melem units and on the stability of the structure.

Formation of a Hydrogen-Bonded Heptazine Framework by Self-Assembly of Melem into a Hexagonal Channel Structure

Sophia J. Makowski, Pia Köstler, and Wolfgang Schnick

published in: *Chem. Eur. J.* **2012**, *18*, 3248. DOI: 10.1002/chem.201103527

Keywords: Crystal structure; Hydrogen bonds; Self-assembly; Solid-state structures; Stacking interactions

Abstract: Self-assembly of melem $C_6N_7(NH_2)_3$ in hot aqueous solution leads to the formation of hydrogen-bonded, hexagonal rosettes of melem units surrounding infinite channels with a diameter of 8.9 Å. The channels are filled with strongly disordered water molecules, which are bound to the melem network through hydrogen bonds. Single-crystals of melem hydrate $C_6N_7(NH_2)_3 \cdot xH_2O$ ($x \approx 2.3$) were obtained by hydrothermal treatment of melem at 200 °C and the crystal structure ($R\ \bar{3}c$, a = 2879.0(4), c = 664.01(13) pm, $V = 4766.4(13) \cdot 10^6$ pm^3, Z = 18) was elucidated by single-crystal X-ray diffraction. With respect to the structural similarity to the well-known adduct between melamine and cyanuric acid, the composition of the obtained product was further analyzed by solid-state NMR spectroscopy. Hydrolysis of melem to cyameluric acid during syntheses at elevated temperatures could thus be ruled out. DTA/TG studies revealed that, during heating of melem hydrate, water molecules can be removed from the channels of the structure to a large extent. The solvent-free framework is stable up to 430 °C without transforming into the denser structure of anhydrous melem. Dehydrated melem hydrate was further characterized by solid-state NMR spectroscopy, powder X-ray diffraction and sorption measurements to investigate structural changes induced by the removal of water from the channels. During dehydration, the hexagonal, layered arrangement of melem units is maintained whereas the formation of additional hydrogen bonds between melem entities requires the stacking mode of hexagonal layers to be altered. It is assumed that layers are shifted perpendicular to the direction of the channels, thereby making them inaccessible for guest molecules.

6.1 Introduction

Self-assembly, that is, the spontaneous arrangement of molecules into ordered structures by weak, reversible interactions, plays not only an important role in biological systems, for example, for protein folding or pairing of nucleotides, but has also attracted considerable interest in synthetic and materials chemistry.[1,2] In supramolecular chemistry or crystal engineering, complex chemical structures determined by several types of noncovalent interactions such as hydrogen bonds, ionic, hydrophobic, van der Waals, or dispersive forces are formed.

Next to the ambition to understand the principles of molecular self-assembly in the solid state, the synthesis of solids that exhibit desired structural motifs such as ordered channels or cavities reminiscent of zeolites, is a relevant goal in crystal engineering.[3] An outstanding example for the noncovalent assembly of molecules resulting in the formation of a channel structure is the 1:1 adduct between the *s*-triazine (C_3N_3) compounds cyanuric acid and melamine (CA·M) (see Scheme 1).[2,4,5,6] In this adduct, cyanuric acid and melamine form hydrogen-bonded rosette-like hexamers that are arranged in planar sheets. Similar rosette-like motifs have been found in adducts between trithiocyanuric acid and melamine[6] or trithiocyanuric acid and 4,4'-bipyridyl.[7] Furthermore, self-assembly of molecules into hydrogen-bonded rosettes has also been reported for single-component systems, for example, derivatives of trimesic acid, trimesic amide, isophthalic acid, or orthoboric acid.[8,9] However, particular stacking of these hexamers resulting in the formation of channels could be observed only in a few cases.[9]

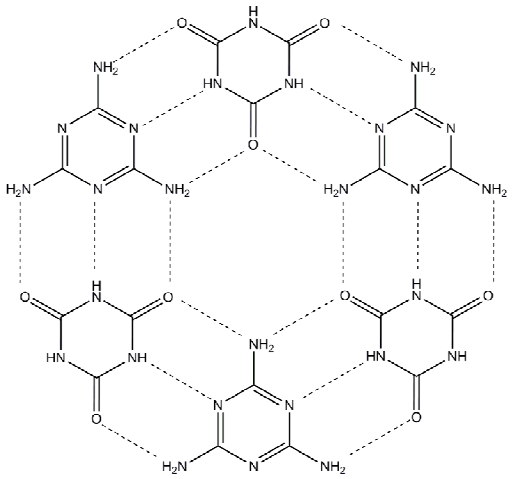

Scheme 1. Hydrogen-bonded rosettes formed between the *s*-triazine compounds isocyanuric acid and melamine.

Among these examples of hydrogen-bonded rosette motifs, the CA·M adduct is certainly the best-studied. Whitesides and co-workers have not only investigated in detail the self-assembly of cyanuric acid and melamine into the respective rosette structures but have also developed concepts for the directed construction of such rosettes. By employing *s*-triazine molecules with sterically bulky substituents or allowing preorganization of building units by interconnecting them with a hub linker,

the formation of rosettes can be favored over the formation of tapes.[2,5] However, whereas numerous compounds based on the CA·M lattice have been extensively studied by many groups, any comparable structures comprising the analogous but larger *s*-heptazine (C_6N_7) compounds cyameluric acid or melem (see Scheme 2) are not known so far.

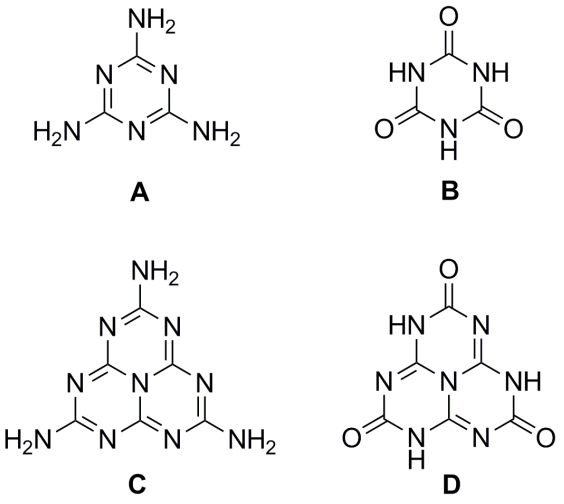

Scheme 2. The *s*-triazine compounds melamine **A** and isocyanuric acid **B**, and the respective *s*-heptazine compounds melem **C** and isocyameluric acid **D**.

The molecular structure of the *s*-heptazine or cyameluric ring system, respectively, has already been postulated by Pauling and Sturdivant in 1937.[10] However, it has not been proven before almost fifty years later when the crystal structure of molecular *s*-heptazine $C_6N_7H_3$ could be solved.[11] Due to the low solubility of *s*-heptazines in common solvents, this building unit is considerably less frequently employed in chemical syntheses than *s*-triazine compounds. However, in the last two decades carbon nitride type compounds have attracted considerable interest as materials for numerous technical applications due to the high thermal and oxidation stability of this class of compounds as well as their semiconducting and catalytic properties.[12] This revival in research of molecular and polymeric carbon nitride type compounds has also initiated substantial progress in the field of *s*-heptazine chemistry. Furthermore, the identification of *s*-heptazine as building block in the polymers melon and poly(heptazine imide)[13,14] and in extended CN_x polymers,[15] as well as quantum chemical calculations that suggest *s*-heptazine as likely building block of graphitic C_3N_4[16,17] have contributed to increased interest in *s*-heptazines. Numerous substituted *s*-heptazines, for example, cyameluric chloride $C_6N_7Cl_3$,[16,18] cyameluric azide $C_6N_7(N_3)_3$,[19] melonates $(C_6N_7(NCN)_3)^{3-}$,[20,21] and several organic derivatives,[22,23] have been synthesized and investigated in detail. The structures of melem[24,25] and cyameluric acid[26,27] as well as of numerous salts[22,28,29,30] have also been solved recently. The employment of melemium and cyamelurate salts has opened access to the chemistry of *s*-heptazines in solution. In addition, the thermal condensation process of melamine leading to melem has been elucidated. Contrary to former assumptions that the condensation might proceed via the intermediate melam $(C_3N_3(NH_2)_2)_2NH$ it could be shown that during thermal treatment of melamine,

crystalline melem is formed via several intermediate melamine-melem adduct phases.[31,32] In the eventually obtained product, melem molecules are arranged in corrugated layers and are interconnected by a dense net of hydrogen bonds both within and between the layers.[24,25] The importance of intermolecular hydrogen bonds for the arrangement of melem units has been demonstrated not only for the assembly of melem molecules in the crystal but also for monolayers of melem on Ag(111), as has been investigated by scanning tunneling microscopy studies recently.[33]

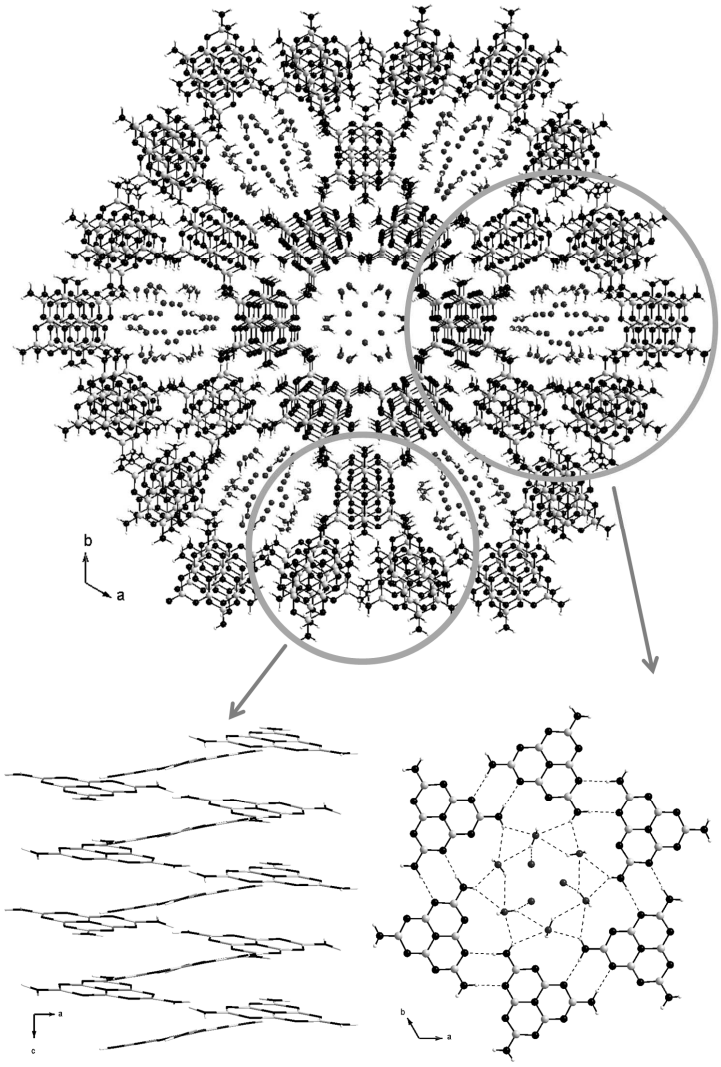

Figure 1. Crystal structure of melem hydrate **2**. (Top) Representation of the porous structure with hexagonal channels along *c*, filled with water molecules; (Bottom, left) Arrangement of melem molecules in helices along *c*; (Bottom, right) Rosette formed of six melem molecules with a diameter of 8.9 Å (van der Waals radii subtracted), filled with water; dashed lines represent hydrogen bonds.

In this contribution, we report on the self-assembly of melem in aqueous solution, thus providing the first example of a structure with a hydrogen-bonded rosette-like pattern, comparable to the CA·M adduct, that comprises *s*-heptazine units. The importance of solvent molecules for the formation of such rosettes and of hexagonal channels in this compound in comparison to structures obtained under anhydrous conditions is exposed. Furthermore, we demonstrate the strength of intermolecular hydrogen bonds in this material, which stabilize the hexagonal arrangement of melem units even in the dehydrated material.

6.2 Results and Discussion

Synthesis and Crystal Structure

The *s*-heptazine compound melem **1** is commonly synthesized by thermal treatment of less condensed C/N/H compounds such as melamine $C_3N_3(NH_2)_3$ or dicyandiamide $(NH_2)_2CN(CN)$, leading to the elimination of ammonia and subsequent condensation. Crystalline melem of high purity is prepared by heating small amounts of starting materials in sealed ampoules.[24] An alternative approach for the synthesis of larger quantities of melem by heating melamine in open systems has been reported recently.[30,34] In this procedure, a reaction mixture of melem and unreacted melamine is obtained. Final purification by boiling the product in water to remove unreacted melamine yields melem as a hydrate **2**, which has not been structurally characterized so far.[30,34] By reacting melem under hydrothermal conditions in an autoclave at 200 °C, we were able to obtain single-crystals of this compound and determine its crystal structure. Crystallographic data for melem hydrate **2** and details of the structure refinement are summarized in Table 1.

Treatment of melem in boiling water breaks up the intermolecular hydrogen bonds and leads to a rearrangement of molecules into a hydrogen-bonded rosette-like network (see Figure 1, bottom right). During the self-assembly of melem in solution, water molecules act as template, resulting in the

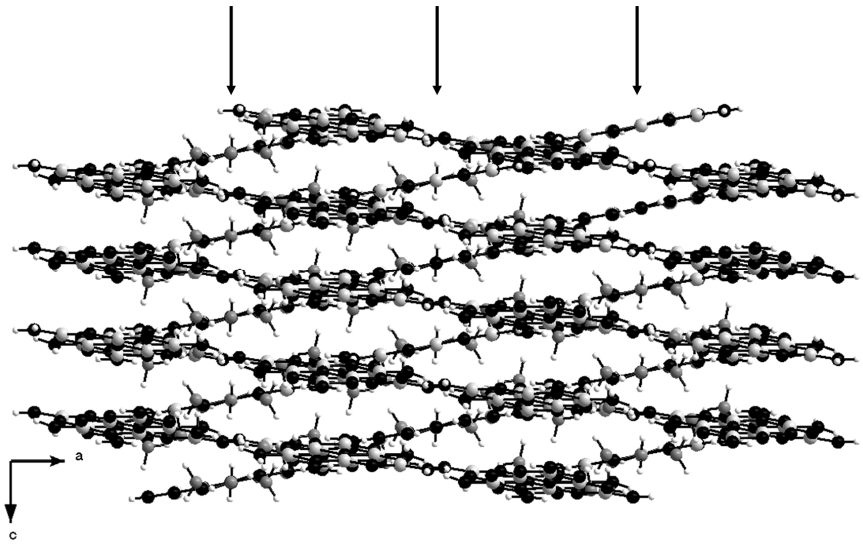

Figure 2. Layered structure of melem hydrate **2**. Arrows indicate the positions of hexagonal channels.

formation of a porous structure in contrast to the denser packed structure of anhydrous melem. The rosettes surround hexagonal channels with a diameter of 8.9 Å (van der Waals radii subtracted) that are filled with water molecules (see Figure 1, top). The self-assembly of molecules in rosettes resulting in the formation of channels resembles the structure of a famous case of noncovalent synthesis, namely the adduct between cyanuric acid and melamine (CA·M). This *s*-triazine (C_3N_3) based compound exhibits cavity diameters of approximately 4Å;[6] the use of the larger *s*-heptazine (C_6N_7) compound melem therefore leads to a remarkable increase in channel diameter by factor 2.2. The melem units are not coplanar but tilted out of the *ab* plane and are arranged in a helix motif along the crystallographic *c* axis (see Figure 1, bottom left) resulting in a corrugated layered structure perpendicular to the channels (see Figure 2). The interlayer distance is 337 pm and, hence, is slightly larger than in anhydrous melem **1** (327 pm).

For the observed assembly of melem units in the structure of melem hydrate, the formation of a dense network of hydrogen bonds appears to be the determining factor (see Table 2). In agreement with the less dense packing of melem molecules in melem hydrate **2** compared to anhydrous melem **1**, in anhydrous melem, each molecule is connected to five other melem molecules each through two hydrogen bonds;[24,25] in melem hydrate, hydrogen bonds are formed only to four further molecules (see Figure 3 and Figure 4). For hydrogen bonds, it is a common approach to estimate their approximate strength based on distances and angles between donors and acceptors. All intermolecular

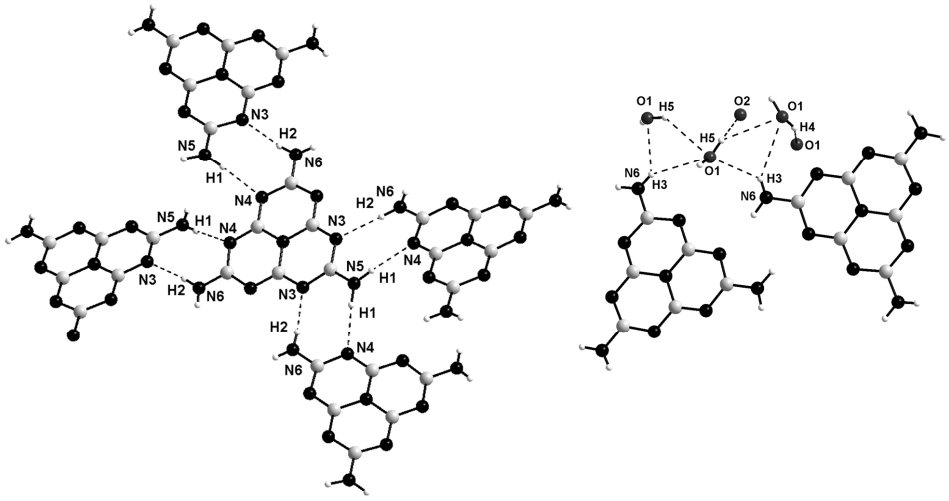

Figure 3. Hydrogen bonds in melem hydrate **2** between melem units (left) and between the melem network and water molecules (right).

Table 1. Crystallographic data and details of the structure refinement for $C_6N_7(NH_2)_3 \cdot 1.98\ H_2O$.

molar mass [g mol^{-1}]	252.85
crystal system	trigonal
space group	$R\ \bar{3}c$ (no. 167)
T [K]	173
diffractometer	Nonius Kappa-CCD
radiation, λ [pm]	Mo-K_α, 71.073
a [pm]	2879.0(4)
c [pm]	664.01(13)
V [10^6 pm^3]	4766.4(13)
Z	18
calculated density [g cm^{-3}]	1.585
crystal size [mm^3]	0.24 x 0.04 x 0.02
absorption coefficient [mm^{-1}]	0.126
diffraction range	$3.72^o \leq \theta \leq 27.38^o$
index range	$-37 \leq h \leq 37$, $-31 \leq k \leq 31$, $-8 \leq l \leq 8$
parameters / restraints	109 / 2
total no. of reflections	4690
no. of independent refl.	1218
no. of observed refl.	769
min./max. residual electron density [e · 10^{-6} pm^{-3}]	-0.282/+0.619
GoF	1.047
final R indices [$I > 2\sigma(I)$][a]	$R1 = 0.0624$, $wR2 = 0.1633$
final R indices (all data)[a]	$R1 = 0.1083$, $wR2 = 0.1892$

[a] $w = [\sigma^2(F_0^2) + (0.1018P)^2 + 6.6517P]^{-1}$, with $P = (F_0^2 + 2\ F_c^2)/3$

N-H···N interactions between melem units can therefore be classified as medium to strong (see Table 2).[35] As can be expected due to the presence of channels in the structure, the water molecules are strongly disordered and are localized on partially occupied sites. Refinement of oxygen occupancies in the single-crystal data of **2** yielded the formula melem·1.98H_2O. The amount of crystal water was further determined by means of elemental analysis (melem-·2.50H_2O) and thermal analysis (melem-·2.33H_2O), resulting in an average formula $C_6N_7(NH_2)_3 \cdot 2.3H_2O$ for melem hydrate **2**. Due to the strong disorder of water molecules in the channels, not all hydrogen

Table 2. Donor-acceptor distances and donor-hydrogen-acceptor angles (pm/°) for the hydrogen-bonding network in $C_6N_7(NH_2)_3 \cdot 1.98H_2O$.

D-H···A	D···A	<D-H···A
N5-H1···N4	304.0	176.10
N6-H2···N3	294.8	173.70
N6-H3···O1	291.6	130.92
O1-H4···O1	348.3	139.43
O1-H5···O2	277.9	134.37

positions could be determined unambiguously from the single-crystal data and were defined by considering reasonable O-H distances and meaningful O-H···O and O-H···N hydrogen-bonding interactions (see Figure 3).

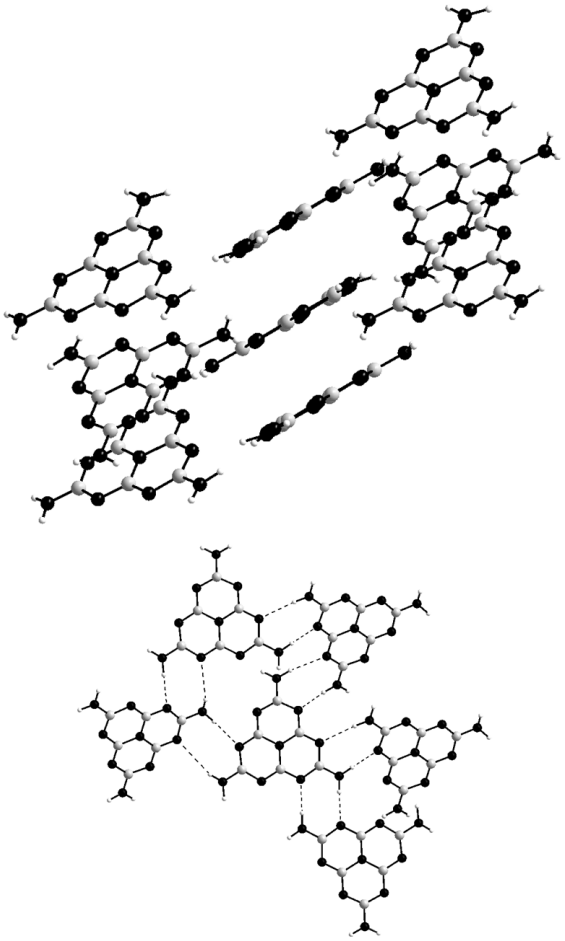

Figure 4. Crystal structure of anhydrous melem **1**. Illustration of the layered structure (top); hydrogen-bonding interactions between melem units (bottom). Structural data for anhydrous melem **1** were taken from the literature.[25]

Interestingly, the above described assembly of melem molecules in hydrogen-bonded rosettes appears to be a preferred arrangement for melem. Scanning tunneling microscopy studies of melem on Ag(111) revealed, among several other polymorphs of melem monolayers, also hydrogen-bonded hexamers of melem;[33] and in the adduct phase 3melem·melamine $3(C_6N_7(NH_2)_3 \cdot (C_3N_3(NH_2)_3)$, the arrangement of melem molecules resembles that of melem hydrate **2**. Whereas the melem rosettes are filled with water in melem hydrate **2**, in the adduct phase (3melem·melamine), a melamine molecule is located in the middle of these voids.[32]

Solid-State NMR Spectroscopy

Because the self-assembly motif of melem hydrate **2** resembles that of the well-known adduct between cyanuric acid and melamine (CA·M), we suspected that, actually, not melem but an analogous adduct between the *s*-heptazine compounds cyameluric acid ($C_6N_7O_3H_3$) and melem ($C_6N_7(NH_2)_3$) might have been formed due to partial hydrolysis of melem. Because the OH and NH_2 groups cannot be unequivocally differentiated by X-ray diffraction, we examined the obtained product by means of solid-state NMR spectroscopy. The observed signals could be assigned

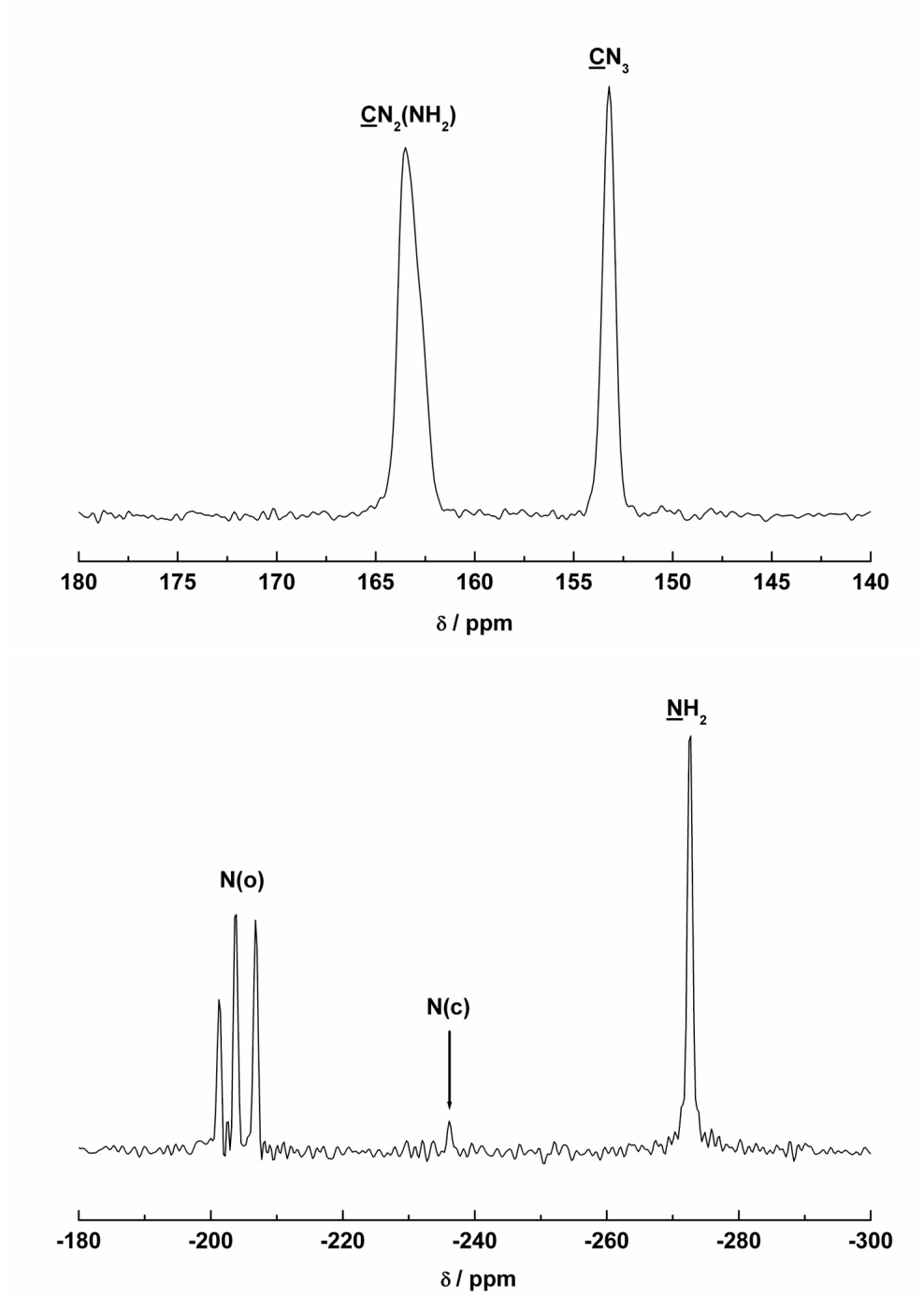

Figure 5. ^{13}C (top) and ^{15}N (bottom) CP-MAS solid-state NMR spectra of as-synthesized melem hydrate **2**, dried at room temperature.

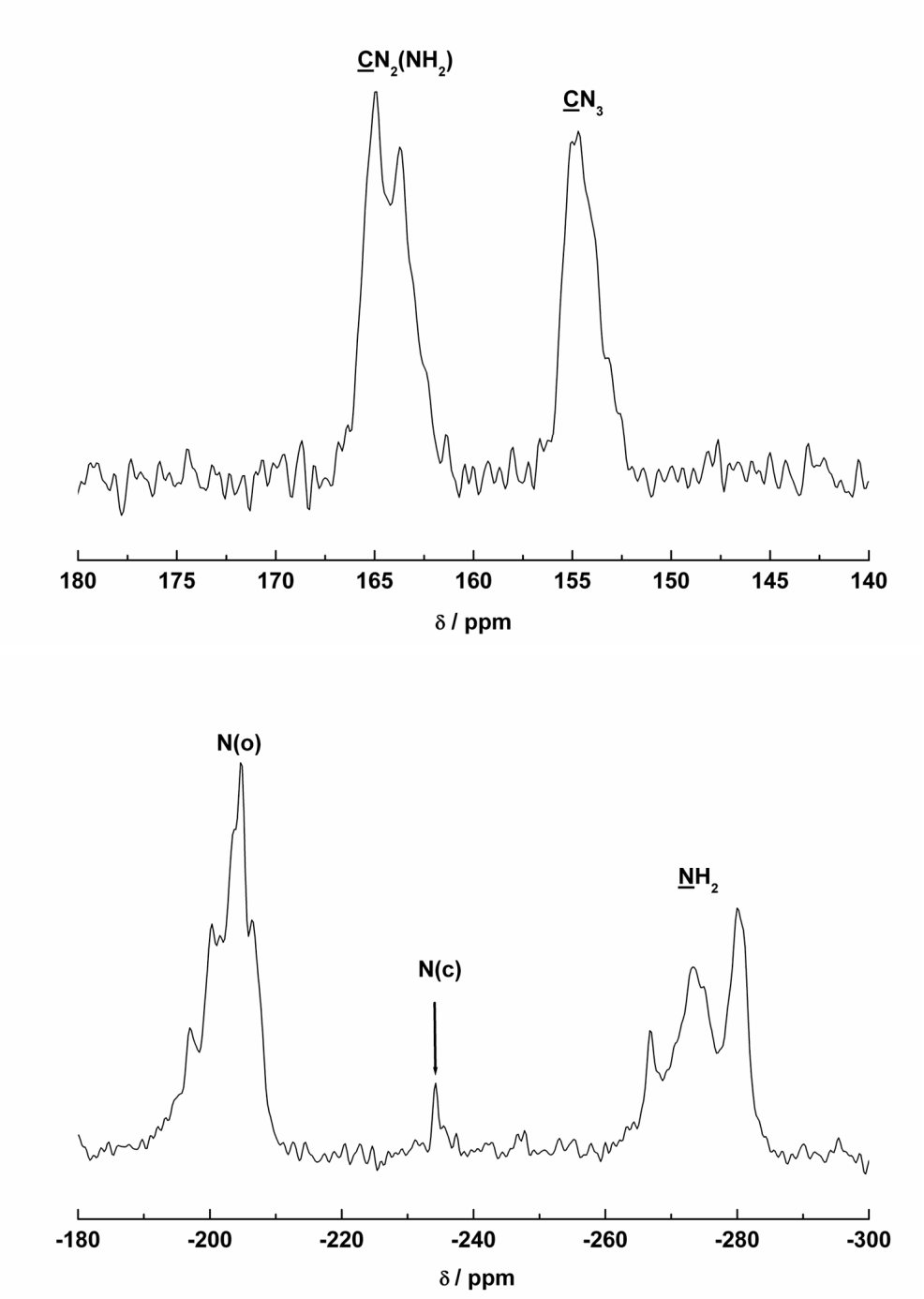

Figure 6. ^{13}C (top) and ^{15}N (bottom) CP-MAS solid-state NMR spectra of melem hydrate **2**, dehydrated at 150 °C under vacuum.

in accordance with solid-state NMR studies of anhydrous melem **1**[24] (compare Scheme 3). The ^{13}C NMR signals of $CN_2(NH_2)$ and CN_3 groups were observed at δ = 163.5 and 153.2 ppm, respectively (see Figure 5, top). For both the CN_3 and $CN_2(NH_2)$ carbon atoms there are each two crystallographic positions but because the chemical surroundings of these atoms basically only differ with respect to hydrogen-bonding interactions of adjacent nitrogen atoms, the respective resonances are not distinctly split. In the ^{15}N spectrum (see Figure 5, bottom) signals can be attributed to the amino groups (δ = -272.7 ppm), the central nitrogen atom of the *s*-heptazine core (δ = -236.2 ppm), and the remaining nitrogen atoms of the ring (δ = -206.9 to -201.3 ppm). Moreover, the multiplicity of signals in the ^{15}N NMR spectrum is in accordance with the number of crystallographic nitrogen positions. Considering the number of signals in the NMR spectra, the presence of an adduct phase between melem and cyameluric acid can be ruled out. Such an adduct phase would lead to splitting of signals both for the outer nitrogen atoms of the ring N(o) and the carbon atoms. Especially for the ^{13}C NMR signal at δ = 163.5 ppm, which corresponds to carbon atoms that are bound either to NH_2 or OH substituents, a splitting would be expected. Elemental analysis and mass spectrometry further confirmed that detectable amounts of cyameluric acid are not formed during the treatment of melem in boiling water. Elemental analysis revealed an atomic ratio C/N = 12:20, matching the formula $C_6N_7(NH_2)_3$, whereas an adduct between melem and cyameluric acid would correspond to a ratio of 12:17. Consistently, an intense peak at m/z = 218.2 ($C_6N_{10}H_6$) occurs in the mass spectrum, but none at m/z = 221.1 ($C_6N_7O_3H_3$) (see the Supporting Information, Figures S1-S2).

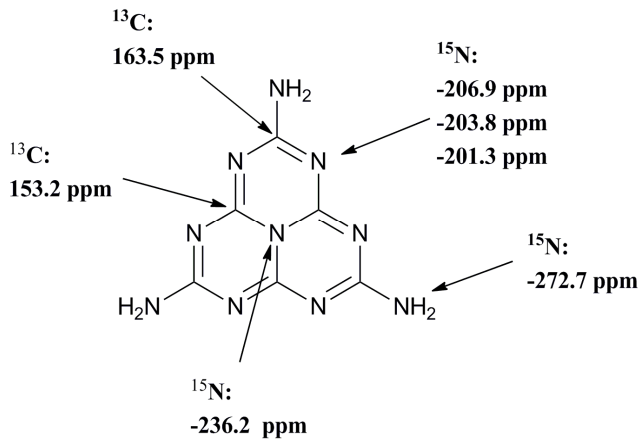

Scheme 3. ^{13}C and ^{15}N NMR chemical shifts observed for melem hydrate **2**.

Furthermore, a dehydrated sample of melem hydrate has been analyzed by solid-state NMR spectroscopy. According to TG/DTA data (see below), crystal water can be largely removed by heating the compound to 150 °C under vacuum overnight. In comparison to as-synthesized melem hydrate, both ^{13}C and ^{15}N spectra of the dehydrated sample (see Figure 6) show a broadening of signals, as expected due to the lower crystallinity of this material. Additionally, splitting of the $CN_2(NH_2)$ signal in the ^{13}C NMR spectrum and the NH_2 signal

in the ^{15}N NMR spectrum are observed, whereas the multiplicity of the remaining signals do not change. Hence, the chemical surroundings of the *s*-heptazine cores remain basically unaltered during the removal of crystal water but those of the amino groups, and, consequently, also of the carbon atoms they are bound to, are different for as-synthesized and dehydrated melem hydrate. Removal of water from the channels corresponds to a withdrawal of hydrogen-bonding donors and acceptors from the structure. Consequently, dehydration causes melem units to form additional hydrogen bonds to other melem entities. The amino groups are affected most by dehydration because N–H···O interactions between the melem framework and crystal water molecules are primarily formed by them (see Figure 3). Therefore, changes in the NMR spectra are mainly observed for the amino groups. Considering the geometric prerequisites for a stable hydrogen bonding network, formation of additional N–H···N interactions is likely to require a shifting of melem units as is discussed in detail below.

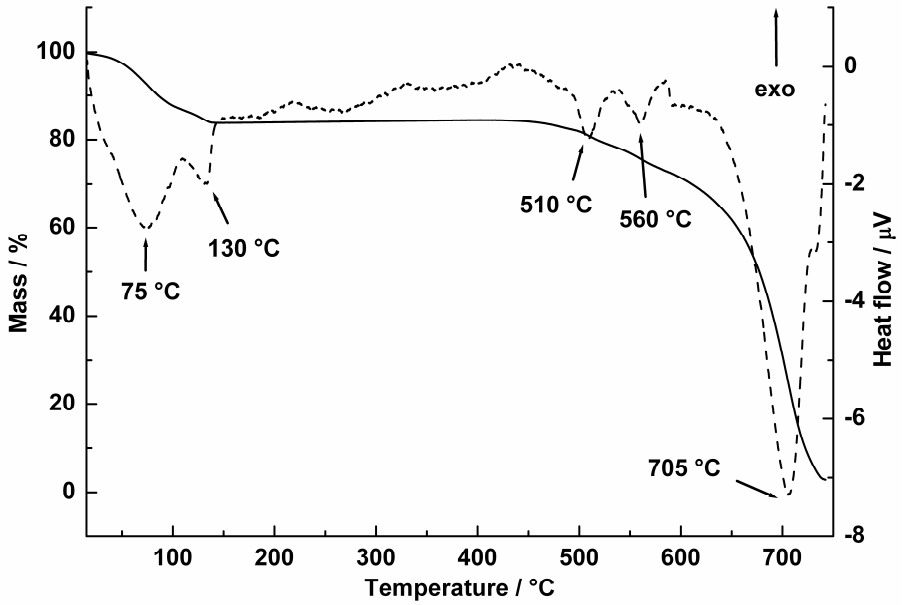

Figure 7. TG (solid) and DTA (dashed) curves of melem hydrate **2** (22.4 mg), measured with a heating rate of 5 $K \cdot min^{-1}$.

Thermal Behavior

The strength of interactions between melem and water molecules as well as the thermal stability of melem hydrate **2** was investigated by TG and DTA measurements. The obtained curves (see Figure 7) show that dehydration of **2** takes place in two steps at 20-150 °C (mass loss observed: 16.1 %, calculated for melem·2.33H_2O: 16.1 %). Subsequently, the dehydrated sample shows thermal stability up to 430 °C. Above this temperature the thermal behavior of **2** is as typically observed for molecular *s*-heptazine compounds in this temperature range.[20,24,26,29] The slow mass loss of 11.4 % at 430-585 °C can presumably be assigned to the release of ammonia and subsequent condensation to a melon like product.[14] Above 585 °C the rapid mass loss of 70.1 % accompanied by a strong endothermic signal in the DTA curve indicates a complete decomposition of the sample into gaseous products. The incipient release of crystal water already at 20 °C is consistent with the above results from single-crystal data, indicating that partly, only weak hydrogen bonds exist between the melem framework and water molecules. During temperature-dependent powder X-ray diffraction (see the Supporting Information, Figure S3) between room temperature and 500 °C, no emergence of any reflections corresponding to crystalline anhydrous melem **1** could be observed. Hence, melem hydrate **2** starts to decompose above 430 °C without previous phase transition to crystalline melem **1**.

In agreement with TG/DTA measurements, melem hydrate can be largely dehydrated by heating to 150 °C under vacuum. However, elemental analysis of a dehydrated sample yielded a total amount of nitrogen, carbon and hydrogen of only 97.8 wt. %. Assignment of the remaining 2.2 wt. % to oxygen results in the formula $C_{6.0}N_{9.9}O_{0.3}H_{6.2}$. This composition can be attributed either to incomplete dehydration of melem hydrate [ca. $C_6N_7(NH_2)_3 \cdot 0.3H_2O$] or to partial hydrolysis [ca. $(C_6N_7(NH_2)_{2.7}(OH)_{0.3}$] due to reaction of melem with crystal water at elevated temperatures. However, because such a small degree of hydrolysis cannot be clearly detected by solid-state NMR or IR spectroscopic analyses, none of these possibilities can be ruled out unambiguously. A comparison of the powder X-ray diffraction patterns of as-synthesized and dehydrated melem hydrate shows that, according to expectation, removal of crystal water significantly decreases the crystallinity of the product (see Figure 8, top). However, the sample does not become completely amorphous; the main reflections in the X-ray diffraction pattern are retained even after dehydration of melem hydrate. Especially, the 110 and 220 reflections, corresponding to a hexagonal pattern, are clearly visible (see Figure 8, bottom). Furthermore, a broad reflection at 2θ = 26-28° is observed that can be attributed to a layered arrangement of melem molecules with an interlayer distance of 320–340 ppm. However,

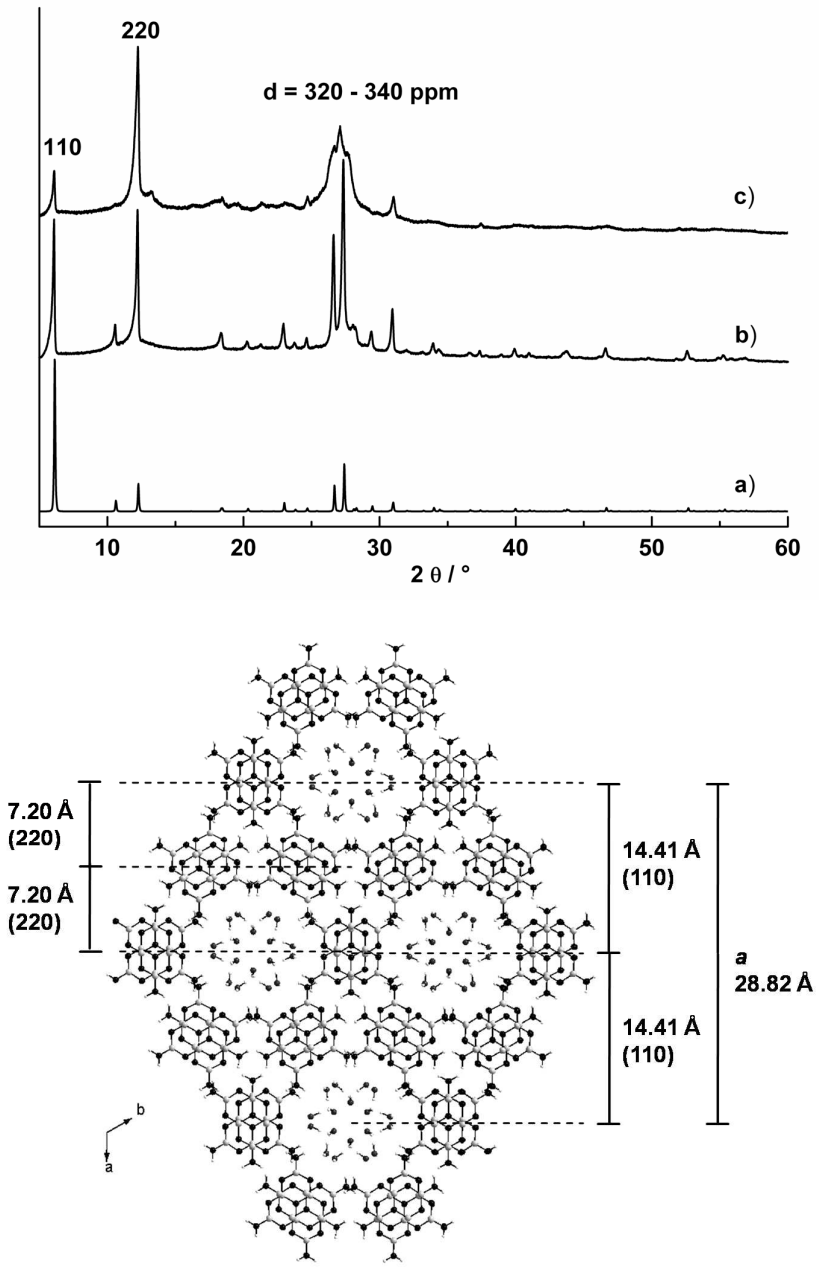

Figure 8. Top: Powder X-ray diffraction patterns (293 K, λ = 154.06 pm) of melem hydrate **2** (top) ; a) calculated pattern based on single-crystal data; b) measured pattern of an as-synthesized sample, dried at room temperature, and c) measured pattern of a sample dehydrated at 150 °C under vacuum. Representation of distances in the structure of melem hydrate corresponding to 110 and 220 reflections (bottom).

there is no evidence that the stacking pattern of hexagonal layers of melem units also remains unaltered. Sorption measurements (see below) indicate that during dehydration of melem hydrate, channels in the structure are blocked. This might be explained by a shifting of layers perpendicular to the *c*-axis. As is discussed above, removal of water causes the amino groups of melem to form additional hydrogen bonds to other melem units. Due to perpetuation of the hexagonal arrangement within the layers, these newly formed hydrogen bonds are most likely formed between the layers. Shifting of the layers might be required so that the amino groups can serve most suitable as donors and acceptors, respectively, for hydrogen bonds.

In summary, the hexagonal structure of melem hydrate does not collapse when water is removed from the channels but the stacking mode of melem layers is probably altered. Because the hydrogen-bonding network interconnecting the melem molecules appears to be strong enough to preserve the main structural features during dehydration, water molecules can essentially be regarded as a template that is required during self-assembly of melem molecules to obtain the porous structure of **2** and not the denser structure of **1**. Melem hydrate, therefore, not only represents an interesting example for the development of a highly symmetric channel structure by self-assembly but also a thermally stable *s*-heptazine-based framework which is predominantly stabilized by strong intermolecular hydrogen bonds between the melem units.

Sorption Measurements

To investigate whether the removal of crystal water makes the channels accessible for other guest molecules, N_2 gas adsorption measurements were performed. After dehydrating a sample of melem hydrate **2** for 12 h at 20 °C and subsequently 6 h at 150 °C, an isotherm was recorded between P/P_o = 0.02 and P/P_o = 0.5. Applying the Brunauer-Emmett-Teller (BET) model to the isotherm resulted in a surface area S_{BET} = 29 $m^2 \cdot g^{-1}$. In comparison to 2D covalent organic frameworks (COFs) with similar pore diameters that exhibit surface areas of 711 $m^2 \cdot g^{-1}$ (COF-1) or 980 $m^2 \cdot g^{-1}$ (COF-6), respectively,[36] it becomes evident that, for dehydrate melem hydrate **2**, perceptible filling of channels with nitrogen does not occur. As is discussed above, this might be due to a shifting of melem layers perpendicular to the direction of the channels, thereby locking the channels and making them inaccessible for guest molecules.

FTIR Spectroscopy

Melem hydrate **2** was further analyzed by FTIR spectroscopy (see Figure 9). In the spectra of both an as-synthesized sample dried at room temperature and of a sample dehydrated at 150 °C, all signals of bending and stretching vibrations of the *s*-heptazine core are in accordance with data of anhydrous melem **1**.[24] In the region of NH and OH stretching vibrations at 2700-3550 cm^{-1}, sharp *ν*(NH) bands, which have been observed for anhydrous melem **1**, are covered by a broad *ν*(OH) signal in the spectrum of as-synthesized melem hydrate but are observable in the spectrum of dehydrated melem hydrate.

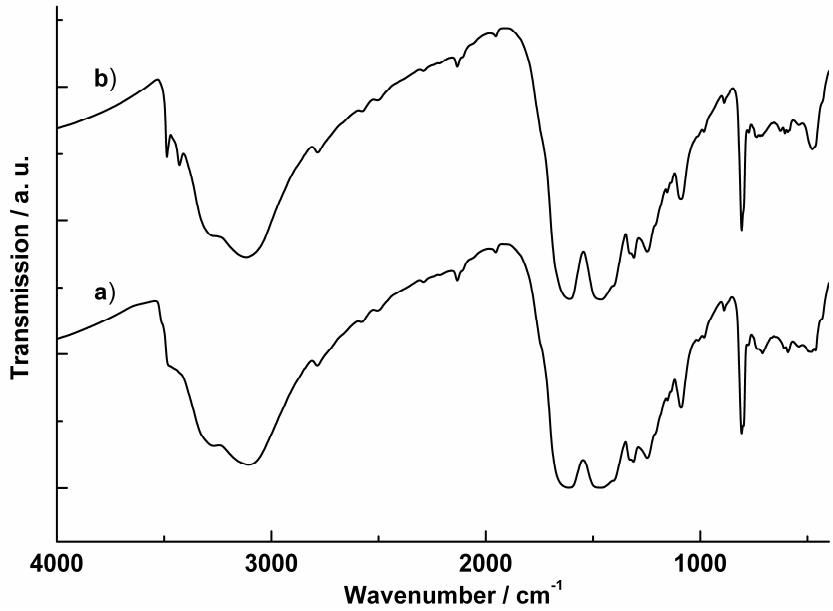

Figure 9. FTIR spectra of a) as-synthesized melem hydrate **2**, dried at room temperature and b) melem hydrate **2**, dehydrated at 150 °C under vacuum.

6.3 Conclusion

In this contribution we describe the self-assembly of melem in aqueous solution, thereby complementing preceding studies on the arrangement of melem units in the solid state and in monolayers on Ag(111). Both in anhydrous melem and in melem hydrate, the formation of numerous intermolecular hydrogen bonds appears to be the main factor determining the development of a specific structure. Although melem is insoluble in aqueous solution, treatment of melem in boiling water induces rearrangement of melem units from a dense to a porous structure. In the presence of solvent molecules, hydrogen bonds in melem are broken up and, during self-assembly into a porous structure, N-H···O interactions between melem and solvent molecules are formed whereas the number of N-H···N bonds between melem units is decreased in comparison to anhydrous melem. Thermal analysis revealed varying degrees of binding strengths for hydrogen bonds present in melem hydrate. Whereas the main part of water can be removed from the material quite easily, small amounts of crystal water remain in the material even at elevated temperatures. Dehydration affects the stacking pattern of melem units but not the hexagonal assembly within the layers. The observation that the hexagonal structure is maintained even when solvent molecules are largely removed demonstrates the potential of a dense network of intermolecular hydrogen bonds between melem units to stabilize a specific arrangement.

The characterization of melem hydrate not only allows for a better understanding of the role of hydrogen-bonding in C/N/H compounds but also establishes a further relationship between the main building blocks in carbon nitride chemistry, namely *s*-triazines and *s*-heptazines. The hydrogen-bonded, rosette-like pattern in *s*-heptazine melem hydrate resembles that of the famous adduct between the *s*-triazine compounds cyanuric acid and melamine. However, because until now a rosette-like assembly could be realized for melem but not for melamine, and for an adduct between cyanuric acid and melamine but not for an analogous adduct between cyameluric acid and melem, it becomes evident that the formation of such structures depends on diverse factors. We have demonstrated that the construction of a symmetric framework by self-assembly is not limited to the well-known CA·M adduct but that it is also possible for an *s*-heptazine compound. The presented results will certainly initiate further synthetic efforts to develop novel hydrogen-bonded networks of various C/N/H compounds or mixtures thereof.

6.4 Experimental Section

Synthesis

Melem hydrate **2** was prepared in preparative amounts according to the procedure described by Sattler et al.[30] starting either from raw or pure crystalline melem. Raw melem was obtained by heating melamine (Fluka, p. a.) in a porcelain crucible covered with a lid in a muffel furnace at 425 °C overnight.[30] To synthesized pure melem,[24] melamine (200 mg, 1.58 mmol, Fluka, p. a.) was placed in a dried Duran glass tube ($\varnothing_{ext.}$ = 16 mm, $\varnothing_{int.}$ = 12 mm). The tube was filled with argon, sealed at a length of 16 cm and placed in an inclined tube furnace. The sample was heated at 1 K·min^{-1} to 450 °C, held at this temperature for 5 h and cooled to RT at 2 K·min^{-1}. From the bottom part of the ampoule, crystalline melem (104 mg, 0.47 mmol, 60 %) could be isolated. Elemental analysis calcd (%) for $C_6N_7(NH_2)_3$: C 33.03, H 2.78, N 64.21; found: C 33.17, H 2.78, N 63.81.

Single crystals of melem hydrate suitable for X-ray diffraction analysis were obtained under hydrothermal conditions. A suspension of raw melem (150.0 mg, 0.69 mmol) in H_2O (20 mL) acidified with a few drops of 2M HCl was filled in a Teflon-lined 40 mL steel autoclave, heated at 0.07 K·min^{-1} to 200 °C and cooled back to RT at 0.25 K·min^{-1}.

For the preparation of larger quantities of melem hydrate, crystalline melem was used as starting material because, in bulk samples of melem hydrate synthesized from raw melem, small amounts of amorphous side phases could be identified by solid-state NMR spectroscopy. Melem was boiled in water at reflux for 30 min, filtered, washed with water and dried at RT, yielding melem hydrate **2** as a colorless powder. MS (DEI+): *m/z* (%): 218 (100) [$C_6N_7(NH_2)_3^+$]; elemental analysis calcd (%) for $C_6N_7(NH_2)_3 \cdot 2.5H_2O$: C 27.38, H 4.21, N 53.21; found: C 27.52, H 4.02, N 53.00.

Dehydration of melem hydrate was performed by heating the compound to 150 °C under vacuum ($1 \cdot 10^{-3}$ mbar) overnight. Elemental analysis calcd (%) for $C_6N_7(NH_2)_3 \cdot 0.3H_2O$: C 32.23, H 2.98, N 62.64; found: C 32.48, H 2.83, N 62.45.

X-ray Structure Determination

Single-crystal X-ray diffraction data of **2** were collected at 173 K with a Kappa CCD diffractometer (Mo-K_α radiation, λ = 71.073 pm). The diffraction intensities were scaled using the SCALEPACK[37] software package and no additional absorption correction was applied. The crystal structure was

solved by direct methods (SHELXS-97) and refined against F^2 by applying the full-matrix least-squares method (SHELXL-97).[38] Hydrogen positions were determined from difference Fourier syntheses considering reasonable oxygen–hydrogen distances and were refined isotropically. All non-hydrogen atoms were refined anisotropically.

Further details of the crystal structure investigation(s) can be obtained from the Fachinformationszentrum Karlsruhe, 76344 Eggenstein-Leopoldshafen, Germany (fax: (+49) 7247-808-666; e-mail: crysdata@fizkarlsruhe.de, http://www.fiz-karlsruhe.de/request_for_deposited_data.html) on quoting the depository number CSD-423755.

Powder X-ray diffraction data under ambient conditions were collected in transmission geometry with a Huber Guinier G670 Imaging Plate diffractometer using Ge(111)-monochromated Cu-$K_{\alpha 1}$ radiation (λ = 154.06 pm).

High-temperature in situ X-ray diffraction measurements were performed on a STOE Stadi P powder diffractometer with an integrated furnace, using Ge(111)-monochromated Mo-$K_{\alpha 1}$ radiation (λ = 70.093 pm). The sample was heated in an unsealed Duran capillary ($\varnothing$ = 0.3 mm) from RT to 500 °C with a ramp of 2 $K \cdot min^{-1}$ and scans were collected in steps of 25 K up to 150 °C and in steps of 50 K at 150-500 °C.

Solid-State NMR Spectroscopy

^{1}H, ^{13}C and ^{15}N MAS NMR spectra were recorded at RT with a Bruker Avance III-500 spectrometer in an external magnetic field of 11.7 T. The measurements were performed with a rotation frequency of 10 kHz using 4 mm standard double-resonance MAS probes (Bruker), which were operated with zirconia rotors. For all experiments, broadband proton decoupling was applied. Both ^{13}C and ^{15}N nuclei were excited via the proton bath by employing a ramped cross-polarization sequence in which the ^{1}H pulse amplitude was decreased linearly by 50 %. Trimethylsilane (TMS) (^{13}C, ^{1}H) and nitromethane (^{15}N) were used as references, respectively.

Thermal Analysis

Thermoanalytical measurements were performed with a Thermoanalyzer TG-DTA92 (Setaram). The sample was heated under inert atmosphere (He) in an alumina crucible from RT to 750 °C with a heating rate of 5 $K \cdot min^{-1}$.

Sorption Measurements

An N_2 adsorption isotherm was recorded at 77 K with an Autosorb iQ Instrument (Quantachrome Instruments). Before measuring the isotherm, the sample was dehydrated under dynamic vacuum for 12 h at 25 °C and subsequently for 6 h at 150 °C. The Brunauer-Emmett-Teller (BET) model was applied to the isotherm between P/P_o = 0.02 and P/P_o = 0.5.

General Techniques

FTIR spectra were recorded under ambient conditions with a Bruker IFS 66v/S spectrometer between 400 and 4000 cm^{-1}. The samples were measured as KBr pellets in an evacuated cell. Direct Electron Ionization (DEI+) (70 eV) mass spectra were measured on a JEOL JMS-700 spectrometer. Elemental analyses for C, H and N were conducted with the elemental analyzer systems Vario EL and Vario Micro (Elementar Analysensysteme GmbH).

Acknowledgements

The authors thank the Deutsche Forschungsgemeinschaft DFG (project SCHN 377/15) and the Fonds der Chemischen Industrie (FCI) for financial support, and the following people for conducting the physical measurements (all Department Chemie, LMU München): Brigitte Breitenstein (mass spectrometry), Stephan Hug (sorption measurements), Dr. Peter Mayer (single-crystal data collection), Christian Minke (solid-state NMR spectroscopy) and Thomas Miller (temperature-dependent X-ray powder diffraction).

6.5 Bibliography

[1] See, for example: a) C. B. Aakeröy, N. R. Champness, C. Janiak, *CrystEngComm* **2010**, *12*, 22-43; b) M. M. Conn, J. Rebek Jr., *Chem. Rev.* **1997**, *97*, 1647-1668; c) R. Custelcean, *Chem. Commun.* **2008**, 295-307; d) G. R. Desiraju, *Angew. Chem.* **2007**, *119*, 8492-8508; *Angew. Chem. Int. Ed.* **2007**, *46*, 8342-8356; e) M. C. Etter, *J. Phys. Chem.* **1991**, *95*, 4601-4610; f) M. C. T. Fyfe, J. F. Stoddart, *Acc. Chem. Res.* **1997**, *30*, 393-401; g) D. S. Lawrence, T. Jiang, M. Levett, *Chem. Rev.* **1995**, *95*, 2229-2260; h) J.-M. Lehn, *Angew. Chem.* **1990**, *102*, 1347-1362; *Angew. Chem. Int. Ed. Engl.* **1990**, *29*, 1304-1319; i) K. Merz, V. Vasylyeva, *CrystEngComm* **2010**, *12*, 3989-4002; j) D. Philp, J. F. Stoddart, *Angew. Chem.* **1996**, *108*, 1242-1286; *Angew. Chem. Int. Ed. Engl.* **1996**, *35*, 1154-1196; k) L. J. Prins, D. N. Reinhoudt, P. Timmerman, *Angew. Chem.* **2001**, *113*, 2446-2492; *Angew. Chem. Int. Ed.* **2001**, *40*, 2382-2426; l) C. M. Reddy, G. R. Krishna, S. Ghosh, *CrystEngComm* **2010**, *12*, 2296-2314; m) G. M. Whitesides, J. P. Mathias, C. T. Seto, *Science* **1991**, *254*, 1312-1319.

[2] G. M. Whitesides, E. E. Simanek, J. P. Mathias, C. T. Seto, D. N. Chin, M. Mammen, D. M. Gordon, *Acc. Chem. Res.* **1995**, *28*, 37-44.

[3] For reviews see, for example: a) G. Couderc, J. Hulliger, *Chem. Soc. Rev.* **2010**, *39*, 1545-1554; b) P. H. Dinolfo, J. T. Hupp, *Chem. Mater.* **2001**, *13*, 3113-3125; c) P. J. Langley, J. Hulliger, *Chem. Soc. Rev.* **1999**, *28*, 279-291.

[4] a) I. S. Choi, X. Li, E. E. Simanek, R. Akaba, G. M. Whitesides, *Chem. Mater.* **1999**, *11*, 684-690; b) X. Li, D. N. Chin, G. M. Whitesides, *J. Org. Chem.* **1996**, *61*, 1779-1786; c) J. P. Mathias, E. E. Simanek, C. T. Seto, G. M. Whitesides, *Angew. Chem.* **1993**, *105*, 1848-1850; *Angew. Chem. Int. Ed. Engl.* **1993**, *32*, 1766-1769; d) C. T. Seto, J. P. Mathias, G. M. Whitesides, *J. Am. Chem. Soc.* **1993**, *115*, 1321-1329; e) C. T. Seto, G. M. Whitesides, *J. Am. Chem. Soc.* **1990**, *112*, 6409-6411; f) C. T. Seto, G. M. Whitesides, *J. Am. Chem. Soc.* **1991**, *113*, 712-713.

[5] a) J. P. Mathias, C. T. Seto, E. E. Simanek, G. M. Whitesides, *J. Am. Chem. Soc.* **1994**, *116*, 1725-1736; b) C. T. Seto, G. M. Whitesides, *J. Am. Chem. Soc.* **1993**, *115*, 905-916.

[6] A. Ranganathan, V. R. Pedireddi, C. N. R. Rao, *J. Am. Chem. Soc.* **1999**, *121*, 1752-1753.

[7] a) V. R. Pedireddi, S. Chatterjee, A. Ranganathan, C. N. R. Rao, *J. Am. Chem. Soc.* **1997**, *119*, 10867-10868; b) A. Ranganathan, V. R. Pedireddi, S. Chatterjee, C. N. R. Rao, *J. Mater. Chem.* **1999**, *9*, 2407-2411.

[8] a) D. J. Duchamp, R. E. Marsh, *Acta Crystallogr., Sect. B* **1969**, *25*, 5-19; b) F. H. Herbstein, M. Kapon, G. M. Reisner, *J. Inclusion Phenom.* **1987**, *5*, 211-217; c) S. V. Kolotuchin, E. E. Fenlon, S. R. Wilson, C. J. Loweth, S. C. Zimmerman, *Angew. Chem.* **1995**, *107*, 2873-2876; *Angew.*

Chem. Int. Ed. Engl. **1995**, *34*, 2654-2657; d) S. V. Kolotuchin, P. A. Thiessen, E. E. Fenlon, S. R. Wilson, C. J. Loweth, S. C. Zimmerman, *Chem. Eur. J.* **1999**, *5*, 2537-2547.

[9] a) A. R. A. Palmans, J. A. J. M. Vekemans, H. Kooijman, A. L. Spek, E. W. Meijer, *Chem. Commun.* **1997**, 2247-2248; b) R. R. Shuvalov, P. C. Burns, *Acta Crystallogr., Sect. C.* **2003**, *59*, i47-i49; c) J. Yang, J.-L. Marendaz, S. J. Geib, A. D. Hamilton, *Tetrahedron Lett.* **1994**, *35*, 3665-3668; d) W. H. Zachariasen, *Acta Crystallogr.* **1954**, *7*, 305-310.

[10] L. Pauling, J. H. Sturdivant, *Proc. Natl. Acad. Sci. U.S.A.* **1937**, *23*, 615-620.

[11] a) R. S. Hosmane, M. A. Rossman, N. J. Leonard, *J. Am. Chem. Soc.* **1982**, *104*, 5497-5499; b) M. Shahbaz, S. Urano, P. R. LeBreton, M. A. Rossman, R. S. Hosmane, N. J. Leonard, *J. Am. Chem. Soc.* **1984**, *106*, 2805-2811.

[12] a) F. Goettmann, A. Fischer, M. Antonietti, A. Thomas, *Angew. Chem.* **2006**, *118*, 4579-4583; *Angew. Chem. Int. Ed.* **2006**, *45*, 4467-4471; b) F. Goettmann, A. Thomas, M. Antonietti, *Angew. Chem.* **2007**, *119*, 2773-2776; *Angew. Chem. Int. Ed.* **2007**, *46*, 2717-2720; c) H. Grueger, C. Kunath, European Patent *EP1436607*; d) H. Sugimura, Y. Sato, N. Tajima, O. Takai, *Surface Coating Technol.* **2001**, *142-144*, 714-718; e) A. Thomas, A. Fischer, F. Goettmann, M. Antonietti, J.-O. Müller, R. Schlögl, J. M. Carlsson, *J. Mater. Chem.* **2008**, *18*, 4893-4908; f) X. Wang, K. Maeda, A. Thomas, K. Takanabe, G. Xin, J. M. Carlsson, K. Domen, M. Antonietti, *Nat. Mater.* **2009**, *8*, 76-80; g) Z. B. Zhou, R. Q. Cui, Q. J. Pang, G. M. Hadi, Z. M. Ding, W. Y. Li, *Solar Energy Mater. Solar Cells* **2002**, *70*, 487-493.

[13] M. Döblinger, B. V. Lotsch, J. Wack, J. Thun, J. Senker, W. Schnick, *Chem. Commun.* **2009**, 1541-1543.

[14] B. V. Lotsch, M. Döblinger, J. Sehnert, L. Seyfarth, J. Senker, O. Oeckler, W. Schnick, *Chem. Eur. J.* **2007**, *13*, 4969-4980.

[15] a) B. V. Lotsch, W. Schnick, *Chem. Mater.* **2006**, *18*, 1891-1900; b) D. R. Miller, J. R. Holst, E. G. Gillan, *Inorg. Chem.* **2007**, *46*, 2767-2774.

[16] E. Kroke, M. Schwarz, E. Horath-Bordon, P. Kroll, B. Noll, A. D. Norman, *New J. Chem.* **2002**, *26*, 508-512.

[17] J. Sehnert, K. Baerwinkel, J. Senker, *J. Phys. Chem.* **2007**, *111*, 10671–10680.

[18] S. Tragl, H.-J. Meyer, *Z. Anorg. Allg. Chem.* **2005**, *631*, 2300-2302.

[19] D. R. Miller, D. C. Swenson, E. G. Gillan, *J. Am. Chem. Soc.* **2004**, *126*, 5372-5373.

[20] a) C. Clauss, J. Wagler, M. Schwarz, A. Schwarzer, E. Kroke, *Z. Anorg. Allg. Chem.* **2010**, *636*, 196-200; b) E. Horvath-Bordon, E. Kroke, I. Svoboda, H. Fuess, R. Riedel, *New J. Chem.* **2005**, *29*, 693-699; c) S. J. Makowski, W. Schnick, *Z. Anorg. Allg. Chem.* **2009**, *635*, 2197-2202; d) A. Sattler, W. Schnick, *Eur. J. Inorg. Chem.* **2009**, 4972-4981.

[21] S. J. Makowski, D. Gunzelmann, J. Senker, W. Schnick, *Z. Anorg. Allg. Chem.* **2009**, *635*, 2434-2439.

[22] N. E. A. El-Gamel, L. Seyfarth, J. Wagler, H. Ehrenberg, M. Schwarz, J. Senker, E. Kroke, *Chem. Eur. J.* **2007**, *13*, 1158-1173.

[23] a) Y. Ke, D. J. Collins, D. Sun, H.-C. Zhou, *Inorg. Chem.* **2006**, *45*, 1897-1899; b) T. Saplinova, V. Bakumov, T. Gmeiner, J. Wagler, M. Schwarz, E. Kroke, *Z. Anorg. Allg. Chem.* **2009**, *635*, 2480-2487; c) T. Saplinova, C. Lehnert, U. Böhme, J. Wagler, E. Kroke, *New J. Chem.* **2010**, *34*, 1893-1908; d) M. R. Schwarz, H. Ehrenberg, M. A. Kloc, E. Kroke, *Heterocycles* **2006**, *68*, 2499-2507; e) A. Schwarzer, E. Kroke, *Chem. Commun.* **2010**, *46*, 2829-2831; f) A. Schwarzer, E. Kroke, *New J. Chem.* **2011**, *35*, 953-958; g) B. Traber, T. Oeser, R. Gleiter, M. Goebel, R. Wortmann, *Eur. J. Org. Chem.* **2004**, 4387-4390.

[24] B. Jürgens, E. Irran, J. Senker, P. Kroll, H. Müller, W. Schnick, *J. Am. Chem. Soc.* **2003**, *125*, 10288–10300.

[25] A. Sattler, W. Schnick, *Z. Anorg. Allg. Chem.* **2006**, *632*, 238-242.

[26] A. Sattler, W. Schnick, *Z. Anorg. Allg. Chem.* **2006**, *632*, 1518-1523.

[27] a) L. Seyfarth, J. Sehnert, N. E. A. El-Gamel, W. Milius, E. Kroke, J. Breu, J. Senker, *J. Mol. Struct.* **2008**, *889*, 217-228; b) J. Wagler, N. E. A. El-Gamel, E. Kroke, *Z. Naturforsch.* **2006**, *61b*, 975-978.

[28] a) N. E. A. El-Gamel, J. Wagler, E. Kroke, *J. Mol. Struct.* **2008**, *888*, 204-213; b) A. Sattler, M. R. Budde, W. Schnick, *Z. Anorg. Allg. Chem.* **2009**, *635*, 1933-1939; c) A. Sattler, W. Schnick, *Z. Anorg. Allg. Chem.* **2006**, *632*, 531-533; d) A. Sattler, W. Schnick, *Z. Anorg. Allg. Chem.* **2008**, *634*, 1063-1066; e) A. Sattler, W. Schnick, *Z. Anorg. Allg. Chem.* **2008**, *634*, 457-460; f) A. Sattler, W. Schnick, *Z. Anorg. Allg. Chem.* **2010**, *636*, 2589-2594; g) A. Sattler, L. Seyfarth, J. Senker, W. Schnick, *Z. Anorg. Allg. Chem.* **2005**, *631*, 2545-2554.

[29] E. Horvath-Bordon, E. Kroke, I. Svoboda, H. Fueß, R. Riedel, S. Neeraj, A. K. Cheetham, *Dalton Trans.* **2004**, 3900-3908.

[30] A. Sattler, S. Schönberger, W. Schnick, *Z. Anorg. Allg. Chem.* **2010**, *636*, 476-482.

[31] B. V. Lotsch, W. Schnick, *Chem. Eur. J.* **2007**, *13*, 4956-4968.

[32] A. Sattler, S. Pagano, M. Zeuner, A. Zurawski, D. Gunzelmann, J. Senker, K. Müller-Buschbaum, W. Schnick, *Chem. Eur. J.* **2009**, *15*, 13161-13170.

[33] J. Eichhorn, S. Schlögl, B. V. Lotsch, W. Schnick, W. M. Heckl, M. Lackinger, *CrystEngComm* **2011**, *13*, 5559-5565.

[34] A. Sattler, Diploma Thesis, University of Munich (LMU), **2005**.

[35] T. Steiner, *Angew. Chem.* **2002**, *114*, 50-80; *Angew. Chem. Int. Ed.* **2002**, *41*, 48-76.

[36] a) A. P. Côté, A. I. Benin, N. W. Ockwig, M. O'Keeffe, A. J. Matzger, O. M. Yaghi, *Science* **2005**, *310*, 1166-1670; b) A. P. Côté, H. M. El-Kaderi, H. Furukawa, J. R. Hunt, O. M. Yaghi, *J. Am. Chem. Soc.* **2007**, *129*, 12914-12915.

[37] Z. Otwinowski, W. Minor, *Methods Enzymol.* **1997**, *276*, 307-326.

[38] a) G. M. Sheldrick, *Acta Crystallogr., Sect. A* **2008**, *64*, 112-122; b) G. M. Sheldrick, *SHELXS-97, Program for the Solution of Crystal Structures*, Universität Göttingen **1997**; c) G. M. Sheldrick, *SHELXL-97, Program for the Refinement of Crystal Structures*, Universität Göttingen **1997**.

7. Cocrystals of Melamine and *N*-Heterocycles

Both the formation of a channel structure in melem hydrate and the stability of this structure during thermal treatment, as has been described in the previous chapter, have demonstrated the relevance of hydrogen bridges for self-assembly of the *s*-heptazine derivative melem $C_6N_7(NH_2)_3$. The same holds true for the *s*-triazine derivative melamine $C_3N_3(NH_2)_3$, which comprises multiple amino groups and nitrogen atoms of the ring as suitable donors and acceptors, respectively, for hydrogen bonds. Formation of cocrystals between melamine and different components has been reported prior to this work. However, adducts of melamine and *N*-heterocycles have been investigated only rarely in this regard. Such compounds are of particular interest because they establish a relation between structurally related carbon nitride type materials and hydrocarbons. In order to investigate the accessibility of such adducts in solution and under solvent-free conditions as well as to study noncovalent interactions in such materials in detail, melamine has been reacted with several *N*-heterocycles. Crystal structures of obtained cocrystals and a discussion of the role of different types of noncovalent interactions in these compounds are presented in this chapter.

Supramolecular hydrogen-bonded structures between melamine and *N*-heterocycles

Sophia J. Makowski, Monika Lacher, Claudia Lermer, and Wolfgang Schnick

published in: *J. Mol. Struct.* **2012**, *1013*, 19. http://dx.doi.org/10.1016/j.molstruc.2012.01.010

Keywords: Co-crystal; Hydrogen bond; Melamine; *N*-Heterocycle; Supramolecular assembly

Abstract. Melamine (M) forms hydrogen bonded adducts with the *N*-heterocycles tris(2-pyridyl)-triazine (TPTZ) and tetrakis(4-*N*-methylpyridinumyl)porphyrin tetratosylate (TMPyP-Tos). The 4:3 adduct 4M·3TPTZ was obtained under solvent-free conditions and the 3:1 adduct 3M·TMPyP-Tos·9H_2O in aqueous solution. In both adduct phases *N*-heterocycles are arranged in π-π stacks and melamine molecules are arranged perpendicular to these stacks. Whereas cohesion between the extended π-systems of *N*-heterocycles is mainly achieved by dispersive interactions no stacking interactions between melamine molecules occur. Melamine units are orientated in such a way to be located most suitable as donors and acceptors, respectively, for a dense hydrogen bonding network. In 4M·3TPTZ all molecules are involved in hydrogen bonding, whereas in 3M·TMPyP-Tos·9H_2O hydrogen bridges are primarily formed between melamine, tosylate and water units and the macrocycle TMPyP is mainly bound by electrostatic interactions.

7.1 Introduction

The *s*-triazine core (C_3N_3) is widely applied as building unit in various fields, such as polymer, supramolecular, solid-state or coordination chemistry. Whereas in solid-state chemistry covalently bound C/N/H networks are obtained by thermal treatment of suitable molecular precursors,[1-8] in supramolecular chemistry frameworks are constructed by self-assembly of molecular building blocks. In these systems cohesion between molecules is achieved by various types of noncovalent interactions such as hydrogen bonds, ionic, hydrophobic, van der Waals or dispersive forces.[9-15] As starting materials for instance melamine $C_3N_3(NH_2)_3$ and its derivatives have been widely employed forming various adduct phases and showing recurring self-assembly motifs such as cyclic rosettes or linear and crinkled tapes. Next to numerous structures based on the famous adduct between cyanuric acid (CA) and melamine (CA·M)[16-25] for instance the formation of adducts between melamine and melem,[26] imides,[27-30] boric acid,[31] trithiocyanuric acid,[20] uracil[32] or 4,4'-bipyridyl[33] has been reported. Furthermore, various molecular salts comprising protonated melaminium ions have been investigated.[34-40] Such adducts are usually prepared by reaction of starting materials in appropriate solvents but for several materials also syntheses under solvent-free conditions have been reported.[29,41]

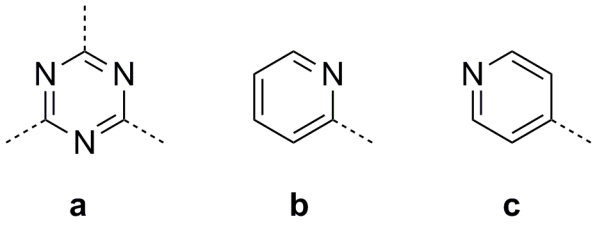

Scheme 1. Six-membered aromatic rings: (a) *s*-triazine (b) 2-pyridyl and (c) 4-pyridyl.

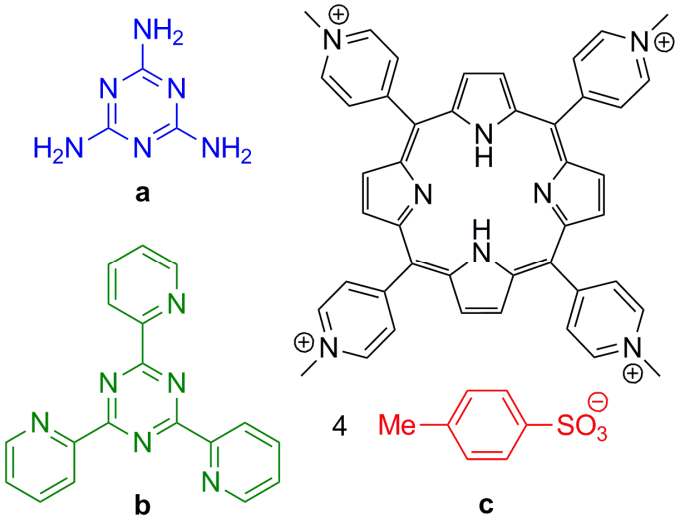

Scheme 2. Molecular structures of: (a) melamine, (b) TPTZ and (c) TMPyP-Tos.

In most of these compounds cohesion between different molecules is mainly achieved by hydrogen bonds and in the case of melaminium salts also by ionic interactions. Contrary, we are especially interested in adducts between melamine and large aromatic cycles in which self-assembly is additionally driven by dispersive interactions. Moreover, we try to employ nitrogen-rich heterocycles in such adducts in order to obtain co-crystals which can be regarded as model systems between carbon nitride type materials and hydrocarbons. These two classes of compounds often show structural similarities but differ with respect to their chemical and physical properties. For employment of functional materials in technical applications often tuning of specific properties is desired, which might for instance be achieved by combining carbon nitride type materials and hydrocarbons in a single compound. However, for the directed synthesis of applicable new materials a detailed knowledge of the factors that affect the arrangement of molecular building blocks in the solid state is an inevitable prerequisite. So far only very few examples of such co-crystals are known, for instance an adduct between melamine and bis(thymine)-*p*-xylyl.[27] Therefore we have investigated the possible formation of adducts between melamine (M) and various nitrogen-rich hydrocarbon cycles both in solution and under solvent-free conditions. For this purpose compounds were employed that comprise the pyridyl core, which represents an aromatic, six-membered ring structurally related to triazine (Scheme 1). In this contribution a structural and thermal characterization of co-crystals between melamine and the *N*-heterocycles tris(2-pyridyl)-triazine (TPTZ) and tetrakis(4-*N*-methyl-pyridinumyl)porphyrin tetratosylate (TMPyP-Tos) (Scheme 2), namely 4M·3TPTZ (**1**) and 3M·TMPyP-Tos·9H_2O (**2**), is reported.

7.2 Experimental

Materials

Melamine (Fluka, ≥ 99 %), 2,4,6-tris(2-pyridyl)-*s*-triazine (TPTZ, Alfa Aesar, 98 %), pyrrole (Aldrich, 98 %), 4-pyridine-carboxaldehyde (Aldrich, 98 %), propionic acid (Grüssing, > 99 %) and methyl tosylate (Fluka, > 97 %) were commercially available and used as received without further purification. TMPyP-Tos was prepared according to literature procedure by reacting pyrrol and 4-pyridine-carboxaldehyde in propionic acid and subsequent treatment with methyl tosylate.[42]

Physical measurements

Thermoanalytical measurements were performed under inert atmosphere (He) with a Thermoanalyzer TG-DTA92 (Setaram). Samples were heated in alumina crucibles from room temperature to 650 °C with a heating rate of 5 K min^{-1}. FTIR spectra were recorded at ambient conditions between 650 and 4000 cm^{-1} on a Spektrum BX II FTIR spectrometer (Perkin Elmer) equipped with a DuraSampler diamond ATR device. Elemental analyses for C, H, N and S were performed with the elemental analyzer systems Vario EL and Vario Micro (Elementar Analysensysteme GmbH).

Preparation of 1

Melamine (200.0 mg, 0.64 mmol) and TPTZ (108 mg, 0.85 mmol) were thoroughly ground and filled in a dried duran glass tube ($ø_{ext.}$ = 10 mm, $ø_{int.}$ = 7 mm). The tube was evacuated, sealed at a length of 12 cm and placed in an inclined tube furnace. The sample was heated at 5 K min^{-1} to 270 °C, held at this temperature for 24 h and cooled to room temperature at 0.05 K min^{-1}. Anal. calculated for $C_{66}H_{60}N_{42}$: C, 54.99; H, 4.20; N, 40.82 wt.%. Found: C, 53.22; H, 4.21; N, 41.84 wt.%. IR (cm^{-1}): 3450-3050(br), 1625(m), 1545(m), 1523(vs), 1448(s), 1429(s), 1366(s), 1246(w), 1150(w), 1092(w), 1043(w), 994(m), 851(w), 815(m), 765(vs), 737(s), 672(vs).

Preparation of 2

Melamine (55.5 mg, 0.44 mmol) was dissolved in 40 ml H_2O and meso-5,10,15,20-tetrakis(4-*N*-methylpyridinumyl)porphyrin tetratosylate (TMPyP-Tos) (200.0 mg, 0.15 mmol) was dissolved in 10 ml H_2O. The solutions were combined, stirred at room temperature for 12 h and subsequently the product was obtained by slow evaporation of solvent at room temperature. Anal. calculated for $C_{81}H_{102}N_{26}O_{21}S_4$: C, 51.09; H, 5.40; N, 19.13; S 6.74 wt.%. Found: C, 50.59; H, 5.43; N, 19.41; S, 6.60 wt.%. IR (cm^{-1}): 3420-3100(br), 1639(m), 1539(m), 1448(m), 1401(w), 1279(w), 1181(s), 1120(s), 1032(s), 1009(s), 969(m), 887(w), 859(w), 815(m), 794(s), 708(m), 682(vs).

Single-crystal X-ray diffraction

Single-crystal X-ray diffraction data of **1** and **2** were collected at 293 K (**1**) and 173 K (**2**), respectively, on a Kappa CCD diffractometer (Mo-K_α radiation, λ = 71.073 pm). The diffraction intensities were scaled using the SCALEPACK[43] software package and no additional absorption correction was applied. The crystal structures were solved by direct methods (SHELXS-97) and refined against F^2 by applying the full-matrix least-squares method (SHELXL-97).[44-46] Hydrogen

positions were calculated according to geometrical criteria and refined isotropically. All non-hydrogen atoms were refined anisotropically.

7.3 Results and discussion

Synthesis

The reaction between melamine (M) and tris(2-pyridyl)-triazine (TPTZ) was performed under solvent-free conditions at 270 °C above the melting point of TPTZ and the reaction between melamine and tetrakis(4-*N*-methyl-pyridinumyl)porphyrin tetratosylate (TMPyP-Tos) in aqueous solution at room temperature. Reason for the choice of TMPyP-Tos as macrocycle was the high solubility of this compound in water which represents the only applicable common solvent for melamine. Single crystals of the adduct phases 4M·3TPTZ (**1**) and 3M·TMPyP-Tos·9H_2O (**2**) were obtained by slow cooling of the reaction mixture or evaporation of the solvent at room temperature, respectively.

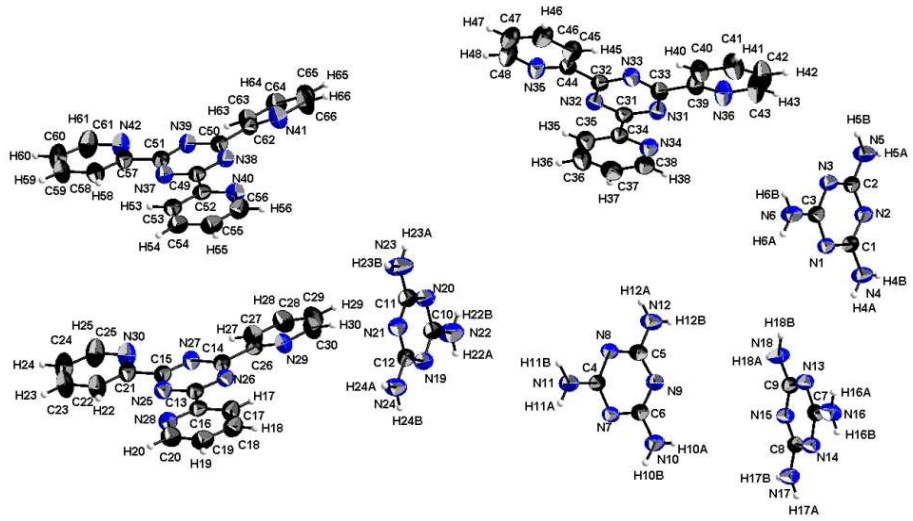

Figure 1. Formula unit of **1** with labeling of atoms. Thermal ellipsoids (except for hydrogen) are drawn at the 50 % probability level.

Crystal structures

4M·3TPTZ (**1**) crystallizes in the monoclinic space group *C*2/*c* and 3M·TMPyP-Tos·9H_2O (**2**) in the triclinic space group $P\ \bar{1}$. Crystallographic data and details of the structure refinement for **1** and **2** are summarized in Table 1 and labeling of atoms for both adduct phases is shown in Figs. 1 and 2. In the crystal structure of **2** a relatively large degree of disorder occurs. Next to disordered oxygen atoms of crystal water and tosylate units also part of the melamine molecules show disorder. As is illustrated in Fig. 2, the respective melamine units (N11-N16, C26-28) occupy two discrete positions with the second position being twisted relatively to the first one by 180° so that atoms C26 and N14 of the first position overlap with atoms N14 and C26 of the second position. Thus all atoms of these melamine molecules as well as neighboring crystal water oxygen atoms (O7, O8, O9) are localized on partially occupied sites. In further figures for clarity only each one of both possible positions is shown.

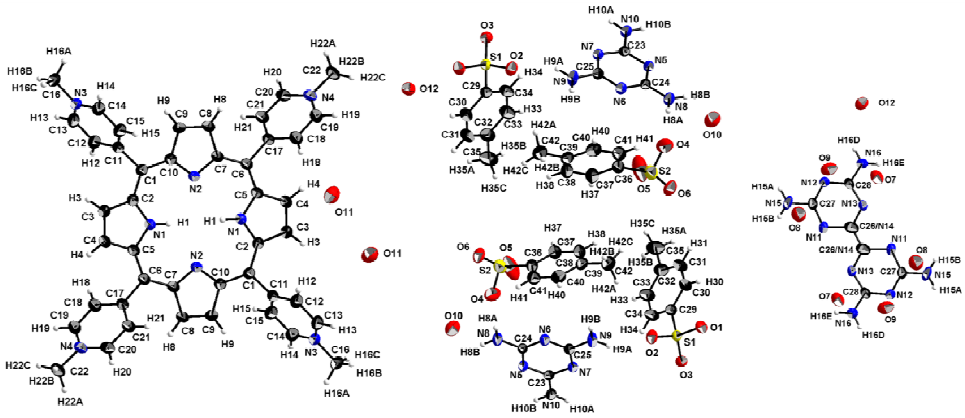

Figure 2. Formula unit of **2** with labeling of atoms and representation of disorder for part of the melamine units. Disorder of crystal water and tosylate oxygen atoms is not shown. Thermal ellipsoids (except for hydrogen) are drawn at the 50 % probability level.

Melamine molecules in **1** and **2** are nearly planar and – except for disordered melamine in **2** – exhibit bond lengths and angles as typically observed for melamine.[47,48] All C–N bonds within the triazine cores and between ring and amino groups are in the range of conjugated bonds (132-135 pm). Angles within the rings are 114-115° (<CNC) and 125-126° (<NCN) and angles between triazine cores and amino groups 116-118°. Bond lengths and angles in the triazine rings of TPTZ resemble those of melamine and also in the pyridyl rings of TPTZ and TMPyP comparable C–N bond lengths (133-

134 pm) are observed. Within the aromatic systems of pyridyl, porphin and phenyl C–C bonds range between 135 and 146 pm while bonds between different aromatic rings or between aromatic rings and methyl groups are slightly larger (148-151 pm). In **1** triazine and pyridyl rings of TPTZ are nearly coplanar with only part of the pyridyl units (C26-30/N29 and NC62-66/N41) being rotated 12-19° relatively to the plane of triazine core and remaining pyridyl rings. Contrary, in **2** pyridyl rings of TMPyP are rotated 61-70° to the porphin plane.

In both **1** and **2** melamine units are arranged perpendicular to the aromatic systems of *N*-heterocycles (Figs. 3 and 4). Between the melamine units stacking interactions are neither present in **1** nor in **2** but melamine molecules are interconnected by hydrogen bonds as is described below. Contrary, the aromatic systems of *N*-heterocycles exhibit varying degrees of π-π stacking. In **1** these dispersive interactions are present between the TPTZ units and in **2** both between tosylate and porphin rings and between tosylate and pyridyl rings. In general, interactions between π-systems are largest between rings with low π-electron density avoiding π-electron repulsion. Factors which further favor π-π stacking are large π-systems and the presence of heteroatoms which lead to polarization.[13] Hence for melamine π-π stacking is less favorable due to electron-donating substituents, the rather small size of the triazine core and the symmetric arrangement of nitrogen atoms

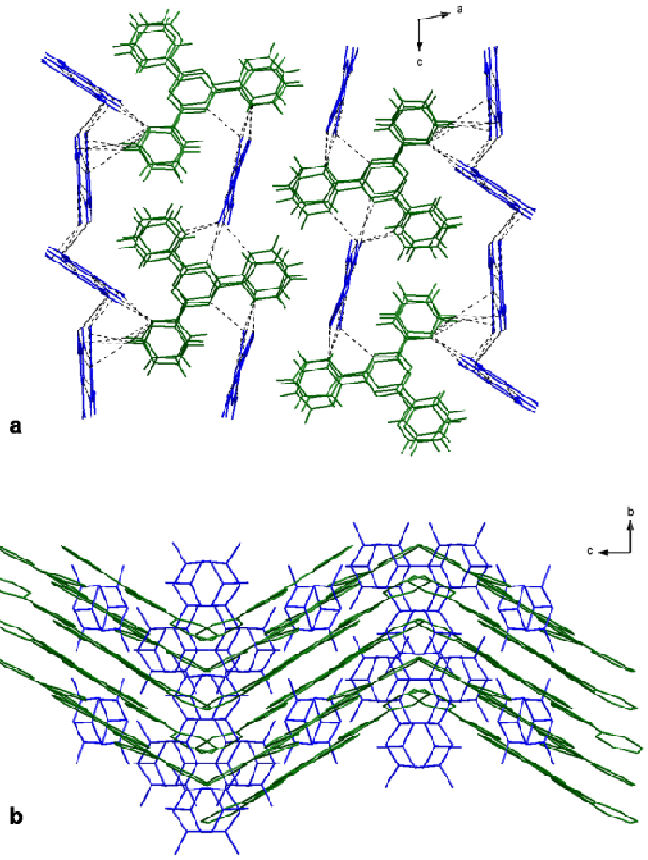

Figure 3. Arrangement of TPTZ (green) and melamine (blue) in 4M·3TPTZ (**1**). (a) Viewed parallel to the direction of TPTZ stacks, dashed lines represent hydrogen bonds. (b) Viewed perpendicular to the direction of TPTZ stacks, hydrogen atoms are omitted for clarity.

within the ring which decreases polarization. At the same time a large number of amino groups and triazine nitrogen atoms are available as donors and acceptors, respectively, for hydrogen bridges. Therefore formation of a stable network of hydrogen bonds has a stronger influence on the arrangement of melamine than dispersive interactions.

In comparison, TPTZ and TMPyP comprise several polarized pyridyl rings, a large number of aromatic rings and in the case of TMPyP furthermore π-electron deficiency as a result of multiple positive charge, making these systems more suitable for dispersive stacking interactions than melamine. However, it has to be noted that stacking of melamine units is not a rare event but has been observed in different adducts.[20,29,38,40] Though, in the presence of stacks of large aromatic systems arrangement of melamine units perpendicular to these stacks as in **1** and **2** appears to be a preferred assembly.[27,33]

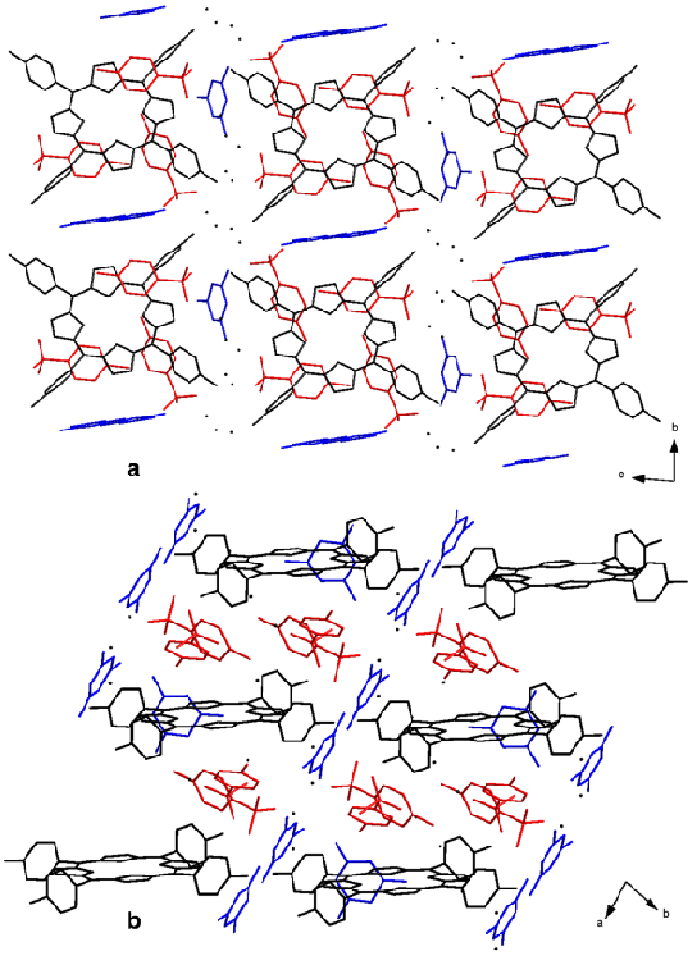

Figure 4. Arrangement of TMPyP (black), tosylate (red), melamine (blue) and crystal water (black) in 3M·TMPyP-Tos·9H_2O (**2**), hydrogen atoms are omitted for clarity. (a) Viewed parallel to the direction of TMPyP stacks, (b) Viewed perpendicular to the direction of TMPyP stacks.

For a rational comparison of π-π stacking interactions numerical values that describe the geometric assembly of involved aromatic rings are a useful tool. Such geometric analysis determining centroid-centroid distances, plane-plane distances, plane-plane angles and displacement angles (angle between centroid-centroid vector and normal to one of the rings) has for instance been performed for a large number of nitrogen-

containing ligands by Janiak.[13] When these values are ascertained for **1** and **2** it becomes clear that stacking interactions between TPTZ units in **1** are stronger than those between tosylate and porphin or tosylate and pyridyl in **2**. Angles between the aromatic planes are close to zero in **1** (≈ 3°) and distinctly larger in **2** (≈15° between tosylate and pyridyl and ≈17° between tosylate and porphin).

Table 1. Crystallographic data and details of the structure refinement for **1** and **2**.

	4M·3TPTZ (**1**)	3M·TMPyP-Tos·9H_2O (**2**)
Molar mass (g mol^{-1})	1440.60	1904.10
Crystal system	Monoclinic	Triclinic
Space group	*C*2/*c* (no. 15)	$P\bar{1}$ (no. 2)
T (K)	293	173
Diffractometer	Nonius Kappa-CCD	Nonius Kappa-CCD
Radiation, λ (pm)	Mo-K_α, 71.073	Mo-K_α, 71.073
a (pm)	4927.6(10)	1045.2(2)
b (pm)	1212.3(2)	1462.8(3)
c (pm)	2301.6(5)	1573.6(3)
α (°)	90	83.26(3)
β (°)	100.85(3)	80.34(3)
γ (°)	90	76.03(3)
V (10^6 pm^3)	13503(5)	2294.2(8)
Z	8	1
Calculated density (g cm^{-3})	1.418	1.364
Crystal size (mm^3)	0.34 x 0.17 x 0.14	0.27 x 0.21 x 0.10
Absorption coefficient (mm^{-1})	0.096	0.188
F(000)	6000	982
Absorption correction	None	None
Diffraction range	$3.13^o \leq \theta \leq 25.35^o$	$3.13^o \leq \theta \leq 27.49°$
Index range	$-59 \leq h \leq 59$, $-14 \leq k \leq 14$	$-12 \leq h \leq 12$, $-17 \leq k \leq 17$
	$-27 \leq l \leq 27$	$-18 \leq l \leq 18$
Parameters / restraints	973 / 0	695 / 0
Total No. of reflections	45655	15445
No. of independent reflections	12348	8325
No. of observed reflections	8235	6281
Min./max. residual electron density (e 10^{-6} pm^{-3})	-0.213 / +0.199	-0.880 / +0.724
GooF	1.021	1.072
Final *R* indices [$I > 2\sigma(I)$]	$R1 = 0.0502$, $wR2 = 0.1296$ [a]	$R1 = 0.0569$, $wR2 = 0.1467$ [b]
Final *R* indices (all data)	$R1 = 0.0829$, $wR2 = 0.1479$ [a]	$R1 = 0.0802$, $wR2 = 0.1589$ [b]

[a] $w = [\sigma^2(F_0^2) + (0.0708P)^2 + 7.5509P]^{-1}$, with $P = (F_0^2 + 2\,F_c^2)/3$

[b] $w = [\sigma^2(F_0^2) + (0.0638P)^2 + 2.1432P]^{-1}$, with $P = (F_0^2 + 2\,F_c^2)/3$

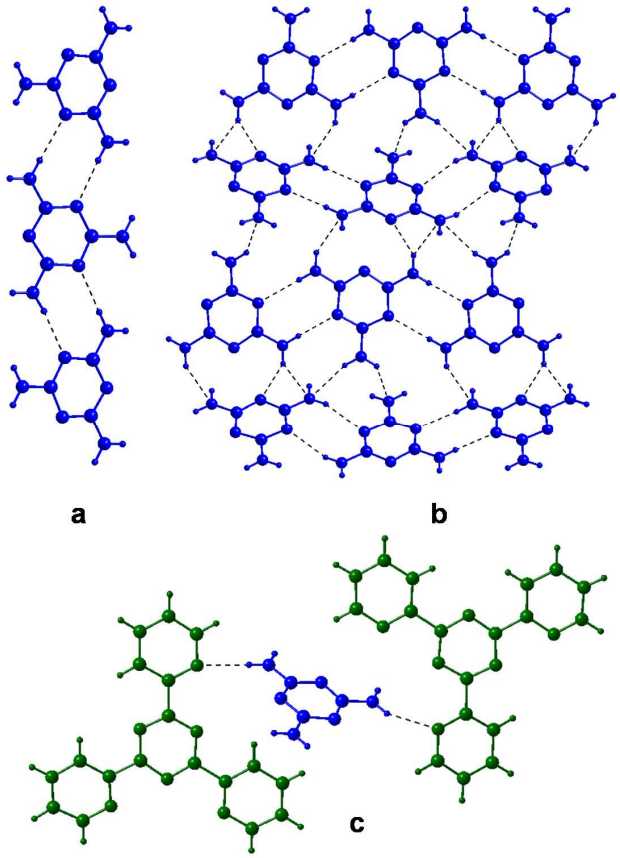

Figure 5. Hydrogen bridge motifs in 4M·3TPTZ **1**. (a) Between melamine units in single melamine strands along *b*. (b) Between melamine units in corrugated melamine sheets parallel to *bc*. (c) Between TPTZ and melamine.

Also plane-plane distances of average 336 pm in **1** are smaller than tosylate-pyridyl and tosylate-porphin distances in **2** which amount to average values of 398 pm and 363 pm, respectively. In all cases the aromatic rings are parallel displaced resulting in centroid-centroid distances that are larger than the respective plane-plane distances, namely 430 pm between TPTZ units, 427 pm between tosylate and pyridyl rings and 421 pm between tosylate and porphin. Consistently, displacement angles of 34° between TPTZ, 19° between tosylate and pyridyl and 29° between tosylate and porphin have been determined. All these values are in the range of frequently observed distances and angles between nitrogen-containing aromatic systems with the exception of rather large plane-plane angles in **2**.[13]

In both adduct phases **1** and **2** a dense network of hydrogen bridges is formed (Figs. 5 and 6). Due to comprehensive disorder of crystal water oxygen atoms in **2** in this compound hydrogen positions of water molecules were not determined. Thus, in the following the description of hydrogen bonding interactions in **2** refers only to hydrogen bridges between M and TMPyP-Tos but not to hydrogen bonds involving crystal water molecules. However, O···N distances between crystal water and melamine (271-320 pm) as well as O···O distances between the water molecules (273-298 pm) and between crystal water and sulfonate (272-309 pm) indicate that all water molecules are involved in the hydrogen bonding network. Intermolecular hydrogen bridges between melamine units are alike in **1** and **2**. In both compounds melamine entities are arranged in strands along *b* and *a*, respectively, with a double N–H···N bridge betweeneach two melamine units (Figs. 5a and 6).

Table 2. Hydrogen bond distances and angles (in pm °) for **1** and **2**.

D-H···A	H···A	D···A	<D-H···A
4M·3TPTZ (**1**)			
N12-H12A···N1^{i}	211.5	297.4	177.82
N23-H23A···N19^{i}	212.4	294.3	159.13
N5-H5B···N7^{i}	212.9	297.2	166.34
N4-H4A···N8^{i}	213.2	298.4	171.32
N10-H10B···N3^{i}	214.8	300.8	179.59
N18-H18B···N13^{i}	217.2	303.2	177.72
N24-H24B···N20^{i}	220.5	306.3	175.46
N17-H17A···N14^{i}	226.0	307.4	158.14
N22-H22B···N16^{ii}	265.8	326.3	128.48
N22-H22A···N17^{ii}	270.6	343.8	143.67
N24-H24A···N18^{ii}	292.0	357.9	134.78
N23-H23B···N15^{ii}	294.0	358.0	132.82
N23-H23B···N17^{ii}	294.1	358.3	132.95
N17-H17B···N35^{iii}	221.3	307.2	175.98
N18-H18A···N29^{iii}	228.2	311.7	163.95
N16-H16A···N41^{iii}	237.0	297.2	127.43
N6-H6A···N42^{iii}	238.6	319.1	156.17
N6-H6B···N30^{iii}	243.1	320.6	150.24
N5-H5A···N36^{iii}	246.1	309.4	130.94
N11-H11A···N34^{iii}	250.7	306.9	123.80
N11-H11B···N28^{iii}	254.9	326.1	140.77
N12-H12B···N42^{iii}	263.3	332.2	138.06
N16-H16B···N40^{iii}	266.6	315.7	117.55
N11-H11B···N25^{iii}	268.2	325.9	125.66
3M·TMPyP-Tos·9H_2O (**2**)			
N16-H16E···O1	210.6	292.6	159.05
N8-H8B···O2	217.4	302.0	168.19
N9-H9B···O2	218.3	287.9	137.88
N10-H10B···O3	219.2	300.7	158.25
N15-H15A···O4	236.0	316.1	155.07
N9-H9A···N6^{i}	210.9	296.6	174.42
N10-H10A···N7^{i}	216.3	301.3	169.95
N1-H1···N2^{iv}	233.9	288.9	122.04
N1-H1···N2^{iv}	241.1	294.7	120.91
N15-H15A···S2	284.3	343.4	127.40

(i) Intermolecular interactions within the melamine strands.

(ii) Intermolecular interactions between two melamine strands.

(iii) Intermolecular interactions between melamine and TPTZ.

(iv) Intramolecular interactions in TMPyP.

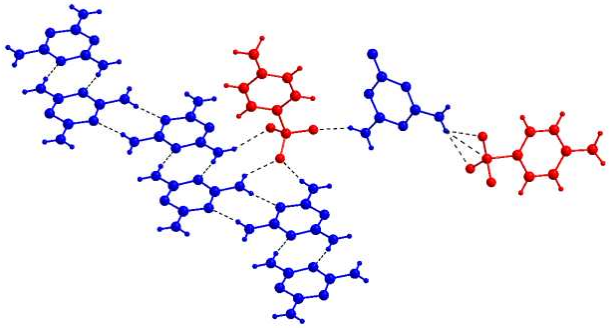

Figure 6. Hydrogen bridge motifs in 3M·TMPyP-Tos·9H_2O **2** between melamine units in melamine strands along *a* and between tosylate and melamine.

In **1** half of these strands are further interconnected by hydrogen bonds resulting in corrugated sheets of melamine entities (Fig. 5b). However, these additional interactions are only weak as becomes evident by comparing geometric parameters of different N–H···N bridges in **1** (Table 2).[49]

Hydrogen bonds between the strands exhibit significantly larger hydrogen-donor and donor-acceptor distances than those hydrogen bridges within the strands. The connection between melamine and TPTZ or melamine and Tos, respectively, is achieved by N–H···N, N–H···O and N–H···S interactions with the amino groups of melamine acting as donors and the pyridyl nitrogen atoms of TPTZ and the sulfonate groups of tosylate acting as acceptors. In contrast, TMPyP is not involved in any common hydrogen bonds neither to melamine nor to tosylate and also hydrogen bridges to crystal water molecules are only weak as is indicated by relatively large N···O distances of 324-340 pm. Whereas in adduct **1** hydrogen bridges are required for cohesion between the uncharged components M and TPTZ, in **2** the positively charged macrocycle TMPyP is mainly bound by electrostatic interactions.

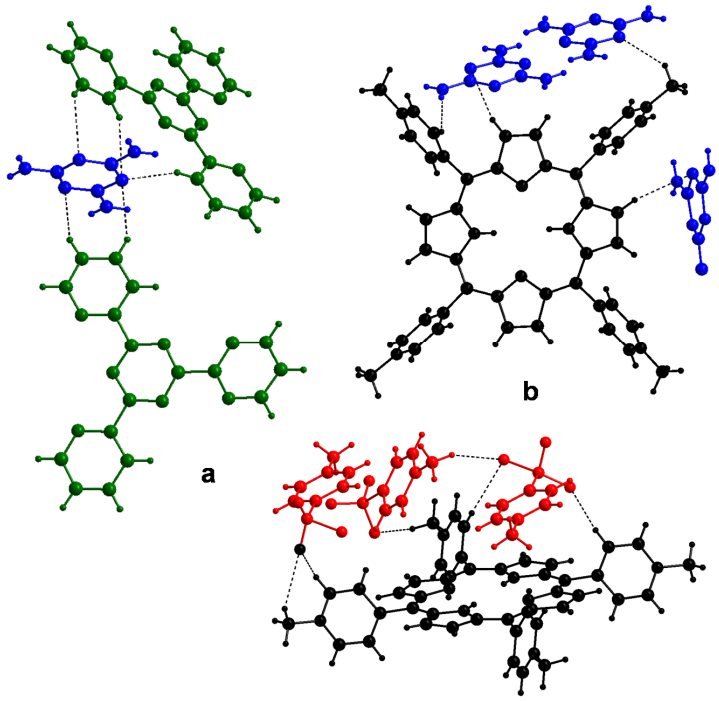

Figure 7. Exemplary illustration of nonconventional hydrogen bridges in **1** and **2**. (a) C–H···N bonds between TPTZ and M in**1**. (b) C–H···N bonds between TMPyP and M in**2**. (c) C–H···O bonds between TMPyP and Tos in **2**.

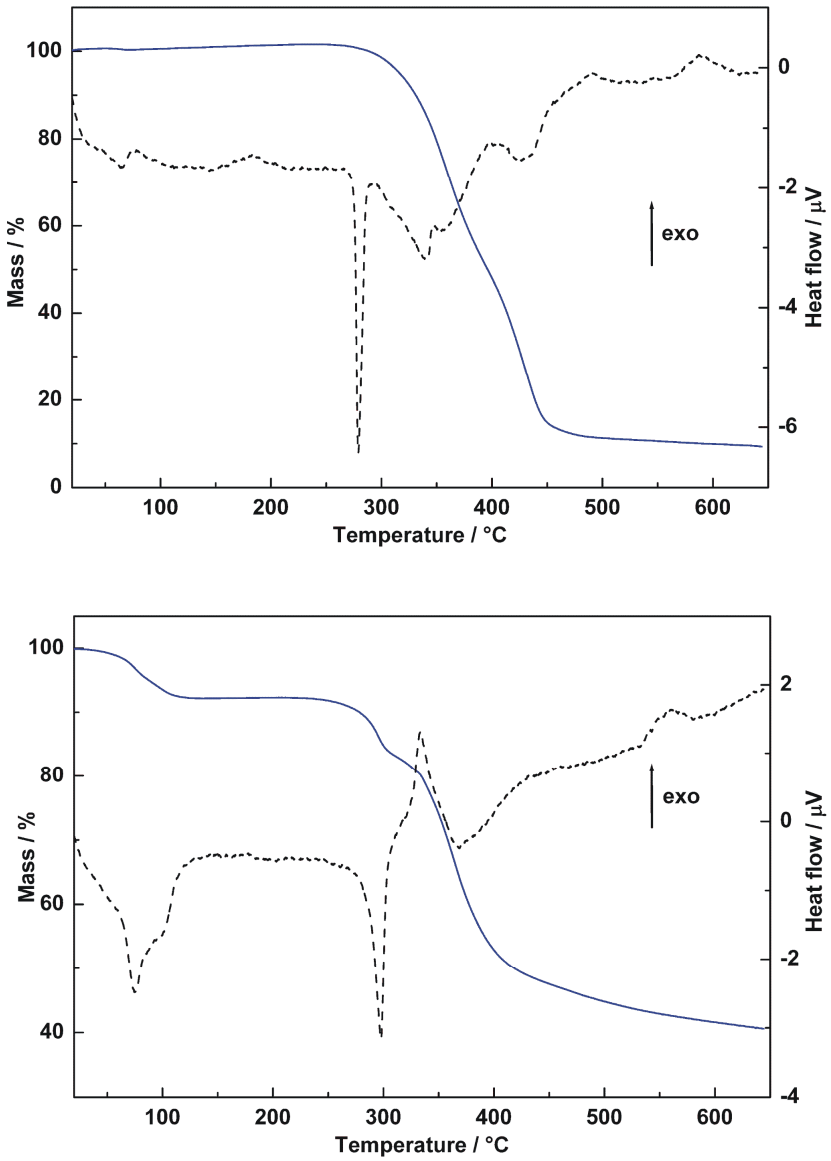

Figure 8. TG (solid) and DTA (dashed) curves of (a) **1** (19.5 mg) and (b) **2** (25.9 mg).

However, taking also weak hydrogen bridges with C–H groups as donors into account, numerous C–H···N and C–H··O bonds between TMPyP and melamine and tosylate, respectively, can be observed in the crystal structure of **2**. Similarly, also in **1** nonconventional C–H···N bridges are formed between

TPTZ and melamine (Fig. 7). Though, compared to the common hydrogen bridges in **1** and **2** (Table 2) which can be classified as medium strong, the C–H···X interactions are distinctly weaker (H···A = 245-298 pm (**1**) / 241-299 pm (**2**), D···A = 329-378 pm (**1**) / 301-385 pm (**2**), <D–H···A = 129-157° (**1**) / 121-160° (**2**)).[49]

Thermal behavior

For adduct phases **1** and **2** TG and DTA measurements were performed (Fig. 8). In the DTA curve of **1** a sharp endothermic signal at 279 °C can be attributed to melting of the sample which is followed by nearly complete decomposition between 300 and 450 °C. In **2** crystal water is released at 20-140 °C (mass loss *observed*: 7.79 %, *calculated*: 8.50 %) during which the compound becomes amorphous. Decreasing crystallinity of **2** as a result of the partial loss of crystal water can already be observed when the sample is stored at room temperature for several days. Decomposition of **2** starts at 245 °C accompanied by an endothermic DTA signal and subsequently continues steadily during further heating. In comparison, the single components melamine, TPTZ and TMPyP-Tos either exhibit sublimation at 345 °C (M), melting at 250 °C (TPTZ) or decomposition at 390 °C (TMPyP-Tos) (see Supporting information, Figs. S1-S3). Because thermal events of adduct phases **1** and **2** and not of individual components occur it can be concluded that interactions between M and TPTZ or M and TMPyP-Tos are present even at elevated temperatures. Adduct **1** shows higher thermal stability than its components which is in accordance with expectation considering that **1** was formed at a synthesis temperature of 270 °C. Whereas **1** decomposes almost completely below 450 °C, decomposition of **2** occurs distinctly slower so that almost 50 wt.% are still present at 650 °C. This resembles the thermal behavior of TMPYP-Tos in this temperature range, probably indicating the formation of thermally stable polymeric compounds.

7.4 Conclusion

In this contribution the formation of two novel co-crystals between melamine and *N*-heterocycles by self-recognition has been reported. The combination of melamine and large, nitrogen-rich aromatic systems allows for a detailed analysis of different types of noncovalent interactions in these adduct phases. Whereas for melamine the dominating factor for a specific self-assembly is the formation of

hydrogen bridges, the arrangement of larger *N*-heterocycles in the crystal is also influenced by dispersive interactions. Consistently, in both co-crystals stacking of heterocycles with melamine molecules orientated perpendicular to these stacks appears as recurring motif. The formation of hydrogen-bonded melamine strands, which represents a commonly observed motif in melamine co-crystals, further illustrates the strong influence of intermolecular hydrogen bridges on the arrangement of melamine units in the solid state. The observed assemblies reflect electron-donating and electron-withdrawing factors in the molecular components as well as the available amount of suitable donor and acceptor sites for hydrogen bridges. The appearance of recurring self-assembly motifs in these adduct phases adds to a deeper understanding of the factors which influence the arrangement of molecular building blocks in such systems. Thus the presented results might contribute to a rational preparation of specific melamine containing materials via crystal engineering in the future.

Acknowledgement

The authors would like to thank the Deutsche Forschungsgemeinschaft DFG (project SCHN 377/15) and the Fonds der Chemischen Industrie (FCI) for financial support, Dr. Peter Mayer (Department Chemie, LMU München) for the single-crystal data collection and PD Dr. Oliver Oeckler (Department Chemie, LMU München) for fruitful discussion.

Appendix A. Supplementary material

CCDC 852974 and 852975 contain the supplementary crystallographic data for this paper. These data can be obtained free of charge via http://www.ccdc.cam.ac.uk/conts/retrieving.html (or from the Cambridge Crystallographic Data Centre, 12, Union Road, Cambridge CB2 1EZ, UK; fax: +44 1223 336033). TG and DTA measurements of melamine, TPTZ and TMPyP-Tos are provided as supporting information (Figs. S1-S3). Supporting information is available free of charge via the Internet. Supplementary data associated with this article can be found, in the online version, at doi:10.1016/ j.molstruc.2012.01.010.

7.5 Bibliography

[1] G. Goglio, D. Foy, G. Demazeau, *Mater. Sci. Eng. R* **2008**, *58*, 195.

[2] E. Horvath-Bordon, R. Riedel, P. F. McMillan, P. Kroll, G. Miehe, P. A. v. Aken, A. Zerr, P. Hoppe, O. Shebanova, I. McLaren, S. Lauterbach, E. Kroke, R. Boehler, *Angew. Chem.* **2007**, *119*, 1498; *Angew. Chem. Int. Ed.* **2007**, *46*, 1476.

[3] E. Kroke, M. Schwarz, *Coord. Chem. Rev.* **2004**, *248*, 493.

[4] B. V. Lotsch, M. Döblinger, J. Sehnert, L. Seyfarth, J. Senker, O. Oeckler, W. Schnick, *Chem. Eur. J.* **2007**, *13*, 4969.

[5] A. Thomas, A. Fischer, F. Goettmann, M. Antonietti, J.-O. Müller, R. Schlögl, J. M. Carlsson, *J. Mater. Chem.* **2008**, *18*, 4893.

[6] E. Wirnhier, M. Döblinger, D. Gunzelmann, J. Senker, B. V. Lotsch, W. Schnick, *Chem. Eur. J.* **2011**, *17*, 3213.

[7] Z. Zhang, K. Leinenweber, M. Bauer, L. A. J. Garvie, P. F. McMillan, G. H. Wolf, *J. Am. Chem. Soc.* **2001**, *123*, 7788.

[8] M. Döblinger, B. V. Lotsch, J. Wack, J. Thun, J. Senker, W. Schnick, *Chem. Commun.* **2009**, 1541.

[9] C. B. Aakeröy, N. R. Champness, C. Janiak, *CrystEngComm* **2010**, *12*, 22.

[10] R. Custelcean, *Chem. Commun.* **2008**, 295.

[11] G. R. Desiraju, *Angew. Chem.* **2007**, *119*, 8492; *Angew. Chem. Int. Ed.* **2007**, *46*, 8342.

[12] S. Grimme, *Angew. Chem.* **2008**, *120*, 3478; *Angew. Chem. Int. Ed.* **2008**, *47*, 3430.

[13] C. Janiak, *J. Chem. Soc., Dalton Trans.* **2000**, 3885.

[14] K. Merz, V. Vasylyeva, *CrystEngComm* **2010**, *12*, 3989.

[15] C. M. Reddy, G. R. Krishna, S. Ghosh, *CrystEngComm* **2010**, *12*, 2296.

[16] I. S. Choi, X. Li, E. E. Simanek, R. Akaba, G. M. Whitesides, *Chem. Mater.* **1999**, *11*, 684.

[17] X. Li, D. N. Chin, G. M. Whitesides, *J. Org. Chem.* **1996**, *61*, 1779.

[18] J. P. Mathias, C. T. Seto, E. E. Simanek, G. M. Whitesides, *J. Am. Chem. Soc.* **1994**, *116*, 1725.

[19] J. P. Mathias, E. E. Simanek, C. T. Seto, G. M. Whitesides, *Angew. Chem.* **1993**, *105*, 1848; *Angew. Chem. Int. Ed. Engl.* **1993**, *32*, 1766.

[20] A. Ranganathan, V. R. Pedireddi, C. N. R. Rao, *J. Am. Chem. Soc.* **1999**, *121*, 1752.

[21] C. T. Seto, J. P. Mathias, G. M. Whitesides, *J. Am. Chem. Soc.* **1993**, *115*, 1321.

[22] C. T. Seto, G. M. Whitesides, *J. Am. Chem. Soc.* **1990**, *112*, 6409.

[23] C. T. Seto, G. M. Whitesides, *J. Am. Chem. Soc.* **1991**, *113*, 712.

[24] C. T. Seto, G. M. Whitesides, *J. Am. Chem. Soc.* **1993**, *115*, 905.

[25] G. M. Whitesides, E. E. Simanek, J. P. Mathias, C. T. Seto, D. N. Chin, M. Mammen, D. M. Gordon, *Acc. Chem. Res.* **1995**, *28*, 37.

[26] A. Sattler, S. Pagano, M. Zeuner, A. Zurawski, D. Gunzelmann, J. Senker, K. Müller-Buschbaum, W. Schnick, *Chem. Eur. J.* **2009**, *15*, 13161.

[27] J. Hamblin, S. P. Argent, A. J. Blake, C. Wilson, N. R. Champness, *CrystEngComm* **2008**, *10*, 1782.

[28] R. F. M. Lange, F. H. Beijer, R. P. Sijbesma, R. W. W. Hooft, H. Kooijman, A. L. Spek, J. Kroon, E. W. Meijer, *Angew. Chem.* **1997**, *109*, 1006; *Angew. Chem. Int. Ed. Engl.* **1997**, *36*, 969.

[29] G. J. Perpétuo, J. Janczak, *Acta Crystallogr., Sect. C* **2007**, *63*, o301.

[30] H. Tukada, Y. Mazaki, *Chem. Lett.* **1997**, 441.

[31] A. Roy, A. Choudhury, C. N. R. Rao, *J. Mol. Struct.* **2002**, *613*, 61.

[32] R. Thomas, G. U. Kulkarni, *Beilstein J. Org. Chem.* **2007**, *17*, doi:10.1186/1860-5397-3-17.

[33] K. Sivashankar, A. Ranganathan, V. R. Pedireddi, C. N. R. Rao, *J. Mol. Struct.* **2001**, *559*, 41.

[34] A. Huczyński, J. Janczak, B. Brzezinski, *J. Mol. Struct.* **2009**, *922*, 77.

[35] J. Janczak, G. J. Perpétuo, *Acta Crystallogr., Sect. C* **2008**, *64*, o91.

[36] A. N. Lazar, O. Danylyuk, K. Suwinska, A. W. Coleman, *New J. Chem.* **2006**, *30*, 59.

[37] B. V. Lotsch, W. Schnick, *Chem. Mater.* **2006**, *18*, 1891.

[38] G. J. Perpétuo, J. Janczak, *J. Mol. Struct.* **2008**, *891*, 429.

[39] X.-L. Zhang, X.-M. Chen, *Cryst. Growth Des.* **2005**, *5*, 617.

[40] X.-L. Zhang, B.-H. Ye, X.-M. Chen, *Cryst. Growth Des.* **2005**, *5*, 1609.

[41] D. Braga, F. Grepioni, L. Maini, P. P. Mazzeo, K. Rubini, *Thermochim. Acta* **2010**, *507-508*, 1.

[42] C. Romera, L. Sabater, A. Garofalo, I. M. Dixon, G. Pratviel, *Inorg. Chem.* **2010**, *49*, 8558.

[43] Z. Otwinowski, W. Minor, *Methods Enzymol.* **1997**, *276*, 307.

[44] G. M. Sheldrick, *Acta Crystallogr., Sect. A* **2008**, *64*, 112.

[45] G. M. Sheldrick, *SHELXS-97, Program for the Solution of Crystal Structures, Universität Göttingen* **1997**.

[46] G. M. Sheldrick, *SHELXL-97, Program for the Refinement of Crystal Structures, Universität Göttingen* **1997**.

[47] A. Cousson, B. Nicolai, F. Fillaux, *Acta Crystallogr., Sect. E* **2005**, *61*, o222.

[48] J. N. Varghese, A. M. O'Connel, E. N. Maslen, *Acta Crystallogr., Sect. B* **1977**, *33*, 2102.

[49] T. Steiner, *Angew. Chem.* **2002**, *114*, 50; *Angew. Chem. Int. Ed.* **2002**, *41*, 48.

8. DFT-D3 investigations of noncovalent interactions in triazine derivatives

All calculations in this chapter were carried out by Helge Krieg (University of Münster, advisor: Prof. Dr. S. Grimme), who also wrote major parts of this chapter. I provided the idea for these calculations and the crystallographic data of 4M·3TPTZ and 3-tptz, and was involved in scientific discussion. The results presented in this chapter will also be published as part of the doctoral thesis of Helge Krieg.

In the previous chapter, synthesis and structural characterization of adduct phases between melamine and *N*-heterocycles have been presented. Detailed analysis of structural data has revealed that different types of noncovalent interactions contribute with varying extent to the observed assembly of molecules in these cocrystals. Whereas the arrangement of melamine units is mainly determined by hydrogen bonds, for the assembly of larger *N*-heterocycles dispersive interactions also play a relevant role. Especially the 4:3 adduct between melamine and tris(2-pyridyl)-triazine (2-TPTZ) represents a suitable system to study the influence of different *N*-heterocycles on the arrangement of molecular building blocks in such cocrystals in detail. This compound is built up exclusively of the six-membered aromatic rings *s*-triazine and 2-pyridyl. In this chapter, the strength of dispersive interactions between *s*-triazine and 2-pyridyl rings in the adduct phase 4M·3TPTZ is investigated in detail by employing density functional theory including dispersion corrections (DFT-D3). Interaction energies are computed for adduct 4M·3TPTZ, its components melamine and 2-TPTZ, and additionally for tris(3-pyridyl)-triazine (3-TPTZ). Taking advantage of a complementary approach to analyze noncovalent interactions in such phases by employing both single-crystal data and theoretical studies allows for an enhanced understanding with which relative impact different types of noncovalent forces contribute to a specific self-assembly of aromatic C/N/H cycles in the solid state.

Investigation of non-covalently bound triazine derivatives with density functional theory including dispersion corrections (DFT-D3)

Helge Krieg, Jonas Moellmann, Stefan Grimme, Sophia J. Makowski, and Wolfgang Schnick

unpublished results

Keywords: DFT-D; Density functional theory; Dispersion; Molecular crystal; Solid state; Triazine

Abstract. We investigate the non-covalent interactions in different molecular crystals of triazine derivatives (melamine)$_4$·(2,4,6-tris(2'-pyridinyl)-1,3,5-triazine)$_3$ (432tptz), 2,4,6-tris(2'-pyridinyl)-1,3,5-triazine (2tptz), 2,4,6-tris(3'-pyridinyl)-1,3,5-triazine (3tptz) and melamine. Twenty-six smaller complexes are chosen (mainly from crystallographic data) as model systems to study the non-covalent interactions with density functional theory including dispersion corrections (DFT-D3). The applied density functionals are two GGAs (BLYP-D3, PBE-D3), one meta GGA (TPSS-D3) and the recently proposed double-hybrid density functional PWPB95-D3. In order to investigate the interaction with neighboring molecules we studied the crystals of 2tptz and 3tptz using PBE-D3 with periodic boundary conditions. The results clearly show that the structures are mainly bound by dispersion forces and the application of the dispersion correction to DFT is crucial. The computed binding energies of melamine are -5.0 and -10.3 kcal·mol^{-1} in its π-stacked and hydrogen bonded model systems, respectively. The interaction energy of 2tptz in a model dimer with two stacked pyridinyle moieties is -10.5 kcal·mol^{-1} based on the fixed geometry taken from crystallographic data and nearly twice as strong for the relaxed gas phase structure. The complexation energy of a trimer of 2tptz molecules is computed to be -27.2 kcal·mol^{-1} while for the 3tptz dimer complex we obtain an interaction energy of -15.8 kcal·mol^{-1}.

8.1 Introduction

Carbon nitride type materials are valuable compounds because of their interesting physicochemical and structural properties. Two dimensional layered materials offer interesting electric properties for the field of semiconductor technology and are promising candidates for catalysts without the presence of any metal. For a recent review see the paper of Antonietti *et al*.[1] In contrast to these covalently bound frameworks the carbon nitrogen cycles triazine and heptazine can also form supramolecular networks, in which molecules are interconnected by non-covalent interactions. A prominent example is the hydrogen-bonded, rosette-like structure of an adduct between melamine and cyanuric acid.[2,3] Recently, a related structure has been reported for the larger heptazine compound melem hydrate,[4] demonstrating the importance of hydrogen bonds and other non-covalent forces for the assembly of building units in such molecular crystals. Besides, triazines can also form cocrystals with other heterocyclic compounds. These molecular frameworks can be considered as the intersection between inorganic carbon nitrides and organic molecules in the solid phase connected via non-covalent interactions.

This work investigates the interaction between different model systems of triazine derivatives that are promising precursors for the synthesis of such molecular crystals. The focus is on the structures of 2,4,6-tris(2'-pyridinyl)-1,3,5-triazine (**2tptz**) and 2,4,6-tris(3'-pyridinyl)-1,3,5-triazine (**3tptz**)[5,6] whose crystallographic data can be compared to the recently reported crystal structure of (melamine)$_4$·(2,4,6-tris(2'-pyridinyl)-1,3,5-triazine)$_3$ (**432tptz**, structure 1, see Figure 1).[7] We selected five different binding motifs from the crystal structure as model systems for 432tptz (see Figure 1): three dimer interactions of 2tptz molecules (compounds 1a to 1c), the trimer 1d and one complex of 2tptz with melamine (compound 1e). The π-complex (compound 1f) is chosen to investigate the interaction of 2tptz with melamine for a stacked conformation

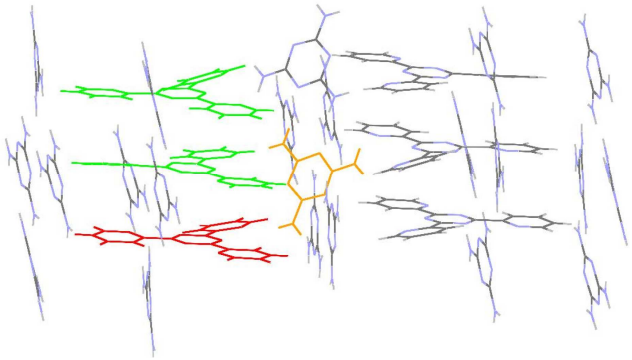

Figure 1. Model systems of 432tptz taken from crystallographic data:[7] dimer 1a (green), dimer 1b (red plus lower green), dimer 1c (upper green plus red), trimer 1d (both green and red) and dimer 1e (lower green plus orange).

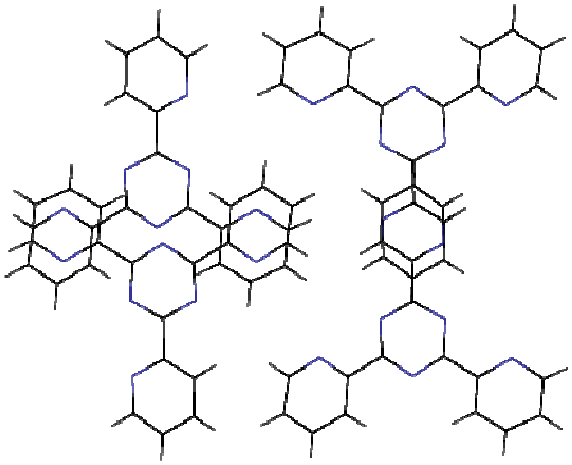

Figure 2. Model systems of 2tptz taken from crystallographic data:[9] dimer 2a (left), dimer 2b (right).

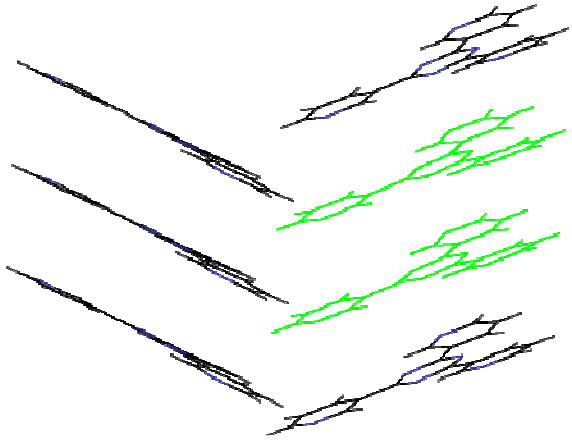

Figure 3. Model system of 3tptz taken from crystallographic data:[6] dimer 3a (green).

(see Figure 14 in the supporting information). So far two crystal structures of 2tptz at different temperatures have been reported.[8,9] Because both 1 and 3 have been prepared at elevated temperatures also for 2 the modification which is formed at higher temperatures[9] (structure 2) is chosen for comparison in this work. There are two different motifs of interaction between the 2tptz molecules that both have been taken as model systems for crystal structure 2 (compounds 2a and 2b, see Figure 2). The model system for the description of 3tptz is the fully stacked dimer structure shown in Figure 3 (structure 3a). In order to quantify the different contributions of pyridinyle and triazine rings to the interaction energy of 3tptz three further model systems are investigated that contain a decreasing number of pyridinyle moieties (structures 3b-3d). The interaction between melamine molecules is modeled using four systems: a π-stacked melamine dimer and a planar hydrogen bonded one (structures 4a and 4b, see Figures 4a and 4b), as well as the corresponding complexes taken from crystallographic data reported by Cousson *et al.*[10] (structures 4c and 4d, see Figure 4c).

The method applied in this work is density functional theory including a dispersion correction (DFT-D3).[11] Depending on the underlying density functional DFT-D3 scales only as N^{3-5} (with system size N) while covering a large fraction of electron correlation effects. Especially in combination with double hybrid density functionals, the method has been shown to give very accurate results over a wide variety of systems in spite of employing modest triple-ζ basis sets.[12] For a recent benchmark which demonstrates the high accuracy of DFT-D3 for a wide range of systems see Ref.[13]. Based on results of DFT-D3 computations we will answer the questions of how strong the non-covalent

interactions of the model systems are, how strong the influence of stacked pyridinyle moieties is and how conformational differences in the fragments regarding rotation around the pyridinyle moieties change the interaction energy.

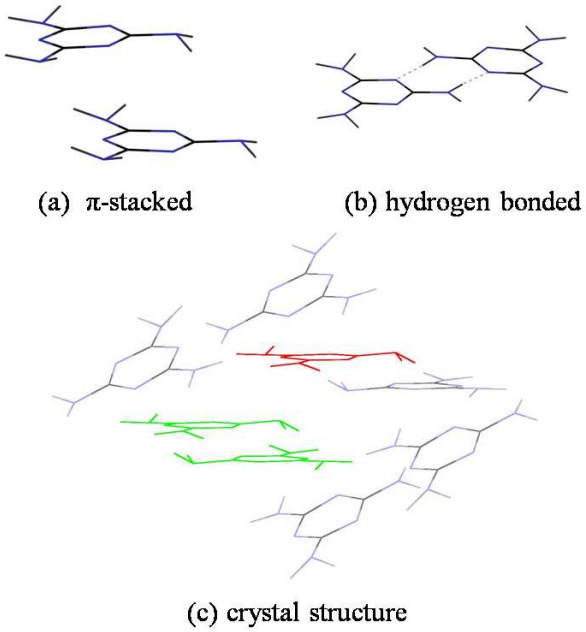

Figure 4. Model systems of melamine: π-stacked dimer (4a), hydrogen bonded dimer (4b) and the corresponding dimer structures 4c (right green with red) and 4d (green) taken from crystallographic data.[10]

8.2 Computational methods

The computations are based on fully optimized and fixed crystallographic geometries (with optimized positions of the hydrogen atoms only). We apply BLYP-D3[14,15] in combination with a triple-ζ Ahlrichs type basis set (def2-TZVP)[16,17] to the geometry optimization of all model systems. The optimizations are performed with the Turbomole 6.3 program[18,19] employing the resolution-of-the-identity approximation (RI)[20,21] for the evaluation of the Coulomb integrals (RI-J[21]) with Weigend's optimized *def2*-auxiliary basis sets.[22] Subsequent single point energies are computed with BLYP-D3 and PWPB95-D3. The currently most accurate description (based on a comparison of nearly 50 density functionals[23]) of non-covalent interactions with DFT is obtained with double hybrid density functionals that contain a certain amount of non-local Fock exchange, employ virtual orbitals via a Møller-Plesset second order perturbation theory (MP2[24,25]) contribution and furthermore include a dispersion correction. From this class of density functionals PWPB95-D3[26-30] has proven to be very robust and accurate in the description of many different properties such as non-covalent interactions and was found to be significantly less dependent on the size of the basis set than other double hybrid density functionals.[12] The computations with PWPB95-D3 in combination with the def2-TZVP basis set are carried out with a modified version of Turbomole 5.9. The interaction energy E_{int}^{DFT-D} of the model systems is calculated as the difference of energies between the complex and the single fragments at infinite distance with the frozen geometry of the

fragments in the complex state. The energies are corrected for dispersive interactions using our standard dispersion correction (denoted -D3).[11,31,32]

Our computations show that the particular type of GGA is only of minor influence on the resulting minimum geometry of compounds 2a, 4a and 4b. The increase of the basis set size to quadruple-ζ during the optimization is only of small importance for the resulting optimum gas phase geometry. BLYP-D3/def2-TZVP optimized geometries are sufficient for this study. A detailed analysis of functional and basis set dependence can be found in the supporting information. Test calculations for compound 4a show that on the quadruple-ζ level the basis set superposition error (BSSE) contributes about 8% to the binding energy with PWPB95-D3. On triple-ζ level the contribution is even larger than 20%. Therefore we employ the counterpoise correction of Boys and Bernardi[33,34] with this functional. In the case of the GGAs in combination with a quadruple-ζ basis set the BSSE is only about 2% and a correction is not necessary. In order to differentiate between the influence of bulk effects and the influence of the applied method on the relaxed geometries and energies we additionally investigate the crystal structure of compounds 2 and 3 using PBE-D3 with periodic boundary conditions via the plane-wave based VASP program.[35-39] The computations are based on starting geometries taken from crystallographic data. The interaction energy of the dimers in the bulk, $E_{int}^{periodic}$, is calculated from the difference between the energy of the fully relaxed crystal structure and the energy of the monomers in the bulk. The latter is approximated by computation of the single fragments located within a large unit cell. The closest distance between atoms of adjacent unit cells is 37.8 Bohr which is chosen quite conservatively in order to eliminate nearly any intermonomer interactions. We apply two k-points (±0.25,0,0) to the sampling of the Brillouin zone for the bulk system and use the projector augmented wave method[38,40] for both, the gas phase and bulk systems. The cutoff for the plane wave basis set is 800 eV.

8.3 Results and discussion

Geometries

The agreement between the crystal structures of 2tptz and 3tptz taken from experiment and their crystal structures optimized using periodic boundary conditions is very good (cf. Figure 15 in the supporting information). We find low root mean square deviations (RMSD) of 0.18 Å and 0.12 Å,

respectively, as calculated from the difference between the two sets of coordinates.[41] The mean bond lengths of C–C and C–N are nearly identical for both structures, whereas C–H bonds are on average 17% longer in the optimized structures. This clearly results from the inaccuracy of the measurement of hydrogen positions. Deviations of bond angles (C–C–C, C–N–C, C–C–H) are below 1%. In order to investigate the influence of packing on the geometry we fully optimized the model complexes in the gas phase and compared the resulting structures to model dimers that have been optimized with fixed positions of heavy atoms. In most of the cases relaxation leads to a shortening of the intermonomer distance and at the same time to an enlargement of the rotation of pyridinyle moieties. We find a decrement of the distance between the fragments' centers of mass of 0.9 Å on average and an increment of 7 degrees for the dihedral angles between the triazine ring and the pyridinyle moieties. Especially for compounds 1a-1d a twist of the monomers relative to their position in the crystal is observed (cf. Figures 1-11 in the supporting information). The RMSD is 1.2 Å on average reflecting considerable differences between the structures that mainly result from different rotational conformations of the pyridinyle moieties. The observed conformational differences in the gas phase are attributed to the absence of interactions with surrounding molecules in the bulk. The potential energy surface of the different model systems is expected to be very flat due to a low rotational barrier of the pyridinyle moieties. Biphenyle for example has a similar electronic structure as (2'-pyridinyl)-1,3,5-triazine. Rubio *et al.*[42] report a maximum rotational barrier of only 3.1 kcal·mol^{-1} based on high-level *ab initio* calculations. The experimental value computed from gas phase diffraction data is even lower (1.5 kcal·mol^{-1}).[43] Therefore one can expect that the different rotational conformations of the investigated model systems are energetically very close lying.

A collection of all coordinates can be found in the supporting information.

Interaction energies

We discuss the computed interaction energies beginning with the different systems to model melamine 4a-4d. An overview of DFT-D3 results based on different density functionals can be found in the supporting information. The interaction energy based on counterpoise corrected PWPB95-D3/def2-TZVP is -11.2 kcal·mol^{-1} for the hydrogen bonded complex 4b. The value for the π-stacked model system lies about 2.4 kcal·mol^{-1} above. This difference is more pronounced for systems 4c and 4d that have directly been extracted from crystallographic data (-5.0 and -10.3 kcal·mol^{-1}, respectively). For all of the model complexes we find that a complete relaxation of the geometry leads to a decrement of

the distance between the fragments' centers of mass and consequently to lower interaction energies compared to results based on structures with fixed positions of heavy atoms during the optimization. But independent of the type of the underlying geometry optimization the hydrogen bonded structure 4d is about 5 kcal·mol^{-1} more stable than the stacked conformation. The dispersion energy makes up about 17% of the interaction energy of the hydrogen bonded conformation and 62% of the binding energy of the stacked one.

Regarding the stacking motifs of the 2tptz model systems 2a and 2b it is clear that the binding energy will mainly consist of dispersion energy. The energies computed by PWPB95-D3/def2-TZVP including counterpoise correction are -7.9 and -10.5 kcal·mol^{-1} for the conformations with one and two π-stacked pyridinyle moieties, respectively. We find a dispersion contribution of about -5 kcal·mol^{-1} for both systems making up 55% of the interaction energy on average. Comparing the interaction energies of systems 2a and 2b we find that doubling the number of π-stacked pyridinyle moieties does not lead to twice the interaction energy. This must be attributed to the slightly stronger repulsive contribution of the other parts of structure 2b because of the closer distance between its monomers. Fully relaxing the geometries of complexes 2a and 2b leads to significant shortenings of the interfragment distances and strongly lowers the binding energies. The interaction energy of model system 2b with two π-stacked pyridinyle moieties is lowered by more than 80% compared to the result based on an optimization with fixed positions of the heavy atoms. Based on density functional computations with periodic boundary conditions we find an interaction energy ($E_{int}^{periodic}$) of -42.1 kcal·mol^{-1} per molecule of compound 2. Restricting the analysis to dimer interactions within the unit cell we have two types of π-stacked interactions that are modeled by systems 2a and 2b. The sum of both π-stacked interaction energies (E_{int}^{DFT-D}) computed from the model systems is -18.4 kcal·mol^{-1}. The remaining difference to the total value in the bulk results from other non-covalent dimer interactions within the unit cell and from interactions to all molecules in the periodic environment. The non-covalent interaction between 2tptz fragments as modeled by 2a and 2b contributes 44% to the total crystallization energy per molecule of structure 2.

Regarding the type of non-covalent bonding between the monomers of 3tptz our results agree with the findings for the model systems discussed above. An amount of 60% of the computed binding energies (E_{int}^{DFT-D}) results from the dispersion contribution. Each added π-stacked pyridinyle moiety contributes approximately 4.5 kcal·mol^{-1} to the total complexation energy and the dispersive interaction between the two triazine centers adds another 2.4 kcal·mol^{-1}. This can be seen from the PWPB95-D3/def2-

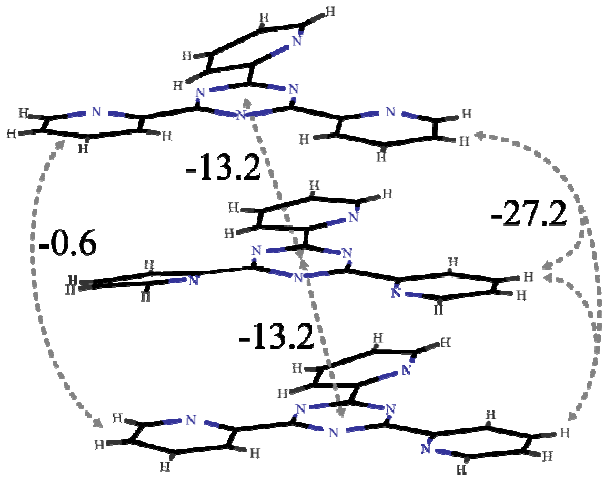

Figure 5. Interaction energies $E_{int}^{DFT\text{-}D}$ (kcal·mol^{-1}) of trimer 1d computed with counterpoise corrected PWPB95-D3/def2-TZVP. Deformation energy of the monomers is neglected.

TZVP interaction energies for compounds 3a to 3d that uniformly decrease by about 4.5 kcal·mol^{-1} starting from -15.8 kcal·mol^{-1} for compound 3a with three stacked pyridinyle moieties. Hence, the value of dispersion energy between two pyridinyle units is almost twice as large as that between two triazine moieties although both cycles are of similar size. The interaction energy in the bulk ($E_{int}^{periodic}$) is -39.4 kcal·mol^{-1} per molecule of compound 3tptz. Compared to $E_{int}^{DFT\text{-}D}$ of model system 3a we find a contribution of 40% of this type of interaction to the total crystallization energy per molecule which agrees very well with our findings for 2tptz. The stacked conformations modeled by structures 2a, 2b and 3a clearly contribute an important part to the total crystallization energy but in order to accurately estimate the total crystallization energy in the bulk based on a sum of interaction energies of the constituting dimers one must also consider other types of non-covalent interactions than π-stacking.

Model systems 1a to 1d consist of 2tptz fragments and show similar trends for the binding energy as compounds 2a and 2b. The 2tptz fragments are π-stacked in a parallel displaced fashion with significant dispersion interaction between all three pyridinyle moieties. The distance between the fragments' centers of mass is about 8% larger for the upper dimer than for the lower one within the π-stacked trimer 1d but the computed interaction energies $E_{int}^{DFT\text{-}D}$ agree with a value of -13.2 kcal·mol^{-1}. The computed interaction energy of the t-shaped model complex of 2tptz with melamine (1e) is below 50% of this value resulting from a weaker dispersion interaction between 2tptz and melamine than between the π-stacked fragments of 2tptz. Our results show that there is no significant contribution to the binding energy of the trimer (1d) due to cooperative effects. The sum of the counterpoise corrected binding energies of the dimers is -27.0 kcal·mol^{-1} and differs by only 0.2 kcal·mol^{-1} from the predicted binding energy of the trimer (see Figure 5). Compared to the different model systems of stacked 2tptz or 3tptz molecules the dispersion interaction of 2tptz with melamine is significantly weaker

independent of the type of conformation. Between 2tptz and melamine other types of interactions such as hydrogen bonds seem to be of prior importance. From the different combinations and conformations of 2tptz and melamine molecules the π-stacked conformation of 2tptz molecules and the hydrogen bonded conformation of melamine molecules are the most stable ones. This could be the reason why 432tptz crystallizes with both of these binding motifs but does not contain any stacked conformations of 2tptz with melamine.

8.4 Summary

We investigated the non-covalent interactions in different molecular crystals of triazine derivatives with density functional theory with dispersion corrections (DFT-D3). We find very good agreement between the crystal structures extracted from crystallographic data and crystal structures optimized in the bulk with periodic boundary conditions. Analyzing the non-covalent interactions in the bulk based on model complexes of dimers in the gas phase leads to meaningful results only if the gas phase geometries are optimized with fixed positions of the heavy atoms. Full relaxation results in different minima that can no longer be reasonably compared to the investigated crystal structures. The strongest interaction is found for π-stacked arrangements of 3tptz fragments. Non-covalent interactions between π-stacked 2tptz fragments are 2.6 kcal·mol^{-1} weaker but still stronger than all remaining investigated interactions. Each stacked pyridinyle moiety adds approximately -4.5 kcal·mol^{-1} to the total binding energy. The hydrogen bonded model complex of melamine is about 5 kcal·mol^{-1} more stable than the π-stacked conformation. Our results clearly show that the structures are mainly bound by dispersion interaction and the application of dispersion corrections to DFT is crucial in the study of this and related systems.

Acknowledgement

This work was supported by the Deutsche Forschungsgemeinschaft in the framework of the SFB 858 and by grants 793/1-1 and SCHN 377/15 and by the Fonds der Chemischen Industrie. The authors thank C. Mück-Lichtenfeld for technical assistance.

Supporting Information: The supporting information contains coordinates of the investigated complexes and further computational details.

8.5 Bibliography

[1] Y. Wang, X. Wang, M. Antonietti, *Angew. Chem.* **2012**, *124*, 70–92; *Angew. Chem. Int. Ed.* **2012**, *51*, 68–70 .

[2] C. T. Seto, G. M. Whitesides, *J. Am. Chem. Soc.* **1990**, *112*, 6409–6411.

[3] A. Ranganathan, V. R. Pedireddi, C. N. R. Rao, *J. Am. Chem. Soc.* **1999**, *121*, 1752–1753.

[4] S. J. Makowski, P. Köstler, W. Schnick, *Chem. Eur. J.* **2012**, *in press*, DOI: 10.1002/ chem.201103527.

[5] H. L. Anderson, S. Anderson, J. K. M. Sanders, *J. Chem. Soc., Perkin Trans. 1*, **1995**, 2231–2245.

[6] Single-crystals of 3tptz were obtained by heating small amounts of 3tptz in a sealed duran ampoule, filled with argon (with 2 $K \cdot min^{-1}$ to 310 °C, held at 310 °C for 48 h, with 0.05 $K \cdot min^{-1}$ to RT). 3tptz crystallizes in the orthorhombic space group *Pnma* with a disorder of the nitrogen atom in one of the pyrimidyl rings. However, for the calculations this disorder has not been taken into account and calculations have been performed in space group $P\ \bar{1}$. PCCDC 867801 contains the crystallographic data for 3tptz (space group *Pnma*). These data can be obtained free of charge via http://www.ccdc.cam.ac.uk/conts/retrieving.html (or from the Cambridge Crystallographic Data Centre, 12, Union Road, Cambridge CB2 1EZ, UK; fax: +44 1223 336033).

[7] S. J. Makowski, M. Lacher, C. Lermer, W. Schnick, *J. Mol. Struct.* **2012**, *1013*, 19–25.

[8] M. G. B. Drew, M. J. Hudson, P. B. Iveson, M. L. Russell, C. Madic, *Acta Crystallogr., Sect. C*, **1998**, *54*, 985–987.

[9] J. Janczak, M. Śledź, R. Kubiak, *J. Mol. Struct.* **2003**, *659*, 71–79.

[10] A. Cousson, B. Nicolaï, F. Fillaux, *Acta Crystallogr., Sect. E* **2005**, *61*, o222–o224.

[11] S. Grimme, J. Antony, S. Ehrlich, H. Krieg, *J. Chem. Phys.* **2010**, *132*, 154104.

[12] L. Goerigk, S. Grimme, *Phys. Chem. Chem. Phys.* **2011**, *13*, 6670–6688.

[13] L. Goerigk, H. Kruse, S. Grimme, *ChemPhysChem.* **2011**, *12*, 3421–3433.

[14] C. Lee, W. Yang, R. Parr, *Phys. Rev. B* **1988**, *37*, 785–789.

[15] A. D. Becke, *Phys. Rev. A* **1988**, *38*, 3098–3100.

[16] A. Schäfer, C. Huber, R. Ahlrichs, *J. Chem. Phys.* **1994**, *100*, 5829–5835.

[17] D. Rappoport, F. Furche, *J. Chem. Phys.* **2010**, *133*, 134105.

[18] R. Ahlrichs, M. Bär, M. Häser, H. Horn, C. Kölmel, *Chem. Phys. Lett.* **1989**, *162*, 165–169.

[19] R. Ahlrichs, F. Furche, C. Hättig, W. Klopper, M. Sierka, F.Weigend, TURBOMOLE, Turbomole GmbH, Karlsruhe, **2009**.

[20] K. Eichkorn, F. Weigend, O. Treutler, R. Ahlrichs, *Theor. Chim. Acta* **1997**, *97*, 119–124.

[21] K. Eichkorn, O. Treutler, H. Öhm, M. Häser, R. Ahlrichs, *Chem. Phys. Lett.* **1995**, *240*, 283–289.

[22] F. Weigend, *Phys. Chem. Chem. Phys.* **2006**, *8*, 1057–1065.

[23] L. Goerigk, S. Grimme, *J. Chem. Theory Comput.* **2010**, *6*, 107–126.

[24] C. Møller, M. S. Plesset, *Phys. Rev.* **1934**, *46*, 618–622.

[25] D. Cremer, *Encyclopedia of Computational Chemisty*; Wiley: New York, **1998**, pp. 1706–1735.

[26] J. P. Perdew, *Proceedings of the 21st Annual International Symposium on the Electronic Structure of Solids*, Akademie Verlag: Berlin, **1991**, pp. 11-20.

[27] A. D. Becke, *J. Chem. Phys.* **1996**, *104*, 1040–1046.

[28] S. Grimme, *J. Chem. Phys.* **2003**, *118*, 9095–9102.

[29] Y. Jung, R. C. Lochan, A. D. Dutoi, M. Head-Gordon, *J. Chem. Phys.* **2004**, *121*, 9793–9802.

[30] L. Goerigk, S. Grimme, *J. Chem. Theory Comput.* **2011**, *7*, 291–309.

[31] S. Grimme, *J. Comput. Chem.* **2004**, *25*, 1463–1473.

[32] S. Grimme, *J. Comput. Chem.* **2006**, *27*, 1787–1799.

[33] S. F. Boys, F. Bernardi, *Mol. Phys.* **2002**, *100*, 65–73.

[34] F. Duijneveldt, J. van Duijneveldt-van de Rijdt, J. Lenthe, *Chem. Rev.* **1994**, *94*, 1873–1855.

[35] G. Kresse, J. Hafner, *Phys. Rev. B* **1993**, *47*, 558–561.

[36] G. Kresse, J. Furthmüller, *Comput. Mat. Sci.* **1996**, *6*, 15–50.

[37] G. Kresse, J. Furthmüller, *Phys. Rev. B* **1996**, *54*, 11169–11186.

[38] G. Kresse, D. Joubert, *Phys. Rev. B* **1999**, *59*, 1758–1775.

[39] J. Moellmann, S. Grimme, *Phys. Chem. Chem. Phys.* **2010**, *12*, 8500–8504.

[40] P. E. Blöchl, *Phys. Rev. B* **1994**, *50*, 17953–17979.

[41] E. A. Coutsias, C. Seok, K. A. Dill, *J. Comput. Chem.* **2004**, *25*, 1849–1857.

[42] M. Rubio, M. Merchán, E. Ortí, *Theor. Chim. Acta* **1995**, *91*, 17–29.

[43] A. Almenningen, L. Bastiansen, O. Fernholt, B. N. Cyvin, S. J. Cyvin, S. Samdal, *J. Mol. Struct.* **1985**, *128*, 59–76.

9. Discussion and Outlook

In this thesis it has been demonstrated how novel materials comprising the *s*-triazine and *s*-heptazine core, respectively, can be obtained by taking advantage of several types of noncovalent interactions. On the one hand, supramolecular materials have been investigated in which a specific arrangement of molecular building blocks is determined by interplay of hydrogen bridges, dispersive and electrostatic interactions; on the other hand, molecular salts and coordination compounds have been described in which additionally strong Coulomb and coordinative interactions are important for the assembly of building units. It has been shown how employment of molecular building blocks which have been used only rarely in this regard so far, enables preparation of interesting novel compounds. In this context attention has been paid especially to *s*-heptazine derivatives and to molecules which do not represent classical inorganic carbon nitride type materials but can rather be placed between such compounds and organic hydrocarbons. Continuing research in this area could take up investigations which have not been completed yet, for instance analysis of materials which have been prepared but not fully characterized in the course of this work. Additionally, the insight into possibilities and limitations regarding syntheses of such materials gained in this thesis should contribute to a more facile preparation of novel compounds. Thereby systematic investigations of specific classes of compounds could be complemented and several materials possibly featuring interesting properties be obtained.

9.1 Molecular Salts and Coordination Compounds

In this study it has been shown that next to several cyamelurates and melonates with divalent transition metal ions, which have been reported prior to this work,[1,2] also melonates with trivalent rare-earth ions can be synthesized as novel *s*-heptazine based coordination compounds (see chapter 3). Preparation of crystalline *s*-heptazine materials with multivalent cations in this thesis as well as by *Clauss*[1] and *Sattler*[2] has been realized by two different methods which both circumvent the problem that in general *s*-heptazine salts with multivalent cations exhibit low solubility, therefore impeding synthesis of highly crystalline materials. In the case of transition metal cyamelurates reactions in

ammonia solutions have increased solubility and allowed for single-crystal growth by recrystallization. Another method which facilitates growth of single-crystals even of compounds that precipitate immediately during metathesis reactions in solution has been employed in the case of copper and rare-earth melonates. Single-crystals of these materials have been obtained by slow diffusion reactions, thereby retarding nucleation and crystal growth. Utilization of one of these strategies might enable access to several novel *s*-heptazine compounds with multivalent cations, e. g. further transition metal cyamelurates and melonates or rare-earth cyamelurates.

On the one hand, such compounds are of interest with respect to the large variety of structures that can be formed. Because in *s*-heptazine based building blocks such as melonate or cyamelurate not only functional side chains but also nitrogen atoms of the ring represent potential coordination sites numerous coordination motifs and resulting network structures are conceivable. On the other hand, *s*-heptazine coordination compounds are likely to exhibit manifold properties dependent on the respective metal ions. For instance, in this thesis it has been reported that Tb^{3+} melonate exhibits photoluminescence under UV excitation in analogy to Tb^{3+} dicyanamides and tricyanomelaminates.[3] In this regard photoluminescence studies of Ln^{3+} cyamelurates would contribute to a systematic investigation of luminescent *s*-heptazine materials. Moreover, synthesis and characterization of carbon nitride type materials with divalent rare-earth ions or doping of alkaline earth compounds with Eu^{2+} would be of considerable interest. Because preparation of such materials requires non-oxidative reaction conditions liquid ammonia might present a suitable solvent. However, first attempts to prepare the respective Ln^{2+} dicyanamides by metathesis reactions between $EuCl_2$ and alkali or alkaline earth dicyanamides in liquid ammonia have not been successful so far.[4] Next to photoluminescence of rare-earth materials further physical properties might be of interest and should be studied once the respective compounds have been synthesized, for instance magnetic behavior of *s*-heptazine salts with transition metal ions.

Novel coordination compounds can presumably also be obtained by employing triazine tricarboxylate as ligand under suitable reaction conditions. Comprehensive studies of coordination motifs and stacking modes of triazine tricarboxylate in several salts in this thesis have provided an overview of possible structures (see chapter 4). The appearance of the recurring coordination motif of two adjacent carboxylate groups and the intermediate nitrogen atom of the triazine ring, and the observed dependence of stability of triazine tricarboxylate on the ionic radii of counterions allow for an estimation of feasible structures. So far only one structurally characterized triazine tricarboxylate comprising transition metal ions is known, namely K{Fe(1,3,5-triazine-2,4,6-tricarboxylate)-

$(H_2O)_2\}\cdot 2H_2O$.[5] Investigating the hydrolysis stability of triazine tricarboxylate in the presence of different transition metal salts has shown that additionally a triazine tricarboxylate material with Mn^{2+} ions can be synthesized (see chapter 4.2). However, structural characterization of this compound has not been performed in the course of this work. By employing for instance crystallization by slow diffusion reactions, as has been described for *s*-heptazine coordination frameworks above, synthesis of crystalline Mn^{2+} triazine tricarboxylate might be possible. Additionally, measurements of magnetic properties for this material and comparison to magnetic behavior of Fe^{2+} triazine tricarboxylate[5] would valuably contribute to a comprehensive characterization of transition metal triazine tricarboxylates. Triazine tricarboxylate coordination frameworks with various ions might furthermore be obtained by avoiding hydrolysis of triazine tricarboxylate units in aqueous solution, for instance by employment of large metal ions, addition of a second, strongly coordinating ligand, or use of anhydrous solvents such as suitable ionic liquids. Pre-examinations have shown adequate solubility of the starting material potassium triazine tricarboxylate in 1-ethyl-3-methylimidazolium ethyl sulfate and 1-ethyl-3-methylimidazolium acetate.[6]

For the attempted synthesis of further *s*-triazine and *s*-heptazine based coordination compounds the electronic structure of these ring systems and its influence on possible structural motifs should be kept in mind. Both the *s*-triazine and the *s*-heptazine core represent electron-poor aromatic cycles and therefore coordination of metal ions by π-electrons of the rings, resulting for instance in sandwich-type complexes, has not been reported so far. Moreover, considering the preferred arrangement of both melonate and triazine tricarboxylate units into layered structures, as has been observed for all materials investigated in this thesis, construction of three-dimensional porous MOFs comprising solely melonate or triazine tricarboxylate as linkers appears rather unlikely. It is assumed that for this purpose indeed a combination of such ligands with further building blocks is required. Next to utilization of extended ligands such as *s*-triazine tribenzoate,[7] *s*-triazine-tris(4-pyridyl)[8] or *s*-heptazine tribenzoate[9] preparation of mixed-ligand coordination compounds might provide access to such three-dimensional frameworks. Whereas combination of two different *s*-triazine based building blocks capable of metal coordination causes formation of a layered structure, as has been shown for adducts between alkali triazine tricarboxylates and cyanuric acid in this work (see chapter 5), employment of non-cyclic spacers might avoid such arrangement. For instance more linear compounds such as dicyanamide $(N(CN)_2)^-$ should be considered in this regard.

9.2 Supramolecular Compounds

Facile transformation of the dense structure of anhydrous melem into the channel structure of melem hydrate by treatment in boiling water has illustrated the potential of noncovalent interactions for the construction of supramolecular carbon nitride type frameworks (see chapter 6). The influence of numerous hydrogen bonding interactions with slightly differing bond strengths on the arrangement of molecular building blocks both during synthesis and thermal treatment of melem hydrate has been demonstrated. Solid-state NMR spectra of as-synthesized and dehydrated melem hydrate have shown distinctive differences as a result of varying hydrogen bonding motifs. Progressive NMR investigations could provide more detailed information about hydrogen bridges in the dehydrated material. Thorough structural characterization by solid-state NMR might be achieved by ^{15}N doping of melem hydrate as has for instance been demonstrated for the structure elucidation of melon and anhydrous melem.[10]

Next to further analysis of melem hydrate, variations of self-assembly motifs might be achieved by functionalization of melem units. As has been investigated in detail by *Whitesides* et al. for the adduct between cyanuric acid and melamine (CA·M) for instance bulky substituents strongly affect self-assembly of building blocks into specific structures.[11] Possibly even further stabilization of the structure can be achieved this way, allowing for maintenance of channels during removal of solvent molecules, and therefore preparation of a porous material. Synthesis of several symmetric and asymmetric substituted melem units, which might represent suitable building blocks for this purpose, has been reported by *Kroke* et al..[12] Synthetic strategies described in these publications might also be applicable for the preparation of further functionalized *s*-heptazine derivatives. Moreover, structural changes might also be achieved by the reaction of either melem or substituted derivatives in different solvents, thereby allowing not only for varying hydrogen bonding motifs between melem units but also between melem and solvent molecules.

Moreover, it has been demonstrated in this work that the formation of highly symmetric hydrogen-bonded structures by self-assembly of molecular C/N/H compounds is not limited to the well-known *s*-triazine based CA·M adduct, but also feasible for an *s*-heptazine material. Similar effects on the assembly of molecular building blocks by treatment of materials in suitable solvents and under appropriate reaction conditions are considered possible for further *s*-triazine and *s*-heptazine compounds or mixtures of these. In this regard for instance an adduct of melem and cyameluric acid would be of considerable interest. Considering hydrogen bonding motifs in melem hydrate and CA·M

such an adduct is conceivable. However, by heating suspensions of melem and cyameluric acid in water under similar conditions as have been employed for the preparation of melem hydrate, so far no such adduct could be obtained. These attempts only yielded mixtures of melem hydrate and cyameluric acid hydrate, or decomposition products of cyameluric acid. Preferred formation of melem hydrate indicates that an adduct between melem and cyameluric acid would have to be prepared under modified conditions if it can be obtained at all. Furthermore, supramolecular assemblies comprising melam ($C_3N_3(NH_2)_2)_2NH$ should be taken into account. Until recently this compound could be obtained only in small amounts as side phase during thermal condensation of melamine to melem[13] but meanwhile *Wirnhier* has developed a method to prepare phase pure samples of melam in large quantities,[14] so that it could be employed as building block in supramolecular structures.

As further example of hydrogen-bonded supramolecular structures, co-crystals of melamine and *N*-heterocycles have been presented in this thesis (see chapter 7). In these compounds the structurally related six-membered rings benzene, pyridyl and triazine as well as the macrocycle porphin have been employed. Therefore, it has been demonstrated that model systems between carbon nitrides type materials and hydrocarbons can easily be obtained by supramolecular synthesis. Observation of recurring self-assembly motifs and detailed analysis of different types of noncovalent interactions in these compounds have contributed to a deeper understanding of the factors which influence the arrangement of building blocks in such materials. Interplay of hydrogen bonds, electrostatic and dispersive interactions on the respective assemblies has been examined experimentally by analysis of crystal structures and thermal behavior (see chapter 7) as well as theoretically by DFT calculations (see chapter 8). Further insight into intermolecular interactions in such adduct phases might be achieved by varying the relative importance of different bonding types and thereby examining their particular influence on the structures. For instance, the impact of dispersive interactions could be decreased by employing porphyrin salts with non-aromatic counterions instead of tosylate units. Moreover, preparation and characterization of similar adducts between *s*-heptazine compounds and *N*-heterocycles would be of particular interest. For this purpose presumably substituted *s*-heptazine derivatives have to be prepared in order to achieve sufficient solubility of starting materials. As described above, synthetic methods developed by *Kroke* et al. might be utilized in this regard.[12] Moreover, water-soluble melemium salts,[15] which have been reported by *Sattler*, might be suitable starting materials for the synthesis of adducts which contain *s*-heptazine units. With a large number of cocrystals that comprise *s*-triazine and *s*-heptazine rings at hand, and especially by utilization of both experimental data and theoretical calculations, comprehensive knowledge about interactions in

s-triazine and *s*-heptazine based supramolecular compounds could be achieved. Detailed understanding of these factors might contribute to a more rational synthesis of such materials through crystal engineering in the future. This way *s*-triazine and *s*-heptazine derivatives might be employed as building blocks of interesting novel materials, which ideally exhibit not only specific structures but also desired properties and could therefore be employed for various applications.

9.3 Bibliography

[1] C. Clauss, H. Schmidt, A. Schwarzer, E. Kroke, *Z. Anorg. Allg. Chem.* **2011**, *637*, 2246.

[2] A. Sattler, M. R. Budde, W. Schnick, *Z. Anorg. Allg. Chem.* **2009**, *635*, 1933.

[3] a) A. Nag, B. V. Lotsch, J. Schmedt a. d. Günne, O. Oeckler, P. J. Schmidt, W. Schnick, *Chem. Eur. J.* **2007**, *13*, 3512; b) A. Nag, P. J. Schmidt, W. Schnick, *Chem. Mater.* **2006**, *18*, 5738.

[4] A. Zurawski, S. J. Makowski, W. Schnick, *unpublished results*.

[5] J.-R. Galán-Mascarós, J.-M. Clemente-Juan, K. R. Dunbar, *J. Chem. Soc., Dalton Trans.* **2002**, 2710.

[6] S. Manzori Ostad, Bachelor Thesis, University of Munich (LMU), **2010**.

[7] a) S. Ma, X.-S. Wang, E. S. Manis, C. D. Collier, H.-C. Zhou, *Inorg. Chem.* **2007**, *46*, 3432; b) S. Ma, X.-S. Wang, D. Yuan, H.-C. Zhou, *Angew. Chem.* **2008**, *120*, 4198; *Angew. Chem. Int. Ed.* **2008**, *47*, 4130; c) S. Ma, D. Yuan, X.-S. Wang, H.-C. Zhou, *Inorg. Chem.* **2009**, *48*, 2072; d) S. Ma, H.-C. Zhou, *J. Am. Chem. Soc.* **2006**, *128*, 11734; e) Y. K. Park, S. B. Choi, H. Kim, K. Kim, B.-H. Won, K. Choi, J.-S. Choi, W.-S. Ahn, N. Won, S. Kim, D. H. Jung, S.-H. Choi, G.-H. Kim, S.-S. Cha, Y. H. Jhon, J. K. Yang, J. Kim, *Angew. Chem.* **2007**, *119*, 8378; *Angew. Chem. Int. Ed.* **2007**, *46*, 8230; f) D. Sun, Y. Ke, D. J. Collins, G. A. Lorigan, H.-C. Zhou, *Inorg. Chem.* **2007**, *46*, 2725; g) D. Sun, S. Ma, Y. Ke, D. J. Collins, H.-C. Zhou, *J. Am. Chem. Soc.* **2006**, *128*, 3896; h) D. Sun, S. Ma, Y. Ke, T. M. Petersen, H.-C. Zhou, *Chem. Commun.* **2005**, 2663.

[8] a) J. P. Barrio, J.-N. Rebilly, B. Carter, D. Bradshaw, J. Bacsa, A. Y. Ganin, H. Park, A. Trewin, R. Vaidhyanathan, A. I. Cooper, J. E. Warren, M. J. Rosseinsky, *Chem. Eur. J.* **2008**, *14*, 4521; b) D. N. Dybtsev, H. Chun, K. Kim, *Chem. Commun.* **2004**, 1594; c) M.-X. Li, Z.-X. Miao, M. Shao, S.-W. Liang, S.-R. Zhu, *Inorg. Chem.* **2008**, *47*, 4481; d) W. Li, M.-X. Li, M. Shao, S.-R. Zhu, *Inorg. Chem. Commun.* **2007**, *10*, 753.

[9] a) Y. Ke, D. J. Collins, D. Sun, H.-C. Zhou, *Inorg. Chem.* **2006**, *45*, 1897; b) S. Ma, D. Sun, M. Ambrogio, J. A. Fillinger, S. Parkin, H.-C. Zhou, *J. Am. Chem. Soc.* **2007**, *129*, 1858.

[10] a) B. Jürgens, E. Irran, J. Senker, P. Kroll, H. Müller, W. Schnick, *J. Am. Chem. Soc.* **2003**, *125*, 10288; b) B. V. Lotsch, M. Döblinger, J. Sehnert, L. Seyfarth, J. Senker, O. Oeckler, W. Schnick, *Chem. Eur. J.* **2007**, *13*, 4969.

[11] a) J. P. Mathias, E. E. Simanek, J. A. Zerkowski, C. T. Seto, G. M. Whitesides, *J. Am. Chem. Soc.* **1994**, *116*, 4316; b) G. M. Whitesides, E. E. Simanek, J. P. Mathias, C. T. Seto, D. N. Chin, M. Mammen, D. M. Gordon, *Acc. Chem. Res.* **1995**, *28*, 37.

[12] a) T. Saplinova, V. Bakumov, T. Gmeiner, J. Wagler, M. Schwarz, E. Kroke, *Z. Anorg. Allg. Chem.* **2009**, *635*, 2480; b) T. Saplinova, C. Lehnert, U. Böhme, J. Wagler, E. Kroke, *New J. Chem.* **2010**, *34*, 1893; c) M. R. Schwarz, H. Ehrenberg, M. A. Kloc, E. Kroke, *Heterocycles* **2006**, *68*, 2499; d) A. Schwarzer, E. Kroke, *Chem. Commun.* **2010**, *46*, 2829; e) A. Schwarzer, E. Kroke, *New J. Chem.* **2011**, *35*, 953.

[13] B. V. Lotsch, W. Schnick, *Chem. Eur. J.* **2007**, *13*, 4956.

[14] E. Wirnhier, W. Schnick, *in preparation*.

[15] a) A. Sattler, W. Schnick, *Z. Anorg. Allg. Chem.* **2008**, *634*, 457; b) A. Sattler, W. Schnick, *Z. Anorg. Allg. Chem.* **2010**, *636*, 2589; c) A. Sattler, S. Schönberger, W. Schnick, *Z. Anorg. Allg. Chem.* **2010**, *636*, 476; d) A. Sattler, L. Seyfarth, J. Senker, W. Schnick, *Z. Anorg. Allg. Chem.* **2005**, *631*, 2545.

10. Appendix

10.1 Supporting Information

Supporting information for chapter 3

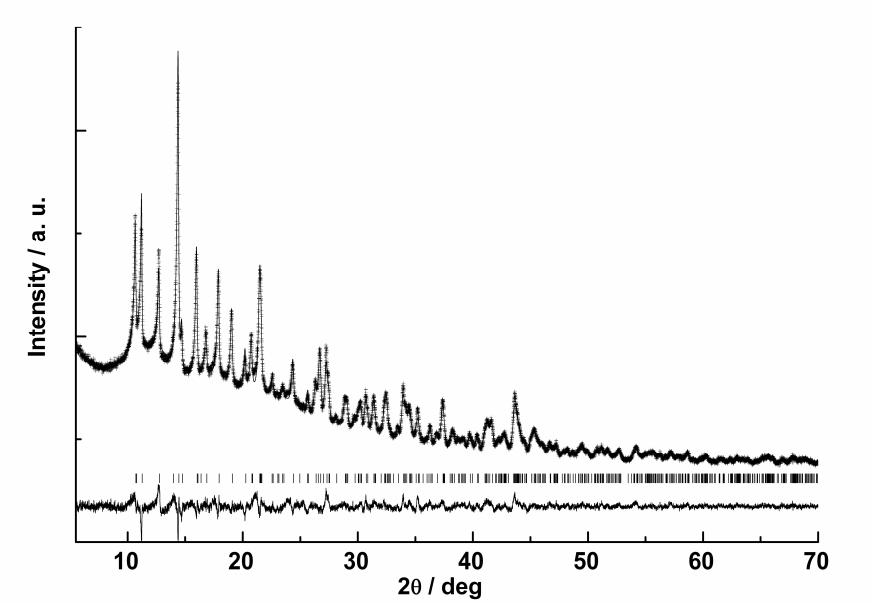

Figure S1. Observed (crosses) and calculated (line) X-ray powder diffraction patterns as well as difference profile of the Rietveld refinement of $PrC_6N_7(NCN)_3 \cdot 8H_2O$ **7c**. Bragg peaks are indicated by vertical lines. (λ = 154.06 pm, T = 298 K).

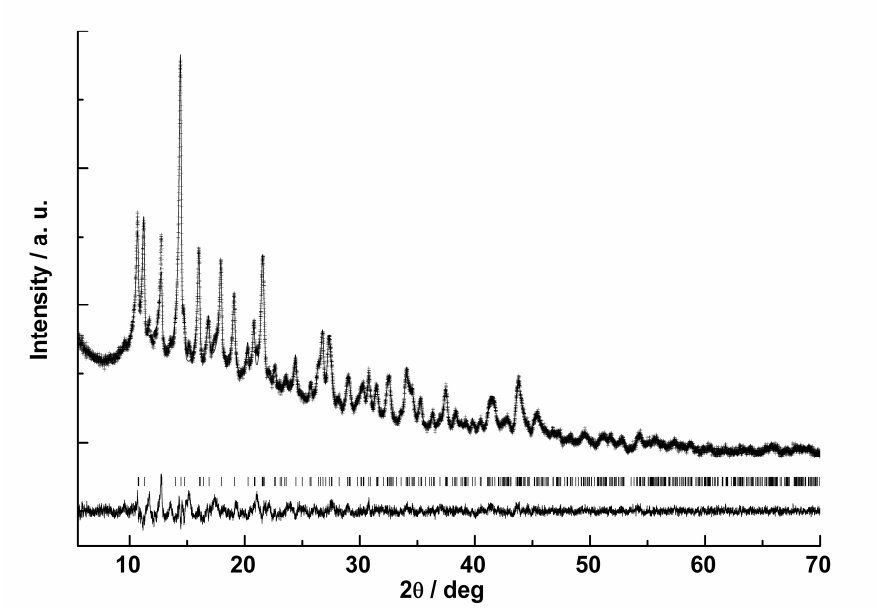

Figure S2. Observed (crosses) and calculated (line) X-ray powder diffraction patterns as well as difference profile of the Rietveld refinement of $NdC_6N_7(NCN)_3 \cdot 8H_2O$ **7d**. Bragg peaks are indicated by vertical lines. (λ = 154.06 pm, T = 298 K).

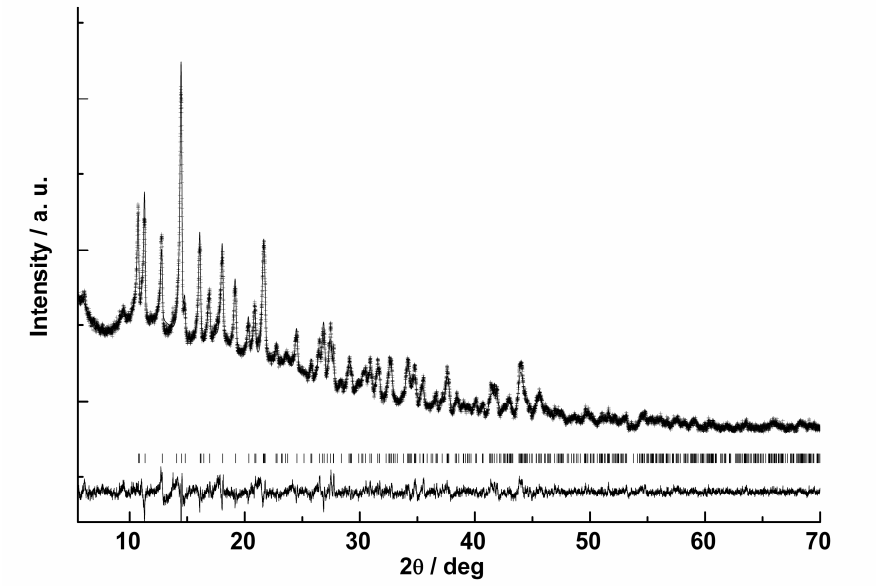

Figure S3. Observed (crosses) and calculated (line) X-ray powder diffraction patterns as well as difference profile of the Rietveld refinement of $SmC_6N_7(NCN)_3 \cdot 8H_2O$ **7e**. Bragg peaks are indicated by vertical lines. (λ = 154.06 pm, T = 298 K).

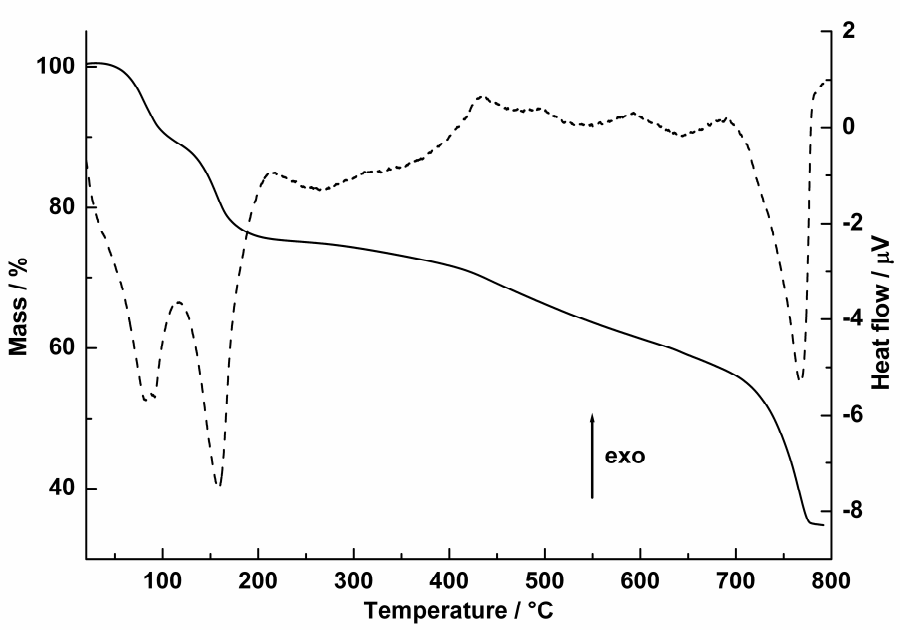

Figure S4. TG (solid) and DTA (dashed) curves of $CeC_6N_7(NCN)_3 \cdot 8H_2O$ **7b** (34.8 mg), measured with a heating rate of 5 $K \cdot min^{-1}$.

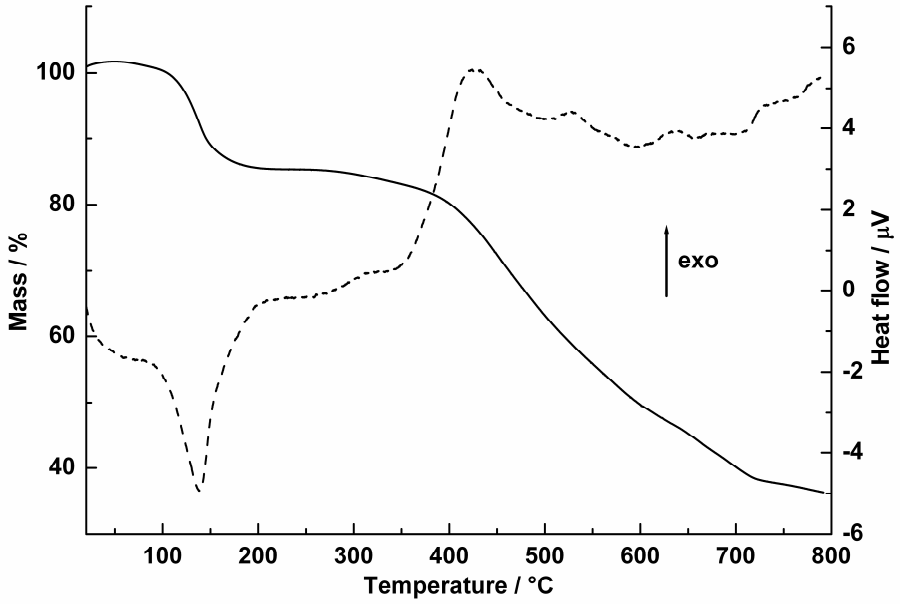

Figure S5. TG (solid) and DTA (dashed) curves of $PrC_6N_7(NCN)_3 \cdot 8H_2O$ **7c** (21.0 mg), measured with a heating rate of 5 $K \cdot min^{-1}$.

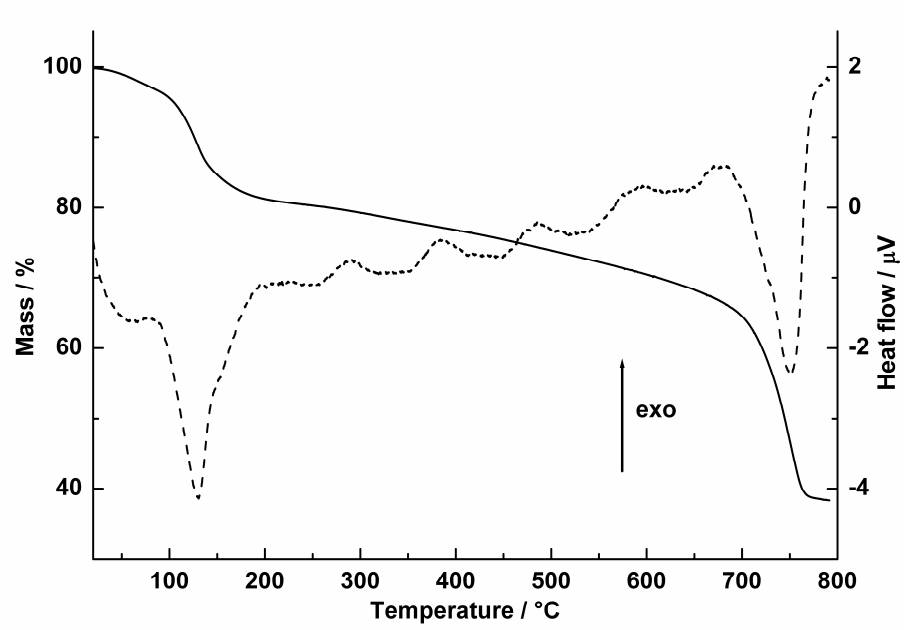

Figure S6. TG (solid) and DTA (dashed) curves of $NdC_6N_7(NCN)_3 \cdot 8H_2O$ **7d** (19.0 mg), measured with a heating rate of 5 $K \cdot min^{-1}$.

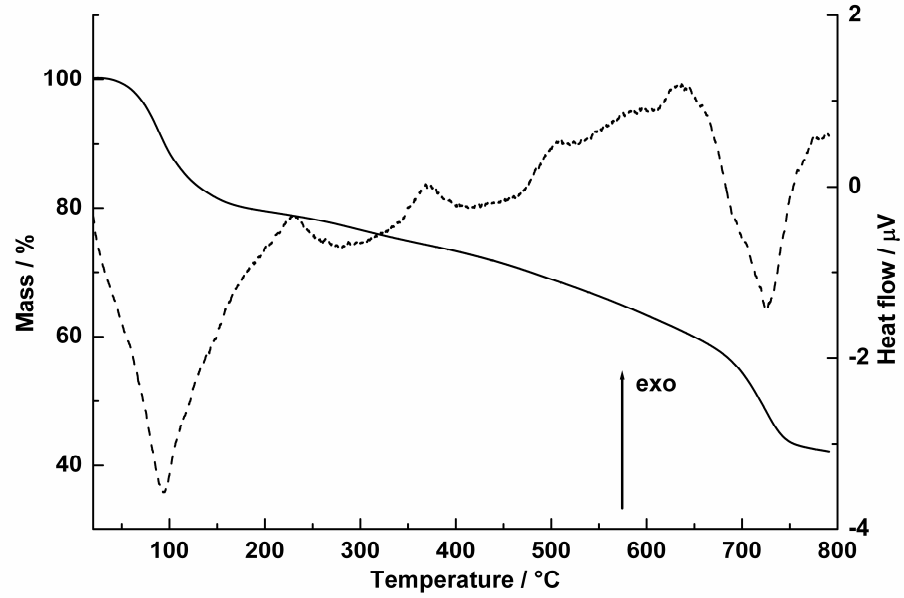

Figure S7. TG (solid) and DTA (dashed) curves of $SmC_6N_7(NCN)_3 \cdot 8H_2O$ **7e** (22.4 mg), measured with a heating rate of 5 $K \cdot min^{-1}$.

Supporting information for chapter 6

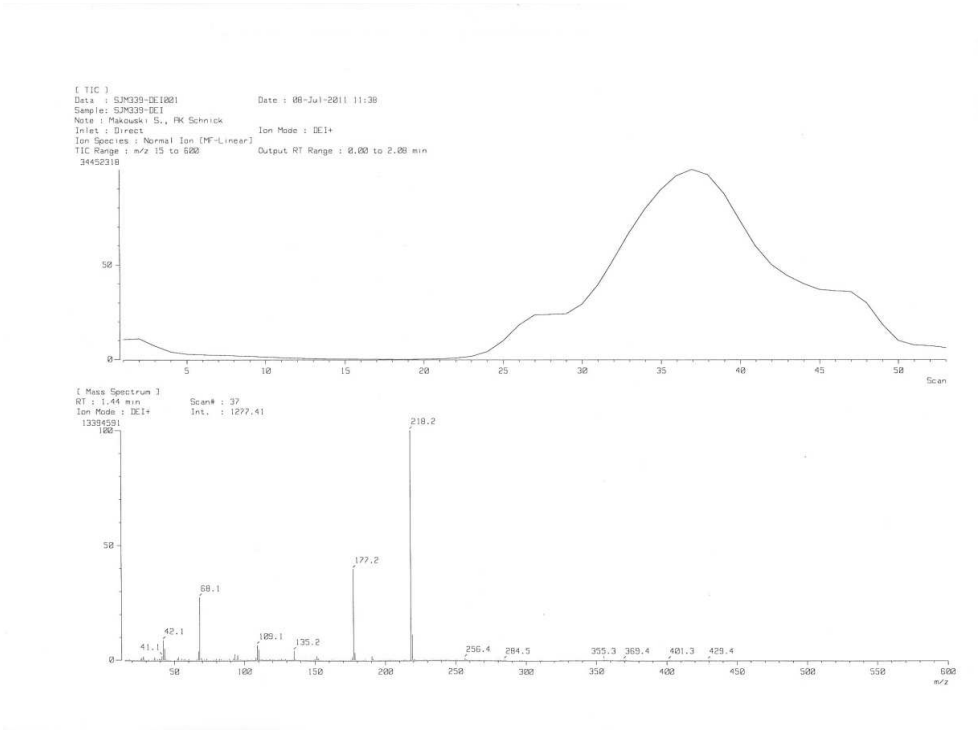

Figure S1. DEI+ mass spectrum of melem hydrate **2**. *m/z* (%): 218.2 (100) [M^+], 178.2 (3) [M^+–NCN], 177.2 (40) [M^+–NCNH], 135.2 (5) [$C_4N_6H_3^+$], 109.1 (6) [$C_3N_5H_3^+$], 93.1 (3) [$C_3N_4H^+$], 68.1 (28) [$C_3N_2H_4^+$], 42.1 (9) [$CN_2H_2^+$], 41.1 (2) [CN_2H^+], 28.1 (2) [CNH_2^+].

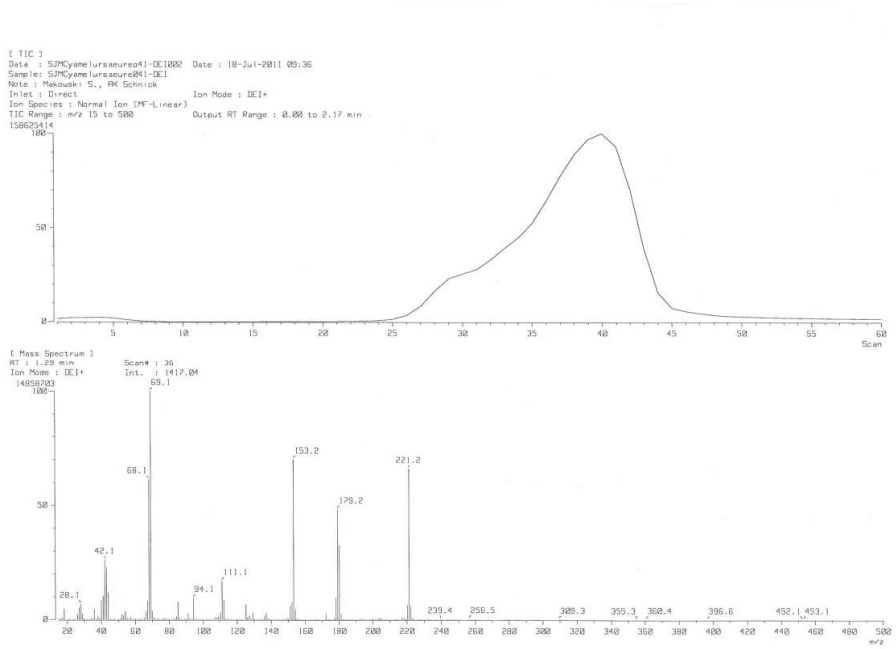

Figure S2. DEI+ mass spectrum of cyameluric acid, demonstrating the possibility to detect cyameluric acid in MS spectra. Spectrum was recorded under the same conditions as used for the MS spectrum of **2**. *m/z* (%): 221.2 (65) [M^+], 220.2 (6) [M^+–H], 179.2 (48) [M^+–NCO], 153.2 (70) [$C_4N_5O_2H_3^+$], 152.2 (6) [$C_4N_5O_2H_2^+$], 111.1 (17) [$C_3N_4OH_3^+$], 69.1 (100) [$C_2N_3H_3^+$], 68.1 (61) [$C_2N_3H_2^+$], 42.1 (18) [$CN_2H_2^+$], 41.1 (11) [CN_2H^+], 28.1 (8) [CO^+].

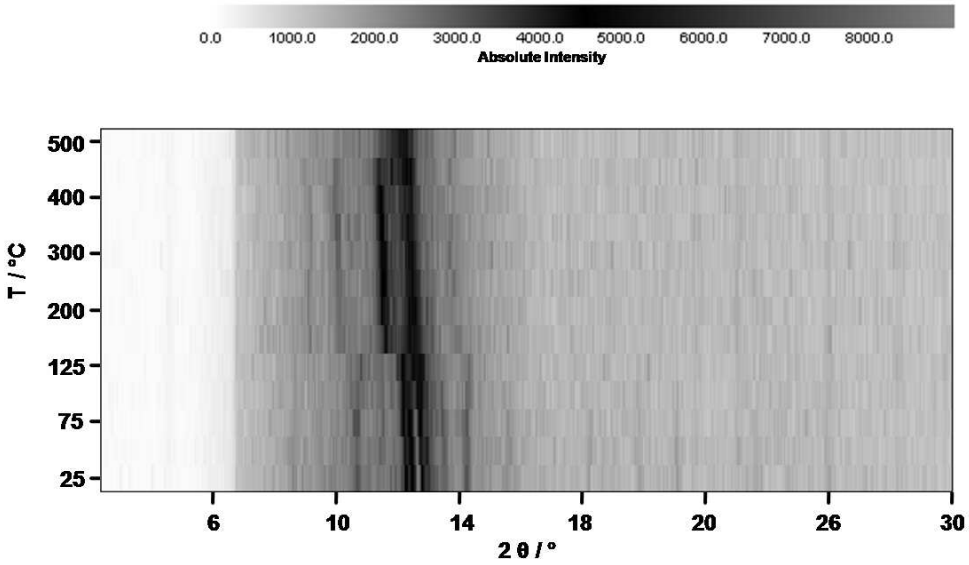

Figure S3. In situ temperature-dependent X-ray diffraction measurement of melem hydrate **2**, recorded between room temperature and 500 °C (λ = 70.093 pm).

Supporting information for chapter 7

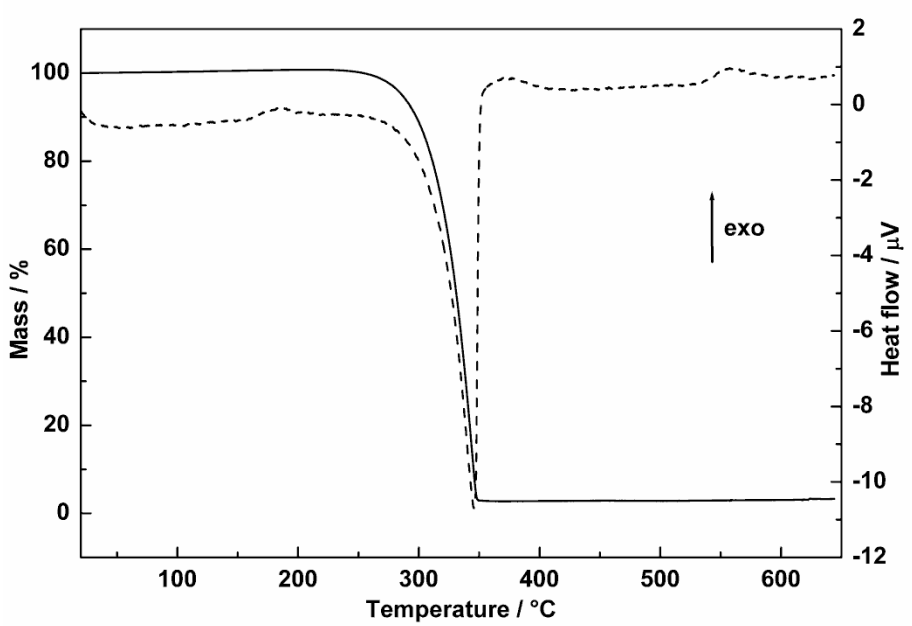

Figure S1. TG (solid) and DTA (dashed) curves of melamine (19.5 mg).

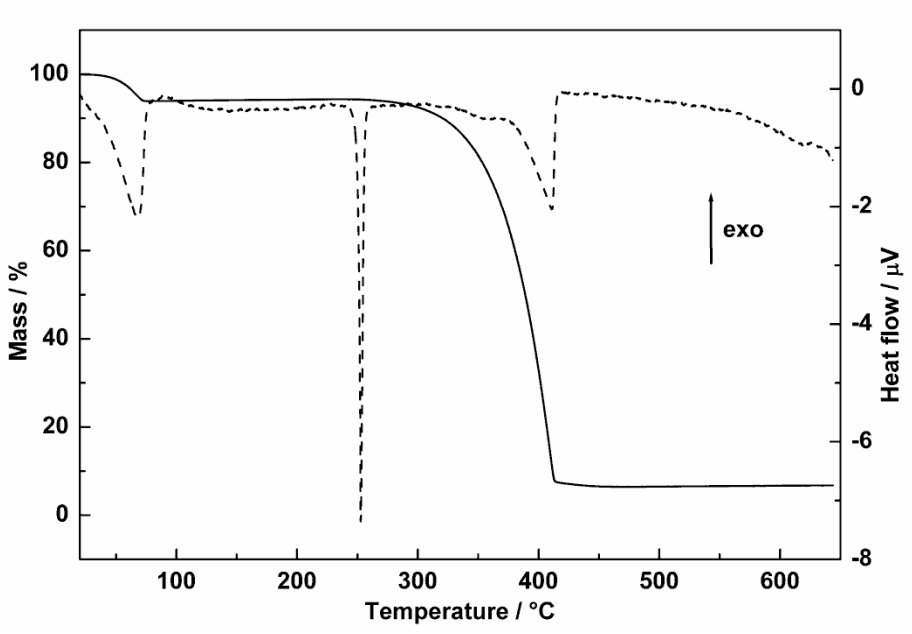

Figure S2. TG (solid) and DTA (dashed) curves of TPTZ (17.0 mg).

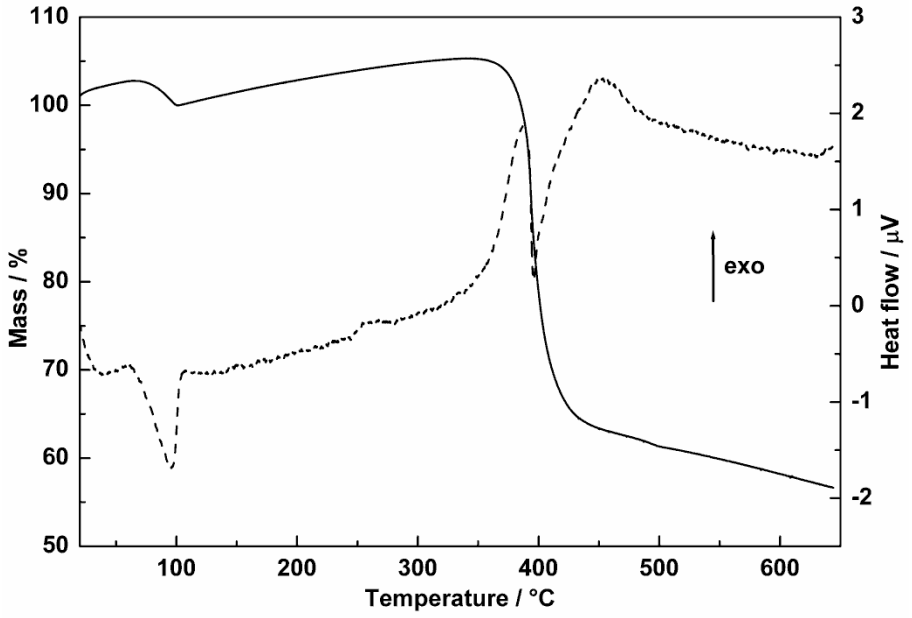

Figure S3. TG (solid) and DTA (dashed) curves of TMPyP-Tos (13.4 mg).

Supporting information for chapter 8

The supplementary material contains:

Table 1 Comparison of interaction energies of the model complexes 1a-4d computed from density functional theory (E_{int}^{DFT-D}) and DFT including dispersion correction (E_{int}^{DFT-D3}) based on BLYP-D3/def2-TZVP optimized geometries. The PWPB95 computations employ the def2-TZVP basis set, otherwise the def2-QZVP basis set is applied. Deformation energy of the monomers is neglected. All energies in kcal·mol^{-1}.

	BLYP[1,2]		oTPSS[3,4]		PWPB95[5–9]		PWPB95[a]	
complex	E_{int}^{DFT-D}	E_{int}^{DFT-D3}	E_{int}^{DFT-D}	E_{int}^{DFT-D3}	E_{int}^{DFT-D}	E_{int}^{DFT-D3}	E_{int}^{DFT-D}	E_{int}^{DFT-D3}
based on fully relaxed geometries								
1a	12.5	–20.4	12.1	–17.8	–9.5	–19.4	–6.8	–16.6
1b	10.5	–26.9	10.0	–24.0	–15.3	–26.6	–10.1	–21.4
1c	11.7	–20.3	10.9	–18.2	–10.0	–19.6	–6.4	–16.1
1d	26.3	–47.7	25.5	–41.7	–23.4	–46.4	–17.0	–40.1
1e	–3.2	–12.9	–3.3	–12.1	–6.6	–9.8	–6.0	–9.2
1f	0.6	–18.9	0.4	–17.1	–7.2	–13.1	–6.1	–12.0
2a	6.4	–15.0	5.8	–13.5	–8.0	–14.6	–6.1	–12.7
2b	6.7	–22.6	6.2	–20.4	–12.8	–21.9	–10.3	–19.4
3a	14.3	–19.4	13.6	–17.0	–9.0	–19.2	–6.3	–16.5
4a	2.5	–10.4	2.7	–8.8	–6.9	–10.5	–5.2	–8.8
4b	–8.2	–13.6	–9.0	–13.8	–10.4	–12.1	–9.6	–11.2
4c	2.2	–8.8	2.4	–7.4	–2.8	–5.9	–1.9	–5.0
4d	–8.3	–13.6	–9.0	–13.8	–9.1	–10.8	–8.6	–10.3
based on structures optimized with fixed positions of heavy atoms								
1a	9.9	–17.3	9.2	–15.9	–7.1	–15.5	–4.7	–13.2
1b	9.4	–17.5	8.6	–16.2	–7.1	–15.5	–4.8	–13.2
1c	0.1	–0.7	–3.5	–4.2	–0.1	–0.6	0.0	–0.6
1d	19.3	–35.5	17.8	–32.7	–14.6	–32.0	–9.8	–27.2
1e	–0.9	–10.0	–0.9	–9.1	–4.0	–7.0	–3.4	–6.4
2a	3.8	–10.4	3.4	–9.6	–4.6	–9.2	–3.3	–7.9
2b	4.0	–12.5	3.0	–12.2	–6.4	–11.9	–5.0	–10.5
3a	12.5	–19.1	11.7	–17.2	–8.7	–18.3	–6.1	–15.8
3b	9.2	–13.7	8.6	–12.3	–6.2	–13.0	–4.3	–11.2
3c	6.0	–8.4	5.6	–7.5	–3.6	–7.8	–2.6	–6.7
3d	2.4	–3.1	2.1	–2.9	–1.2	–2.7	–0.9	–2.4
4c	2.6	–6.9	2.5	–6.2	–1.9	–4.6	–1.1	–3.8
4d	–7.3	–12.9	–8.1	–13.1	–8.2	–9.9	–7.7	–9.5

[a]counterpoise corrected.

Influence of the density functional on the optimized geometry

Figure 1 presents an overlay of resulting geometries of model system 2a optimized with BLYP-D3,[1,2] PBE-D3[10] and TPSS-D3[3] using triple-ζ basis sets. Compared to the initial geometry of the dimer in the solid phase (black structure in Figure 1) two main differences of the DFT-D3 optimized gas phase geometries can be identified. First, the distance between the fragments' centers of mass is shorter because they are not as much parallel displaced as they are in the crystal phase (6.5 Å based on fully relaxed geometries predicted by all density functionals (DF) vs. 7.4 Å based on structures with fixed positions of the heavy atoms). Second, the rotational conformation of the pyridinyle moieties differs strongly. While the stacked pyridinyle moiety is rotated by 31 degrees out of plane of the triazine ring in the solid phase, these moieties are stacked in a more planar way for the fully relaxed gas phase structures (9 degrees).

The agreement of the resulting geometries optimized with different density functionals is very good. The optimization converges to the same minimum structure with only minor differences in the dihedral angle of the pyridinyle moieties. The root mean square deviation (RMSD) as calculated from the difference between the two sets of coordinates of BLYP-D3/def2-TZVP optimized geometries and PBE-D3/def2-TZVP optimized ones is 0.12 Å.[11] Compared to TPSS-D3 the RMSD is only 0.02 Å higher.

We obtain similar results for the melamine dimer in its π-stacked and hydrogen-bonded conformations. The distance between the π-stacked fragments' centers of mass is 3.7 Å (±0.05 Å depending on the DF) compared to 6.2 Å for the hydrogen bonded conformation (all DF). The RMSD between BLYP-D3 and PBE-D3 optimized geometries of compound 4a is 0.05 Å. Compared to TPSS-D3 the agreement is even better (0.03 Å). For model system 4b all optimizations lead to minimum geometries that can be considered identical due to the low RMSD value of 0.02 Å.

Based on free optimizations with BLYP-D3 and basis sets of increasing size (def2-TZVP, def2-TZVPD, def2-QZVP) we find an average distance between the monomers' centers of mass of 6.5 Å compared to 6.1 Å for the dimer based on optimization with fixed positions of heavy atoms. The RMSD between def2-TZVP and def2-TZVPD optimized geometries is 0.02 Å and compared to def2-QZVP the RMSD is even below 0.02 Å which reflects the good agreement of the different minimum geometries. Figures 2 and 3 present overlays of melamine structures 4c and 4d optimized with three different density functionals. The RMSD between the fully relaxed structures is always below 0.05 Å.

Our computations show that the particular type of GGA or meta GGA is only of minor influence on the resulting minimum geometry of compounds 2a and 4a to 4d. The increase of the basis set size to quadruple-ζ during the optimization is also only of small importance for the resulting optimum gas phase geometry (see below). The same can be expected for compounds 2b, 3a and 1a-1f because of the similar bonding situation in these structures. Therefore BLYP-D3/def2-TZVP optimized geometries are sufficient for this study. Figures 4 to 11 present overlays of fully relaxed structures of model systems 2b, 3a, 1a, 1b, 1d, 1e, 4c and 4d with their crystal reference.

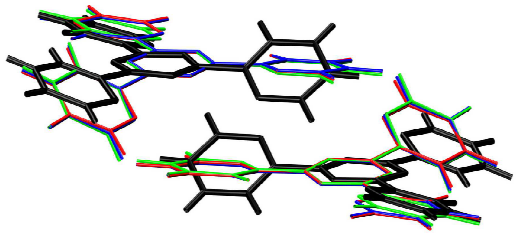

(a) sideview

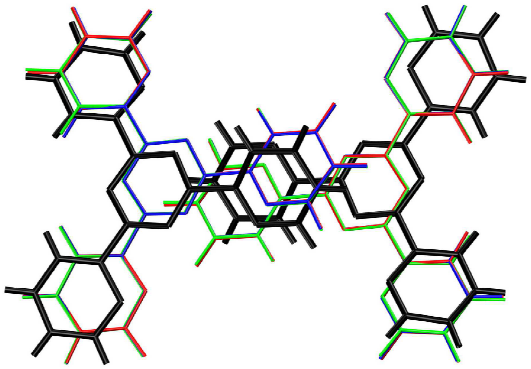

(b) topview

Figure 1. Overlay of geometries of dimer 2a resulting from geometry optimization with BLYP-D3 (green), PBE-D3 (blue) and TPSS-D3 (red). Always the def2-TZVP basis set is applied. For comparison the starting geometry taken from crystallographic data[12] is shown in black.

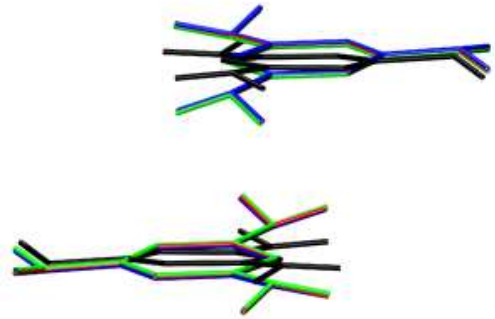

(a) sideview

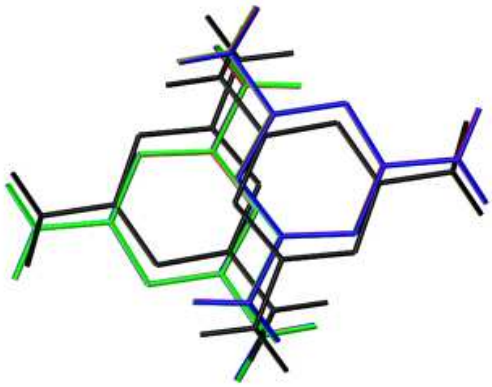

(b) topview

Figure 2. Overlay of geometries of dimer 4c resulting from geometry optimization with BLYP-D3 (green), PBE-D3 (blue) and TPSS-D3 (red). Always the def2-TZVP basis set is applied. For comparison the starting geometry taken from crystallographic data[13] is shown in black.

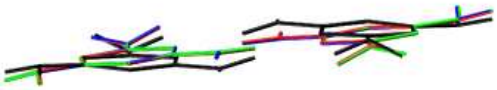

(a) sideview

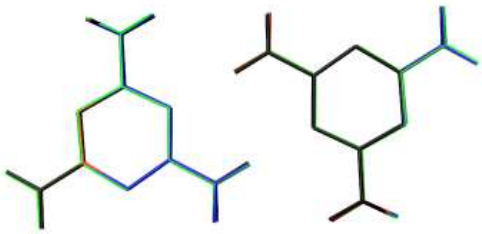

(b) topview

Figure 3. Overlay of geometries of dimer 4d resulting from geometry optimization with BLYP-D3 (green), PBE-D3 (blue) and TPSS-D3 (red). Always the def2-TZVP basis set is applied. For comparison the starting geometry taken from crystallographic data[13] is shown in black.

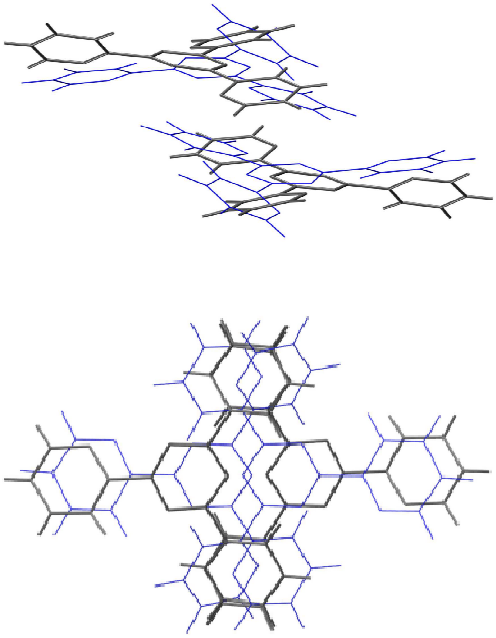

Figure 4. BLYP-D3/def2-TZVP optimized geometries (blue) of compound 2b. For comparison the initial geometries taken from crystallographic data[12] are shown in black. Top: sideview, bottom: topview.

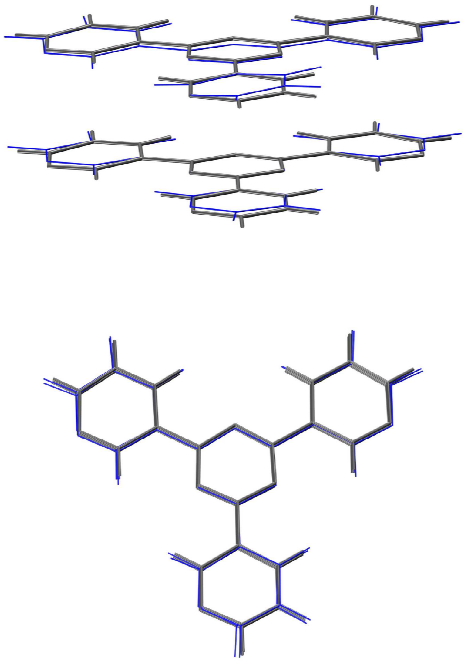

Figure 5. BLYP-D3/def2-TZVP optimized geometries (blue) of compound 3a. For comparison the initial geometries taken from crystallographic data[14] are shown in black. Top: sideview, bottom: topview.

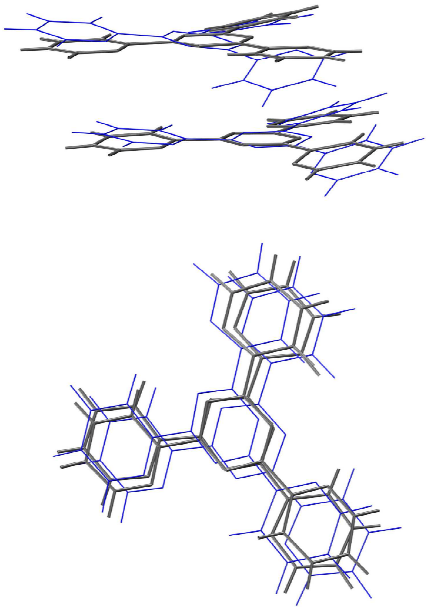

Figure 6. BLYP-D3/def2-TZVP optimized geometries (blue) of compound 1a. For comparison the initial geometries taken from crystallographic data[15] are shown in black. Top: sideview, bottom: topview.

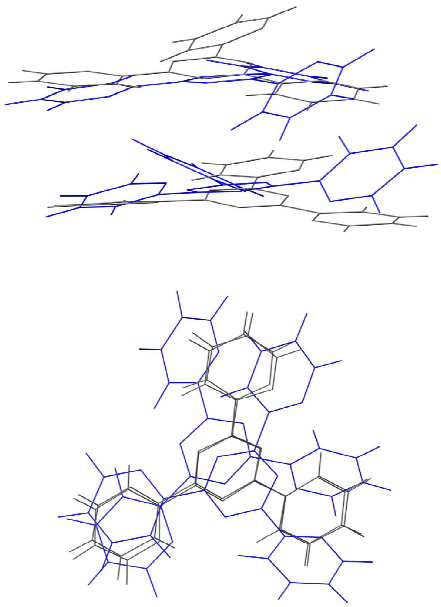

Figure 7. BLYP-D3/def2-TZVP optimized geometries (blue) of compound 1b. For comparison the initial geometries taken from crystallographic data[15] are shown in black. Top: sideview, bottom: topview.

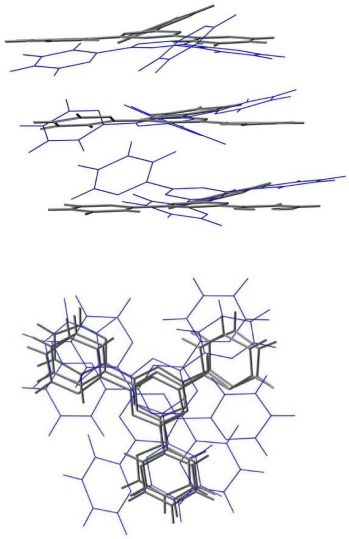

Figure 8. BLYP-D3/def2-TZVP optimized geometries (blue) of compound 1d. For comparison the initial geometries taken from crystallographic data[15] are shown in black. Top: sideview, bottom: topview.

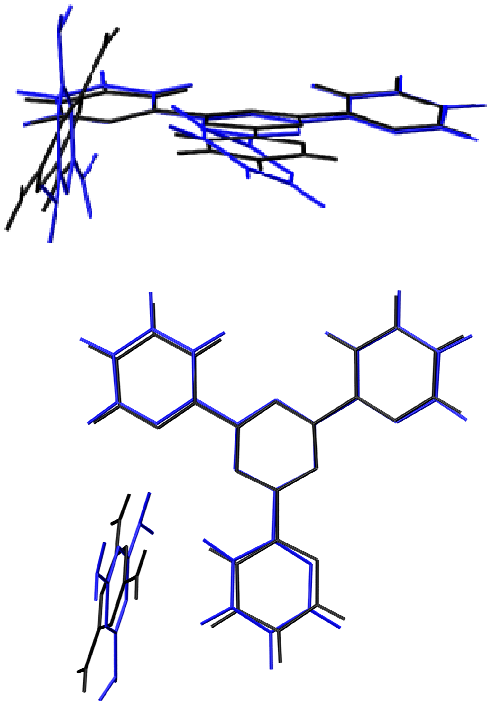

Figure 9. BLYP-D3/def2-TZVP optimized geometries (blue) of compound 1e. For comparison the initial geometries taken from crystallographic data[15] are shown in black. Top: sideview, bottom: topview.

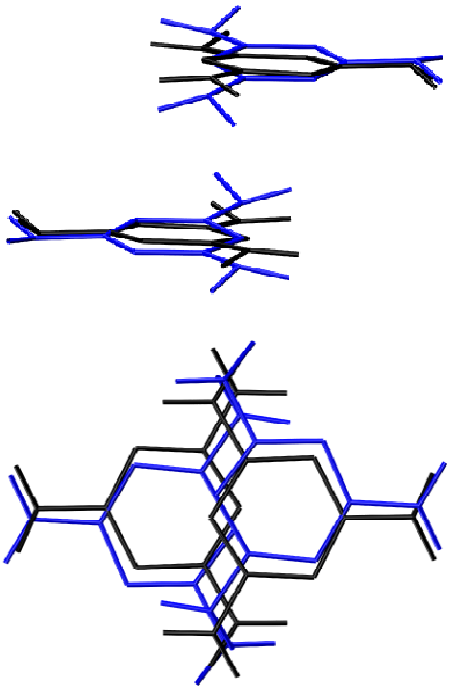

Figure 10. BLYP-D3/def2-TZVP optimized geometries (blue) of compound 4c. For comparison the initial geometries taken from crystallographic data[13] are shown in black. Top: sideview, bottom: topview.

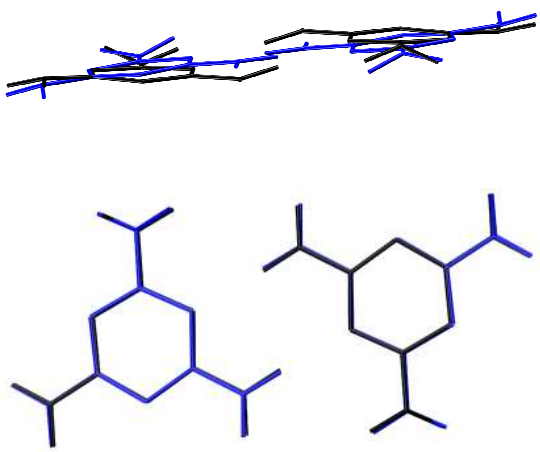

Figure 11. BLYP-D3/def2-TZVP optimized geometries (blue) of compound 4d. For comparison the initial geometries taken from crystallographic data[13] are shown in black. Top: sideview, bottom: topview.

Basis set effect

Figure 12 presents the optimized geometries of dimer 2a based on computations with BLYP-D3 and three basis sets of increasing size (def2-TZVP, def2-TZVPD and def2-QZVP). Increasing the size of the basis set during the optimization procedure shows only moderate basis set effects to the energy. The binding energy rises by 0.6 kcal·mol^{-1} going from def2-TZVP to def2-QZVP corresponding to 4% of the predicted total value of -15.0 kcal·mol^{-1} with BLYP-D3/def2-QZVP/BLYP-D3/def2-TZVP. The results confirm that using triple-ζ basis sets during the optimization leads to negligible deviations of the interaction energy.

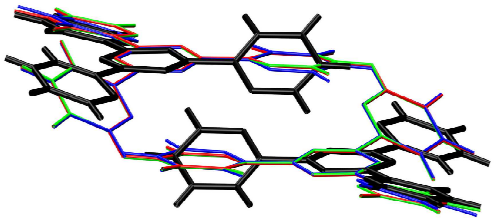

(a) sideview

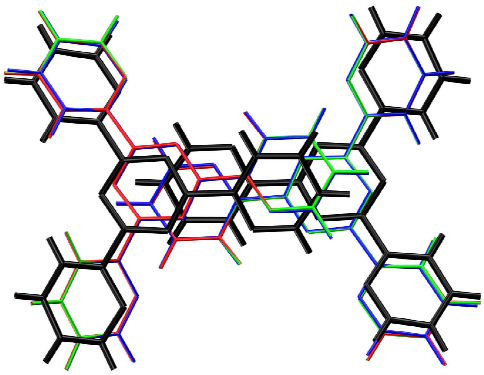

(b) topview

Figure 12. Overlay of geometries of dimer 2a resulting from geometry optimization with BLYP-D3 and def2-TZVP (green), def2-TZVPD (red) and def2-QZVP (blue) basis set. For comparison the starting geometry taken from crystallographic data[12] is shown in black.

Basis set superposition error

The basis set superposition error is large on the triple-ζ level. Applying the counterpoise correction to the PWPB95-D3/def2-TZVPP calculations raises the interaction energies of model systems 4a to 4d by 1.0 kcal·mol^{-1} on average which is about 11% of their average binding energy. For the 2tptz model systems 2a and 2b the counterpoise correction gives a contribution of +1.9 and +2.5 kcal·mol^{-1} to the complexation energy. The results for 3tptz show that the BSSE increases by 0.7 kcal·mol^{-1} per π-stacked pyridinyle moiety and reaches up to 2.5 kcal·mol^{-1} for model system 3a. It gives a nearly constant contribution of 14% to the binding energies computed with PWPB95-D3/def2-TZVP independent of the number of stacked pyridinyle moieties. In case of model systems 1a to 1f the basis set superposition error adds +2.7 kcal·mol^{-1} or 16% on average to the binding energy of the model systems. We find the largest percental contribution of BSSE to the total binding energy for the lower dimer 1b (24%). The largest absolute BSSE of +6.3 kcal·mol^{-1} is found for the trimer of 2tptz molecules. Compared to PWPB95-D3/def2-TZVPP the basis set superposition error for the (meta) GGA computations with quadruple-ζ basis sets is below 5% and is neglected.

Frozen monomer approximation

Compared to the frozen monomer based binding energies we find a contribution of 3% to 8% to E_{int}^{DFT-D} of the model systems of compound 1 if the deformation energy of the monomers is included. It is 1.7 kcal·mol^{-1} on average computed with BLYP-D3/def2-QZVP. Though the resulting error of the frozen monomer approximation is acceptable on a relative scale, the absolute values can contribute up to 3 kcal·mol^{-1} to the binding energy. The conformation of the relaxed and complexated monomers differs mainly in the rotational angles between the pyridinyle moieties and the triazine ring (cf. Figure 13). Their barrier of rotation is small and relaxation via reorientation of the pyridinyle moieties is easily possible. The deformation energy ranges from -0.2 to -1.2 kcal·mol^{-1} and is 0.8 kcal·mol^{-1} per 2tptz monomer on average computed with BLYP-D3/def2-QZVP. In the case of the model systems of melamine we find a similar picture. Computations based on relaxed monomer geometries (BLYP-D3/def2-QZVP//BLYP-D3/def2-TZVP) predict binding energies that are on average 1.3 kcal·mol^{-1} above the energies computed from frozen monomer geometries. Based on relaxed monomer geometries of model systems 2a and 2b we find interaction energies of -14.0 and -21.2 kcal·mol^{-1} with BLYP-D3/def2-QZVP. The computed binding energies rise by 1.0 and 1.4 kcal·mol^{-1} compared to results based on frozen monomer geometries. For the model systems of 3tptz the observed shift is only +0.1 kcal·mol^{-1}. The deformation energy of the monomers can decrease the binding energy of the model systems by >1 kcal·mol^{-1} and highly accurate computations must account for this contribution.

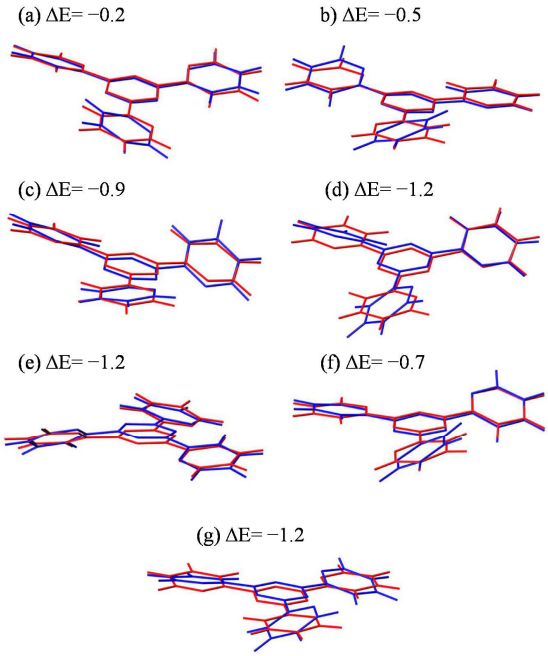

Figure 13. Overlay of 2tptz monomers with the geometry of the complexated state (blue) and their fully relaxed structure (red). (a)/(b) Monomers of model system 1a. (c)/(d) Monomers of model system 1b. (e)-(g) Monomers of model system 1d. The fully relaxed geometry of the complex as well as the monomers is obtained with BLYP-D3/def2-TZVP. The relative energies ($\Delta E = E^{relaxed} - E^{frozen}$) between both of the monomers' conformations are calculated with BLYP-D3/def2-QZVP (all values in kcal·mol^{-1}).

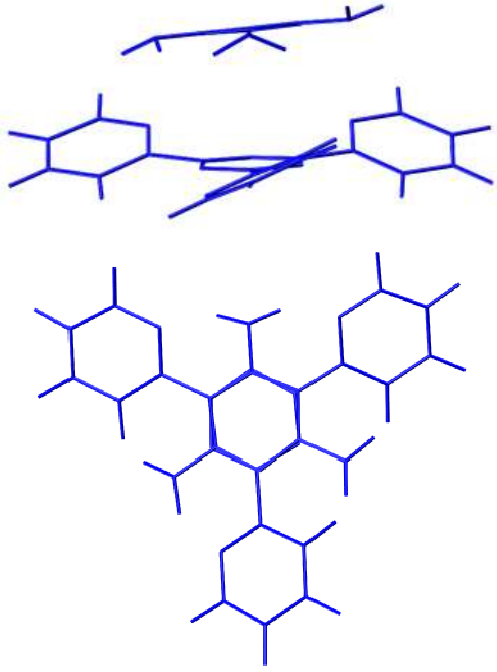

Figure 14. π-stacked model system 1f optimized with BLYP-D3/def2-TZVP. Top: sideview, bottom: topview.

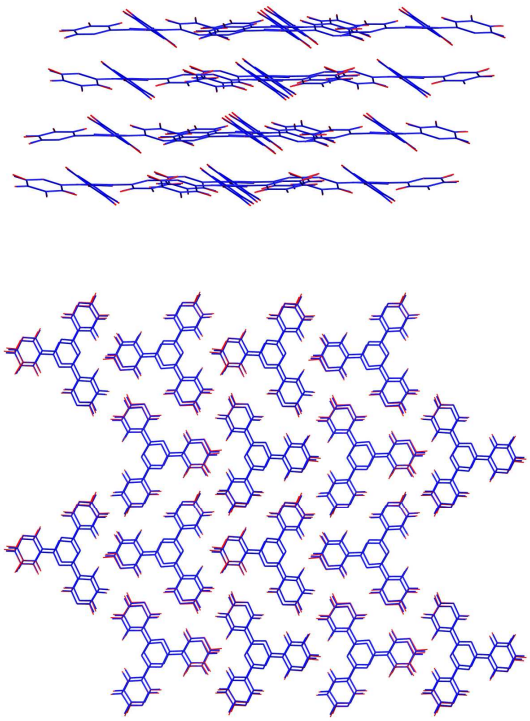

Figure 15. Overlay of crystal structures taken from crystallographic data[12,14] (blue) with fully relaxed structures computed with PBE-D3 using periodic boundary conditions (red). Top: 2tptz,[12] bottom: 3tptz.[14]

Listing 1. Fully relaxed XYZ coordinates of compounds 1a to 4d in atomic units. Based on optimization with BLYP-D3/def2-TZVP.

#1A				4.3432	5.7001	0.2148	n
0.0272	1.8268	-3.4837	n	-0.5775	-0.7373	3.8026	c
-0.4949	-2.6483	-3.2871	n	3.1176	-1.8027	1.8688	c
-3.6543	0.0884	-1.5710	n	2.1204	2.3335	2.4336	c
3.7526	-2.9491	-6.5210	n	2.6274	5.0876	2.0016	c
-2.9275	-6.6846	-0.9818	n	4.7594	8.1586	-0.2321	c
-4.9841	4.9523	-0.0314	n	6.1413	8.5869	-1.7039	h
-2.6875	-2.2228	-2.0722	c	3.5305	10.1161	1.0621	c
0.8069	-0.5602	-3.9338	c	3.9553	12.0807	0.6223	h
-2.2192	2.0487	-2.3072	c	1.7579	9.4713	2.9115	c
-3.0832	4.6808	-1.7136	c	0.7467	10.9279	3.9552	h
-1.8738	6.7584	-2.8539	c	1.2854	6.9215	3.3848	c
-0.3291	6.4303	-4.1643	h	-0.1030	6.3228	4.7727	h
-2.6733	9.1932	-2.2371	c	-3.0664	-1.4584	4.9335	c
-1.7641	10.8319	-3.0856	h	-5.1331	0.2035	4.7226	c
-4.6363	9.4860	-0.4944	c	-4.9289	1.9752	3.7053	h
-5.3168	11.3491	0.0524	h	-7.4521	-0.5450	5.7334	c
-5.7173	7.3064	0.5523	c	-9.0980	0.6800	5.5684	h
-7.2430	7.4614	1.9337	h	-7.6289	-2.8962	6.9242	c
3.3699	-0.8820	-5.0736	c	-9.3999	-3.5536	7.7411	h
5.2793	0.8778	-4.4997	c	-5.4621	-4.4178	7.0320	c
4.8950	2.4631	-3.2509	h	-5.5317	-6.2702	7.9387	h
7.7008	0.4449	-5.4547	c	4.7919	-3.7919	0.7685	c
9.2399	1.7267	-4.9847	h	3.7117	-6.0331	-0.1705	c
8.1165	-1.6744	-6.9726	c	1.6809	-6.3255	-0.0830	h
9.9767	-2.0856	-7.7510	h	5.3000	-7.7924	-1.3300	c
6.0789	-3.2986	-7.4587	c	4.5162	-9.5127	-2.1423	h
6.3352	-4.9692	-8.6429	h	7.8879	-7.2873	-1.4617	c
-4.1336	-4.4378	-1.0669	c	9.1933	-8.6084	-2.3489	h
-6.6146	-4.1062	-0.1668	c	8.7829	-5.0106	-0.4405	c
-7.4781	-2.2469	-0.2463	h	10.7957	-4.5585	-0.5045	h
-7.8811	-6.1796	0.8572	c	**#1B**			
-9.7951	-5.9730	1.5826	h	-0.7862	2.4364	-3.2560	n
-6.6373	-8.5063	0.9624	c	-2.2374	-1.7899	-2.6266	n
-7.5424	-10.1713	1.7634	h	-5.0252	1.6671	-1.9234	n
-4.1649	-8.6514	0.0211	c	4.0185	0.5900	-4.1733	n
-3.1271	-10.4336	0.0896	h	-6.2919	-5.0579	-1.9931	n
3.8028	0.6361	1.5779	n	-2.0871	7.4732	-4.0025	n
0.9448	-2.5845	2.9558	n	-4.4940	-0.8237	-2.0028	c
-0.0755	1.7537	3.5910	n	-0.4265	-0.0807	-3.1851	c

7.2876	-3.2707	0.6305	n	-3.1176	3.2109	-2.6184	c
-3.2237	-3.7440	6.0562	n	-3.6698	5.9901	-2.6636	c
-2.5575	9.9611	-4.0520	c	4.9868	5.3188	-0.1059	h
-1.2454	11.1045	-5.1617	h	2.6869	8.6437	0.6268	c
-4.5827	11.1015	-2.7813	c	3.8693	9.9340	-0.4545	h
-4.8627	13.1378	-2.8823	h	0.4974	9.5024	1.8289	c
-6.2191	9.5548	-1.3985	c	-0.0759	11.4752	1.7323	h
-7.8143	10.3572	-0.3753	h	-0.9903	7.7469	3.1380	c
-5.7672	6.9579	-1.3423	c	-2.7232	8.3492	4.0816	h
-6.9818	5.6792	-0.2928	h	7.9147	-2.3162	1.8727	c
-6.5855	-2.6136	-1.3289	c	8.4754	-4.9090	2.0930	c
-8.7436	-1.7258	-0.0499	c	6.9730	-6.2252	2.5683	h
-8.8859	0.2637	0.4345	h	10.9492	-5.7146	1.6613	c
-10.6506	-3.4386	0.5705	c	11.4350	-7.7088	1.8122	h
-12.3354	-2.8063	1.5696	h	12.7826	-3.9201	1.0268	c
-10.3562	-5.9733	-0.1140	c	14.7353	-4.4619	0.6686	h
-11.7973	-7.3751	0.3240	h	12.0452	-1.3793	0.8689	c
-8.1461	-6.6753	-1.3952	c	13.4263	0.0775	0.3875	h
-7.8511	-8.6362	-1.9662	h	**#1C**			
2.1644	-1.1002	-3.6969	c	1.4815	0.3799	2.2878	n
2.6010	-3.7241	-3.5928	c	3.1537	-3.8054	2.2909	n
1.0520	-4.9957	-3.1513	h	5.3764	-0.4644	0.2138	n
5.0490	-4.6156	-4.0078	c	-1.0071	-5.3946	5.0616	n
5.4492	-6.6306	-3.9028	h	6.6994	-7.1873	0.3949	n
6.9716	-2.8776	-4.5051	c	5.2867	4.4408	-1.6899	n
8.9154	-3.4847	-4.7969	h	5.0916	-2.9006	0.9169	c
6.3542	-0.3003	-4.5613	c	1.4010	-2.0872	2.9434	c
7.8169	1.1125	-4.9036	h	3.5090	1.0997	0.9271	c
3.4924	-3.2088	2.6796	n	3.6467	3.8229	0.1641	c
0.4245	0.0877	2.7792	n	2.0853	5.6184	1.3526	c
4.7689	1.0698	2.0750	n	0.7798	5.0160	2.8169	h
9.6792	-0.5732	1.2764	n	2.2290	8.1368	0.5912	c
-0.4590	-6.6841	2.7539	n	1.0180	9.5566	1.4563	h
-0.4326	5.2805	3.3064	n	3.9114	8.7855	-1.3365	c
1.1087	-2.3635	2.9109	c	4.0677	10.7215	-2.0145	h
5.2524	-1.4169	2.2414	c	5.3895	6.8681	-2.4093	c
2.3251	1.7293	2.3723	c	6.7160	7.3040	-3.9293	h
-0.9584	-4.2483	3.3269	c	-0.8029	-2.9089	4.5251	c
-3.3066	-3.4451	4.2846	c	-2.5581	-1.1102	5.4026	c
-3.6100	-1.4516	4.6730	h	-2.3407	0.8624	4.8832	h
-5.1904	-5.2439	4.6947	c	-4.5755	-1.9158	6.8974	c
-7.0267	-4.6802	5.4293	h	-5.9736	-0.5649	7.5673	h
-4.6878	-7.7674	4.1047	c	-4.7870	-4.4839	7.4651	c
-6.1076	-9.2315	4.3727	h	-6.3403	-5.2038	8.6053	h
-2.3030	-8.3790	3.1264	c	-2.9577	-6.1370	6.4922	c
-1.8573	-10.3281	2.6149	h	-3.0746	-8.1619	6.8766	h

1.7066	4.4771	2.1698	c	7.1230	-4.6929	0.0788	c
3.3196	6.0915	0.8069	c	9.3551	-3.7431	-1.0200	c
9.5795	-1.7160	-1.2544	h	6.6263	-0.3058	1.7492	n
11.2120	-5.4470	-1.7981	c	0.8427	-0.8441	9.1808	n
12.9610	-4.7672	-2.6442	h	4.5262	-6.7391	2.7912	n
10.7837	-8.0347	-1.4748	c	8.3590	3.8464	-0.9707	n
12.1777	-9.4331	-2.0545	h	5.4696	-2.2330	2.9638	c
8.4959	-8.7976	-0.3750	c	3.2738	0.4479	5.4989	c
8.0892	-10.8024	-0.0991	h	5.9954	2.0199	2.5441	c
-3.2436	-1.5474	-1.8132	n	7.0574	4.2686	1.1846	c
-1.6675	2.4584	-3.1266	n	6.5956	6.7169	2.1195	c
-5.2734	2.2247	-0.4268	n	5.5026	6.9455	3.8402	h
-8.8613	-0.7075	2.0446	n	7.5121	8.7893	0.7733	c
0.8868	-3.8586	-3.9792	n	7.1638	10.7016	1.4466	h
-2.5096	7.6283	-3.5805	n	8.8531	8.3638	-1.4619	c
-1.5508	-0.0879	-3.0208	c	9.5931	9.9222	-2.5831	h
-5.0691	-0.3082	-0.5476	c	9.2209	5.8602	-2.2434	c
-3.5548	3.5129	-1.7990	c	10.2526	5.4554	-3.9848	h
0.6637	-1.3300	-4.2649	c	1.2203	0.9225	7.3787	c
2.4639	0.1385	-5.5591	c	-0.3021	3.0880	7.1105	c
2.2107	2.1691	-5.6959	h	0.0146	4.3916	5.5548	h
4.5829	-1.0636	-6.5699	c	-2.3053	3.4203	8.7934	c
6.0318	0.0318	-7.5347	h	-3.5574	5.0423	8.6009	h
4.8303	-3.6739	-6.2722	c	-2.7017	1.6191	10.6820	c
6.4685	-4.6850	-6.9973	h	-4.2467	1.7999	12.0298	h
2.9267	-4.9813	-4.9677	c	-1.0723	-0.4693	10.7950	c
3.0726	-7.0162	-4.6671	h	-1.3296	-1.9152	12.2450	h
-3.7601	6.3390	-1.7702	c	6.0087	-4.8307	1.9738	c
-5.1946	7.5415	0.1223	c	7.9402	-5.1831	0.1765	c
-6.1994	6.4013	1.5037	h	9.0561	-3.5736	-0.4342	h
-5.2891	10.1779	0.1593	c	8.3289	-7.5945	-0.8153	c
-6.3664	11.1609	1.6115	h	9.7923	-7.9135	-2.2255	h
-3.9843	11.5258	-1.7027	c	6.7883	-9.5738	0.0103	c
-4.0086	13.5828	-1.7515	h	7.0089	-11.4830	-0.7247	h
-2.6460	10.1568	-3.5348	c	4.9238	-9.0408	1.8161	c
-1.6247	11.1437	-5.0326	h	3.6825	-10.5400	2.5032	h
-6.9644	-1.9047	0.8264	c	-0.8550	1.6535	1.0670	n
-6.7021	-4.5535	0.8203	c	0.5878	-2.2464	-0.6824	n
-5.1151	-5.4077	-0.1622	h	2.0485	1.6529	-2.3845	n
-8.4809	-6.0045	2.1168	c	-4.0980	-1.0574	4.1726	n
-8.3141	-8.0547	2.1596	h	3.0347	-4.6438	-4.7251	n
-10.4558	-4.7799	3.3726	c	0.0440	6.8446	1.5117	n
-11.8863	-5.8355	4.4088	h	2.0040	-0.8954	-2.2909	c
-10.5528	-2.1339	3.2774	c	-0.8119	-0.8922	0.9685	c
-12.0653	-1.1121	4.2417	h	0.5910	2.8283	-0.6584	c
#1D				0.6669	5.6549	-0.6557	c

4.3473	2.4970	4.4236	n	0.1616	9.3738	1.5448	c
3.7981	-1.9599	4.8611	n	-0.3424	10.2772	3.3299	h
0.8717	10.8387	-0.5426	c	-7.0349	7.4242	4.6874	h
0.9202	12.8911	-0.4045	h	-6.3078	9.1614	1.0504	c
1.4958	9.5960	-2.7886	c	-6.3848	11.1032	1.7279	h
2.0450	10.6585	-4.4629	h	-5.7861	8.6593	-1.4963	c
1.4050	6.9636	-2.8486	c	-5.4466	10.2084	-2.8164	h
1.8915	5.9069	-4.5386	h	-8.3096	-4.5242	-0.3138	c
3.7254	-2.2872	-4.0453	c	-7.6643	-7.0379	-0.9081	c
5.9834	-1.1409	-4.8573	c	-6.2808	-7.3992	-2.3816	h
6.4929	0.7229	-4.1624	h	-8.8180	-8.9936	0.4324	c
7.5754	-2.5060	-6.4573	c	-8.3429	-10.9545	0.0262	h
9.3569	-1.6917	-7.0904	h	-10.5839	-8.3892	2.3028	c
6.8570	-4.9363	-7.2058	c	-11.5327	-9.8523	3.3959	h
8.0375	-6.0640	-8.4590	h	-11.1183	-5.8322	2.7413	c
4.5723	-5.9118	-6.2855	c	-12.4971	-5.2879	4.1782	h
3.9501	-7.8038	-6.8248	h	**#1E**			
-2.3443	-2.3467	2.8363	c	4.2483	-2.6175	-0.4429	n
-1.9067	-4.9476	3.1591	c	0.9630	0.4781	-0.2619	n
-0.4253	-5.8705	2.0844	h	5.2722	1.7682	-0.1571	n
-3.3627	-6.2588	4.9243	c	0.4514	-6.1557	-1.6230	n
-3.0580	-8.2703	5.2291	h	-0.5151	5.4653	-0.3218	n
-5.2004	-4.9465	6.2871	c	9.3419	-3.7259	-0.8030	n
-6.3935	-5.8967	7.6673	h	2.7726	2.2519	-0.1504	c
-5.4887	-2.3500	5.8388	c	1.7981	-1.9326	-0.4094	c
-6.9138	-1.2675	6.8627	h	5.9115	-0.7023	-0.3049	c
-5.5837	-3.0140	-3.6731	n	8.6804	-1.3183	-0.2813	c
-4.4359	1.3324	-3.9650	n	11.8041	-4.3109	-0.7751	c
-7.3113	-0.0332	-0.7691	n	12.2701	-6.2725	-1.2167	h
-10.0158	-3.9284	1.4870	n	13.7244	-2.5689	-0.2213	c
-2.7853	-3.9857	-7.9898	n	15.6956	-3.1587	-0.2173	h
-5.6498	6.3216	-2.4682	n	13.0317	-0.0778	0.3184	c
-4.3422	-1.0868	-4.7685	c	14.4566	1.3397	0.7614	h
-7.0253	-2.3925	-1.6681	c	10.4733	0.5675	0.2818	c
-5.9485	1.7564	-1.9620	c	9.8474	2.4809	0.6820	h
-2.6537	-1.6500	-6.9714	c	1.9668	4.9661	0.0058	c
-0.9726	0.2111	-7.8593	c	3.7427	6.8854	0.4870	c
-0.9562	2.0604	-6.9721	h	5.7217	6.3950	0.7210	h
0.6749	-0.3999	-9.8256	c	2.9086	9.3838	0.6526	c
2.0300	0.9863	-10.5152	h	4.2449	10.9024	1.0311	h
0.5699	-2.8241	-10.8657	c	0.3380	9.8986	0.3268	c
1.8315	-3.3931	-12.3881	h	-0.3945	11.8171	0.4426	h
-1.2094	-4.5299	-9.8921	c	-1.2934	7.8709	-0.1639	c
-1.3607	-6.4337	-10.6759	h	-3.3128	8.1811	-0.4459	h
-6.0746	4.3656	-0.8860	c	-0.1804	-3.9493	-0.5068	c
-6.5720	4.6725	1.7083	c	-2.5819	-3.4822	0.5334	c

-6.7770	3.0106	2.8943	h	-2.9955	-1.6709	1.4038	h
-6.6818	7.1181	2.6829	c	-4.4118	-5.3796	0.4010	c
-6.2910	-5.0671	1.1774	h	-4.7959	7.6900	2.4815	c
-3.7819	-7.6615	-0.7700	c	-6.7343	8.0566	3.0885	h
-5.1517	-9.1879	-0.9371	h	-3.6635	-4.1972	1.5994	c
-1.3330	-7.9494	-1.7471	c	-6.1747	-3.7576	2.3517	c
-0.7818	-9.7058	-2.6805	h	-6.6885	-1.9284	3.1320	h
-10.2619	-1.5970	1.6985	n	-7.9451	-5.6917	2.0560	c
-8.4622	-0.2946	-2.2764	n	-9.8994	-5.4137	2.6387	h
-6.7360	1.2874	1.6316	n	-7.1641	-7.9814	0.9939	c
-11.7920	-3.1353	-2.1083	n	-8.4805	-9.5374	0.7155	h
-11.9849	-2.8534	-3.9915	h	-4.6275	-8.2321	0.2726	c
-13.3131	-3.7529	-1.1250	h	-3.9562	-9.9791	-0.5950	h
-5.0022	2.3924	-2.2370	n	-0.6743	2.7058	-4.5082	n
-3.4329	3.0791	-1.3261	h	-1.7599	-1.6781	-3.9583	n
-4.8433	1.9673	-4.0965	h	2.6105	-0.4265	-4.1636	n
-8.6094	0.0758	5.3954	n	-4.8569	1.4032	-4.2728	n
-7.1152	0.8776	6.2800	h	-6.0392	0.0947	-3.5238	h
-9.6573	-1.2189	6.3349	h	-5.2700	3.2402	-3.9192	h
-6.7806	1.0920	-0.9243	c	1.4652	-4.5987	-3.3735	n
-10.1247	-1.5899	-0.8545	c	3.2057	-4.7535	-2.5549	h
-8.5248	-0.0870	2.8104	c	0.1105	-5.6525	-2.4872	h
#1F				3.5596	3.8242	-4.6594	n
0.7241	-2.8163	1.9581	n	5.3411	3.2526	-5.0672	h
-2.6042	0.2408	1.9098	n	2.9729	5.4961	-5.3850	h
1.6883	1.5906	1.9740	n	0.7520	-2.1702	-3.8679	c
-2.8975	-6.4044	0.5698	n	-2.3381	0.7826	-4.2496	c
-4.0357	5.2742	2.5930	n	1.7631	1.9502	-4.4772	c
5.8316	-3.6392	0.7899	n	**#2A**			
-0.8206	2.0482	1.9614	c	-1.9640	4.5321	-2.5280	n
-1.7304	-2.1512	1.8591	c	-2.7205	2.0943	-2.5507	c
2.3563	-0.8664	1.9577	c	-3.0230	0.7022	-4.6657	n
5.1256	-1.4415	1.8812	c	-2.5578	1.9309	-6.8336	c
8.3090	-4.1629	0.6800	c	-1.8608	4.3754	-7.0232	n
8.8177	-5.9354	-0.2450	h	-1.5473	5.5824	-4.7943	c
10.1887	-2.5773	1.6632	c	-3.1603	0.8718	-0.0395	c
12.1707	-3.1139	1.5364	h	-4.1736	-1.4730	-0.0387	n
9.4471	-0.3057	2.7900	c	-4.4852	-2.6151	2.1972	c
10.8440	0.9836	3.5786	h	-5.2771	-4.5193	2.1371	h
6.8776	0.2864	2.8845	c	-3.8209	-1.5113	4.5165	c
6.2076	2.0422	3.7127	h	-4.0796	-2.5529	6.2721	h
-1.6416	4.7529	1.8805	c	-2.7725	0.9122	4.5033	c
0.0483	6.6193	1.0221	c	-2.1355	1.8093	6.2405	h
1.9375	6.0788	0.4278	h	-2.4378	2.1336	2.1881	c
-0.7842	9.1181	0.8991	c	-1.5719	3.9901	2.0738	h
0.4700	10.6019	0.2199	h	-2.7737	0.4841	-9.2596	c

-3.2564	9.6779	1.6467	c	-2.0739	-1.9677	-9.2086	n
-3.9858	11.6009	1.5821	h	-2.2480	-3.2872	-11.3677	c
-1.6407	-5.2567	-11.2723	h	-1.8013	-12.4246	1.0155	h
-3.1404	-2.2674	-13.6433	c	-1.1009	-13.1605	4.9878	c
-3.2610	-3.4385	-15.3305	h	-1.8067	-15.0922	4.9266	h
-3.8527	0.2772	-13.6832	c	-0.1929	-12.0979	7.2295	c
-4.5530	1.1476	-15.4116	h	-0.1665	-13.1865	8.9760	h
-3.6460	1.6878	-11.4629	c	0.6778	-9.6075	7.1948	c
-4.1512	3.6780	-11.4042	h	1.3784	-8.6911	8.8928	h
-0.6315	8.2628	-4.8985	c	**#2B**			
0.2428	9.2809	-2.7284	n	-4.2714	-2.1124	1.4178	n
1.0902	11.6668	-2.7985	c	-5.8949	-0.2692	0.7329	c
1.8013	12.4246	-1.0155	h	-5.5638	2.2132	1.1551	n
1.1009	13.1605	-4.9878	c	-3.3395	2.8227	2.2341	c
1.8067	15.0922	-4.9266	h	-1.5699	1.1371	2.9525	n
0.1929	12.0979	-7.2295	c	-2.1431	-1.3161	2.5600	c
0.1665	13.1865	-8.9760	h	-8.2173	-1.1024	-0.6565	c
-0.6778	9.6075	-7.1948	c	-9.2843	0.5662	-2.2671	n
-1.3784	8.6911	-8.8928	h	-11.3593	-0.1742	-3.5225	c
1.9640	-4.5321	2.5280	n	-12.1670	1.2062	-4.8265	h
2.7205	-2.0943	2.5507	c	-12.4793	-2.5575	-3.2349	c
3.0230	-0.7022	4.6657	n	-14.1772	-3.0416	-4.2911	h
2.5578	-1.9309	6.8336	c	-11.3540	-4.2800	-1.5768	c
1.8608	-4.3754	7.0232	n	-12.1564	-6.1552	-1.3028	h
1.5473	-5.5824	4.7943	c	-9.1757	-3.5548	-0.2769	c
3.1603	-0.8718	0.0395	c	-8.2060	-4.8303	1.0082	h
4.1736	1.4730	0.0387	n	-2.7153	5.5606	2.5794	c
4.4852	2.6151	-2.1972	c	-4.6645	7.2054	2.6575	n
5.2771	4.5193	-2.1371	h	-4.1164	9.6647	2.9118	c
3.8209	1.5113	-4.5165	c	-5.7318	10.9470	2.9934	h
4.0796	2.5529	-6.2721	h	-1.6451	10.6117	3.0642	c
2.7725	-0.9122	-4.5033	c	-1.3186	12.6352	3.2477	h
2.1355	-1.8093	-6.2405	h	0.3617	8.8978	2.9669	c
2.4378	-2.1336	-2.1881	c	2.3121	9.5473	3.0473	h
1.5719	-3.9901	-2.0738	h	-0.1729	6.3257	2.7376	c
2.7737	-0.4841	9.2596	c	1.3310	4.9355	2.6139	h
2.0739	1.9677	9.2086	n	-0.2337	-3.2429	3.3571	c
2.2480	3.2872	11.3677	c	-0.9761	-5.6877	3.3826	n
1.6407	5.2567	11.2723	h	0.7687	-7.4344	3.9413	c
3.1404	2.2674	13.6433	c	0.1136	-9.3911	3.9553	h
3.2610	3.4385	15.3305	h	3.3131	-6.8713	4.4293	c
3.8527	-0.2772	13.6832	c	4.6633	-8.3846	4.7725	h
4.5530	-1.1476	15.4116	h	4.0662	-4.3420	4.4218	c
3.6460	-1.6878	11.4629	c	6.0314	-3.8034	4.6938	h
4.1512	-3.6780	11.4042	h	2.2502	-2.4929	3.9294	c
0.6315	-8.2628	4.8985	c	2.7443	-0.5018	3.8901	h

-0.2428	-9.2809	2.7284	n	4.2714	2.1124	-1.4178	n
-1.0902	-11.6668	2.7985	c	5.8949	0.2692	-0.7329	c
5.5638	-2.2132	-1.1551	n	4.7174	-9.0685	-2.1976	n
3.3395	-2.8227	-2.2341	c	-7.9990	0.3059	-5.1667	c
1.5699	-1.1371	-2.9525	n	-10.0065	0.4566	-5.6119	h
2.1431	1.3161	-2.5600	c	3.5679	-6.8233	-2.4613	c
8.2173	1.1024	0.6565	c	1.5662	-6.8643	-2.9307	h
9.2843	-0.5662	2.2671	n	3.5357	7.0308	-2.4500	c
11.3593	0.1742	3.5225	c	1.5365	7.0634	-2.9319	h
12.1670	-1.2062	4.8265	h	-4.2845	-2.1754	-4.3295	c
12.4793	2.5575	3.2349	c	-3.3113	-3.9702	-4.1086	h
14.1772	3.0416	4.2911	h	4.6747	9.2803	-2.1795	n
11.3540	4.2800	1.5768	c	-4.2974	2.3817	-4.2501	c
12.1564	6.1552	1.3028	h	-3.3273	4.1732	-3.9667	h
9.1757	3.5548	0.2769	c	7.3549	4.7437	-1.4789	c
8.2060	4.8303	-1.0082	h	8.3685	2.9768	-1.2153	h
2.7153	-5.5606	-2.5794	c	-0.2223	0.0988	-3.3284	c
4.6645	-7.2054	-2.6575	n	7.3789	-4.5195	-1.5034	c
4.1164	-9.6647	-2.9118	c	8.3849	-2.7484	-1.2383	h
5.7318	-10.9470	-2.9934	h	8.5887	-6.8417	-1.2187	c
1.6451	-10.6117	-3.0642	c	10.5840	-6.9446	-0.7274	h
1.3186	-12.6352	-3.2477	h	8.5530	7.0710	-1.1875	c
-0.3617	-8.8978	-2.9669	c	10.5463	7.1827	-0.6905	h
-2.3121	-9.5473	-3.0473	h	7.1415	9.2800	-1.5576	c
0.1729	-6.3257	-2.7376	c	8.0232	11.1336	-1.3478	h
-1.3310	-4.9355	-2.6139	h	7.1868	-9.0571	-1.5859	c
0.2337	3.2429	-3.3571	c	8.0780	-10.9064	-1.3795	h
0.9761	5.6877	-3.3826	n	0.1367	-4.4910	3.2099	c
-0.7687	7.4344	-3.9413	c	0.0568	4.6893	3.1967	c
-0.1136	9.3911	-3.9553	h	-3.7416	-2.1865	2.3910	n
-3.3131	6.8713	-4.4293	c	0.0682	0.0993	3.1367	n
-4.6633	8.3846	-4.7725	h	-3.7830	2.3165	2.3810	n
-4.0662	4.3420	-4.4218	c	-1.2859	2.2492	2.8847	c
-6.0314	3.8034	-4.6938	h	-1.2469	-2.0725	2.8939	c
-2.2502	2.4929	-3.9294	c	-7.6711	0.0167	1.5481	c
-2.7443	0.5018	-3.8901	h	-11.5767	-2.2176	0.8174	c
#3A				-12.6744	-3.9531	0.6946	h
4.7984	-4.4796	-2.1394	c	-11.4858	2.3447	0.5024	n
4.7769	4.6928	-2.1234	c	0.0694	-9.0796	3.0186	n
0.9440	-2.1533	-3.0539	n	-12.7280	0.1274	0.3846	c
4.7250	0.1052	-2.1102	n	-14.7365	0.2378	-0.0757	h
0.9361	2.3524	-3.0424	n	-1.0660	-6.8277	2.7575	c
3.4085	2.2640	-2.4398	c	-3.0324	-6.8512	2.1531	h
3.4169	-2.0559	-2.4492	c	-1.1802	7.0071	2.7355	c
-2.9485	0.0964	-3.9797	c	-3.1450	7.0029	2.1247	h
-6.8453	-2.0651	-4.9333	c	-9.0113	-2.2744	1.4083	c

-7.9430	-3.7829	-5.2033	h	-8.0292	-4.0449	1.7533	h
-6.7626	2.5043	-4.8307	n	-0.0746	9.2743	2.9948	n
-9.0142	2.2706	1.0688	c	**#4B**			
-8.0291	4.0745	1.1284	h	6.0052	1.0783	0.0354	c
2.5990	4.7813	3.9673	c	6.2057	5.3444	0.0466	c
3.6175	3.0320	4.3161	h	2.3812	3.4012	0.0451	c
-4.9307	0.0547	2.1369	c	7.2031	-1.2276	0.0971	n
2.6812	-4.5452	3.9747	c	7.6121	7.5129	-0.0211	n
3.6754	-2.7812	4.3199	h	-0.1710	3.5307	0.0420	n
3.8770	-6.8744	4.2583	c	3.6748	5.6099	0.0586	n
5.8483	-6.9887	4.8325	h	3.4548	1.0627	0.0389	n
3.7613	7.1267	4.2495	c	7.4998	3.1380	0.0362	n
5.7298	7.2698	4.8267	h	6.1911	-2.7588	-0.4426	h
2.3578	9.3122	3.7400	c	9.0702	-1.2194	-0.3272	h
3.2210	11.1759	3.9192	h	9.4881	7.3770	0.3207	h
2.5042	-9.0810	3.7580	c	6.7185	9.1687	0.3192	h
3.3938	-10.9317	3.9417	h	-0.9493	5.2752	-0.0325	h
#4A				-1.2884	1.9317	-0.0054	h
-2.7512	0.8236	-1.2610	c	-6.2107	-5.3399	-0.0946	c
-3.5785	-2.9375	0.5879	c	-2.3836	-3.4133	0.1109	c
-3.6101	0.6286	2.9197	c	-5.9916	-1.0748	-0.1092	c
-2.1059	2.1978	-3.3559	n	-7.6325	-7.4996	-0.0935	n
-3.6996	-5.5376	0.4439	n	0.1638	-3.5517	0.2709	n
-3.7698	1.8013	5.2419	n	-7.1739	1.2340	-0.2610	n
-3.9128	-1.9018	2.8922	n	-3.4455	-1.0710	0.0358	n
-3.0636	2.1087	0.9251	n	-7.4929	-3.1280	-0.1786	n
-3.0341	-1.6974	-1.5641	n	-3.6845	-5.6165	0.0428	n
-1.3415	3.9228	-3.0147	h	-9.4835	-7.3503	-0.5492	h
-1.3199	1.2005	-4.7924	h	-6.7338	-9.1638	-0.3745	h
-4.0008	-6.2676	-1.3023	h	0.9351	-5.2983	0.3629	h
-4.5512	-6.4206	1.9162	h	1.2898	-1.9592	0.2644	h
-4.6244	0.7989	6.6336	h	-6.1889	2.7699	0.3132	h
-4.0812	3.6918	5.2096	h	-9.0633	1.2376	0.0487	h
4.1416	1.7706	-2.6945	c	**#4C**			
3.0221	-1.9525	-0.9176	c	-2.8645	-2.7409	-2.0872	c
3.0120	1.6292	1.4257	c	-2.5680	1.4778	-1.4681	c
4.7970	3.1528	-4.8032	n	-5.3522	-0.8270	0.8118	c
2.6610	-4.5093	-1.1032	n	-1.9978	-4.9140	-3.2324	n
2.6386	2.8222	3.6932	n	-1.4564	3.7476	-2.0262	n
2.6016	-0.8849	1.3578	n	-7.2476	-0.9553	2.5660	n
3.7897	3.0768	-0.5359	n	-4.3830	1.4766	0.3241	n
3.7993	-0.7314	-3.0280	n	-4.6463	-3.0295	-0.2839	n
5.5256	4.8945	-4.4775	h	-1.7704	-0.5585	-2.7948	n
5.5245	2.1601	-6.2715	h	-3.1444	-6.4451	-3.1326	h
2.4772	-5.1856	-2.8861	h	-0.9907	-4.6691	-4.8437	h
1.5156	-5.2908	0.2235	h	0.2377	3.6382	-2.9184	h

1.4980	1.9115	4.9387	h	-1.5773	5.0817	-0.6530	h
2.4406	4.7253	3.5988	h	-7.7693	-2.6797	3.2057	h
-7.5625	0.5831	3.6567	h	0.0130	2.3328	-0.1696	h
2.8645	2.7409	2.0872	c	6.8410	-6.0772	-0.4425	h
2.5680	-1.4778	1.4681	c	3.5961	-5.7409	-0.6174	h
5.3522	0.8270	-0.8118	c				
1.9978	4.9140	3.2324	n				
1.4564	-3.7476	2.0262	n				
7.2476	0.9553	-2.5660	n				
4.3830	-1.4766	-0.3241	n				
4.6463	3.0295	0.2839	n				
1.7704	0.5585	2.7948	n				
3.1444	6.4451	3.1326	h				
0.9907	4.6691	4.8437	h				
-0.2377	-3.6382	2.9184	h				
1.5773	-5.0817	0.6530	h				
7.7693	2.6797	-3.2057	h				
7.5625	-0.5831	-3.6567	h				
#4D							
-8.1333	-0.9698	0.1096	c				
-3.8768	-1.4977	0.1783	c				
-5.5814	2.4549	0.1265	c				
-10.5140	-1.9778	0.1416	n				
-1.8329	-3.0309	0.2399	n				
-5.2824	5.0358	0.0519	n				
-3.4589	1.0412	0.1610	n				
-7.9720	1.5835	0.0995	n				
-6.1839	-2.6051	0.1468	n				
-11.9844	-0.8154	-0.2361	h				
-10.6978	-3.8531	-0.1830	h				
-2.1598	-4.9141	0.2607	h				
-0.0130	-2.3328	0.1696	h				
-6.8410	6.0772	0.4425	h				
-3.5961	5.7409	0.6174	h				
8.1333	0.9698	-0.1096	c				
3.8768	1.4977	-0.1783	c				
5.5814	-2.4549	-0.1265	c				
10.5140	1.9778	-0.1416	n				
1.8329	3.0309	-0.2399	n				
5.2824	-5.0358	-0.0519	n				
3.4589	-1.0412	-0.1610	n				
7.9720	-1.5835	-0.0995	n				
6.1839	2.6051	-0.1468	n				
11.9844	0.8154	0.2361	h				
10.6978	3.8531	0.1830	h				
2.1598	4.9141	-0.2607	h				

Listing 2. XYZ coordinates of compounds 1a to 4d in atomic units. Based on optimization with BLYP-D3/def2-TZVP and fixed positions of heavy atoms.

#1A				1.4395	-1.4790	2.9603	c
-1.2242	1.3395	-2.9594	n	5.4936	-1.1874	1.7076	c
-3.0998	-2.6966	-2.5038	n	3.1980	2.3310	2.3280	c
-5.4665	1.0190	-1.6226	n	2.9626	5.1302	2.3041	c
1.4137	-4.8847	-3.7522	n	4.6570	8.9039	1.1478	c
-7.4982	-5.4089	-2.0124	n	6.1985	9.8942	0.1911	h
-5.7233	6.1886	-1.3211	n	2.7271	10.2271	2.2243	c
-5.2084	-1.4838	-1.8161	c	2.7158	12.2857	2.1551	h
-1.1553	-1.1771	-3.0358	c	0.8305	8.9178	3.3695	c
-3.4168	2.3425	-2.2352	c	-0.7609	9.9037	4.2283	h
-3.5543	5.1589	-2.1533	c	0.9166	6.3317	3.3946	c
-1.5311	6.6003	-2.9422	c	-0.5767	5.2166	4.2573	h
0.1939	5.6774	-3.5631	h	-0.8355	-3.0058	3.6790	c
-1.7453	9.1870	-2.9223	c	-2.9476	-1.8005	4.6323	c
-0.1641	10.3539	-3.5368	h	-2.9618	0.2427	4.8201	h
-3.9371	10.2599	-2.0999	c	-5.0185	-3.2335	5.2954	c
-4.1838	12.3041	-2.0555	h	-6.7100	-2.3144	6.0274	h
-5.8666	8.6945	-1.3135	c	-4.9228	-5.7727	5.0034	c
-7.6446	9.4957	-0.6297	h	-6.5208	-6.9772	5.4883	h
1.2963	-2.3519	-3.7586	c	-2.7457	-6.8257	4.0427	c
3.3437	-0.8368	-4.3780	c	-2.6174	-8.8672	3.7585	h
3.1682	1.2059	-4.3052	h	7.8815	-2.4681	0.9712	c
5.6066	-1.9721	-5.0142	c	8.0366	-5.0651	1.0395	c
7.2572	-0.8237	-5.4482	h	6.4190	-6.1574	1.6787	h
5.7291	-4.5676	-5.0553	c	10.2256	-6.2144	0.2334	c
7.4765	-5.5419	-5.5398	h	10.3716	-8.2694	0.2460	h
3.6079	-5.9270	-4.4107	c	12.1700	-4.7596	-0.5971	c
3.6588	-7.9922	-4.3941	h	13.9313	-5.5940	-1.2645	h
-7.4698	-3.0412	-1.1828	c	11.8972	-2.1818	-0.5319	c
-9.4080	-2.0086	0.2051	c	13.4396	-0.9489	-1.1391	h
-9.2996	-0.0441	0.7969	h	**#1B**			
-11.4694	-3.4963	0.7851	c	-0.3718	1.5265	-3.3001	n
-13.0278	-2.7140	1.8825	h	-2.0038	-2.6228	-2.7646	n
-11.5078	-5.9332	-0.0187	c	-4.6556	0.9145	-2.1730	n
-13.0904	-7.1825	0.4028	h	4.2051	-0.5094	-4.5570	n
-9.5070	-6.7961	-1.3965	c	-6.1307	-5.7088	-1.9860	n
-9.4899	-8.7404	-2.0981	h	-1.2580	6.5422	-3.7570	n
5.4184	1.3335	1.6606	n	-4.2202	-1.5526	-2.2322	c
3.5553	-2.6955	2.3405	n	-0.1379	-0.9851	-3.2827	c
1.1642	1.0115	3.0001	n	-2.6806	2.3706	-2.7282	c
9.7911	-1.0070	0.2205	n	-3.0931	5.1494	-2.7267	c
-0.7157	-5.5009	3.3645	n	-1.5901	9.0409	-3.7496	c
4.8298	6.3892	1.1651	n	-0.0670	10.1418	-4.6091	h

-3.6497	10.2218	-2.7506	c	4.2511	10.9448	2.3232	h
-3.7838	12.2771	-2.7853	h	0.3893	10.2059	3.2490	c
-5.5110	8.7769	-1.7161	c	-0.1685	12.1853	3.3636	h
-7.1877	9.6494	-0.8954	h	-1.3415	8.3462	3.6839	c
-5.2611	6.2013	-1.7210	c	-3.2981	8.8403	4.1337	h
-6.6989	4.9804	-0.9095	h	7.4283	-1.5572	1.3915	c
-6.4246	-3.2316	-1.6448	c	7.9313	-4.1098	1.2868	c
-8.6523	-2.1778	-0.7794	c	6.4342	-5.4487	1.7136	h
-8.7879	-0.1442	-0.5419	h	10.3241	-4.8988	0.6156	c
-10.6566	-3.7494	-0.2365	c	10.7576	-6.9100	0.5164	h
-12.4298	-2.9531	0.4480	h	12.1149	-3.1277	0.0858	c
-10.3851	-6.2724	-0.5569	c	14.0307	-3.6644	-0.4489	h
-11.9173	-7.5867	-0.1478	h	11.4626	-0.6245	0.2199	c
-8.1019	-7.1700	-1.4246	c	12.8561	0.8403	-0.2066	h
-7.8231	-9.1979	-1.7071	h	**#1C**			
2.3592	-2.1003	-3.9192	c	5.5918	1.3414	3.8913	n
2.6765	-4.6830	-3.8777	c	7.1595	-2.7150	2.8407	n
1.1237	-5.8845	-3.2770	h	9.1315	0.9749	1.2038	n
4.9704	-5.6784	-4.5917	c	3.3070	-4.8538	5.5429	n
5.2533	-7.7190	-4.5756	h	11.1048	-5.4760	0.9026	n
6.8552	-4.0904	-5.3076	c	9.3287	6.1416	0.8200	n
8.7011	-4.7976	-5.8845	h	8.9262	-1.5251	1.4794	c
6.4154	-1.5364	-5.2218	c	5.5250	-1.1744	3.9929	c
7.9090	-0.1972	-5.7106	h	7.4229	2.3206	2.4679	c
3.1418	-2.4425	2.5816	n	7.5558	5.1353	2.3372	c
0.2480	0.8646	3.4122	n	5.9329	6.5984	3.7580	c
4.4477	1.8363	2.2053	n	4.5229	5.6903	4.9422	h
9.1652	0.2139	0.8644	n	6.1564	9.1825	3.6604	c
-0.7106	-5.8471	3.1459	n	4.9008	10.3702	4.7818	h
-0.8396	5.8965	3.5866	n	7.9545	10.2318	2.1447	c
0.8639	-1.5692	3.2221	c	8.1950	12.2729	2.0152	h
4.8572	-0.6510	2.0955	c	9.4886	8.6458	0.7580	c
2.1010	2.4862	2.8711	c	10.9398	9.4276	-0.4881	h
-1.1579	-3.4395	3.7574	c	3.4476	-2.3224	5.5027	c
-3.4225	-2.6480	4.8194	c	1.7455	-0.7852	6.7720	c
-3.6909	-0.6573	5.2492	h	1.9363	1.2551	6.6583	h
-5.2718	-4.4143	5.2976	c	-0.1829	-1.8958	8.1366	c
-7.0595	-3.8394	6.1426	h	-1.5556	-0.7330	9.1381	h
-4.8461	-6.8793	4.6432	c	-0.3130	-4.4898	8.2233	c
-6.2736	-8.3316	4.9454	h	-1.7902	-5.4490	9.2904	h
-2.5616	-7.4992	3.5699	c	1.4517	-5.8721	6.9051	c
-2.1724	-9.4476	3.0056	h	1.3817	-7.9369	6.9230	h
1.5289	5.2395	2.9998	c	10.8245	-3.1070	0.1251	c
3.3988	6.9909	2.5299	c	12.1928	-2.0945	-1.8375	c
5.2884	6.3485	2.0451	h	11.9144	-0.1285	-2.3662	h
2.8041	9.5238	2.6835	c	13.9216	-3.6046	-3.0745	c

15.0258	-2.8384	-4.6360	h	11.2151	-5.4566	0.7889	n
14.2018	-6.0428	-2.3244	c	9.4390	6.1610	0.7063	n
15.5332	-7.3105	-3.2535	h	9.0365	-1.5057	1.3657	c
12.7730	-6.8849	-0.3506	c	5.6353	-1.1550	3.8792	c
12.9708	-8.8303	0.3195	h	7.5332	2.3400	2.3542	c
-7.5392	-2.6442	-2.4508	n	7.6661	5.1547	2.2235	c
-5.3276	0.8231	-4.2081	n	6.0432	6.6178	3.6443	c
-8.7850	1.5537	-1.4602	n	4.6166	5.7136	4.8104	h
-12.5574	-0.3352	1.5206	n	6.2667	9.2019	3.5467	c
-4.0522	-5.8320	-4.5554	n	4.9969	10.3855	4.6542	h
-4.6068	5.9074	-4.6125	n	8.0648	10.2512	2.0310	c
-5.7188	-1.6424	-3.8807	c	8.3037	12.2927	1.8998	h
-9.0140	-0.9531	-1.2873	c	9.5989	8.6652	0.6443	c
-6.9011	2.3364	-2.9472	c	11.0509	9.4471	-0.6012	h
-3.9765	-3.3952	-5.2089	c	3.5579	-2.3031	5.3890	c
-2.3260	-2.4696	-7.0259	c	1.8558	-0.7658	6.6583	c
-2.3303	-0.4624	-7.4636	h	2.0168	1.2750	6.5227	h
-0.7257	-4.1285	-8.2322	c	-0.0726	-1.8764	8.0229	c
0.5672	-3.4490	-9.6844	h	-1.4713	-0.7102	8.9796	h
-0.7625	-6.6221	-7.5492	c	-0.2027	-4.4704	8.1096	c
0.4942	-7.9957	-8.4290	h	-1.6982	-5.4254	9.1533	h
-2.4345	-7.3776	-5.7084	c	1.5620	-5.8527	6.7914	c
-2.5032	-9.3549	-5.1139	h	1.4837	-7.9172	6.7953	h
-6.5406	5.1177	-3.1904	c	10.9348	-3.0877	0.0113	c
-8.1625	6.7607	-1.9845	c	12.3031	-2.0751	-1.9512	c
-9.7074	6.0148	-0.8541	h	12.0225	-0.1089	-2.4770	h
-7.7813	9.3234	-2.2668	c	14.0319	-3.5852	-3.1882	c
-9.0472	10.6613	-1.3441	h	15.1390	-2.8186	-4.7477	h
-5.7976	10.1404	-3.6860	c	14.3120	-6.0234	-2.4381	c
-5.4182	12.1484	-3.9448	h	15.6468	-7.2898	-3.3647	h
-4.2860	8.3814	-4.8103	c	12.8833	-6.8655	-0.4643	c
-2.6837	8.9845	-5.9704	h	13.0824	-8.8103	0.2073	h
-11.0793	-2.0041	0.3117	c	-2.1086	1.4354	1.6666	n
-11.3939	-4.5810	0.5134	c	-0.6282	-2.6135	0.4091	n
-10.1239	-5.8350	-0.5037	h	1.4414	1.0673	-1.0274	n
-13.3122	-5.5050	2.0183	c	-5.7656	-0.8576	4.5022	n
-13.5921	-7.5374	2.2015	h	3.0166	-5.4655	-1.9872	n
-14.8390	-3.8390	3.2501	c	-1.3318	6.4835	1.9217	n
-16.3799	-4.4837	4.4556	h	1.1683	-1.4200	-0.8907	c
-14.3958	-1.3032	2.9628	c	-2.2230	-1.0845	1.6542	c
-15.5834	0.0789	3.9365	h	-0.2322	2.4087	0.2873	c
#1D				0.0284	5.2050	0.2233	c
5.7021	1.3608	3.7776	n	-1.1355	8.9960	1.8732	c
7.2698	-2.6956	2.7269	n	-2.2610	10.0024	3.2847	h
9.2418	0.9943	1.0901	n	0.3331	10.2988	0.2058	c
3.4173	-4.8344	5.4291	n	0.3849	12.3576	0.2589	h

1.7182	8.9698	-1.5082	c	-5.3010	12.1675	-4.0504	h
2.9297	9.9387	-2.8633	h	-4.1757	8.4007	-4.9240	c
1.6002	6.3848	-1.4961	c	-2.5627	9.0035	-6.0679	h
2.6841	5.2531	-2.8222	h	-10.9690	-1.9847	0.1980	c
3.0509	-2.9714	-2.3302	c	-11.2836	-4.5616	0.3996	c
4.7313	-1.7887	-3.9426	c	-10.0074	-5.8130	-0.6113	h
4.6957	0.2539	-4.1330	h	-13.2019	-5.4857	1.9045	c
6.4416	-3.2442	-5.2612	c	-13.4776	-7.5182	2.0928	h
7.7982	-2.3429	-6.5223	h	-14.7287	-3.8197	3.1364	c
6.4220	-5.7824	-4.9475	c	-16.2703	-4.4648	4.3413	h
7.7528	-7.0039	-5.9364	h	-14.2855	-1.2838	2.8491	c
4.6845	-6.8121	-3.3065	c	-15.4720	0.0988	3.8235	h
4.6340	-8.8529	-2.9930	h	**#1E**			
-4.2370	-2.3392	3.1557	c	4.3209	-2.7185	-0.0629	n
-4.4346	-4.9342	3.1504	c	0.9472	0.2444	0.0126	n
-3.1679	-6.0394	1.9720	h	5.1733	1.6706	0.0056	n
-6.2364	-6.0598	4.6501	c	0.8619	-6.5502	-0.2242	n
-6.4136	-8.1122	4.6752	h	-0.6134	5.2097	-0.2541	n
-7.7710	-4.5843	6.0835	c	9.3184	-3.6317	-0.6484	n
-9.2266	-5.3963	7.2933	h	2.6971	2.0552	0.0178	c
-7.5077	-2.0096	5.9235	c	1.8715	-2.1170	-0.0249	c
-8.7592	-0.7590	6.9878	h	5.8889	-0.7407	-0.0443	c
-7.4289	-2.6248	-2.5645	n	8.6489	-1.2603	-0.1028	c
-5.2173	0.8425	-4.3219	n	11.7884	-4.1330	-0.6858	c
-8.6747	1.5731	-1.5740	n	12.2918	-6.0819	-1.1532	h
-12.4471	-0.3158	1.4069	n	13.6233	-2.3952	-0.1887	c
-3.9419	-5.8126	-4.6691	n	15.6087	-2.9429	-0.2302	h
-4.4965	5.9268	-4.7263	n	12.9132	0.0181	0.3540	c
-5.6085	-1.6230	-3.9944	c	14.3242	1.4648	0.7567	h
-8.9037	-0.9337	-1.4011	c	10.3967	0.6205	0.3734	c
-6.7908	2.3558	-3.0609	c	9.7538	2.5288	0.7798	h
-3.8662	-3.3758	-5.3227	c	1.8456	4.7566	0.0415	c
-2.2157	-2.4502	-7.1396	c	3.6050	6.6594	0.3672	c
-2.2143	-0.4416	-7.5697	h	5.5874	6.1787	0.5850	h
-0.6154	-4.1091	-8.3460	c	2.7886	9.1322	0.3968	c
0.6908	-3.4272	-9.7846	h	4.1488	10.6599	0.6470	h
-0.6522	-6.6027	-7.6630	c	0.2948	9.6254	0.1155	c
0.6168	-7.9717	-8.5308	h	-0.4396	11.5487	0.1326	h
-2.3242	-7.3582	-5.8221	c	-1.3346	7.6206	-0.1971	c
-2.3810	-9.3316	-5.2159	h	-3.3591	7.9482	-0.4406	h
-6.4303	5.1371	-3.3042	c	-0.0167	-4.1949	-0.0651	c
-8.0522	6.7801	-2.0982	c	-2.5584	-3.6414	0.0152	c
-9.5836	6.0318	-0.9522	h	-3.1784	-1.6940	0.1987	h
-7.6710	9.3428	-2.3805	c	-4.2738	-5.5892	-0.1470	c
-8.9306	10.6801	-1.4485	h	-6.2921	-5.1766	-0.1007	h
-5.6873	10.1598	-3.7997	c	-3.4152	-7.9971	-0.3727	c

-4.7103	-9.5921	-0.5272	h	0.3127	8.7487	-3.5076	n
-0.8537	-8.3997	-0.3589	c	1.1902	11.0906	-3.4996	c
-0.0909	-10.3154	-0.4855	h	1.9695	11.7309	-1.6937	h
-10.0081	-1.6269	1.4269	n	1.1709	12.7042	-5.5211	c
-9.2627	0.9117	-2.2447	n	1.9109	14.6159	-5.3395	h
-6.4077	1.0979	1.2232	n	0.2110	11.8123	-7.7417	c
-12.7233	-1.6441	-1.9822	n	0.1444	12.9993	-9.4242	h
-13.3241	-0.7975	-3.5867	h	-0.6761	9.3776	-7.8296	c
-13.9597	-2.6642	-0.9403	h	-1.4356	8.5951	-9.5709	h
-5.6932	3.3661	-2.3741	n	2.0997	-4.1664	3.5197	n
-3.8773	3.6110	-1.7413	h	2.8824	-1.7719	3.7148	c
-6.0570	3.5677	-4.2419	h	3.3169	-0.5149	5.8834	n
-7.1076	-1.3951	4.6576	n	2.8965	-1.8834	7.9911	c
-5.4351	-0.7756	5.3416	h	2.0132	-4.2572	8.0250	n
-8.0674	-2.7806	5.5557	h	1.6180	-5.2916	5.7579	c
-7.1560	1.7239	-1.0890	c	3.3633	-0.4342	1.2771	c
-10.6191	-0.7471	-0.8690	c	2.9473	2.0723	1.2967	n
-7.8639	-0.6173	2.3791	c	3.3460	3.2685	-0.9040	c
#2A				2.8694	5.2751	-0.9160	h
-2.0997	4.1664	-3.5197	n	4.2298	2.1421	-3.0493	c
-2.8824	1.7719	-3.7148	c	4.5318	3.2629	-4.7507	h
-3.3169	0.5149	-5.8834	n	4.6920	-0.4152	-3.0117	c
-2.8965	1.8834	-7.9911	c	5.3783	-1.4097	-4.6774	h
-2.0132	4.2572	-8.0250	n	4.1832	-1.7184	-0.8036	c
-1.6180	5.2916	-5.7579	c	4.4189	-3.7588	-0.7092	h
-3.3633	0.4342	-1.2771	c	3.4709	-0.6946	10.4610	c
-2.9473	-2.0723	-1.2967	n	3.6819	1.9775	10.5274	n
-3.3460	-3.2685	0.9040	c	4.2192	3.0219	12.8915	c
-2.8694	-5.2751	0.9160	h	4.3433	5.0758	12.9382	h
-4.2298	-2.1421	3.0493	c	4.5640	1.5039	14.9687	c
-4.5318	-3.2629	4.7507	h	5.0125	2.3227	16.8052	h
-4.6920	0.4152	3.0117	c	4.3560	-1.0536	14.6763	c
-5.3783	1.4097	4.6774	h	4.6506	-2.2466	16.3355	h
-4.1832	1.7184	0.8036	c	3.7715	-2.1303	12.4754	c
-4.4189	3.7588	0.7092	h	3.5742	-4.1718	12.3194	h
-3.4709	0.6946	-10.4610	c	0.6132	-7.9103	5.7023	c
-3.6819	-1.9775	-10.5274	n	-0.3127	-8.7487	3.5076	n
-4.2192	-3.0219	-12.8915	c	-1.1902	-11.0906	3.4996	c
-4.3433	-5.0758	-12.9382	h	-1.9695	-11.7309	1.6937	h
-4.5640	-1.5039	-14.9687	c	-1.1709	-12.7042	5.5211	c
-5.0125	-2.3227	-16.8052	h	-1.9109	-14.6159	5.3395	h
-4.3560	1.0536	-14.6763	c	-0.2110	-11.8123	7.7417	c
-4.6506	2.2466	-16.3355	h	-0.1444	-12.9993	9.4242	h
-3.7715	2.1303	-12.4754	c	0.6761	-9.3776	7.8296	c
-3.5742	4.1718	-12.3194	h	1.4356	-8.5951	9.5709	h
-0.6132	7.9103	-5.7023	c	**#2B**			

-6.0683	-2.4828	1.4531	n	14.8272	2.6498	1.8239	c
-7.6199	-0.6065	0.7776	c	16.7018	3.0758	2.5630	h
-7.0956	1.8801	0.8945	n	13.7189	4.1477	0.0122	c
-4.7717	2.4210	1.7882	c	14.6768	5.8048	-0.7440	h
-3.0261	0.6984	2.4219	n	11.3150	3.5145	-0.7963	c
-3.7527	-1.7067	2.1901	c	10.3204	4.6816	-2.1667	h
-10.1767	-1.3908	-0.1227	c	4.0911	-5.1172	-2.1209	c
-11.2464	0.1276	-1.8566	n	5.5595	-6.9342	-0.8051	n
-13.5292	-0.5968	-2.6913	c	4.8523	-9.4518	-1.1660	c
-14.3557	0.6136	-4.1476	h	5.9607	-10.8364	-0.1213	h
-14.8272	-2.6498	-1.8239	c	2.8886	-10.0678	-2.7478	c
-16.7018	-3.0758	-2.5630	h	2.3556	-12.0355	-3.0440	h
-13.7189	-4.1477	-0.0122	c	1.6296	-8.1616	-3.9523	c
-14.6768	-5.8048	0.7440	h	0.0706	-8.6683	-5.2061	h
-11.3150	-3.5145	0.7963	c	2.1873	-5.7295	-3.6075	c
-10.3204	-4.6816	2.1667	h	1.1024	-4.2565	-4.5464	h
-4.0911	5.1172	2.1209	c	1.8711	3.6820	-2.8446	c
-5.5595	6.9342	0.8051	n	2.3626	6.0428	-2.0949	n
-4.8523	9.4518	1.1660	c	0.6643	7.7738	-2.7063	c
-5.9607	10.8364	0.1213	h	1.0735	9.6858	-2.0333	h
-2.8886	10.0678	2.7478	c	-1.4910	7.3416	-4.0696	c
-2.3556	12.0355	3.0440	h	-2.7957	8.8752	-4.4844	h
-1.6296	8.1616	3.9523	c	-1.9529	4.9191	-4.8221	c
-0.0706	8.6683	5.2061	h	-3.6592	4.4421	-5.8706	h
-2.1873	5.7295	3.6075	c	-0.2530	3.0682	-4.1839	c
-1.1024	4.2565	4.5464	h	-0.5814	1.1124	-4.7198	h
-1.8711	-3.6820	2.8446	c	**#3A**			
-2.3626	-6.0428	2.0949	n	4.6145	-4.4302	-2.1815	c
-0.6643	-7.7738	2.7063	c	4.5938	4.6629	-2.1775	c
-1.0735	-9.6858	2.0333	h	0.7798	-2.1253	-3.0365	n
1.4910	-7.3416	4.0696	c	4.5473	0.1191	-2.1361	n
2.7957	-8.8752	4.4844	h	0.7747	2.3511	-3.0259	n
1.9529	-4.9191	4.8221	c	3.2290	2.2552	-2.4531	c
3.6592	-4.4421	5.8706	h	3.2416	-2.0283	-2.4519	c
0.2530	-3.0682	4.1839	c	-3.0684	0.1058	-4.0013	c
0.5814	-1.1124	4.7198	h	-6.8163	-2.1610	-5.0526	c
6.0683	2.4828	-1.4531	n	-7.8334	-3.9298	-5.3253	h
7.6199	0.6065	-0.7776	c	-6.8418	2.3822	-5.0527	n
7.0956	-1.8801	-0.8945	n	4.6386	-8.9552	-2.4341	n
4.7717	-2.4210	-1.7882	c	-7.9665	0.0633	-5.3768	c
3.0261	-0.6984	-2.4219	n	-9.9544	0.1735	-5.9207	h
3.7527	1.7067	-2.1901	c	3.4291	-6.7256	-2.6548	c
10.1767	1.3908	0.1227	c	1.4511	-6.7980	-3.2101	h
11.2464	-0.1276	1.8566	n	3.4064	6.9519	-2.6430	c
13.5292	0.5968	2.6913	c	1.4257	7.0170	-3.1912	h
14.3557	-0.6136	4.1476	h	-4.3705	-2.1327	-4.3665	c

-3.3464	-3.8928	-4.0693	h	5.8897	-6.7647	4.9154	h
4.5997	9.1968	-2.4334	n	3.8830	6.9416	4.3593	c
-4.3719	2.3299	-4.3557	c	5.8654	7.0025	4.9108	h
-3.4626	4.1539	-4.0832	h	2.6110	9.0993	3.8515	c
7.1054	4.7280	-1.4561	c	3.5359	10.9393	3.9792	h
8.0576	2.9449	-1.0749	h	2.6445	-8.8751	3.8596	c
-0.3534	0.1056	-3.3123	c	3.5722	-10.7127	3.9971	h
7.1246	-4.4821	-1.4615	c	**#3B**			
8.0682	-2.6940	-1.0834	h	6.0331	2.3168	-1.8400	c
8.3705	-6.7015	-1.2227	c	2.2191	-4.4714	-2.6990	n
10.3491	-6.7549	-0.6529	h	5.9867	-2.2269	-1.7986	n
8.3457	6.9520	-1.2246	c	2.2140	0.0051	-2.6884	n
10.3246	7.0135	-0.6568	h	4.6684	-0.0908	-2.1156	c
7.0736	9.1097	-1.7324	c	4.6810	-4.3743	-2.1143	c
7.9941	10.9518	-1.5847	h	-1.6291	-2.2402	-3.6638	c
7.1071	-8.8648	-1.7243	c	-5.3769	-4.5071	-4.7150	c
8.0304	-10.7044	-1.5671	h	-6.3943	-6.2758	-4.9877	h
0.1518	-4.4406	3.4024	c	-5.4024	0.0362	-4.7151	n
0.1311	4.6525	3.4063	c	-6.5271	-2.2827	-5.0393	c
-3.6829	-2.1357	2.5474	n	-8.5150	-2.1724	-5.5832	h
0.0847	0.1088	3.4477	n	4.8458	4.6059	-2.3055	c
-3.6880	2.3408	2.5580	n	2.8651	4.6731	-2.8542	h
-1.2336	2.2449	3.1308	c	-2.9311	-4.4788	-4.0290	c
-1.2210	-2.0386	3.1320	c	-1.9042	-6.2377	-3.7329	h
-7.5311	0.0955	1.5825	c	6.0391	6.8508	-2.0959	n
-11.2789	-2.1714	0.5313	c	-2.9325	-0.0161	-4.0181	c
-12.2919	-3.9411	0.2429	h	-2.0242	1.8086	-3.7466	h
-11.3044	2.3719	0.5312	n	8.5448	2.3820	-1.1186	c
0.1760	-8.9656	3.1497	n	9.4951	0.5972	-0.7375	h
-12.4291	0.0530	0.2070	c	1.0860	-2.2404	-2.9748	c
-14.4127	0.1607	-0.3579	h	9.7850	4.6059	-0.8871	c
-1.0335	-6.7359	2.9291	c	11.7637	4.6664	-0.3187	h
-3.0066	-6.8034	2.3535	h	8.5130	6.7636	-1.3948	c
-1.0562	6.9416	2.9409	c	9.4330	8.6059	-1.2470	h
-3.0312	7.0020	2.3695	h	1.5705	2.3065	3.7439	c
-8.8331	-2.1431	1.2174	c	-2.2435	-4.4817	2.8849	n
-7.8007	-3.9027	1.4890	h	1.5240	-2.2373	3.7853	n
0.1371	9.1865	3.1504	n	-2.2486	-0.0053	2.8955	n
-8.8345	2.3196	1.2282	c	0.2057	-0.1011	3.4683	c
-7.9180	4.1436	1.4707	h	0.2183	-4.3847	3.4695	c
2.6428	4.7177	4.1278	c	-6.0917	-2.2506	1.9201	c
3.6008	2.9339	4.4898	h	-9.8396	-4.5174	0.8688	c
-4.8160	0.0952	2.2715	c	-10.8527	-6.2872	0.5802	h
2.6619	-4.4924	4.1224	c	-9.8651	0.0258	0.8688	n
3.6108	-2.7034	4.4817	h	-10.9898	-2.2931	0.5446	c
3.9078	-6.7119	4.3611	c	-12.9732	-2.1852	-0.0204	h

0.3831	4.5955	3.2784	c	-4.5299	2.4360	2.2417	c
-1.5918	4.6581	2.7067	h	-3.6122	4.2599	2.4838	h
-7.3938	-4.4891	1.5549	c	-0.5114	0.2116	3.2850	c
-6.3585	-6.2476	1.8265	h	4.0902	-3.7061	4.3782	h
1.5764	6.8405	3.4880	n	8.5499	-3.6960	-1.1894	h
-7.3952	-0.0265	1.5657	c	8.5347	4.1587	-1.1961	h
-6.4799	1.7983	1.8078	h	4.0746	4.1485	4.3715	h
4.0821	2.3716	4.4653	c	**#3D**			
5.0392	0.5867	4.8274	h	-4.6222	-2.2163	0.0000	c
-3.3767	-2.2508	2.6091	c	-3.4916	-2.4974	-2.2332	n
5.3224	4.5956	4.6968	c	-1.0296	-3.0819	-2.1375	c
7.3046	4.6553	5.2484	h	0.2785	-3.3925	0.0000	n
4.0503	6.7533	4.1890	c	-1.0296	-3.0819	2.1375	c
4.9749	8.5933	4.3168	h	-3.4916	-2.4974	2.2332	n
1.2260	-6.1681	3.6988	h	0.9710	3.0864	2.2353	n
5.6864	-6.1579	-1.8686	h	3.4253	2.5134	2.1380	c
#3C				4.7411	2.1914	0.0000	n
5.0844	-2.0090	-2.0230	n	3.4253	2.5134	-2.1380	c
8.8520	0.2355	-1.1226	n	0.9710	3.0864	-2.2353	n
5.0793	2.4675	-2.0124	n	-0.1596	3.3676	0.0000	c
7.5337	2.3716	-1.4396	c	-2.1691	3.8357	0.0000	h
7.5463	-1.9119	-1.4384	c	-6.6289	-1.7342	0.0000	h
1.2362	0.2222	-2.9878	c	-0.0250	-3.3197	-3.9218	h
-2.5116	-2.0447	-4.0391	c	4.4351	2.2480	-3.9299	h
-3.5286	-3.8135	-4.3128	h	4.4351	2.2480	3.9299	h
-2.5371	2.4986	-4.0392	n	-0.0250	-3.3197	3.9218	h
-3.6618	0.1797	-4.3633	c	**#4C**			
-5.6497	0.2896	-4.9076	h	-2.5000	-2.0009	-2.0718	c
-0.0658	-2.0163	-3.3530	c	-2.8048	2.2650	-1.7425	c
0.9603	-3.7762	-3.0581	h	-5.1978	-0.2368	0.7613	c
-0.0672	2.4463	-3.3422	c	-1.4395	-4.0643	-3.0746	n
0.8433	4.2702	-3.0709	h	-2.1075	4.5878	-2.4837	n
3.9513	0.2220	-2.2989	c	-7.0495	-0.5319	2.5236	n
0.6218	-2.0193	3.5608	n	-4.5297	2.1196	0.1309	n
4.3893	0.2251	4.4612	n	-4.2388	-2.3650	-0.2303	n
0.6167	2.4571	3.5715	n	-1.7699	0.2776	-2.9442	n
3.0710	2.3613	4.1443	c	-1.7506	-5.7312	-2.1923	h
3.0836	-1.9222	4.1455	c	0.1849	-3.8428	-4.0628	h
-3.2264	0.2119	2.5960	c	-0.5390	4.7579	-3.5652	h
-6.9743	-2.0550	1.5448	c	-2.6873	6.0787	-1.4386	h
-7.9872	-3.8248	1.2563	h	-7.2914	-2.2764	3.2681	h
-6.9998	2.4883	1.5447	n	-7.5441	0.9915	3.5688	h
-8.1245	0.1694	1.2205	c	2.5000	2.0009	2.0718	c
-10.1079	0.2769	0.6555	h	2.8048	-2.2650	1.7425	c
-4.5285	-2.0267	2.2309	c	5.1978	0.2368	-0.7613	c
-3.4946	-3.7862	2.5020	h	1.4395	4.0643	3.0746	n

2.1075	-4.5878	2.4837	n
7.0495	0.5319	-2.5236	n
4.5297	-2.1196	-0.1309	n
4.2388	2.3650	0.2303	n
1.7699	-0.2776	2.9442	n
1.7506	5.7312	2.1923	h
-0.1849	3.8428	4.0628	h
0.5390	-4.7579	3.5652	h
2.6873	-6.0787	1.4386	h
7.2914	2.2764	-3.2681	h
7.5441	-0.9915	-3.5688	h
#4D			
-8.0718	-0.9876	0.1045	c
-3.8340	-1.4938	-0.3250	c
-5.4984	2.4373	-0.1496	c
-10.3869	-1.9528	0.4158	n
-1.8056	-3.0002	-0.5434	n
-5.2349	4.9928	-0.2956	n
-3.4097	1.0213	-0.3184	n
-7.8658	1.5628	0.1013	n
-6.1192	-2.5986	-0.1736	n
-11.8923	-0.7764	0.3932	h
-10.6435	-3.8370	0.2286	h
-2.1166	-4.8746	-0.3139	h
-0.0045	-2.2897	-0.2914	h
-6.7435	6.0608	0.1966	h
-3.4900	5.7516	-0.1208	h
8.0718	0.9876	-0.1045	c
3.8340	1.4938	0.3250	c
5.4984	-2.4373	0.1496	c
10.3869	1.9528	-0.4158	n
1.8056	3.0002	0.5434	n
5.2349	-4.9928	0.2956	n
3.4097	-1.0213	0.3184	n
7.8658	-1.5628	-0.1013	n
6.1192	2.5986	0.1736	n
11.8923	0.7764	-0.3932	h
10.6435	3.8370	-0.2286	h
2.1166	4.8746	0.3139	h
0.0045	2.2897	0.2914	h
6.7435	-6.0608	-0.1966	h
3.4900	-5.7516	0.1208	h

References

[1] C. Lee, W. Yang, R. Parr, *Phys. Rev. B* **1988**, *37*, 785–789.

[2] A. D. Becke, *Phys. Rev. A* **1988**, *38*, 3098–3100.

[3] J. Tao, J. Perdew, V. Staroverov, G. Scuseria, *Phys. Rev. Lett.* **2003**, *91*, 146401.

[4] L. Goerigk, S. Grimme, *J. Chem. Theory Comput.* **2010**, *6*, 107–126.

[5] J. P. Perdew, *Proceedings of the 21st Annual International Symposium on the Electronic Structure of Solids*, Akademie Verlag: Berlin, **1991**, pp. 11-20.

[6] A. D. Becke, *J. Chem Phys.* **1996**, *104*, 1040–1046.

[7] Y. Jung, R. C. Lochan, A. D. Dutoi, M. Head-Gordon, *J. Chem. Phys.* **2004**, *121*, 9793–9802.

[8] S. Grimme, *J. Chem. Phys.* **2003**, *118*, 9095–9102.

[9] L. Goerigk, S. Grimme, *J. Chem. Theory Comput.* **2011**, *7*, 291–309.

[10] J. P. Perdew, K. Burke, M. Ernzerhof, *Phys. Rev. Lett.* **1996**, *77*, 3865–3868.

[11] E. A. Coutsias, C. Seok, K. A. Dill, *J. Comput. Chem.* **2004**, *25*, 1849–1857.

[12] J. Janczak, M. Śledź, R. Kubiak, *J. Mol. Struct.* **2003**, *659*, 71–79.

[13] A. Cousson, B. Nicolaï, F. Fillaux, *Acta Crystallogr., Sect. E* **2005**, *61*, o222–o224.

[14] Single-crystals of 3tptz were obtained by heating small amounts of 3tptz in a sealed duran ampoule, filled with argon (with 2 $K \cdot min^{-1}$ to 310 °C, held at 310 °C for 48 h, with 0.05 $K \cdot min^{-1}$ to RT). 3tptz crystallizes in the orthorhombic space group *Pnma* with a disorder of the nitrogen atom in one of the pyrimidyl rings. However, for the calculations this disorder has not been taken into account and calculations have been performed in space group $P\ \bar{1}$. PCCDC 867801 contains the crystallographic data for 3tptz (space group *Pnma*). These data can be obtained free of charge via http://www.ccdc.cam.ac.uk/conts/retrieving.html (or from the Cambridge Crystallographic Data Centre, 12, Union Road, Cambridge CB2 1EZ, UK; fax: +44 1223 336033).

[15] S. J. Makowski, M. Lacher, C. Lermer, W. Schnick, *J. Mol. Struct.* **2012**, *1013*, 19–25.

10.2 List of Publications

A - Publications published as part of this thesis

Rare-Earth Melonates $LnC_6N_7(NCN)_3 \cdot xH_2O$ (Ln = La, Ce, Pr, Nd, Sm, Eu, Tb; x = 8-12): Synthesis, Crystal Structures, Thermal Behavior, and Photoluminescence Properties of Heptazine Salts with Trivalent Cations

S. J. Makowski, A. Schwarze, P. J. Schmidt, W. Schnick, *Eur. J. Inorg. Chem.* **2012**, 1832

Supramolecular Hydrogen-Bonded Structures between Melamine and *N*-Heterocycles

S. J. Makowski, M. Lacher, C. Lermer, W. Schnick, *J. Mol. Struct.* **2012**, *1013*, 19

Formation of a Hydrogen-Bonded Heptazine Framework by Self-Assembly of Melem into a Hexagonal Channel Structure

S. J. Makowski, P. Köstler, W. Schnick, *Chem. Eur. J.* **2012**, *18*, 3248

Investigation of the Hydrolysis Stability of Triazine Tricarboxylate in the Presence of Transition Metal(II) Ions and Synthesis and Crystal Structure of the Alkaline Earth Triazine Tricarboxylates $M_3[C_3N_3(CO_2)_3]_2 \cdot 12H_2O$ (M = Sr, Ba)

S. J. Makowski, E. Calta, M. Hörmannsdorfer, W. Schnick, *Z. Anorg. Allg. Chem.* **2012**, *638*, 345

Formation of Cocrystals between Alkali Triazine Tricarboxylates and Cyanuric Acid – Reactivity Considerations and Structural Characterization of the Adduct Phases $M_3[C_3N_3(CO_2)_3]$ $[C_3N_3O_3H_3] \cdot H_2O$ (M = K, Rb)

S. J. Makowski, E. Calta, M. Lacher, W. Schnick, *Z. Anorg. Allg. Chem.* **2011**, *638*, 88

Novel Alkali Triazine Tricarboxylates $Li_3[C_3N_3(CO_2)_3] \cdot 4H_2O$, $Rb_3[C_3N_3(CO_2)_3] \cdot 2H_2O$ and $Cs_3[C_3N_3(CO_2)_3] \cdot 2H_2O$ – Synthesis, Crystal Structure and Thermal Behavior

S. J. Makowski, E. Calta, W. Schnick, *Z. Anorg. Allg. Chem.* **2011**, *637*, 2142

$K_3[C_3N_3(COO)_3]\cdot 2H_2O$ – Crystal Structure of a New Alkali Derivative of the Multidentate Ligand Triazine Tricarboxylate

S. J. Makowski, M. Hörmannsdorfer, W. Schnick, *Z. Anorg. Allg. Chem.* **2010**, *636*, 2584

B - Publications published prior to this thesis

Protonated Melonate $Ca[HC_6N_7(NCN)_3]\cdot 7H_2O$ - Synthesis, Crystal Structure, and Thermal Properties

S. J. Makowski, D. Gunzelmann, J. Senker, W. Schnick, *Z. Anorg. Allg. Chem.* **2009**, *635*, 2434

$Rb_3[C_6N_7(NCN)_3]\cdot 3H_2O$ and $Cs_3[C_6N_7(NCN)_3]\cdot 3H_2O$ – Synthesis, Crystal Structure and Thermal Behavior of Two Novel Alkali Melonates

S. J. Makowski, W. Schnick, *Z. Anorg. Allg. Chem.* **2009**, *635*, 2197

Coupled Spin Ordering in the Ln_2LiRuO_6 Double Perovskites

S. J. Makowski, J. A. Rodgers, P. F. Henry, J. P. Attfield, J.-W. G. Bos, *Chem. Mater.* **2009**, *21*, 264

10.3 CSD and CCDC numbers

Crystallographic data were deposited with the Cambridge Crystallographic Data Centre (CCDC, http://www.ccdc.cam.ac.uk/data_request/cif; 12 Union Road, Cambridge CB2 1EZ, UK (Fax: +44-1223-336-033; or E-Mail: deposit@ccdc.cam.ac.uk) or the Fachinformationszentrum Karlsruhe (76344 Eggenstein-Leopoldshafen, Germany, fax: (+49)7247-808-666; e-mail: crysdata@fiz-karlsruhe.de) and are available on quoting the respective CSD/CCDC depository numbers.

$LaC_6N_7(NCN)_3 \cdot 8H_2O$	CSD 423756
$CeC_6N_7(NCN)_3 \cdot 8H_2O$	CSD 423757
$PrC_6N_7(NCN)_3 \cdot 8H_2O$	CSD 423758
$NdC_6N_7(NCN)_3 \cdot 8H_2O$	CSD 423759
$SmC_6N_7(NCN)_3 \cdot 8H_2O$	CSD 423760
$Li_3[C_3N_3(CO_2)_3] \cdot 4H_2O$	CCDC 827795
$K_3[C_3N_3(CO_2)_3] \cdot 2H_2O$	CCDC 784049
$Rb_3[C_3N_3(CO_2)_3] \cdot 2H_2O$	CCDC 827796
$Cs_3[C_3N_3(CO_2)_3] \cdot 2H_2O$	CCDC 827797
$Sr_3[C_3N_3(CO_2)_3]_2 \cdot 12H_2O$	CCDC 834692
$Ba_3[C_3N_3(CO_2)_3]_2 \cdot 12H_2O$	CCDC 834693
$K_3[C_3N_3(CO_2)_3][C_3N_3O_3H_3] \cdot H_2O$	CCDC 834102
$Rb_3[C_3N_3(CO_2)_3][C_3N_3O_3H_3] \cdot H_2O$	CCDC 834103
$C_6N_7(NH_2)_3 \cdot 1.98H_2O$	CSD 423755
4M·3TPTZ	CCDC 852974
3M·TMPyP-Tos·$9H_2O$	CCDC 852975
3-tptz	CCDC 867801

10.4 List of Abbreviations

A	acceptor
anal.	analytical
ATR	attenuated total reflectance
a. u.	arbitrary units
BET	Brunauer-Emmet-Teller
br.	broad
BSSE	basis set superposition error
CA	cyanuric acid
calcd.	calculated
CAS	Chemical Abstracts Service
CCD	charge coupled device
CCDC	Crystallographic Data Centre
cf.	confer
cm	centimeter
CN	coordination number
COF	covalent organic framework
CP	cross polarization
CSD	Cambridge Structural Database
CTF	covalent triazine framework
D	donor
DEI	direct electron ionization
dens.	density
DFT	density functional theory
DTA	differential thermal analysis
E_{int}^{DFT}	interaction energy based on density functional computations
E_{int}^{DFT-D3}	interaction energy based on density functional computations with dispersion correction
e. g.	*exempli gratia*, for example

$E_{int}^{periodic}$	interaction energy based on density functional computations with periodic boundary conditions
et al.	*et alii*, and others
eV	electron Volt
ext.	external
F_c	calculated structure factor
F_o	observed structure factor
FT	Fourier transformation
GGA	generalized gradient approximation
GoF	goodness of fit
GooF	goodness of fit
h	hour
HSAB	hard and soft acids and bases
I	intensity
ICP-AES	inductively coupled plasma - atomic emission spectrometry
i. e.	*id est*, that is
int.	internal
IPDS	imaging plate diffraction system
IR	infrared
kcal	kilocalorie
kHz	kilohertz
Ln	lanthanide
m	medium
M	molar
M	melamine
MAS	magic angle spinning
max.	maximum
mbar	millibar
min	minute
min.	minimum
mL	milliliter
mm	millimeter
mmol	millimol

MOF	metal organic framework
MS	mass spectrometry
NMR	nuclear magnetic resonance
no.	number
p. a.	*pro analysis*, for analysis
pm	picometer
ref.	reflection
Ref.	reference
res.	residual
RMSD	root mean square deviation
s	strong
TG	thermogravimetry
TMPyP-Tos	tetrakis(4-*N*-methylpyridinumyl)porphyrin tetratosylate
TMS	trimethylsilane
TPTZ	tris(2-pyridyl)-triazine
2tptz	tris(2-pyridyl)-triazine
3tptz	tris(3-pyridyl)-triazine
432tptz	$(melamine)_4 \cdot (tris(2\text{-}pyridyl)\text{-}triazine)_3$
TPymT	2,4,6-tris(2-pyrimidyl)-*s*-triazine
TTC	*s*-triazine tricarboxylate
UV	ultra violet
VASP	Vienna Ab Initio Simulation
v. d. Waals	van der Waals
vs	very strong
w	weak
wt.	weight
Z	formula units per unit cell